

**FUNCTIONAL ANALYSIS OF THE MOUSE RBBP6 GENE USING
INTERFERENCE RNA**

Ashley Pretorius



A thesis submitted in fulfilment of the requirement for the degree of Doctor Philosophiae
in the Faculty of Science, University of the Western Cape.

Supervisor: Prof D. Jasper G. Rees

November 2007

ABSTRACT

Functional analysis of the mouse RBBP6 gene using interference RNA

A. Pretorius

PhD thesis, Department of Biotechnology, Faculty of Science, University of the Western Cape

A novel hamster gene homologous to the human cDNA clone 21C4 was identified in a genetic screen to identify new genes involved in the MHC class I antigen processing and presentation pathway. The identified gene however showed no significant matches to sequences in the Genbank Database and was subsequently named the Domain Without No name (DWNN). The corresponding human gene was found to be located on chromosome 16p12.2, upstream of the previously identified RBBP6/PACT/P2P-R gene. Analysis of cDNA sequences showed that the sequence coded for the previously unidentified N-terminus of the RBBP6 protein (Dlamini *et al*, in prep), which was named the DWNN domain.

RBBP6 is one of the few proteins identified that has been shown to interact with both p53 and Rb, suggesting a possible model for the integration of the regulation of transcription, cell cycle control and apoptosis. Over-expression of the mouse homolog P2P-R has been shown to lead to cell cycle arrest and apoptosis. The conserved mechanisms of

programmed cell death play a fundamentally important role in tissue homeostasis, embryogenesis and cellular defense and had only recently been subjected to molecular analysis.

The aim of this thesis was to investigate the cellular role of the mouse RBBP6 gene using the interference RNA (RNAi) gene targeting technology and also to understand the relevance of two promoters for the RBBP6 gene.

Genetic analysis showed the presence of two promoters for RBBP6 namely Promoter 0 (P0) and Promoter 1 (P1) both being responsible for the different RBBP6 transcripts. The Enhanced Green Fluorescent Protein (EGFP) and the Red Fluorescent Protein (DsRed1) were both placed under the transcriptional control of P0 and P1. Promoter activities were measured using FACS and Real-Time qRT-PCR. The results showed P0 to have a higher level of transcriptional activity than P1 before and after camptothecin-induced apoptosis.

RNAi was used to target the expression of the RBBP6 gene. Several small interference RNA (siRNA) constructs were designed that would result in the expression of two distinct siRNA oligonucleotides designated DWNN-A and DWNN-B targeting different regions of the gene. Two stable siRNA-expressing cell lines were established, namely RU6A and GU6B expressing DWNN-A and DWNN-B respectively. Fluorescence microscopy and Real-Time qRT-PCR analysis were used to evaluate the effect on RBBP6 expression following (i) transient transfections of the siRNA constructs into the parental cell line NIH 3T3 cell line (ii) as well as expression in the stable cell lines RU6A

and GU6B. The silencing effect of the DWNN-A oligonucleotide appeared to be more potent than that exerted by DWNN-B.

Both stable lines were used in assays to determine the effect of RBBP6 silencing on apoptosis. The stable cell lines proved to be significantly more resistant to apoptosis induced by camptothecin compared to the parental NIH 3T3 cell line. Furthermore complementing the stable cell lines with the full-length DWNN-200 cDNA, restored sensitivity to camptothecin and the degree of cell death observed in the parental cell line. In addition, over-expression of the RBBP6 protein showed an increase in the apoptotic population following camptothecin-induced apoptosis. Apoptosis mediated through RBBP6 was shown to be dependent on p53 expression and possibly follows an intrinsic pathway. Finally, the siRNA stable expressing cell lines RU6A and GU6B were also shown to be restricted in the G1 phase of the cell cycle implicating the RBBP6 gene in cell cycle progression.

From the study the RBBP6 Promoters showed an increase in transcriptional activity following the induction of apoptosis. Furthermore the involvement of the RBBP6 was implicated in the processes of apoptosis and the cell cycle although the exact mechanisms have not been fully elucidated.

Keywords:

Apoptosis

Real-Time qRT-PCR

Cell cycle

Interference RNA (RNAi)

Homologous recombination

Promoter

p53

Retinoblastoma

PACT

RBBP6



DECLARATION.

I declare that “**Functional analysis of the mouse RBBP6 gene using Interference RNA**” is my own work that has not been submitted for any degree or examination in any other university and that all the sources I have used or quoted have been indicated and acknowledged by complete references.

Ashley Pretorius



November 2007

Signed:.....

TABLE OF CONTENTS

ABSTRACT.....	I
DECLARATION.....	V
TABLE OF CONTENTS.....	VI
LIST OF TABLES.....	X
LIST OF FIGURES.....	XI
ABBREVIATIONS.....	XVIII
ACKNOWLEDGEMENTS	XXI
CHAPTER 1: LITERATURE REVIEW.....	1
1.1 INTRODUCTION	1
1.2 THE IMMUNE SYSTEM.....	3
1.2.1 Classes of T lymphocytes	4
1.2.2 MHC class 1 presentation pathway.....	7
1.3 CTL KILLING	10
1.3.1 Granule mediated exocytic killing	11
1.3.2 Receptor mediated CTL killing (see figure 1.2).....	13
1.3.3 The role of Caspases in CTL killing.....	14
1.4 APOPTOSIS.....	16
1.4.1 Introduction.....	16
1.4.2 Characteristics of Apoptosis.....	17
1.4.3 Components of the Apoptotic pathway.....	19
1.4.4 The Apoptotic pathways	22
1.4.5 Regulation of the Apoptotic Proteins.....	29
1.5 THE P53 GENE.....	30
1.5.1 Functions of the p53 gene.....	31
1.5.2 p53-activating pathways	33
1.5.3 Control of p53.....	34
1.6 RETINOBLASTOMA (RB) GENE.....	36
1.6.1 RB function in the cell cycle	37
1.6.2 Function of Rb in apoptosis.....	39
1.7 THE DWNN GENE FAMILY	40
1.7.1 Identification of the DWNN domain.....	40
1.7.2 Structure of DWNN	43
1.7.3 DWNN/RBBP6 homologues	45
1.7.4 Homo sapiens RBBP6.....	46
1.7.5 Mus musculus RBBP6 (NM 011247)	47
1.7.6 Saccharomyces cerevisiae RBBP6 (NP 012864).....	51
1.7.7 Other RBBP6 homologues.....	53
1.8 ZINC FINGERS	53
1.9 ROLE OF RING FINGERS IN UBIQUITIN PATHWAY	54
1.9.1 DWNN ubiquitin homology.....	54
1.9.2 Ubiquitin	55
1.9.3 The ubiquitin pathway.....	56
1.9.4 Functional relationship between DWNN and the RING finger.....	57
1.10 GENE TARGETING.....	59
1.10.1 Homologous recombination.....	60
1.10.2 Embryonic Stem (ES) cells.....	61
1.10.3 Designing of HR vectors.....	61
1.10.4 The use of site-specific recombinases.....	67
1.10.5 Applications of gene targeting.....	68

1.11	ANTISENSE RNAs	71
1.12	INTERFERENCE RNA (RNAi)	72
1.12.1	Mechanism of RNAi	74
1.12.2	Dicer	76
1.12.3	Role of RNA pol III	79
1.12.4	Applications of RNAi	82
1.13	AIMS	83
CHAPTER 2: MATERIALS AND METHODS		85
2.1	MATERIALS AND SUPPLIERS	85
2.2	GENERAL STOCK SOLUTIONS AND BUFFERS	88
2.3	BACTERIAL CULTURE	91
2.3.1	Bacterial strains	91
2.3.2	Selection	91
2.3.3	Storage of bacterial strains and clones	91
2.4	CLONING VECTORS	92
2.4.1	pGEM [®] -T Easy Vector (Promega)	92
2.4.2	pCR [®] -XL-TOPO [®] Cloning Vector (Invitrogen)	93
2.4.3	pEGFP-C1 (Clontech)	94
2.4.4	pDsRed1-C1 vector (Clontech)	95
2.5	PREPARATION OF COMPETENT E. COLI CELLS FOR TRANSFORMATION	96
2.6	BACTERIAL TRANSFORMATIONS (COHEN ET AL., 1972)	96
2.7	PREPARATION OF PLASMID DNA	97
2.7.1	Small-scale plasmid preparation (minipreps)	97
2.7.2	Large-scale preparation of plasmid DNA	98
2.7.3	Double CsCl/ethidium bromide fractionation	99
2.8	MANIPULATION OF PLASMID DNA	100
2.8.1	Ethanol precipitation	100
2.8.2	Phenol/chloroform extraction	101
2.8.3	Restriction enzyme digests	101
2.8.4	Ligation of DNA	102
2.9	AGAROSE GEL ELECTROPHORESIS OF DNA	102
2.9.1	DNA molecular weight markers	103
2.9.2	Purification of DNA fragments using the GFX- purification kit	104
2.10	POLYMERASE CHAIN REACTION (PCR) AMPLIFICATION	104
2.10.1	Standard PCR	104
2.10.2	PCR amplification of plasmid DNA	105
2.10.3	Colony PCR	106
2.11	SEQUENCING OF DOUBLE STRANDED DNA	106
2.12	ISOLATION OF GENOMIC DNA FROM CULTURED CELLS	108
2.13	CELL CULTURE	109
2.13.1	Cell lines	109
2.13.2	Tissue culture media	109
2.13.3	Propagation and storage of cell lines	110
2.13.4	Transfection of cell lines	110
2.14	IMMUNOFLUORESCENCE	112
2.14.1	Fixation and permeabilization of cells	112
2.14.2	Immunostaining of cells	112
2.15	FACS ANALYSIS	113
2.16	APOPTOSIS ASSAYS	113
2.16.1	The screening of camptothecin as an inducer of apoptosis	113
2.16.2	APOPercentage [™] Apoptosis Assay	114
2.16.3	Annexin V-PE assay	114
2.16.4	APO-Direct/TUNEL assay	115
2.17	CELL CYCLE ANALYSIS	116
2.18	RNA ISOLATION	116

2.19	AGAROSE GEL ELECTROPHORESIS OF RNA	117
2.20.	cDNA SYNTHESIS.....	118
2.21	REAL-TIME QUANTITATIVE RT-PCR	119
2.22	QUANTITATION OF REAL-TIME QRT-PCR RESULTS.....	120
2.22.1	The standard curve.....	120
2.23	ANNEALING OF siRNA OLIGONUCLEOTIDES.....	122
CHAPTER 3: EXPRESSION ANALYSIS OF THE RBBP6 PROMOTERS IN MAMMALIAN CELL CULTURE.....		123
3.1	INTRODUCTION.....	123
3.2	CLONING OF P0 AND P1 INTO pGEM®-T EASY.....	125
3.2.1	PCR amplification of promoters.....	125
3.2.2.	Cloning of P0 and P1 PCR products.....	127
3.3	PREPARATION OF pEGFP-C1 AND pDsRED1 PROMOTER CONSTRUCTS.....	129
3.3.1.	Preparing pEGFP-C1 and pDsRed-C1 cloning vectors.....	129
3.3.2	Digestion and purification of inserts.....	130
3.3.3.	Cloning of P0 and P1 into pEGFP-C1 and pDsRed-C1	130
3.4	EVALUATION OF THE EXPRESSION OF EGFP AND DSRED1 IN VIVO.....	134
3.4.1.	Transfection of constructs.....	134
3.4.2	Fluorescence microscopy.....	135
3.4.2.	Quantification of fluorescence	136
3.5	THE EFFECT OF APOPTOSIS ON PROMOTER ACTIVITY.....	138
3.5.1	Induction of Apoptosis.....	139
3.5.2	The effect of apoptosis on promoter activity.....	139
3.6	SUMMARY.....	141
CHAPTER 4: INTERFERENCE RNA – CONSTRUCTION OF MOUSE RBBP6 siRNA VECTORS		145
4.1	INTRODUCTION.....	145
4.2	AMPLIFICATION OF THE RNA POL III PROMOTERS.....	147
4.3	CLONING OF H1 AND U6 PROMOTERS.....	148
4.3.1	Deletion of the MCS from pEGFP-C1 and pDsRed-C1 vectors.....	148
4.3.2	Preparing pG-MCS and pR-MCS as cloning vectors	150
4.3.3	Cloning of the U6 and H1 promoters.....	150
4.3.4	Screening for recombinant clones.....	151
4.4	CLONING OF siRNA OLIGONUCLEOTIDES.....	152
4.4.1	Identifying siRNA oligonucleotides	152
4.4.2	Annealing of siRNA oligonucleotides.....	153
4.4.3	Cloning of siRNA oligonucleotides.....	153
4.4.4	Sequencing of recombinant siRNA clones.....	154
4.5	SUMMARY.....	155
CHAPTER 5: INTERFERENCE RNA – EVALUATING THE EFFECT OF THE siRNA CONSTRUCTS ON THE EXPRESSION OF RBBP6		157
5.1	INTRODUCTION.....	157
5.2	TRANSIENT TRANSFECTIONS OF CELLS	158
5.2.1.	Transfection of mouse NIH 3T3 cells with siRNA constructs.....	158
5.2.2	Fluorescence microscopy.....	159
5.2.3	Real-Time qRT-PCR.....	161
5.3	GENERATING THE STABLE siRNA EXPRESSING CELL LINES RU6A AND GU6 B.....	162
5.3.1	Cell culture.....	162
5.3.2	Fluorescence microscopy.....	163
5.3.3	Real-Time qRT-PCR.....	164
5.4	SUMMARY.....	165

CHAPTER 6: THE EFFECT OF RBBP6 SILENCING ON APOPTOSIS.....	167
6.1 INTRODUCTION.....	167
6.2 DETERMINING THE OPTIMUM CONCENTRATION OF CAMPTOTHECIN.....	170
6.2.1 The Annexin V-PE assay.....	170
6.3 THE EFFECT OF RBBP6 SILENCING ON APOPTOSIS.....	171
6.3.1 Annexin V-PE assay.....	171
6.3.2 APOPercentage™ assay.....	172
6.3.3 Complementing stable cell lines with a full-length RBBP6 cDNA.....	173
6.4 OVER-EXPRESSING THE RBBP6 PROTEIN AND THE EFFECT ON APOPTOSIS.....	174
6.4.1 The effect of increased concentration of RBBP6 on Apoptosis.....	176
6.5 THE EFFECT ON P53 EXPRESSION.....	177
6.6 INVESTIGATION OF THE RBBP6 APOPTOTIC PATHWAY.....	180
6.8 SUMMARY.....	182
CHAPTER 7: THE EFFECT OF SILENCING OF THE RBBP6 GENE ON THE CELL CYCLE	188
7.1 INTRODUCTION.....	188
7.2 CELL CYCLE ANALYSIS OF RU6A AND GU6B.....	191
7.2 THE EFFECT OF APOPTOSIS ON THE CELL CYCLE.....	194
7.3 SUMMARY.....	195
CHAPTER 8: GENERAL DISCUSSION.....	197
8.1 INTRODUCTION.....	197
8.2 EXPRESSION ANALYSIS OF THE RBBP6 PROMOTERS IN CELL CULTURE (CHAPTER THREE).....	199
8.3 INTERFERENCE RNA – CONSTRUCTION OF MOUSE RBBP6 siRNA VECTORS. (CHAPTER FOUR).....	201
8.4 INTERFERENCE RNA – TESTING THE EFFECT OF THE siRNA CONSTRUCTS ON THE EXPRESSION OF RBBP6 (CHAPTER FIVE).....	202
8.5 THE EFFECT OF RBBP6 SILENCING ON APOPTOSIS. (CHAPTER SIX).....	204
8.6 THE EFFECT OF RBBP6 SILENCING ON THE CELL CYCLE. (CHAPTER SEVEN).....	208
8.7 CONCLUSION.....	211
8.8 FUTURE WORK.....	212
REFERENCES.....	214

LIST OF TABLES

Table 2.1	The sequencing reaction protocol
Table 2.2	PCR cycles for sequencing
Table 2.3	Represents the reagents used for the first strand cDNA synthesis reaction
Table 2.4	Represents the PCR conditions used in Real-Time Quantitative PCR
Table 2.5	Descriptive statistics of two candidate housekeeping genes (HKG) based on their crossing point (CP/ C_T) values
Table 3.1	Oligonucleotides used in chapter three
Table 3.2	List of promoter constructs with the nomenclature used in the subsequent sections of chapter three
Table 4.1	Parameters used for the design of siRNA oligonucleotides using the iRNAi v1.0 software
Table 4.2.	List of oligonucleotides used in the construction of siRNA vectors
Table 4.3.	List of siRNA constructs generated and the nomenclature used in the subsequent chapters
Table 6.1	List of oligonucleotides used in chapter six

LIST OF FIGURES

- Figure 1.1** Represents the MHC class 1 antigen processing and presentation pathway
- Figure 1.2** Diagrammatic representation of the two pathways by which CTLs kill their target cells
- Figure 1.3.** Diagrammatically represents the morphological changes associated with apoptosis
- Figure 1.4** A diagrammatical representation of the general structure of procaspase
- Figure 1.5** Diagrammatically represents the two mechanisms by which apoptosis occur
- Figure 1.6** Represents a diagrammatical representation of the regulation of the cell cycle by p53
- Figure 1.7** The p53-Mdm-2 negative feedback loop
- Figure 1.8** Represents the Retinoblastoma pathway of cell proliferation control
- Figure 1.9** Sequence alignment of DWNN homologues from a range of eukaryotic genomes
- Figure 1.10** Shows the neighbour joining tree of the DWNN gene from different taxa
- Figure 1.11** Diagrammatic representation of the RBBP6 partial cDNAs, including the full-length RBBP6 protein

- Figure 1.12** The domain structure of the RBBP6 family of proteins
- Figure 1.13** Shows the three-dimensional structure of the DWNN domain
- Figure 1.14** Diagrammatical representation of the ubiquitination pathway
- Figure 1.15** Schematic representation of the steps involved in producing a 'knock-out' mouse
- Figure 1.16** Represents a working model of the RNA interference mechanism
- Figure 1.17** Represent the interaction of Dicer and RISC (RNA-induced silencing complex)
- Figure 2.1** Represents the circular map of pGEM[®]-T Easy cloning vector indicating unique restriction recognition sequences in the multiple cloning site (MCS)
- Figure 2.2** Shows the sequence surrounding the TA cloning site and the diagrammatic representation of the pCR[®]-XL-TOPO[®] cloning vector map
- Figure 2.3** Represents the circular map and MCS of the pEGFP-C1 vector
- Figure 2.4** Represents the circular map of the pDsRed1-C1 vector and the MCS
- Figure 2.5** Agarose gel showing the sizes of the molecular weight markers pTZ and pKG 2
- Figure 3.1** Diagrammatically represents the different DWNN transcripts resulting from the activity of Promoter 0 (P0) and Promoter 1 (P1) using EST data and RT-PCR analysis
- Figure 3.2** Nucleotide sequence for the human RBBP6 Promoter 0 gene

- Figure 3.3** Nucleotide sequence for the human RBBP6 Promoter 1 gene
- Figure 3.4** PCR amplification of the human RBBP6 Promoter 0 (P0) gene
- Figure 3.5** PCR amplification of the human RBBP6 Promoter 1 (P1) gene
- Figure 3.6** PCR based screening method to identify P0 pGEM[®]-T Easy recombinants
- Figure 3.7** PCR based screening method to identify P1 pCR[®]-XL-TOPO[®] recombinants
- Figure 3.8** Restriction digestion of the pEGFP-C1 vector deleting the CMV promoter
- Figure 3.9** PCR identification of P0-pEGFP-C1 recombinant clones
- Figure 3.10** Restriction analysis of the pEGFP-C1 promoter constructs
- Figure 3.11** BLAST search results for the pEGFP-C1 P0 construct
- Figure 3.12** BLAST search results for the pDsRed-C1 P1 construct
- Figure 3.13** Sequence alignment of pEGFP-C1 P0
- Figure 3.14** Sequence alignment of pDsRed-C1 P1
- Figure 3.15(i)** Fluorescence microscopy analysis of EGFP expression in Hek 293T cells
- Figure 3.15(ii)** Fluorescence microscopy analysis of DsRed1 expression in Hek 293T cells
- Figure 3.16(i)** FACS analysis of EGFP expression in the Hek 293T cells
- Figure 3.16(ii)** FACS analysis of DsRed1 expression in the Hek 293T cells
- Figure 3.17** Represents the *gapdh* standard curve

- Figure 3.18(i)** Expression analysis of EGFP and DsRed1 in Hek 293T cells using Real-Time qRT-PCR
- Figure 3.18(ii)** Expression analysis of EGFP and DsRed1 using Real-Time qRT-PCR
- Figure 3.19** FACS analysis of EGFP and DsRed1 expression in Hek 293T cells following the induction of apoptosis
- Figure 3.20(i)** Expression analysis of EGFP and DsRed1 after camptothecin (cpt)-induced apoptosis using Real-Time qRT-PCR
- Figure 3.20(ii)** Expression analysis of EGFP and DsRed1 following the induction of apoptosis
- Figure 4.1** PCR amplification of the RNA Pol III U6 and H1 promoters
- Figure 4.2** A diagrammatical representation of the deletion of the MCS (Multiple Cloning Site) from pDsRed-C1 cloning vector
- Figure 4.3** The PCR strategy used to identify GU6A recombinant clones
- Figure 4.4** The PCR strategy used to identify RH1 recombinant clones
- Figure 4.5** The PCR strategy used to identify pU6A and pU6B siRNA recombinant clones
- Figure 4.6** Sequence data and BLAST results for the RNA Pol III mouse U6 promoter
- Figure 4.7** Sequence data and BLAST results for the DWNN-A siRNA oligonucleotide
- Figure 4.8** Represents the map for the siRNA construct GU6B

- Figure 5.1** Fluorescence microscopy analysis of the localization of the RBBP6 protein in the NIH 3T3 cells transiently transfected with the siRNA construct RH1B
- Figure 5.2** Fluorescence microscopy analysis of the localization of the RBBP6 protein in the NIH 3T3 cells transiently transfected with the siRNA construct RU6A
- Figure 5.3** Fluorescence microscopy analysis of the localization of the RBBP6 protein in the NIH 3T3 cells transiently transfected with the siRNA construct GU6B
- Figure 5.4** Isolation of total RNA from cultured NIH 3T3 cells
- Figure 5.5** Expression analysis of the RBBP6 gene using Real-Time qRT-PCR
- Figure 5.6** The expression level of the RBBP6 gene in cells transiently transfected with different siRNA constructs
- Figure 5.7** Fluorescence microscopy analysis of the localization of the RBBP6 protein in the stable siRNA expressing cell line, RU6A
- Figure 5.8** Isolation of total RNA from cultured NIH 3T3 cells
- Figure 5.9** Expression level of the RBBP6 gene as determined using Real-Time qRT-PCR analysis
- Figure 5.10** The level of expression of the RBBP6 gene
- Figure 6.1a** LDH release assay of the three hygromycin B/CTL resistant clones, compared to the Y10 parental cell line on exposure to the HA-specific K^k restricted CTL clones HA8 and HA11

- Figure 6.1b** LDH release assay of the three-hygromycin B/CTL resistant clones, compared to the Y10 parental cell line on exposure to different concentrations of staurosporine
- Figure 6.2(i)** Apoptosis analysis of the parental NIH 3T3 cell line using the Annexin V-PE assay following treatment with camptothecin.
- Figure 6.2(ii)** Flow cytometric data for the NIH 3T3 cell line following the induction of apoptosis
- Figure 6.2(iii)** Flow cytometric data for the NIH 3T3, RU6A and GU6B cell lines following the induction of apoptosis.
- Figure 6.3** *APOPercentage*TM assay demonstrating the percentage cell death in different cell lines following camptothecin-induced apoptosis
- Figure 6.4** TUNEL assay measuring apoptosis in the NIH 3T3 cell line
- Figure 6.5** *APOPercentage*TM demonstrating the percentage cell death in the NIH 3T3 cell line
- Figure 6.6** Expression analysis of the p53 gene using Real-Time qRT-PCR
- Figure 6.7** Shows the relative expression ratios of the pro-apoptotic Bax versus the anti-apoptotic Bcl-2 gene
- Figure 7.1** Represents a schematic representation of the cell cycle and proteins that regulate the different checkpoints
- Figure 7.2** FACS results of the cell cycle analysis of the NIH 3T3, RU6A and GU6B cell lines at the 12-point
- Figure 7.3** FACS results of the cell cycle analysis of the NIH 3T3, RU6A and GU6B cell lines at the 18-point

Figure 7.4 FACS results of the cell cycle analysis of the NIH 3T3, RU6A and GU6B cell lines at the 24-point

Figure 7.5 FACS results of the cell cycle analysis of the NIH 3T3, RU6A and GU6B cell lines at the 48-point

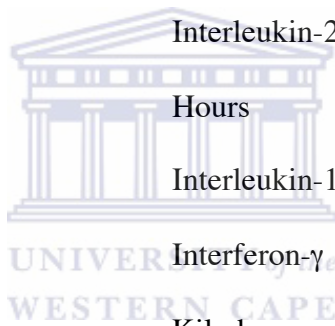
Figure 7.6 Represent the cell cycle results measured on a FACS instrument following camptothecin-induced apoptosis



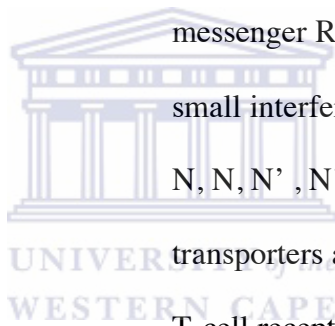
ABBREVIATIONS

AIDS	Acquired immune deficiency syndrome
AMPS	Ammonium persulphate
ATP	Adenosine triphosphate
bp	base pair
BLAST	Basic local alignment search tool
BPB	Bromophenol blue
BSA	Bovine serum albumin
Caspases	Cysteine aspartic acid-specific protease
cDNA	complementary deoxyribonucleic acid
CD	Cluster determinant
CED	Cell death defective
CHO	Chinese hamster ovary
C-terminal	Carboxy terminal
CTL	Cytotoxic T lymphocyte
Da	Dalton
DAPI	4', 6'-Diamidino-2-phenylindole
DMEM	Dulbecco's modified Eagle medium
DMSO	Dimethyl sulphoxide
DNA	Deoxyribonucleic acid
DR	Death receptor
DTT	Dithiothreitol

DWNN	Domain With No name
dNTP	2'-deoxynucleoside 5'-triphosphate
ER	Endoplasmic reticulum
EDTA	Ethylene diamine tetra acetic acid
FACS	Fluorescence activated cell sorter
FCS	Foetal calf serum
FSC	Forward scatter
GFP	Green fluorescent protein
GST	Glutathione-S-transferase
IL-2	Interleukin-2
hrs	Hours
ICE	Interleukin-1 β converting enzyme
IFN- γ	Interferon- γ
kb	Kilo base
kD	Kilo Dalton
LAK cells	Lymphokine activated killer cells
LB	Luria Broth
LFA-1	Lymphocyte function-associated antigen-1
MCS	Multiple cloning site
MHC I	Major histocompatibility complex class I
MHC II	Major histocompatibility complex class II
min	Minutes
MOPS	4-Morpholoine propanesulphonic acid

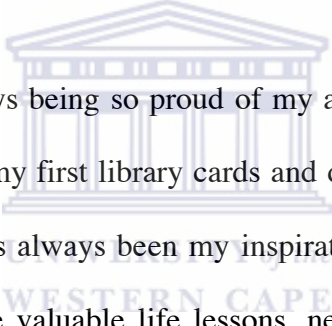


N-terminal	Amino-terminal
PACT	p53-associated cellular protein-testis derived
PAGE	Polyacrylamide gel electrophoresis
PBS	Phosphate buffered saline
PCR	Polymerase chain reaction
RFP	Red fluorescent protein
RIP	Receptor interacting protein
RNA	Ribonucleic acid
RNAi	Interference RNA
mRNA	messenger RNA
siRNA	small interfering RNA
TEMED	N, N, N', N'-tetramethylethylenediamine
TAP	transporters associated with antigen-processing
TCR	T-cell receptor
Th	Pre-T helper
TNF- α	Tumour necrosis factor- α
Tris	2-amino-2-hydroxymethylpropane-1, 3-diol



ACKNOWLEDGEMENTS

I would like to thank the National Research Foundation (NRF) for funding during this project. Prof. D Jasper G Rees for his guidance and intellectual input and also for financial assistance during this project. To Mr MF February for his intellectual input , computational skills and friendship. Dr A Skepu and Miss M Essack for assistance and reagents. Many thanks to my family (cousins, aunts and extended members) for their continual support and encouragement and to my friends for distracting me now and again from the demanding world of research with a good party.



To my brother Shaun for always being so proud of my achievements and just being my brother. Because of you I got my first library cards and discovered my love for reading. To my mother Muriel, who has always been my inspiration to achieve that which I put my mind too. For teaching me valuable life lessons, never to give up and too set my sights always higher. Thank you for your love and support without it this thesis would not have been possible. Thank you that you have taught me by example and just not by word, so that I could see the true meaning of your teaching.

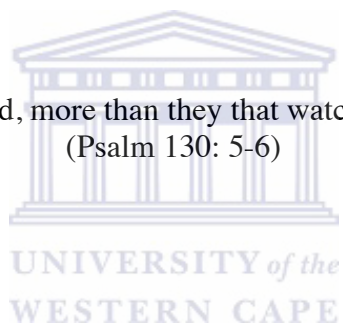
All honour and praise to my heavenly father who has allowed me to walk this path, who blessed me with family and friends that are both caring and supportive, who has allowed various circumstances in my life but have been with me even in my darkest hour.



DEDICATION

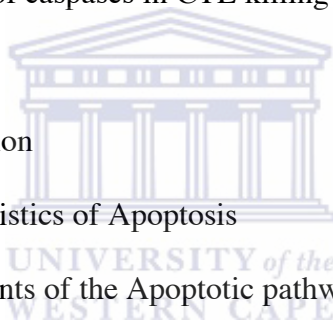
I dedicate this work to mother and brother and to my
Aunt Sissy, who has departed this life but who's memory lives on
in my heart and mind everyday.

I wait for the Lord, more than they that watch for the morning
(Psalm 130: 5-6)



CHAPTER 1: INTRODUCTION

- 1.1 INTRODUCTION
- 1.2 THE IMMUNE SYSTEM
 - 1.2.1 Classes of T lymphocytes
 - 1.2.2 MHC class 1 presentation pathway
- 1.3 CTL KILLING
 - 1.3.1 Granule mediated exocytic killing
 - 1.3.2 Receptor mediated killing
 - 1.3.3 The role of caspases in CTL killing
- 1.4 APOPTOSIS
 - 1.4.1 Introduction
 - 1.4.2 Characteristics of Apoptosis
 - 1.4.3 Components of the Apoptotic pathway
 - 1.4.4 The Apoptotic pathways
 - 1.4.5 Regulation of the Apoptotic Proteins
- 1.5 THE P53 GENE
 - 1.5.1 Functions of the p53 gene
 - 1.5.2 p53 activating pathways
 - 1.5.3 Control of p53
- 1.6 RETINOBLASTOMA (RB) GENE
 - 1.6.1 RB function in the cell cycle
 - 1.6.2 Function of Rb in apoptosis



- 1.7 THE DWNN GENE FAMILY
 - 1.7.1 Identification of DWNN domain
 - 1.7.2 Structure of DWNN
 - 1.7.3 DWNN/RBBP6 homologues
 - 1.7.4 Homo sapiens RBBP6
 - 1.7.5 *Mus musculus* RBBP6
 - 1.7.6 *Saccharomyces cerevisiae* RBBP6
 - 1.7.7 Other RBBP6 homologues
- 1.8 ZINC FINGERS
- 1.9 ROLE OF RING FINGERS IN UBIQUITIN PATHWAY
 - 1.9.1 DWNN ubiquitin homology
 - 1.9.2 Ubiquitin
 - 1.9.3 The ubiquitin pathway
 - 1.9.4 Functional relationship between DWNN and the RING finger
- 1.10 GENE TARGETING
 - 1.10.1 Homologous recombination
 - 1.10.2 Embryonic Stem (ES) cells
 - 1.10.3 Designing of HR vectors
 - 1.10.4 The use of site-specific recombinases
 - 1.10.5 Applications of gene targeting
- 1.11 ANTISENSE RNAs
- 1.12 INTERFERENCE RNA (RNAi)

1.12.1 Mechanism of RNAi

1.12.2 Dicer

1.12.3 Role of RNA pol III

1.12.4 Applications

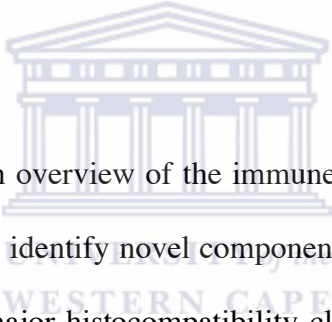
1.13 AIMS



CHAPTER 1: LITERATURE REVIEW

1.1 Introduction

The advent of gene targeting has paved the way for determining the functions of many previously identified genes. With the completion of the human genome project many new genes have been sequenced, but no function(s) could be ascribed to them. To meet this demand, gene target technology has grown rapidly, with new advances and technologies being introduced frequently. This thesis will outline the use of the RNA interference (RNAi) technology to determine the physiological role of the mouse RBBP6 gene.



This chapter will firstly give an overview of the immune system. The DWNN gene was identified in a genetic screen to identify novel components of the antigen processing and presentation pathway via the major histocompatibility class I (MHC class I) molecules. Over 100 cytotoxic T lymphocyte (CTL) resistant cell lines were generated using a promoter trap mutagenesis approach (George, 1995). The system of retrovirus promoter trap mutagenesis involves the insertion of a promoter-less selectable marker gene, hygromycin, into the U3 region of the Long Terminal Repeat (LTR) of the Moloney murine leukaemia virus (MoMLV). Sequences adjacent to the site of integration were identified using a combination of PCR and sequencing. It was expected that identified genes would play a role in the expression, processing or presentation of antigens by MHC class I molecules or in the recognition, adhesion or lytic mechanism of CTLs. Based on

the genes identification from this genetic screen it suggests a potential role for RBBP6 in the immune system.

The mechanisms of apoptosis and CTL are closely linked. Two molecular mechanisms of T-cell mediated cytotoxicity have been demonstrated: (i) killing mediated by the formation of pores in the target cell plasma membrane and (ii) receptor mediated apoptosis (Kupfer *et al.*, 1986). Also, caspases has been shown to be molecular mediators of both CTL killing (Chinnaiyan *et al.*, 1995) and apoptosis (Sarin *et al.*, 1998). Recent studies by several groups had implicated RBBP6 involvement in apoptosis (Gao and Scott, 2003) and the cell cycle (Gao and Scott, 2002). The overview of the immune system will thus be followed on a review of apoptosis, proteins regulating apoptosis and the cell cycle as both systems are closely linked and tightly controlled by the same proteins. Furthermore, RBBP6 is one of the few proteins identified that has been shown to interact with both p53 and Rb (Sakai *et al.*, 1995) with both proteins having demonstrated roles in apoptosis and cell cycle regulation.

This chapter will also review the isolation of the RBBP6 gene, domain organization and interaction with other proteins such as p53 and pRB. Lastly, this chapter will review the different gene targeting strategies with emphasis on the interference RNA (RNAi) technology used in this work to further elucidate the physiological role of the gene.

1.2 The immune system

Different challenges are presented to the immune system by intracellular and extracellular pathogens, both in terms of recognition and the appropriate response. To meet these challenges parallel systems have evolved.

Innate immunity is the first generalised defence against all kinds of pathogens. It provides an immediate, non-specific and rapid protection against the invading pathogen (reviewed by Abbas *et al.*, 1997). The cells of the innate immune system include dendritic cells, macrophages, neutrophils and natural killer cells.

A second response, adaptive immunity, provides a specific defence against pathogens. Adaptive immunity can recognise previously encountered pathogens and reacts faster and more efficiently (reviewed by Abbas *et al.*, 1997). The adaptive immune cells include B and T lymphocytes. There are two types of adaptive immune responses: the humoral and the cell mediated responses.

The humoral response is based on the production of antibodies by the immune system for the recognition and the destruction of the extracellular antigen. This provides protection against bacteria, fungi, parasites and toxins. This type of immune response is mediated by the B lymphocytes.

The cell-mediated response is based on the recognition of an intracellular antigen by T lymphocytes. This immune response destroys cells that are infected with viruses or mutated cells. The next section will focus only on T lymphocytes and their role in cell mediated immune responses.

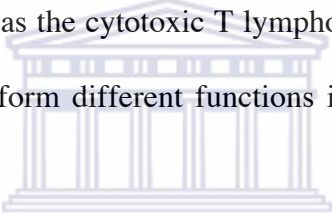
1.2.1 Classes of T lymphocytes

There are two major subpopulations of T cells that develop. Cell surface markers in the thymus can trace the development of both populations. T cells that leave the bone marrow are immature. In the thymus, they mature and are positively or negatively selected depending on the affinity of their T cell receptors (TcRs) for self major histocompatibility (MHC) antigens (Krammer, 2000). MHC antigens are molecules that bind with peptide fragments from foreign and self-protein and present them to the T cells. Every cell produces thousands of MHC molecules. The process of negative or positive selection ensures that T cells with high affinity for self-MHC molecules and peptides are eliminated. The elimination of the self-MHC molecules ensures tolerance to normal tissues and to prevent autoimmunity. T cells develop their specific T cell markers, including TcR, CD3, CD4 or CD8 and CD2, during development and maturation.

There are two types of MHC molecules: the class I and class II molecules. T cells that interact with MHC class II molecules develop into cells expressing CD4⁺ molecules on their surface (Pieters, 1997), and those interacting with MHC class I molecules turn into T lymphocytes that express CD8⁺ antigens (Benoist and Mathis, 1999). Only mature T

cells that produce a functional TcR leave the thymus and enter the secondary lymphoid organs. Mature CD4⁺ T cells function as helper T cells and secrete cytokines that regulate either cellular immune responses or antibody responses. Mature CD8⁺ T cells function as cytotoxic (killer) cells.

The least mature T cells have a T cell receptor (TcR) associated with CD3. In the thymus, the cells express both the CD4 and CD8 markers. These cells are referred to as double positive (CD4⁺CD8⁺). Eventually the cells lose either CD4 or CD8 to become one of the functional subsets. The CD4⁺CD8⁻ cells are called helper T cells (Th cells) whilst the CD4⁻CD8⁺ cells are referred to as the cytotoxic T lymphocytes (CTL). Th cells and CTL both have a TcR, but they perform different functions in the immune system (Clancy, 1998).



1.2.1.1 Helper T cells (Th cells) *TY of the*
WESTERN CAPE

The generation of an immune response, both humoral (by B lymphocytes) and cell-mediated by (CTLs), depends on the activation of Th cells. The importance of Th cells has become apparent because of their involvement in AIDS (Clancy, 1998). There are two subsets of Th cells, Th1 and Th2. Th1 and Th2 are similar and have the same T cell markers and receptors. However, they differ in the cytokines that they secrete upon activation. In addition, the Th1 subset produces the cytokines interleukin-2 (IL-2) and interferon- γ (IFN γ), which are important in cell-mediated immunity. The Th2 subset B cells assist by secreting IL-4, -5 and 6. The cytokines produced by the two subsets are

said to have a cross-regulatory role, meaning that Th1 cytokines down regulate the Th2 responses, and vice versa.

1.2.1.2 Cytotoxic T lymphocytes (CTLs)

CTLs are derived from a lymphocyte stem cell matured in the thymus. These cells are characterised by the presence of a CD8 marker on their surface, and an antigen-specific TcR, which recognises antigens in the context of MHC class I molecules.

The major role of CTL is to kill other cells, especially virus-infected and tumour cells. The cytotoxic T cells must be activated in order to be able to kill. The activation of CTL requires firstly, that the TcR on the CD8⁺ cell interact with an antigen-MHC class I on the surface of a target cell. Secondly, the CD8⁺ T cell must be stimulated by cytokines. Once activated, the CTLs are effective in killing target cells. The killing happens in three steps: (1) conjugate formation between the CTL and the target cell, (2) attack on the membrane of the target cell, and (3) dissociation of the two cells and ultimately death of the target cell.

Major histocompatibility complex (MHC) class I molecules generally present peptides derived from intracellular pathogens to CD8⁺ T cells resulting in a cellular response, whilst those antigens derived from extracellular pathogens are presented to CD4⁺ T cells by MHC class II molecules resulting in a humoral response.

1.2.2 MHC class 1 presentation pathway

MHC class 1 molecules present peptides derived from cytosolic proteins for recognition by CD8⁺ CTL. Evidence for the cytosolic source of class 1 associated peptides initially came from the identification of CTL that recognise fragments of viral nuclear and cytosolic proteins in association with MHC class 1 (Townsend *et al.*, 1985).

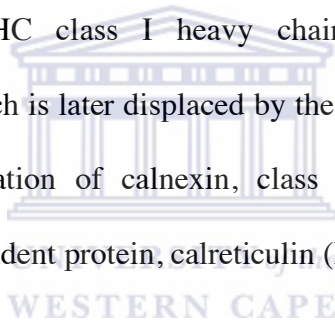
Further studies showed that synthetic peptides will directly prime cells for lysis by CTLs, presumably by binding surface MHC class 1 molecules directly, however priming by native antigens requires their introduction into the cytoplasm before doing so (Morrison *et al.*, 1986). It is well documented that antigens derived from influenza viral nucleoprotein that are apparently excluded from the secretory pathway are efficiently presented to CTLs, suggesting that processing of the antigen occurs in the cytoplasm, rather than in the exocytic pathway (Whitton and Oldstone, 1989, Braciale *et al.* 1987).

Yewdell *et al.*, (1988) showed that mini-genes encoding peptides containing specific CTL epitopes, upon transfection could sensitise cells for lysis by the appropriate CTLs. As these peptides are produced on free ribosomes in the cytoplasm, the intact native antigen is not required for transport of the CTL epitope into the exocytic pathway.

Similarly, transfection of a truncated influenza haemagglutinin gene lacking an amino terminal signal sequence can sensitise cells to lysis by haemagglutinin specific CTL (Yewdell and Bennick, 1989). An important observation noted from this study was that

no core glycosylation of haemagglutinin was detected, showing that the complete molecule does not gain entry into the endoplasmic reticulum (ER).

The basic mechanism of MHC class I presentation is firmly established (see figure 1.1). CTLs recognize small peptides (of between 8 and 11 amino acids in length) from foreign proteins that have been broken down in the cytoplasm of infected or tumour cells. The degradation is mediated in the cytoplasm by the proteases of the proteasome complex. Peptide fragments are transported across the membrane of the endoplasmic reticulum (ER) by the transporters associated with antigen-processing (TAP) proteins. In human cells, newly synthesised MHC class I heavy chains interact with calnexin, a Ca^{2+} dependant chaperone, which is later displaced by the association of β_2 -microglobulin ($\beta_2\text{m}$). Following the dissociation of calnexin, class I- $\beta_2\text{m}$ heterodimers are stably associated with another ER resident protein, calreticulin (Lehner *et al.*, 2000).



Another protein, tapasin, a member of the immunoglobulin (Ig) super family, which is associated with TAP and with MHC class I-calreticulin complexes, acts as a bridge facilitating peptide binding to class I molecules. The class I molecule complexes are released and exported to the cell surface upon stable loading of peptide. Peptides are loaded onto the newly synthesized class I molecules in a groove formed by the alpha helices of the $\alpha 1$ and $\alpha 2$ domains (Elliott *et al.*, 1991). Human HLA molecules are highly polymorphic and most of the polymorphism occurs in the peptide-binding groove.

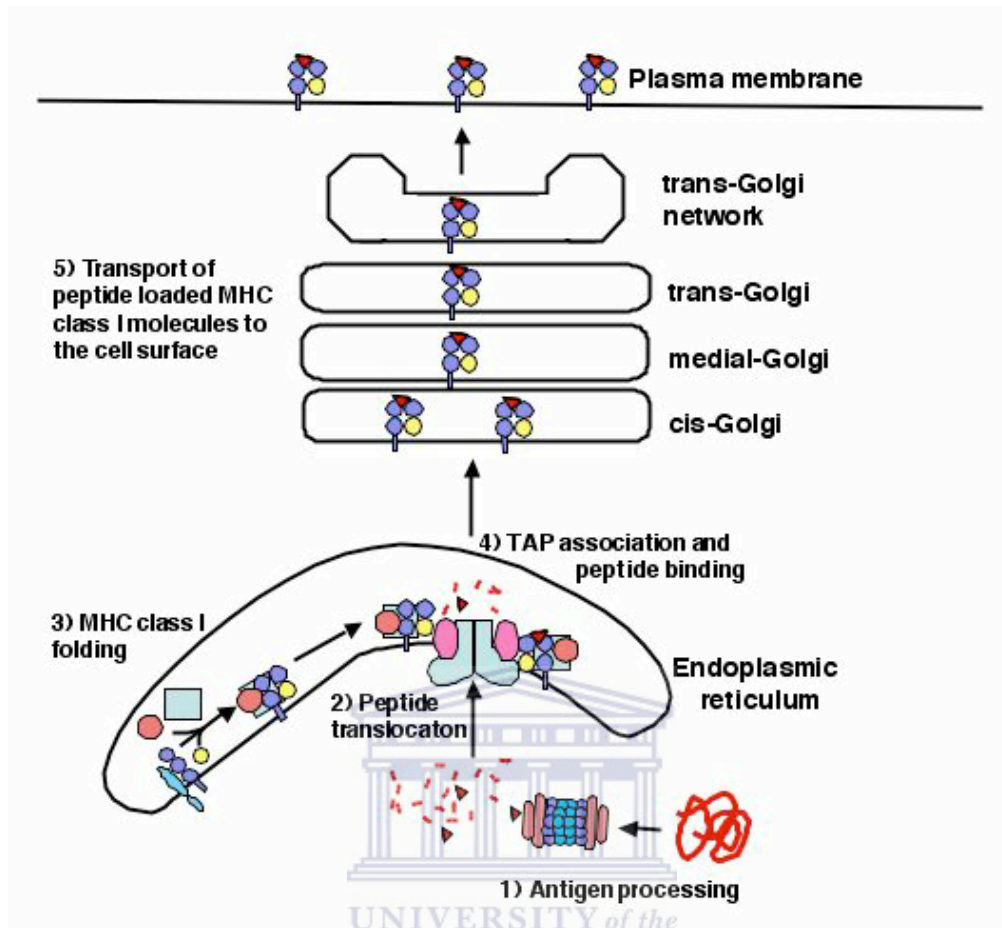


Figure 1.1 Representation of the MHC class I antigen processing and presentation pathway (taken from Lehner *et al.*, 2000).

Consequently, different HLA molecules bind different kinds of peptides (Rotzschke and Falk, 1991). Peptides associated with MHC class I molecules are transported to the cell surface and recognized by CTL, leading to the destruction of the infected cell (Monaco, 1992).

1.3 CTL killing

Two molecular mechanisms of T-cell mediated cytotoxicity have been demonstrated: (i) a membranolytic mechanism initiated by the formation of pores in the target cell plasma membrane by the secretion of molecules of lymphocytic origin such as perforin and granzymes and (ii) receptor mediated apoptosis through the engagement of the target cell surface molecules (Kupfer *et al.*, 1986).

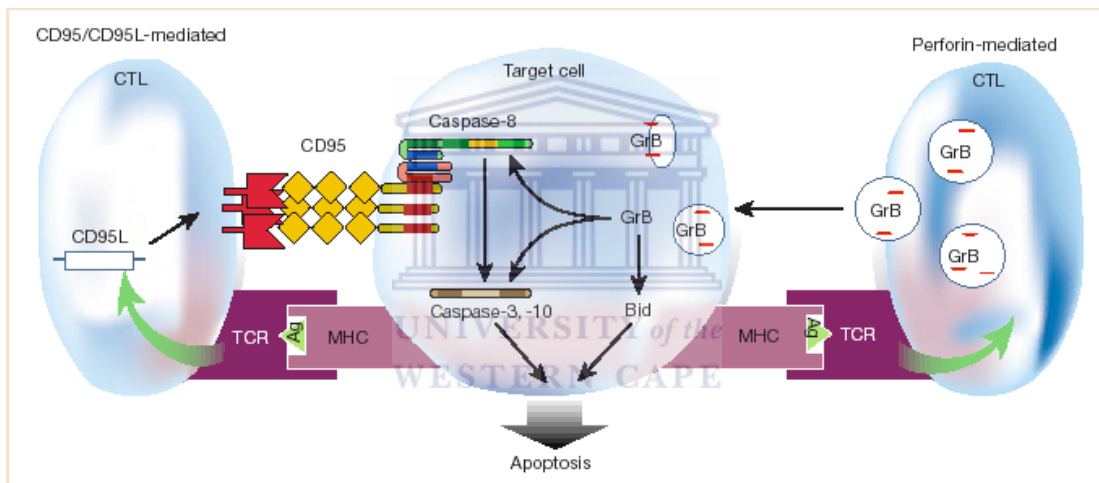


Figure 1.2 Diagrammatic representation of the two pathways by which CTLs kill their target cells: the CD95 (yellow)/CD95L (red) mediated killing and perforin/Granzymes B (GRb) mediated killing (taken from Krammer, 2000).

Binding of the CTL to target cells that results in conjugate formation is one of the first events in lymphocytotoxicity. This binding involves the interaction between the TCR and

MHC class 1 molecules bound to peptide as well as auxiliary cell adhesion molecules (e.g. LFA-1), which increase the avidity of the interaction (see figure 1.2).

1.3.1 Granule mediated exocytic killing

Granule mediated target cell lysis is triggered by compromising the integrity of the plasma membrane due to pore formation from the release of perforin. Extracellular calcium has been found to be necessary for the secretion, binding and polymerisation of perforin (Ishiura *et al.*, 1990). Perforin, which shows homology to complement component C9, is contained in cytoplasmic organelles, which have properties of both secretory granules and lysosomes. The content of the granules is secreted into the contact zone formed by the engagement of the CTL and target cell (see figure 1.2). When cytolytic cells engage their targets there is a change in their shape. This is brought about by the translocation of the Golgi apparatus and the microtubules towards the killer/target interface and is followed by granule content exocytosis (Kupfer *et al.*, 1986).

The perforin-based mechanism was confirmed by the low cytotoxic activity of an activated lymphoid cell population from perforin homozygous *-/-* mice. These mice did not generate a virus specific CTL response to an *in vivo* challenge with lymphocytic choriomeningitis virus, and failed to clear the virus normally, although significant killing activity was demonstrated using perforin-free CTLs, utilizing *in vitro* assays (Walsh *et al.*, 1994).

Dupuis *et al.* (1993) proposed that an additional granule protein called calreticulin regulates the process of cell lysis. Using lysosomal secretory granules, isolated from human Lymphokine Activated Killer (LAK) cells and mouse CTL, the co-localization of perforin and calreticulin was demonstrated. Also, when the release of granule-associated proteins was triggered by TcR complex stimulation, calreticulin was released along with granzymes A and D. Since perforin is activated and becomes lytic in the presence of calcium, a proposed role of calreticulin is to prevent organelle autolysis due to its calcium chelator capacity.

The role of other granule harboured molecules in the process of cytolysis is not clear, as purified granzymes, a group of serine proteases, are not lytic, despite the fact that various protease inhibitors suppress CTL-mediated cytolysis. However, granzymes A and B appears to be involved in the induction of degradation of the nuclear DNA of the target cell, which is observed during CTL attack parallel to the damage of the cytoplasmic membrane (Hayes *et al.*, 1989, Shi *et al.*, 1992).

The first substrate to be identified for granzyme B was caspase 3, which is a member of a family of cysteine proteases involved in inducing apoptosis (Darmon *et al.*, 1995). Multiple caspases have been identified as substrates for granzyme B *in vitro* (Darmon *et al.*, 1995) and this suggests that granzyme B induces apoptosis by triggering the activation of multiple caspases within intact cells.

1.3.2 Receptor mediated CTL killing (see figure 1.2)

Several observations implicated the Fas protein in Ca^{2+} independent target cell lysis, through receptor mediated activation. Firstly, Fas was shown to be a member of a family of membrane proteins that determine the choice of many cell types to grow or die (Itoh, 1991). Other members of this family include the tumour necrosis factor (TNF) receptors.

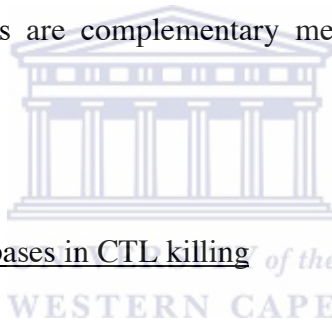
Secondly, a lupus-like systemic autoimmune disease in mice called lymphoproliferative disorder (*lpr*) was shown to result from a retrotransposon insertion into the *fas* locus leading to abnormal transcription and a greatly reduced expression of Fas (Watanabe-Fukunaga *et al.* 1992). This discovery led to the identification of the Fas ligand (FasL), which showed great homology to $\text{TNF}\alpha$, a member of the TNF family of membrane and secreted proteins. Like other TNF family members, FasL is a homodimeric molecule found in a trimeric complex. The crystal structure of lymphotoxin in complex with TNFR1 suggests that each FasL trimer binds three Fas molecules (Crowe *et al.*, 1994). A second autoimmune disease of mice called general lymphoproliferative disorder (*gld*) were shown to be caused by a point mutation in the FasL gene, rendering the protein non-functional (Takahashi *et al.*, 1994, Ramsdell *et al.*, 1994)).

Direct evidence for Fas in receptor mediated CTL lysis was shown using the rat-mouse T cell hybridoma, d10S (Rouvier *et al.*, 1993). This study showed thymocytes from normal MRL-mice were sensitive to killing by d10S T cells but thymocytes derived from MRL-*lpr* donors were resistant to lysis with d10S T cells as there was no expression of Fas on

these cells. Similar results were shown for *gld* mouse mutants using thymocytes (Rouvier *et al.*, 1993).

In contrast to the widespread distribution of Fas, its ligand has a more restricted pattern of expression. The expression of FasL is induced on mature CD4⁺ and CD8⁺ T lymphocytes after their activation (Van Parijs and Abbas, 1996).

When target cells from Fas deficient *lpr* mice and perforin-free CTL were used results showed that killing is completely abolished when both pathways are inhibited. This showed that the two pathways are complementary mechanisms of killing utilised by CTLs (Lowin *et al.*, 1994).

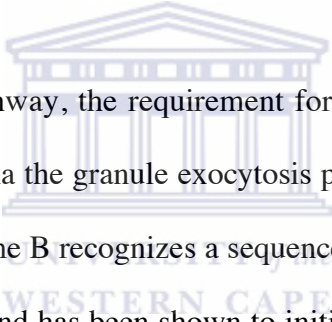


1.3.3 The role of Caspases in CTL killing of the

Various studies have shown that both effector pathways utilised by cytotoxic lymphocytes activates caspases. Chinnaiyan *et al.*, (1995) showed that cross-linking of target cell Fas by FasL on CTL membranes leads to the activation of caspase 8, which transactivates caspase 3 and possibly caspase 10 via the Fas associated death domain (FADD). These caspases will process and activate downstream caspases that, in turn, trigger cell destruction (see figure 1.2).

Furthermore, rapid target cell lysis and apoptotic nuclear damage by this CTL effector pathway have been shown to be blocked by two classes of caspase inhibitors, confirming

the predicted functional importance of caspases in this effector pathways. In a study by Sarin *et al.*, (1997), fluoromethyl ketone caspase inhibitors and baculovirus p35 blocked apoptotic nuclear damage and target cell lysis by the CTL-mediated Fas-Fas ligand pathway. The peptide caspase inhibitors also blocked drug-induced apoptotic cell death in tumour cells. In contrast, the caspase inhibitors blocked CTL granule exocytosis-induced target apoptotic nuclear damage, but did not inhibit target lysis. These results are consistent with those observed by Regner and Mullbacher, (2004) that granzyme B can activate caspases leading to apoptotic nuclear damage, which in turn confirms that target cell lysis by CTL granule exocytosis occurs by a caspase-independent pathway.



For the granule exocytosis pathway, the requirement for caspases in target cell death is less clear. Caspase activation via the granule exocytosis pathway is predicted because the granule serine protease granzyme B recognizes a sequence motif compatible with caspase activation (Thornberry, 1997) and has been shown to initiate processing and activation of several caspases (Talanian *et al.*, 1997). CTL targets undergo rapid caspase-3 processing as shown by *in vitro* experiments (Darmon *et al.*, 1995), thus providing an explanation for apoptotic nuclear damage induced by granzyme B in the presence of sublytic doses of perforin (Shi *et al.*, 1992). However, while CTL from mice lacking granzyme B induce target nuclear damage somewhat more slowly, their potency and rate of target lysis via the granule exocytosis pathway are unaffected by the loss of granzyme B (Shresta *et al.*, 1995). Since no other granule proteases are known to activate caspases directly, these data suggest that target lysis via CTL granule exocytosis might be independent of caspases.

One model to explain these results proposes that granzyme B mediates nuclear damage via caspase activation, but that target lysis occurs as a result of granzyme-induced cleavage of downstream cytoplasmic protein substrates, which are also cleaved by caspases and lead to apoptotic cell destruction. This model predicts that other CTL granule exocytosis-induced cytoplasmic apoptotic damage might be caspase independent if it is part of the postcaspase death pathway. This proposed model was confirmed by Sarin *et al*, (1998) who showed that granzymes activates a postcaspase apoptotic damage pathway that results in mitochondrial potential loss, phosphatidylserine (PS) surface exposure, membrane blebbing, and lysis.

1.4 Apoptosis

1.4.1 Introduction



Apoptosis is a mode of cell death believed to account for most or all of the programmed cell death responsible for tissue modelling in vertebrate development (Ormerod *et al*. 1994). Equally as important as cell division and cell migration, apoptosis allows an organism to tightly control cell numbers and tissue size, and to protect itself from cells that threaten homeostasis. The morphologically observable changes of apoptosis are distinct from the features observed in cells undergoing pathological necrotic cell death. Necrosis refers to the morphology most often seen when cells die from severe and sudden injury, such as ischemia, sustained hyperthermia and physical or chemical trauma. In necrosis there are early changes in mitochondrial shape and function. The cell also rapidly becomes unable to maintain homeostasis, leading to an influx of water and

extracellular ions. Intracellular organelles, including the mitochondria, and the entire cell swell and rupture (Kroemer *et al.*, 1995). Ultimately, the plasma membrane breaks down and the cytoplasmic contents are released into the extracellular fluid. *In vivo*, necrosis is associated with tissue damage resulting in an inflammatory response.

1.4.2 Characteristics of Apoptosis

In contrast to necrosis, there is no marked inflammatory reaction and organelle swelling in apoptotic cells. Several morphological changes are characteristic of this process, like the aggregation of chromatin, nuclear and cytoplasmic condensation and the inclusion of the cytoplasm and nucleus in membrane bound vesicles known as apoptotic bodies (Wyllie, 1997) (see figure 1.3). The engulfment of apoptotic bodies is triggered by changes in the membrane of the apoptotic cells. These changes involve the externalisation of a phospholipid, phosphatidylserine, through the activation of an enzyme called flippase (Williamson *et al.*, 2002). The biochemical markers of apoptosis include DNA fragmentation into nucleosomal fragments (Wyllie, 1997), activation of caspases, a group of aspartate specific cysteine proteases, (Schlegel *et al.*, 1996) and cleavage of various caspase substrates e.g. pre-interleukin-1b, PARP and lamins.

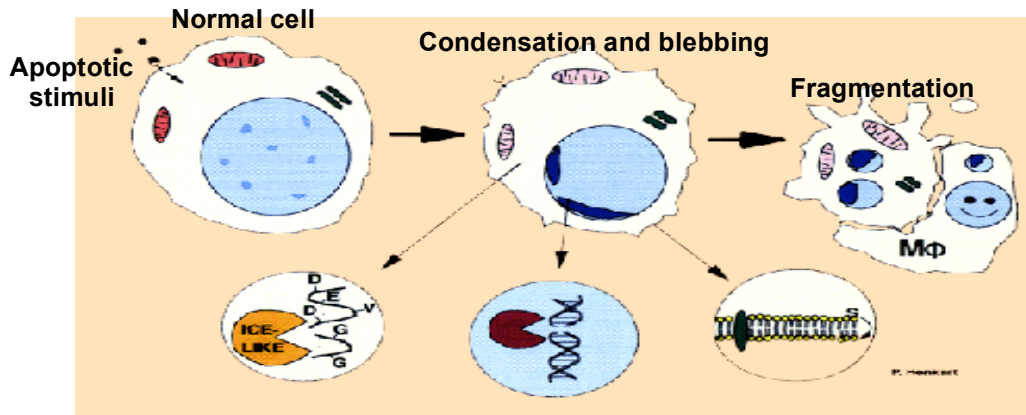


Figure 1.3. Diagrammatically represents the morphological changes associated with apoptosis (modified from www.nih.gov/sigs/aboutapo.html, 3 April 2008).

Apoptosis and necrosis have been regarded as separate modes of cell death, however increasing evidence is now emerging that both represents only the extreme ends of a wide range of possible morphological and biochemical deaths. Kanduc *et al.*, (2002) have shown that the two types of death can occur simultaneously in tissues or cell cultures exposed to the same stimuli and that often the intensity of the initial insult determines if death is apoptotic or necrotic.

Apoptosis has been shown to be an important component of some developmental abnormalities and human diseases. Disorders associated with insufficient apoptosis or failure of apoptosis usually leads to the development of autoimmune diseases and cancer. Excessive apoptosis on the other hand might play a crucial role in the development of many other diseases such as stroke and neuro-degenerative disorders like Parkinson's (Ashkenazi and Dixit, 1998). Suppression of apoptosis may therefore help restore the functionality of the affected tissue. Tomei and Umansky (2001) showed that AIDS is

another example of a disease that has been linked to increased apoptosis in cardiomyocytes.

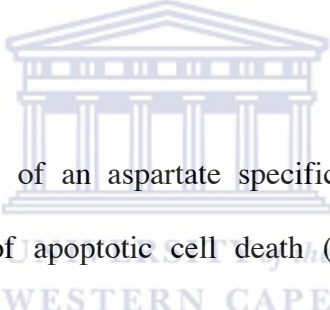
1.4.3 Components of the Apoptotic pathway

Studies in the nematode worm *Caenorhabditis elegans* first shed light on the involvement of three crucial components of the cell death pathway namely the cell death defective (CED) genes. CED-3, CED-4 and CED-9 were implicated as having important roles in the regulation of cell death in *C. elegans* (Hengartner and Horvitz, 1994). The interaction of these gene products is believed to control apoptosis in *C. elegans*. CED-3 and CED-9 are both able to form complexes with CED-4, whilst the association of CED-3 and CED-4 leads to induction of apoptosis. Xue and Horvitz (1997) showed that in unstressed cells CED-4 is unable to form a complex with CED-3, as it is already associated with CED-9 at the mitochondrial membrane. This inhibitory effect of CED-9 is neutralized by another protein, EGL-1 (external germinal layer-1) during apoptosis by promoting the dissociation of CED-4/CED-3 complexes from CED-9 (del Peso *et al.*, 1998).

Homologues of the *C. elegans* death genes have also been identified in vertebrates. The mammalian homologue of CED-9 and EGL-1 is the Bcl-2 protein family (Adams and Cory, 1998) while CED-4 is homologous to Apaf-1 (Zou *et al.*, 1997) and CED-3 is homologous to caspases (Peter *et al.*, 1997).

CED-3 was found to be very similar to a protease involved in the processing of pro-IL-1 β converting enzyme (ICE). Upon its discovery, ICE defined a new class of cysteinyl proteases because it was distinguishable from other cysteinyl proteases. This distinction was made on structural organisation as compared to other families and the absolute requirement for an aspartic residue at the P1 position in the active site (Thornberry *et al.*, 1992) hence the name caspase-1 or cysteine aspartic acid-specific protease-1 (Alnemri *et al.*, 1996). Caspases play a central role in the mechanisms of apoptosis and are also responsible for the many morphological changes observed in apoptotic cells.

1.4.3.1 Caspases



Caspases, which are members of an aspartate specific cysteine protease family, are central molecular mediators of apoptotic cell death (Sarin *et al.* 1998). There are currently 15 identified human caspases which are expressed in an inactive precursor form in many cells and have the hallmark specificity of cleaving protein substrates with aspartic residues at the P1 position (Siegel, 2006).

Caspases share a number of common structural motifs (Wolf and Green, 1999). They consist of a N-terminal pro-domain, a large subunit and a small subunit (Nicholson, 1999) An Aspartate residue between the pro-domain and the large subunit and an interdomain containing 1 or 2 aspartate residues between the large and small subunit (see figure 1.4).

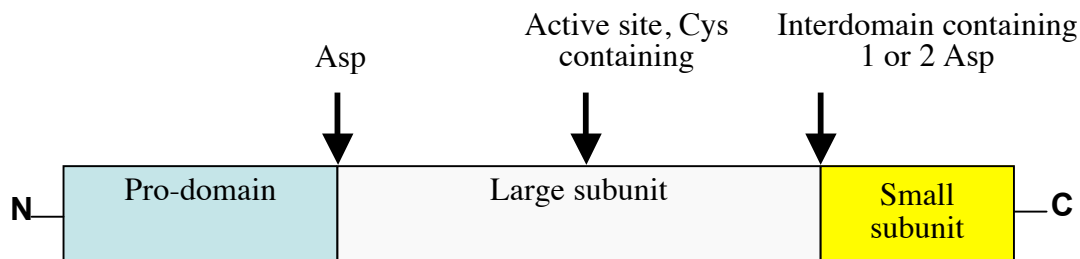
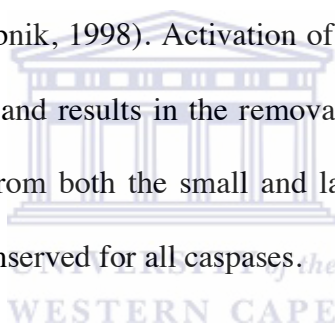


Figure 1.4 A diagrammatical representation of the general structure of procaspase

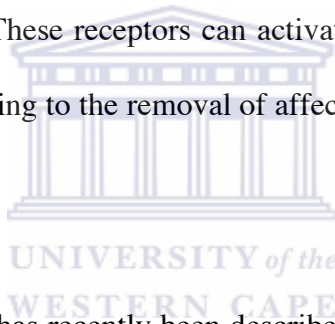
Activation of caspases is a result of proteolytic processing of procaspases at aspartic residues, so that caspases can auto activate and process each other in an activation cascade (Thornberry and Lazebnik, 1998). Activation of pro-caspase is accompanied by proteolysis of the interdomain and results in the removal of the pro-domain. The active site is composed of residues from both the small and large subunits. The residues that constitute the active site are conserved for all caspases.



Caspases were first implicated in apoptosis with the discovery of the *C. elegans* pro-apoptotic gene, CED-3. The connection between caspases and apoptosis was further strengthened with the discovery that there is an extensive similarity between CED-3 and ICE (Miura *et al.*, 1993). Caspases can be categorised into three subfamilies (a) the ICE subfamily of cytokine processors; these include caspases -1, -5, -11, -12, -13, -14 and -15, (b) the CED-3/ CPP32 subfamily of apoptosis executioners, including caspases -3, -6 and -7, and (c) the ICH-1/Nedd-2 subfamily of apoptosis initiators, including caspases -2, -8, -9 and -10 (Nicholson, 1999). The active site for all caspases resides in a pentapeptide with the general structure: QACXG, where X is R, Q or G.

1.4.4 The Apoptotic pathways

Apoptosis is signalled via three major biochemical routes in mammalian cells. Firstly, there is the intrinsic route that responds to most pro-apoptotic signals, which emanates largely from the mitochondrion. This involves the release of caspase activators like cytochrome c, changes in electron transport and loss of mitochondrial transmembrane potential (Green and Reed, 1998 and Green and Kroemer, 1998). Secondly, there is the extrinsic route that enables mammals to direct individual cells to self-destruct. This form of instructive apoptosis is triggered by the ligation of so called “death” receptors (Ashkenazi and Dixit, 1998). These receptors can activate the apoptosis program within seconds of ligand binding, leading to the removal of affected cells from the system within hours.



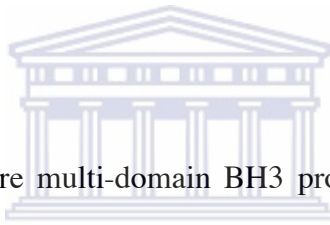
Thirdly, an ER stress pathway has recently been described. Two mechanisms for the ER pathway had been proposed: firstly, a mechanism involving p73 via its two protein isoforms (Dobbelstein *et al.*, 2005) and secondly, a mechanism via homocysteine (Sharma, *et al.*, 2006).

1.4.4.1 The intrinsic pathway

One of the most important regulators of this pathway is the Bcl-2 family of proteins. The Bcl-2 family are key regulators of apoptosis and are over-expressed in many malignancies even without the presence of tumour formation (Reed, 1997). The Bcl-2

family includes pro-apoptotic members such as Bax, Bak, Bad, Bcl-Xs, Bid, Bik, Bim, and Hrk, and anti-apoptotic members such Bcl-2, Bcl-XL, Bcl-W, Bfl-1, and Mcl-1.18.

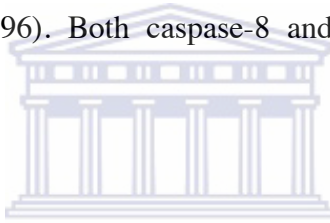
Anti-apoptotic Bcl-2 members act as repressors of apoptosis by blocking the release of cytochrome-c, whereas pro-apoptotic members act as promoters of apoptosis. These effects are more dependent on the balance between Bcl-2 and Bax than on Bcl-2 quantity alone (Zha and Reed, 1997). Following a death signal, pro-apoptotic proteins undergo post-translational modifications that include dephosphorylation and cleavage resulting in their activation and translocation to the mitochondria leading to apoptosis (Scorrano and Korsmeyer, 2003).



All BH3-only molecules require multi-domain BH3 proteins (Bax, Bak) to exert their intrinsic pro-apoptotic activity (Korsmeyer, 1995). In response to apoptotic stimuli, the outer mitochondrial membrane becomes permeable, leading to the release of cytochrome-c and a second mitochondrial-derived activator of caspases called direct IAP-binding protein with low pI. Cytochrome c, once released in the cytosol, interacts with Apaf-1, leading to the activation of caspase-9 pro-enzymes. Active caspase-9 then activates caspase-3, which subsequently activates the rest of the caspase cascade and leads to apoptosis. Activated caspases lead to the cleavage of nuclear lamin and breakdown of the nucleus through caspase-3 (Thornberry and Lazebnik, 1998) (see figure 1.5).

1.4.4.2 The extrinsic pathway

The second apoptotic pathway is through the Fas molecule (see figure 1.5). Fas contain a death domain (DD), which is essential for transmitting apoptotic signals (Nagata, 1997) since there is a tendency for DDs to associate with each other. The assembly of the Fas receptor death-inducing signalling complex (DISC) occurs in a hierarchical manner: the death domain of CD95 binds to the corresponding domain in the adapter molecule Fas-associated death domain (FADD) (Chinnaiyan *et al.*, 1995). The adapter protein FADD also contains a death effector domain (DED), which binds to caspase-8 and caspase 10 (Fernandes-Alnemri *et al.*, 1996). Both caspase-8 and 10 contain two DEDs and a caspase activation domain.



When incorporated into the death inducing signalling complex, caspase-8 is proteolytically activated, possibly in the form of a dimeric complex as observed in caspase-1. Caspase-8 oligomerization drives its activation through self-cleavage (Ashkenazi and Dixit, 1998) and subsequent cleavage of downstream caspases and target proteins such as caspase-9, 3, 6 and 7 and initiates mitochondrial damage.

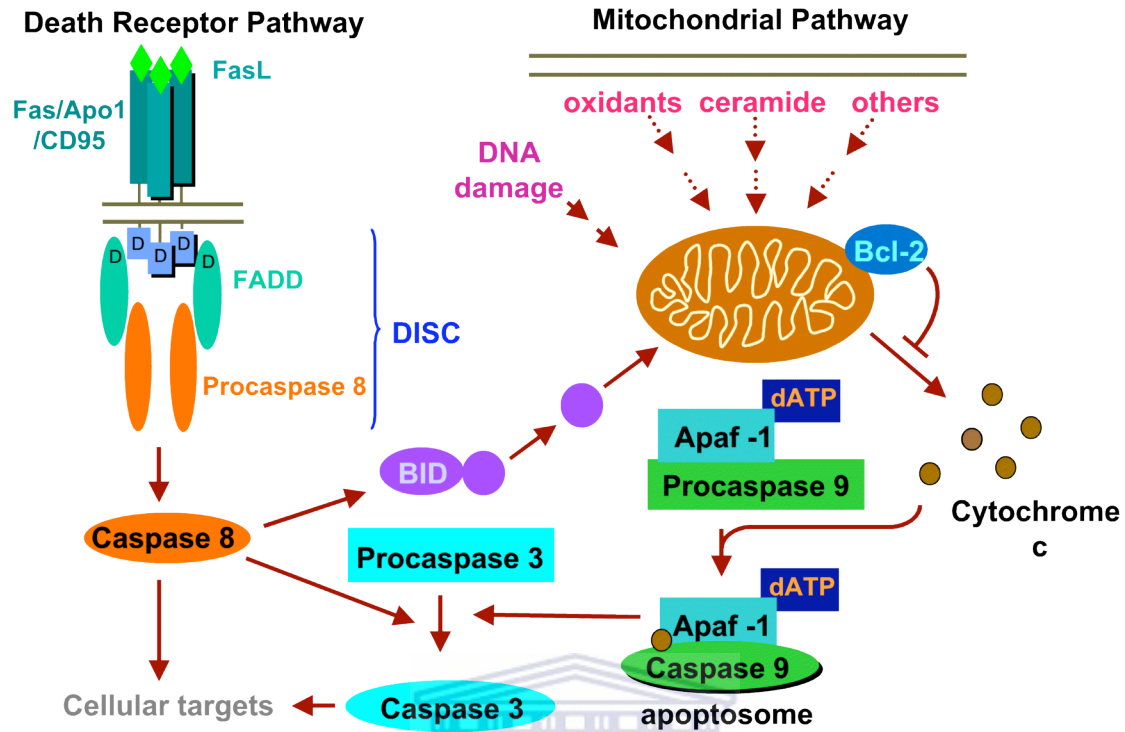
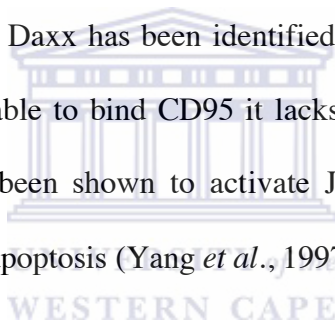


Figure 1.5 Diagrammatically represents two mechanisms by which apoptosis occur (www.nih.gov/sigs/aboutapo.html, 3 April 2008).

It has also been demonstrated that BID, a death agonist member of the Bcl-2 family, is a specific proximal substrate of caspase-8 in the Fas signalling pathway (Li *et al.*, 1998). Cleavage of BID by caspase-8 leads to the release of cytochrome c from the mitochondria. The release of cytochrome c results in the inactivation of the electron transfer chain and triggers caspase-3 activation through Apaf 1 (Krippner *et al.*, 1996), which will induce mitochondrial damage (see figure 1.5). Expression of Bcl inhibits all the apoptotic phenotypes induced by truncated BID, whereas caspase inhibitors inhibit the loss of mitochondrial membrane potential, cell shrinkage, and nuclear condensation, but not cytochrome c release.

The death domain of CD95 and TNFR1 can interact with a second protein called the receptor interacting protein (RIP) (Stanger *et al.*, 1995). This protein is required for the CD95/TNF-induced activation of the transcription factor NF- κ B and hence promotes anti-apoptotic signals (Martinon *et al.*, 2000). As a result, activation of NF- κ B is prevented by cleavage of RIP by activated caspase-8 during the process of apoptosis. Following the recruitment of RIP by either CD95 or TNFR1, RIP interacts with a death adaptor protein called RAIDD (RIP associated ICH/CED-3 homologous protein with a death domain).

A third CD95 binding protein, Daxx has been identified to bind to Fas DD (Kataoka *et al.*, 1998). Although Daxx is able to bind CD95 it lacks a death domain. However, the over-expression of Daxx has been shown to activate JNK (c Jun-N-terminal kinase), which initiates CD95 induced apoptosis (Yang *et al.*, 1997 and Wajant, 2002).



1.4.4.3 The ER stress pathway

1.4.4.3.1 p73

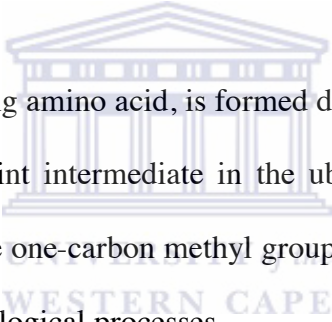
Recently a third apoptotic pathway had been proposed via an ER stress mechanism involving p73. P73, one of two homologues of the tumour suppressor p53, is expressed in different isoforms, as a result of differential promoter usage and alternative splicing (Lee and La Thanque, 1999). Like p53, p73 has long been known to induce programmed cell death (Jost *et al.*, 1997). However, in contrast with p53, the p73 gene has two distinct promoters coding for two protein isoforms with opposite effects. These isoforms contain

a transactivation domain at their amino terminal ends and they are collectively termed TAp73, while the transactivation proficient TAp73 shows pro-apoptotic effects, the amino-terminal-deleted DeltaNp73 has an anti-apoptotic function. Indeed, the relative expression of these two proteins is related to the prognosis of several cancers (Dobbelstein *et al.*, 2005).

The expression of TAp73 is activated by E2F-1 (or the E2F-1 activators adenovirus-E1A and c-MYC), and this appears to be required for E2F-1-induced apoptosis at least in some assay systems (Lissy *et al.*, 2000, Irwin *et al.*, 2000). First, TAp73 induces ER stress via the direct transactivation of Scotin. Second, TAp73 induces the mitochondrial pathway by directly transactivating both Bax and the BH3 only protein PUMA promoters. While the first transactivation is weak, and not sufficient to trigger apoptosis, the induction of PUMA is strong and lethal. Secondly, the promoter of the death receptor CD95 contains a p53 responsive element and preliminary experiments suggest that TAp73 also activates the death receptor pathway through this response element (Dobbelstein *et al.*, 2005). Furthermore, TAp73 is able to transactivate its own second promoter, thus inducing the expression of the anti-apoptotic DeltaNp73 isoform. Therefore, the balance between TAp73 and DeltaNp73 finely regulates cellular sensitivity to death (Dobbelstein *et al.*, 2005).

1.4.4.3.2 Homocysteine

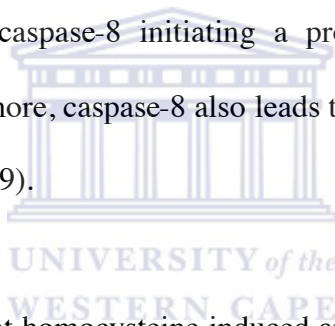
Homocysteine is an independent risk factor for cardiovascular diseases and is also associated with a variety of complex disorders (Eikelboom *et al.*, 1999). Homocysteine-induced modulation of gene expression, through alteration of methylation status or by hitherto unknown mechanisms, is predicted to lead to several pathological conditions either directly or indirectly, including Alzheimer's disease (Clarke *et al.*, 1998), schizophrenia (Applebaum *et al.*, 2004), and non insulin-dependent diabetes (Rudy *et al.*, 2005).



Homocysteine, a thiol containing amino acid, is formed during methionine metabolism in the cell. It is a key branch-point intermediate in the ubiquitous methionine cycle, the function of which is to generate one-carbon methyl groups for transmethylation reactions that are essential for several biological processes.

The major process linking levels of homocysteine with apoptosis and the inflammatory pathway is the ER stress and c-myc mediated signalling. The ER is the destination for secretory and extracellular proteins. It also serves as a site of calcium storage, calcium signalling, and biosynthesis of steroids, cholesterol and other lipids. Increased levels of homocysteine have been shown to alter the cellular redox state resulting in ER stress (Outinen *et al.*, 1998).

Exposure to excess ER stress results in apoptotic cell death. ER stress activates JNKs (c-Jun N-terminal Kinases) that regulate gene expression via phosphorylation and activation of transcription factors such as c-Jun. The activation of JNK is mediated by TNF receptor-associated factor-2 (TRAF2), which transduce signals from ER-resident transmembrane protein kinases (IREs) that act as stress sensors and initiates the unfolded protein response (UPR) (Yoneda *et al.*, 2001). TRAF2 activates the apoptosis-signalling kinase (ASK1) or MAPKKK (mitogen activated protein kinase kinase kinase). Activation of MAPKKK leads to activation of JNK protein kinase that in turn causes apoptosis (Zhang *et al.*, 2001). TRAF1 binds to the TRADD (TNFR-Associated Death Domain), which recruits the activated caspase-8 initiating a proteolytic cascade subsequently resulting in apoptosis. Furthermore, caspase-8 also leads to release of pro-apoptotic factor cytochrome c (Gross *et al.*, 1999).



Mercie *et al.*, 2000, showed that homocysteine induced apoptosis in endothelial cells in a dose dependant manner. Three parameters were used to measure apoptosis, mitochondrial membrane potential, PS exposure and DEVDase activation. They concluded that homocysteine induced apoptosis was independent of caspase-3.

1.4.5 Regulation of the Apoptotic Proteins

Regulators of the apoptotic pathways include transcription factors such as NFκB and activating protein 1 that regulate the FasL gene, because it is a transcriptionally inactive gene (Wajant, 2002). Other inhibitors of the pathway include FAP-1, Fas-associated-

death-domain-protein like interleukin-1-converting enzyme-like inhibitory protein, and the soluble decoy receptors such as DcR3, TRAIL R-3/DcR1, and TRAIL R-4/ DcR2. These decoy receptors antagonize the stimulation of Fas by FasL through competition with the ligand (Pan *et al.*, 1997, Krueger *et al.*, 2001). Other regulators include the ubiquitin proteasome pathway and the tumour suppressor genes p53 and retinoblastoma (Rb).

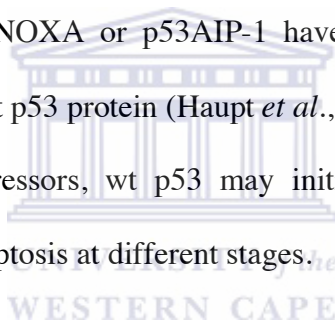
1.5 The p53 gene

The p53 protein was originally identified by the observation that antibodies against the large T antigen from animals bearing tumours produced by SV40 transformed cells co-immunoprecipitates a protein of apparent molecular mass 53 kD, called p53. From these observations it was concluded that p53 interacts with SV40 large T antigen (Chang *et al.*, 1979). Independently, p53 was also identified by its high expression in chemically induced tumours (DeLeo *et al.*, 1979).

Initially classified as an oncogene, p53 is regarded as a “master tumour suppressor” which ensures the integrity of the cell genome by protecting it from the adverse effects of DNA damage. One way in which p53 is thought to potentiate genomic stability, and consequently inhibit tumorigenesis, is by initiating cell cycle arrest, thus allowing repair of damaged DNA prior to DNA synthesis or segregation of the genome (see figure 1.6).

1.5.1 Functions of the p53 gene

Up-regulation and transcriptional activation of p53 leads to an elevation of cell cycle inhibitors, such as p21^{WAF1}, blocking the progression of the cell cycle (el-Deiry *et al.*, 1993, el-Deiry *et al.*, 1994). The induction of a cell cycle block at G1 and G2 by p53 provides the necessary time for the cell to repair genomic damage before entering the critical stages of DNA synthesis and mitosis. However, in tissues where the stressors generate severe and irreparable damage, p53 can initiate apoptosis, thereby, eliminating damaged cells (Haupt *et al.*, 2003). A number of pro-apoptotic factors such as bax, caspase-9, APAF-1, PUMA, NOXA or p53AIP-1 have been shown to be under the transcriptional control of the wt p53 protein (Haupt *et al.*, 2003). Therefore, depending on the cell type and kind of stressors, wt p53 may initiate apoptosis or promote and accelerate the execution of apoptosis at different stages.



In addition, the fact that p53 induction can initiate prolonged cell-cycle arrest suggests that it also provides a prolonged mechanism for permanently removing damaged, and potentially mutated cells from the dividing cell population (Lakin and Jackson, 1999). The ability of p53 to induce arrest within the G1 phase of the cell cycle in response to DNA damage is understood in most detail (Levine, 1997). This arrest is brought about by p53 stimulating transcription of the gene for the cyclin dependant kinase (CdK) inhibitory protein p21^{WAF}. p21^{WAF} is a cyclin-dependant kinase inhibitor that associates with a class of CDKs and inhibits their kinase activities, leading to cell cycle arrest and the

dephosphorylation of pRb. The p21 protein is a p53 inducible protein that inactivates the cyclin/CDK complexes, blocking the cell cycle progression in the G1-S transition.

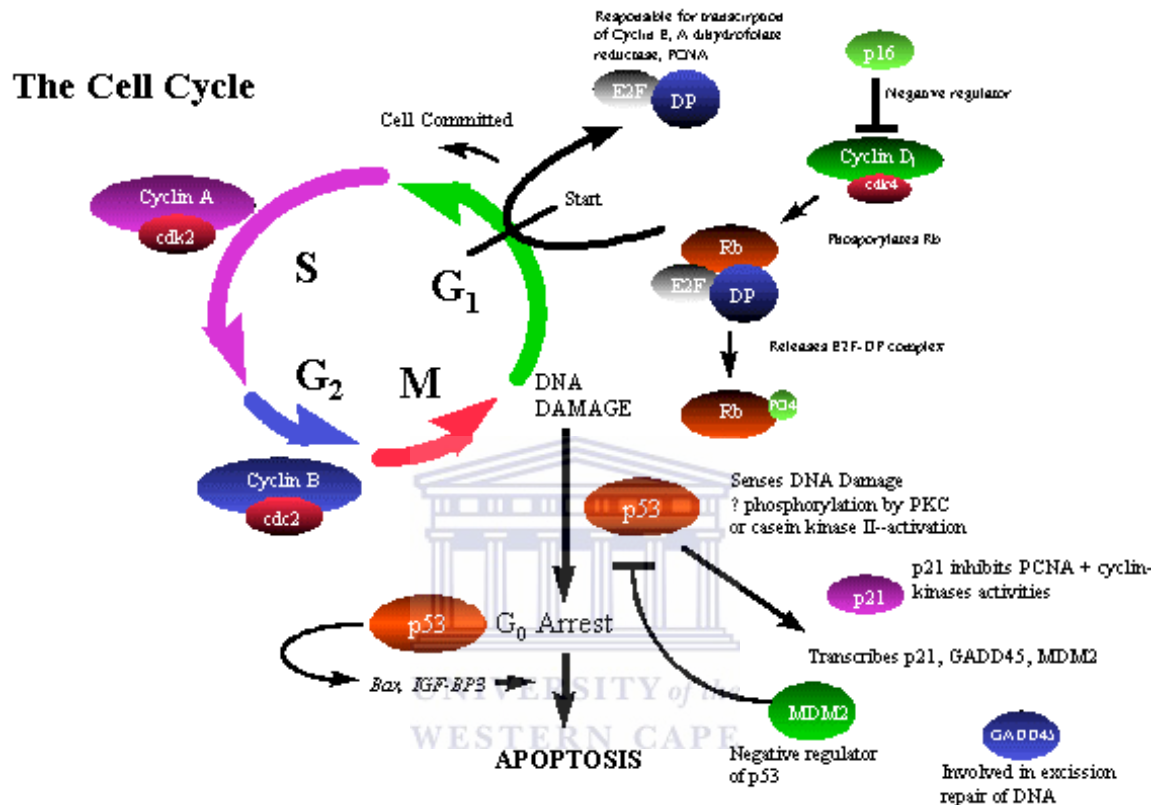


Figure 1.6 Represents a diagrammatical representation of the regulation of the cell cycle by p53.

Furthermore, p53 has been implicated in triggering cell-cycle arrest within the G₂ phase of the cell cycle, and evidence suggests that it is achieved, at least in part, by p53 inducing the expression of the protein 14-3-3 sigma (Hermeking *et al.*, 1997). Another way in which p53 activation can result in the removal of damaged cells is through the

triggering of apoptosis via transcriptional activation of genes that encode pro-apoptotic factors such as Bax (see figure 1.6).

1.5.2 p53-activating pathways

There are three independent pathways that play a role in activating the p53 network. The first pathway is triggered by DNA damage, e.g. ionising radiation. The activation of this pathway depends on two protein kinases: ataxia telangiectasia mutated (ATM) and checkpoint kinase 2 (Chk2) (Carr, 2000). ATM is activated by double stranded breaks in DNA, and in turn stimulates Chk2.

The second pathway is stimulated by aberrant growth signals, resulting from the expression of the oncogenes Ras and Myc. In humans, the activation of the p53 network depends on p14^{ARF} (alternative reading frame) tumour suppressor protein (Lowe and Lin, 2000).

A wide range of chemotherapeutic drugs, UV light and protein kinase inhibitors triggers the third pathway. It involves kinases like ataxia telangiectasia related (ATR) and casein kinase II (Meek, 1999).

All three pathways inhibit the degradation of p53 protein and therefore stabilize p53 at high concentrations. Increased p53 concentrations allow it to bind to particular DNA

sequences and activate transcription of adjacent genes. It is these genes that ultimately lead to cell death or the inhibition of cell division.

1.5.3 Control of p53

At the protein level the regulation of p53 is complex and involves interdependent control by protein-protein association. In normal unstressed cells, the wild type (wt) p53 protein is maintained at low levels primarily due to the action of mouse or human double minute-2 (Mdm-2 or Hdm-2) protein, its downstream transcriptional target (Haupt *et al.*, 1997, Kubbutat *et al.*, 1997). Mdm-2 controls p53 function in two different ways: (i) via the regulation of p53 transcriptional activity and (ii) via the intracellular p53 level (see figure 1.7).

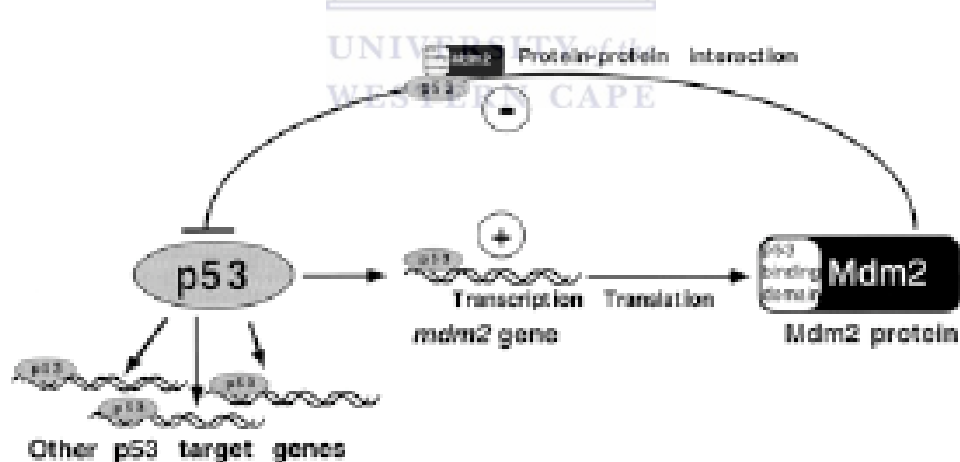


Figure 1.7 The p53-Mdm-2 negative feedback loop (taken from Oren, 1999).

Central to the regulation of p53 is its interaction with Mdm-2 protein which blocks p53's transactivation function by binding to a region of the transactivation domain (Meek,

1999)) and mediates rapid turnover of p53 by targeting it to the 26S proteasome through a mechanism involving Mdm-2 mediated ubiquitination of p53 (Haupt *et al.*, 1997).

In addition to this dual role in regulating p53, the Mdm-2 gene is itself stimulated by p53 transactivation (Zauberman *et al.*, 1995). As a consequence Mdm-2 participates in a negative regulatory loop, which keeps p53 under tight control under normal conditions of cell maintenance, making Mdm-2 pivotal to the regulation of p53 function (Wu *et al.*, 1993) (see figure 1.7). Thus, p53 induces the expression of its own antagonist.

The ability of Mdm-2 to inhibit the activity of p53 has been demonstrated in a study using mdm-2 “knock-out” mice. The mdm-2 double “knock-out” mice are embryonic lethal but p53 and mdm-2 double “knock-out” mice develop to term (Chavez-Reyes *et al.*, 2003). Since one of the most important functions of p53 is its ability to induce apoptosis in response to DNA damage, it is likely that one of the critical roles of mdm-2 would be to inhibit p53-induced apoptosis (Yap *et al.*, 1999).

The Mdm-2 mediated negative regulation of p53 can be abrogated by human alternative reading frame p14 protein (p14ARF) (Kamijo *et al.*, 1997). p14ARF, the product of the INK4a gene generated by alternative splicing, binds to mdm-2, and through this interaction prevents mdm-2 mediated degradation of p53 (Quelle *et al.*, 1997).

Li *et al.*, 2007, suggested that the p53-associated cellular protein-testis derived (PACT) is a negative regulator of p53 mediated by Hdm-2, possibly acting as an E4 ubiquitin ligase.

In their study PACT inhibited the accumulation of p53 by promoting its degradation mediated by Hdm-2 repressing p53-dependant transactivation leading to both apoptosis and cell growth retardation.

1.6 Retinoblastoma (Rb) gene

The retinoblastoma (Rb) gene is one of the best-characterized tumour suppressor genes, and serves as a prototype for genes in this category (Weinberg, 1991). Loss of Rb function plays an essential, rate-limiting role in the development of both familial and sporadic retinoblastoma (Benedict *et al.*, 1988). In familial retinoblastoma multiple tumours occur in the retina of both eyes in the first week of infancy, while in sporadic retinoblastoma a single tumour occurs in one eye. On the basis of statistical analysis of such families, it was suggested that these individuals inherited one defective autosomal allele through the germline and that the wild-type allele is lost during retinal development causing retinoblastoma (Knudson, 1971). Retinoblastoma thus arise through mutations in the retinoblastoma gene, which is located on human chromosome 13q, an area on the human chromosome that is frequently lost in this sporadic form of cancer (Lee *et al.*, 1988).

The earliest indication that the retinoblastoma gene fulfils a role in suppressing cellular proliferation came from studies using DNA tumour viruses. Studies of SV40 large tumour antigen (Tag) (DeCaprio *et al.*, 1988) adenovirus E1A (Whyte *et al.*, 1988), and the human papilloma virus (HPV) E7 protein (Dyson *et al.*, 1989) have uncovered the

molecular mechanisms underlying cellular transformation. All of these oncoproteins have the capacity to bind to and interfere with the growth suppressing properties of pRb and its family members p107 and p130. The molecular basis for their transforming capacity of cells is in part related to the direct binding of these oncoproteins to the pRb family.

The retinoblastoma tumour suppressor gene (Rb) encodes the nuclear phosphoprotein pRb (p105), which have been found mutated or deleted in several types of human cancers including breast cancer (Lee *et al.*, 1988). The Rb protein 105 and other pRb family members p107 and p130 regulate the activity of the E2F transcription factors (Dyson *et al.*, 1994). Complexes consisting of E2F and hyperphosphorylated p105RB repress the transcription of genes that are required for cell cycle progression, and repression is relieved by CDK-mediated phosphorylation of p105Rb (Salcedo *et al.*, 2002). The pRb protein is subject to regulation by many factors including E2F and cyclin D1. The hyperphosphorylated pRb, complexed with a transcription factor, serves as a transcriptional activator of cyclin D1 by binding to its promoter. On the other hand, inactivation of pRb by phosphorylation via the cyclin D/CDK complex in the late G1 phase would not only unleash E2F transcription factors, but would also decrease cyclin D1 expression (Muller *et al.*, 1994).

1.6.1 RB function in the cell cycle

The retinoblastoma gene product, pRb, plays a central role in the decision process of a cell to enter or to exit the cell cycle (Grana *et al.*, 1998). The regulation of the G1 phase

of the cell cycle requires the binding of pRb to a number of cellular proteins, many of which are transcription factors. The best-studied transcription factor is the E2F family. pRb binds to E2F through its large pocket domain and negatively regulates its activity (Weinberg, 1995).

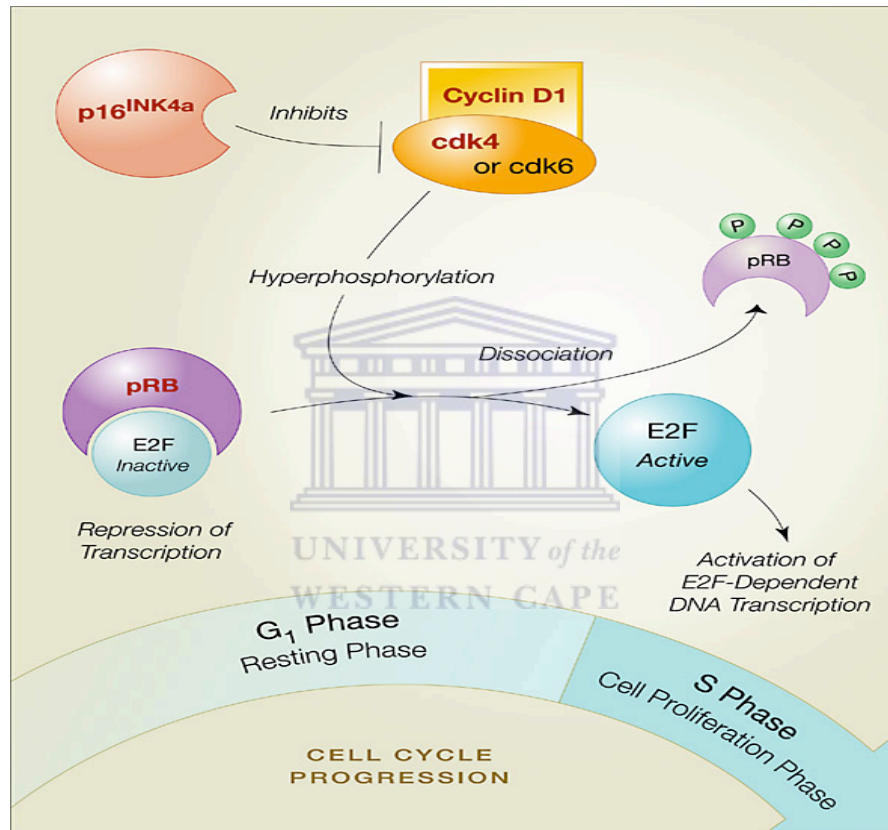
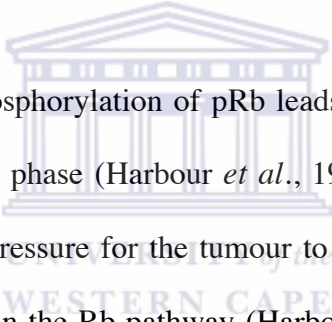


Figure 1.8 Represents the Retinoblastoma pathway of cell proliferation control (taken from Livingston and Shivedasani, 2001).

Progression of a cell through the G₁ and S phase requires inactivation of pRb by phosphorylation. Phosphorylation of pRb by cyclin D-dependent kinases (CDKs) and their cyclin partners (such as cyclin D, Cdk4 or Cdk6 and cyclin E) results in the release of pRb from E2F, leading to progression through the cell cycle (Lundberg and Weinberg,

1998) (see figure 1.8). The Rb protein is present throughout the cell cycle, but its phosphorylation state changes in a cell cycle-dependent manner. Quiescent (G0) cells have un- or hypo-phosphorylated pRb.

When cells are stimulated to divide they transverse quiescence and pRb becomes progressively phosphorylated, permitting cells to enter S phase. This phosphorylation is mediated by G1-cyclins and their associated cyclin d dependent kinases (CdKs), cyclin D-CDK4/6 and cyclin E/A-CDK, and is thought to inactivate pRb function (Kato *et al.*, 1993).



Evidence indicates that the phosphorylation of pRb leads to its loss of function as cells progress through the G1 and S phase (Harbour *et al.*, 1999). Loss of Rb gene function results in creating a selective pressure for the tumour to inactivate p53, which serves to eliminate cells with mutations in the Rb pathway (Harbour and Dean, 2000). Therefore, many tumours have mutations that inactivate both the Rb and p53 genes.

1.6.2 Function of Rb in apoptosis

Rb is inactivated either by a mutation in the gene or by the phosphorylation of the pRb protein in almost all tumours. Loss of Rb gene function triggers the p53 apoptotic pathway (Morgenbesser *et al.*, 1994). This link between the Rb and p53 pathways can be explained by the fact that loss of Rb function leads to the release of E2F, which in turn

triggers apoptosis by activating the tumour suppressor protein ARF expression, which is encoded by the INK4A locus (Pomerantz *et al.*, 1998).

1.7 The DWNN gene family

1.7.1 Identification of the DWNN domain

The Domain With No Name gene (DWNN) was isolated in a genetic screen aimed at identifying novel components of the MHC class I antigen processing and presentation pathway. Several mutant cell lines were generated using a promoter trap mutagenesis strategy (von Melchner and Ruley, 1989). The mutant cell lines were analysed for sensitivity to the CTL specific clones HA8 and HA11 using the Lactate dehydrogenase (LDH) release assay (George, 1995). Analysis of these cell lines showed three lines to be 100 % resistant to killing by the CTL specific clones, HA8 and HA11. One of these lines, the hygromycin B/CTL resistant cell line Mut 7(3xHA8) 3.5hrs, was analysed further to obtain the 5' sequence adjacent to the site of retroviral integration. Sequence analysis of the cell line identified a full-length cDNA clone EST 21C4 (accession number T25012) that showed no significant matches to the Genbank Database. This gene was subsequently named DWNN (domain with no name).

Sequence analysis of the 21C4 clone showed that the mRNA is 1.1 kb long and contains 118 amino acids, encoding a 13 kD protein. Further analysis showed that the sequence encodes a highly conserved region of 80 amino acids and a hydrophobic tail. The DWNN domain (an 80 amino acid region) showed high conservation throughout species, this

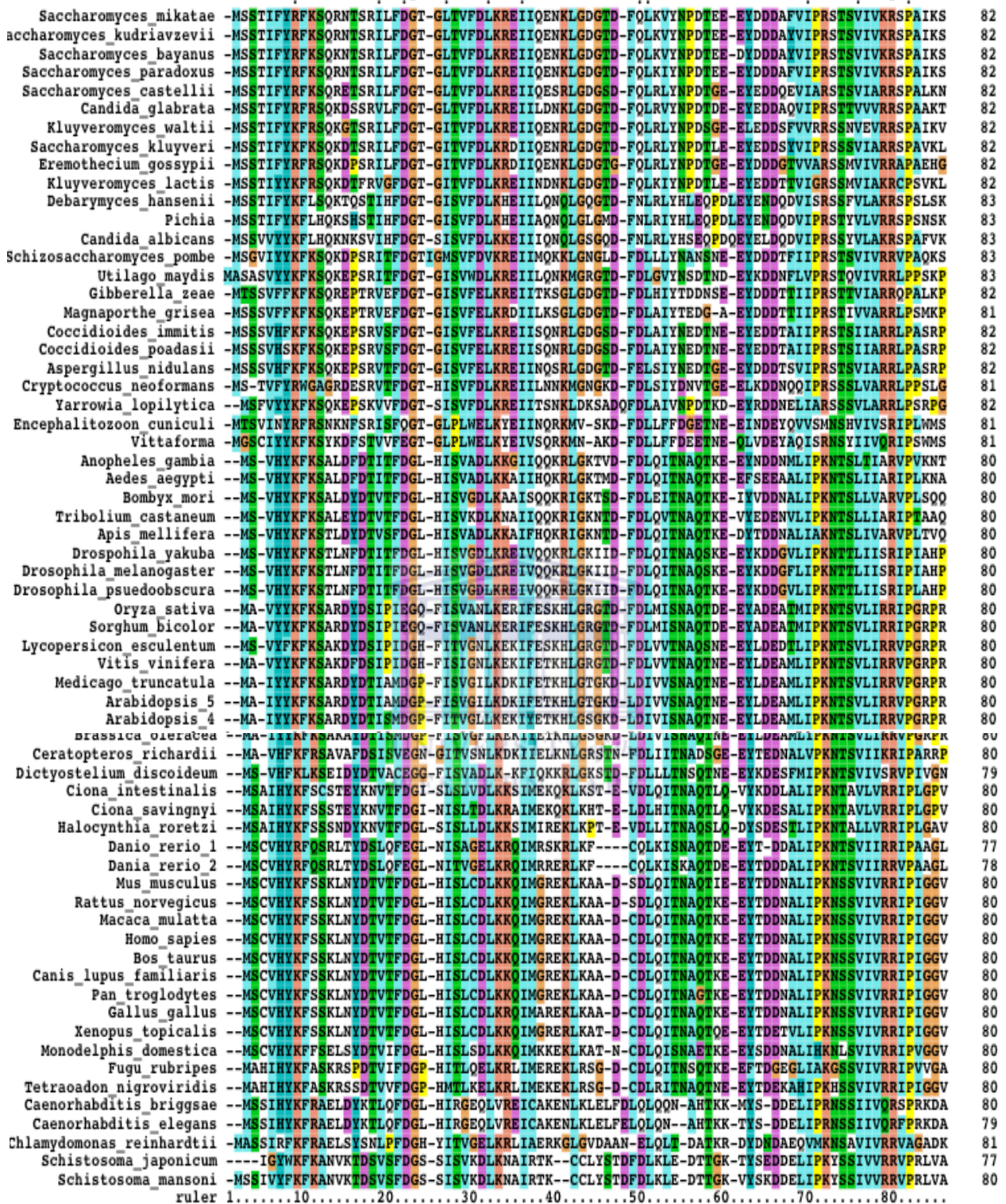


Figure 1.9 Sequence alignment of DWNN homologues from a range of eukaryotic genomes.

The alignment was performed using Clustal X (Jeanmougin *et al.*, 1998)

includes humans, worms, flies, plants, algae and yeast (see figure 1.9). The evolutionary relationship for the DWNN domain in the different taxa is represented by means of a neighbour joining tree in figure 1.10. The corresponding gene was found to be located on human chromosome 16p12.2, upstream of the previously identified RBBP6/PACT/P2P-R gene. Analysis of cDNA sequences showed that the sequence coded for the previously unidentified N-terminus of the RBBP6 protein (Dlamini *et al.*, in prep), which we have named the DWNN domain.

A number of screens have been undertaken to identify proteins that interact with the tumor suppressor proteins p53 and pRb. RBBP6 is one of the few proteins identified that has been shown to interact with both p53 and Rb. Three partial cDNAs from the full length RBBP6 transcript were originally cloned and sequenced in different studies. RBQ-1 (Sakai *et al.*, 1995), corresponding to residues 150–1146 of the human protein, and PACT (p53 associated cellular protein, testis derived) (Simons *et al.*, 1997) corresponding to residues 207–1792, were cloned on the basis of their ability to bind Rb and p53 in both human and mouse cells. P2P-R (Witte and Scott, 1997) corresponding to residues 199–1792, was cloned based on its recognition by two antibodies specific for heterogeneous nuclear ribonucleoproteins (hnRNPs). An alternatively spliced form omitting residues 651–685, corresponding to exon 16 of the full-length gene, has also been reported (Sakai *et al.*, 1995). The Human Gene Mapping Workshop (HGMW)-approved name Retinoblastoma binding protein 6 (RBBP6) will be used for the complete protein and DWNN for the domain in subsequent text (see figure 1.11 for the nomenclature used for the different RBBP6 partial cDNAs).

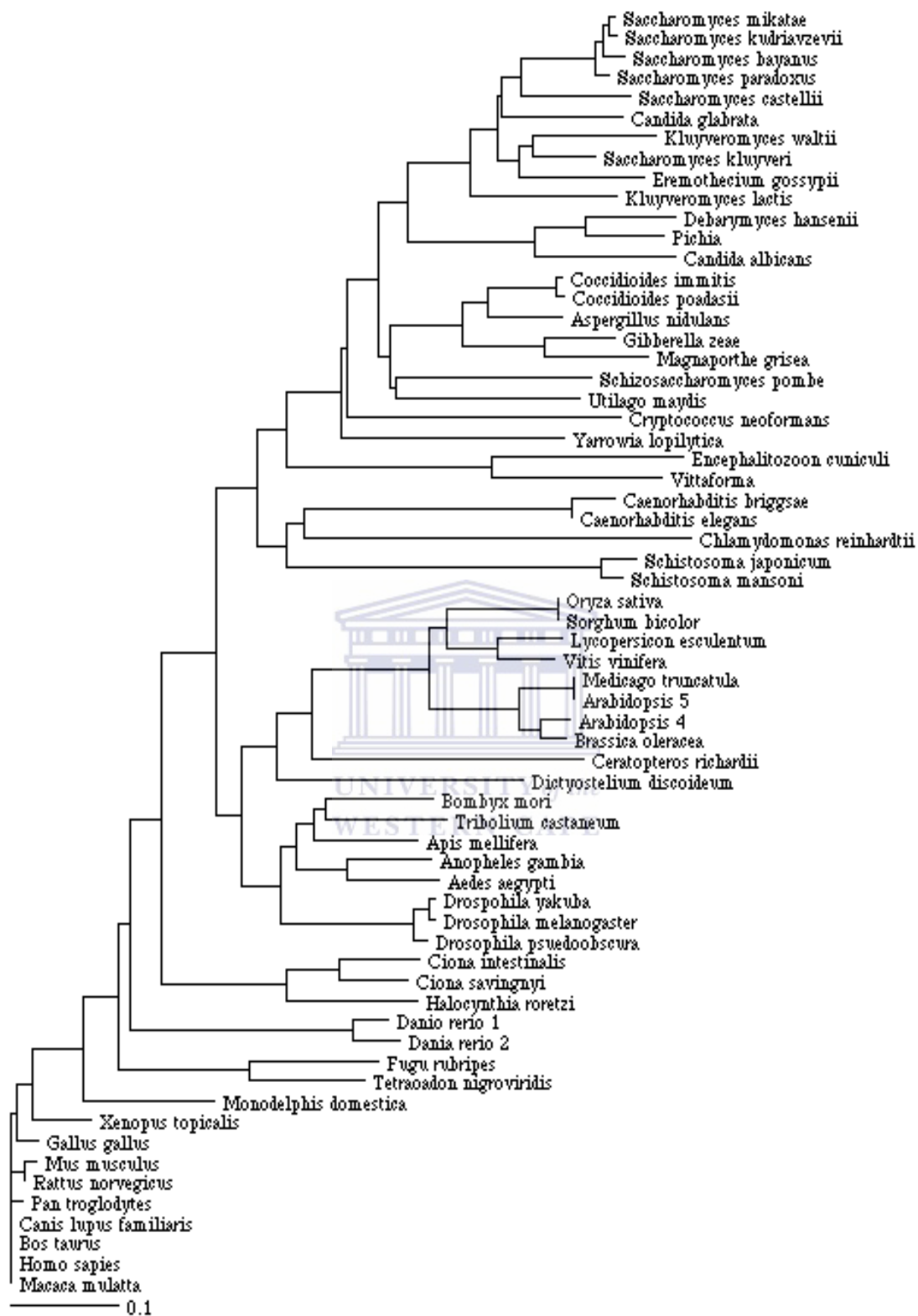


Figure 1.10 Shows the neighbour joining tree of the DWNN gene from different taxa. The tree was drawn using Clustal X (Jeanmougin *et al.*, 1998)

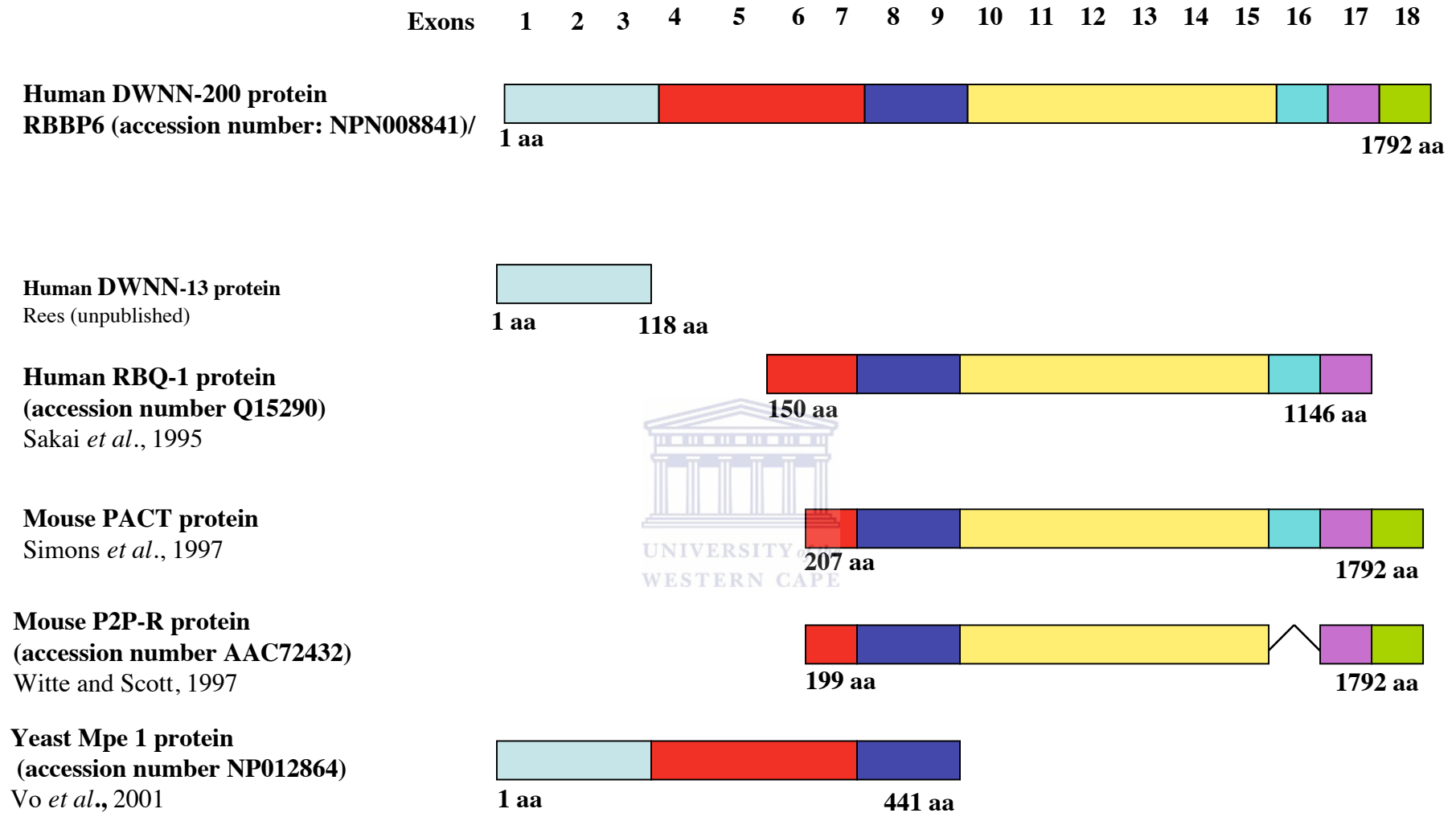


Figure 1.11 Diagrammatic representation of the RBBP6 partial cDNAs, including the full-length RBBP6 protein

Analysis of the RBBP6 locus suggests that three major transcripts of 6.1, 6.0 and 1.1 kb occur, by a combination of alternative splicing and alternative poly-adenylation. These transcripts encode proteins of 1792, 1758 and 118 amino acids, which have been designated RBBP6 isoforms 1, 2 and 3 respectively (Genbank:NP008841, Genbank:NP061173, Genbank:NP116015). Sequence analysis showed that this gene contains 18 exons and consists of several domains. The gene organization is as follows (see figure 1.12).

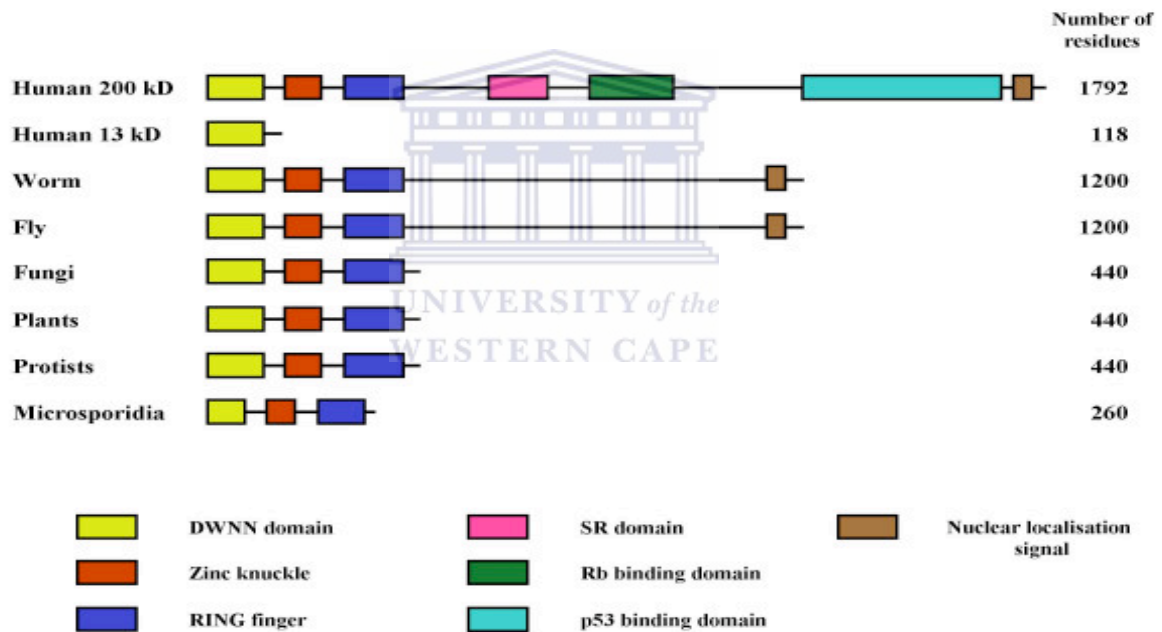


Figure 1.12 The domain structure of the RBBP6 family of proteins. RBBP6 homologues containing a DWNN domain, a zinc knuckle and a RING finger are found in all complete eukaryotic genomes analyzed to date (taken from Pugh *et al.*, 2006).

The conserved DWNN domain spanning exons 1 to 3, a CCHC zinc finger domain spanning exons 5 and 6 and a C3HC4 type of RING finger domain located in exons 7 to 10. CCHC zinc finger domains are known to interact with single stranded RNA or DNA (Fairall, *et al.*, 1993), while the C3HC4 RING finger domain has been shown to have ubiquitin ligase activity (Joazeiro and Weissman, 2000). They are often found in E3 ubiquitin ligases. There is also a SR domain and an Rb-binding domain. Furthermore it contains a p53 binding domain in exon 18 and a proline rich region spanning exons 10 to 15.

1.7.2 Structure of DWNN

Pugh *et al.*, 2006 expressed residues 1–81 of the human RBBP6 gene, corresponding to the DWNN domain, and determined the structure using heteronuclear NMR. Comparison of the representative DWNN structure against the entire Protein Data Base using the Dali server (Holm and Sander, 1993) revealed that the DWNN domain are most similar to human ubiquitin (PDB:1UBI), and the N-terminal ubiquitin-like domain of Isg15 (PDB:1Z2M), with Z-scores of 7.5 and 7.6 respectively. The amino acid sequences of ubiquitin and DWNN are only 18 % identical.

The secondary structure of the protein consists of the elements β 1- β 2- β 3- α - β 4- β 5- β 6- β 7, with the α -helix packing against a five-stranded β -sheet made up of strands β 1, β 2, β 4, β 5 and β 7 in a ubiquitin-like β -grasp topology (see Figure 1.13B). Unlike ubiquitin, DWNN contains an additional short section of anti-parallel β -sheet immediately prior to the α -helix (sheets β 3 and β 6, residues 23–25 and 63–65 respectively). This additional β -sheet has not been seen in other ubiquitin-like proteins. The 310 helix immediately

preceding the last β -strand found in many ubiquitin-like proteins is absent from DWNN. Figure 1.13 shows that the residues corresponding to this helix (ubiquitin: 57–61, underlined in Figure 1.11D) are entirely absent in DWNN.

In addition, Pugh *et al.*, 2006, also confirmed the presence of a second 310 helix at the C-terminal end of the α -helix that is found in many ubiquitin-like proteins; however the loop preceding strand β_4 is two residues longer than the corresponding loop in ubiquitin, so that there is no longer a requirement for a tight helical turn at this position.

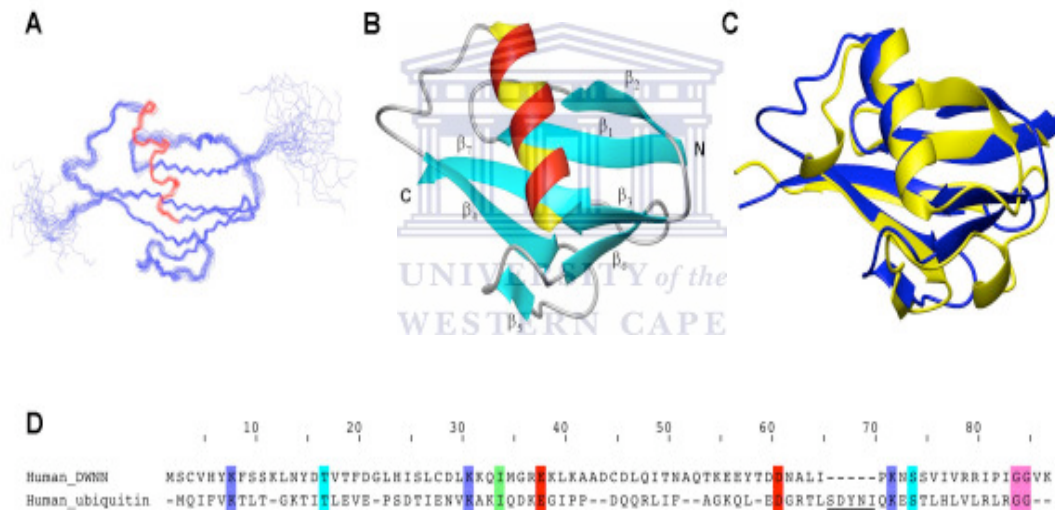


Figure 1.13 Shows the three-dimensional structure of the DWNN domain (taken from Pugh *et al.*, 2006). (A) superposition of the 25 lowest energy conformers, (B) cartoon representation of the overall fold and secondary structure, (C) superposition of the backbone traces of the DWNN domain (in blue) and ubiquitin (1UBI, in yellow) and (D) structural alignment of the primary sequences of DWNN and ubiquitin, determined using the Dali server.

The high level of conservation of G21 (see figure 1.9) may be the consequence of the presence of the extra strand β_3 , which requires the backbone to make a sharp kink at that position. Hydrophobic residues F8, L29, I33, L39, L46, I64, V70, V72 and P76 make up the core of the protein, accounting for their high degree of conservation. The high level of conservation of non-hydrophobic residues Y6, K7, K30, Y57 and R74 suggests a possible functional role for these residues.

In recent years a superfamily of ubiquitin-like domains has been identified (Hochstrasser, 2000 and Hochstrasser, 2000). This superfamily can be divided into the ubiquitin-like proteins (UBL's), which consist solely of the ubiquitin-like domain, and ubiquitin domain proteins (UDP's), which are larger proteins containing one or more ubiquitin-like domains. DWNN are most likely the first example of an ubiquitin-like domain that is alternatively expressed both as a UBL and as a UDP. The role of ubiquitin is discussed in section 1.9.

1.7.3 DWNN/RBBP6 homologues

With the completion of the human genome sequence Sakai *et al.* (1995) the DWNN-200 gene has been officially named RBBP6 (accession number NP 008841). The NCBI BLAST database has (since 1995 to date) revealed a wide range of species containing the RBBP6 gene. Figure 1.12 shows the domain arrangement of the RBBP6 gene in various species. In humans, worms and flies the RBBP6 gene contains the DWNN domain, CCHC zinc motif, C4HC Ring finger domain, as well as the pRb- and p53- binding

domains. In fungi, plants, protists and microsporidia, the RBBP6 domain structure is similar. The RBBP6 gene in these species contains the DWNN domain, CCHC zinc motif and C4HC Ring finger domain only.

1.7.4 Homo sapiens RBBP6

The RBBP6 human gene has been completely sequenced. This gene encodes a protein that binds the underphosphorylated pRb protein (Sakai *et al.*, 1995). Sequence analysis of this gene using AceView indicated that it contains 13 alternatively spliced transcript variants that encode 13 different isoforms. The RBBP6 gene showed high levels of expression in the placenta and various other tissues. The genes expression in oesophageal cancer tissues has also been shown (Yoshitake *et al.*, 2004). When Sakai *et al.*, 1995, described the gene, the full-length sequence of the gene was not known then and they described a partial cDNA and named it RBQ-1.

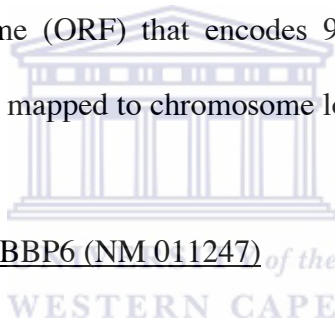
1.7.4.1 RBQ-1 (RBBP6) protein

RBQ-1 (also known as RBBP6) was identified from a human small cell carcinoma (H69c) library as a novel protein of 140 kD and was shown to bind to the Rb gene product. It also showed high homology to the p53 associated cellular protein-testis derived (PACT) protein (Sakai *et al.*, 1995). Two other proteins designated RBQ-2 and RBQ-3 was also identified from that study. All three proteins bind to the underphosphorylated form of pRb. Although all three proteins were identified in the same

study RBQ-1 and RBQ-3 showed no significant homology to each other (Saijo *et al.*, 1995).

RBQ-1 is shorter than that of the mouse PACT protein, 948 amino acids compared to 1583 amino acids of mouse PACT. The overall amino acid homology between mouse PACT and human RBQ-1 is 94 % suggesting that the two proteins are highly conserved (Simons *et al.*, 1997).

The nucleotide sequence of RBQ-1 cDNA was shown to be 3011 bp in length and contains an open reading frame (ORF) that encodes 948 amino acids, with multiple repetitive motifs. The gene was mapped to chromosome location 16p12.2.



1.7.5 *Mus musculus* RBBP6 (NM 011247) of the

Recent data from Ensembl Gene revealed that the mouse contains two transcripts of the RBBP6 gene. The first transcript (Stable ID: ENSMUST00000033043) contains 18 exons and encodes a 1783 residue protein. The second transcript (Stable ID: ENSMUSP00000071519) contains 18 exons but encodes a 1591 residue protein. BLAST analysis has mapped the gene on chromosome 7. According to Mouse Genome Database (MGD), February 2004, the nucleic acid sequence of the mouse RBBP6 shows 82.6 % identity to that of humans.

Two research groups have previously identified the partial cDNAs of the mouse RBBP6 gene and had named them PACT (Simons *et al.*, 1997) and P2P-R (Witte and Scott 1997).

1.7.5.1 PACT

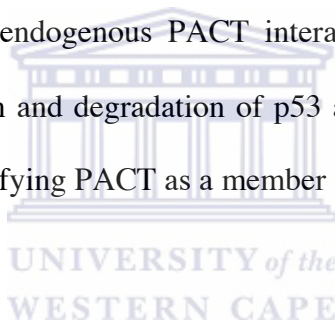
Elucidation of p53 and pRb protein-protein interactions with both viral and cellular proteins has shed light on various functions of these proteins. Binding of p53 and pRb to transforming proteins from several tumour viruses can cause functional inactivation of these tumour suppressor proteins (Lane and Crawford, 1979 and DeCaprio *et al.*, 1988).

Since protein-protein interactions appear to be central in p53 cellular activities Simons *et al.* (1997) set out to identify cellular proteins that may interact with p53. In their study, purified wild type (wt) p53 protein was used as a probe on a mouse testis expression library. From this study a cDNA encoding a novel nuclear protein was isolated, the protein was designated PACT.

Sequence analysis of PACT showed that the cDNA is 5177 bp long coding for 1583 amino acids and contains a 437 bp 3' non-coding region with a polyA signal and tail. This protein contains a serine/arginine (SR) rich region and a very basic lysine rich C-terminus. The SR domain has been shown to be a site in which serines are phosphorylated by specific kinases Gui *et al.*, 1994, whilst the lysine-rich domain has been suggested to play a role in *in vivo* modification. Recombinant PACT protein binds p53 in the wt conformation, but not the mutated forms, and can compete for p53 specific

DNA binding. Gui *et al.* (1994) also showed that the 250 kD PACT protein interacts with both cellular p53 and pRb.

The interaction between PACT and these two tumour suppressor proteins is quite similar in nature to that of the viral oncoproteins. The viral proteins that bind p53 do not bind most mutated forms of p53. In addition, large T antigen binds exclusively to the under-phosphorylated form of pRb. Sakai *et al.*, (1995) showed that RBQ1 also preferentially binds to the under-phosphorylated form of pRb and that EIA can disrupt this interaction. Recently Li *et al.*, 2007, used homologous recombination to “knock-out” PACT. From this study it was shown that endogenous PACT interacted with Hdm-2 and enhance Hdm-2-mediated ubiquitination and degradation of p53 as a result of an increase of the p53-Hdm-2 affinity, thus identifying PACT as a member of negative regulators of p53.



1.7.5.2 Proliferation potential protein related (P2P-R) protein

P2P-R (proliferation potential-related protein), a murine protein highly homologous to PACT, was shown to associate with heterogeneous nuclear ribonucleoprotein (hnRNP) particles (Witte and Scott, 1997). Further analysis indicated that P2P-R is the alternatively spliced form of PACT, lacking the 34 amino acid exon previously described by Saijo *et al.*, 1995, and that P2P-R appears to be the dominant product expressed in multiple murine cell lines (Scott *et al.*, 2003).

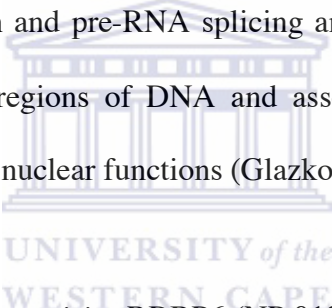
A P2P-R fusion protein derived from a region of the P2P-R cDNA coding for hnRNP association is able to bind single-stranded DNA with P2P-R expression markedly repressed during terminal differentiation (Witte and Scott, 1997). In addition, their study confirmed that P2P-R binds pRb by precipitating pRb from cellular extracts using GST-P2P-R fusion protein. This binding was blocked by E1A protein confirming that P2P-R binds to the pRb pocket domain (Witte and Scott, 1997).

Several lines of evidence place P2P-R at various cellular processes. Scott *et al.* (2003) identified P2P-R as one of many proteins that contribute to genome stability. A role for PACT/P2P-R in RNA metabolism has also been proposed. Evidence showed that P2P-R localises primarily to the nucleoli of interphase murine and human cell lines, (Gao *et al.*, 2002). P2P-R immunoreactivity increases more than ten fold in mitotic cells compared to G0 cells, without an increase in P2P-R mRNA expression. In these mitotic cells, P2P-R localises to the periphery of chromosomes (Gao *et al.*, 2002).

P2P-R promotes apoptosis in a p53- and pRb-independent manner. Transfection and over-expression of near-full length P2P-R restricts cell cycle progression at prometaphase and promotes mitotic apoptosis in Saos2 cells (Gao and Scott, 2002), since Saos2 cells lack p53 and have a non-functional pRb (Masuda *et al.*, 1987 and Shew *et al.*, 1989). Furthermore, a possible pro-apoptotic region exists within P2P-R spanning from amino acid 1156-1314 (Gao and Scott, 2003). Over-expression of this region in MCF-7 cells promotes camptothecin-induced apoptosis. The potential pro-apoptotic region overlaps

with the region of P2P-R that is responsible for p53 and single stranded DNA binding (amino acids 1204-1314).

The SR region of P2P-R can be phosphorylated by the mitotic Cdc2 kinase (Scott *et al.*, 2003), which might explain the earlier observation by Gao *et al.*, 2002, that P2P-R immunoreactivity increases significantly during mitosis. SRPK1a in the SR region also phosphorylates P2P-R. The SR region of P2P-R can bind two factors that associate with matrix associated regions (MARs) of DNA, namely SAF-B and nucleolin (Scott *et al.*, 2003). SAF-B is a MARs binding factor (Renz and Fackelmayer, 1996), which has been reported to couple transcription and pre-RNA splicing and localises to nuclear speckles (Nayler *et al.*, 1998). MARs regions of DNA and associated factors are believed to regulate transcription and other nuclear functions (Glazko *et al.*, 2003).



1.7.6 *Saccharomyces cerevisiae* RBBP6 (NP 012864)

1.7.6.1 Mpe-1 protein

In eukaryotic cells, 3'-end cleavage and polyadenylation are essential steps in the synthesis of functional mRNAs. These processes are involved in transcription termination (Hirose and Manley, 2000) and the export of mature mRNAs from the nucleus (Huang and Carmichael, 1996). In the yeast *Saccharomyces cerevisiae*, two complexes, CFI (cleavage factor I) and CPF (cleavage and polyadenylation factor) and Pab1p are responsible for the specific cleavage and polyadenylation of pre-mRNA. Vo *et al.*, 2001, characterized a novel essential gene, MPE1 (YKL059c), which interacts genetically with the *PCFII* gene encoding a subunit of CFI.

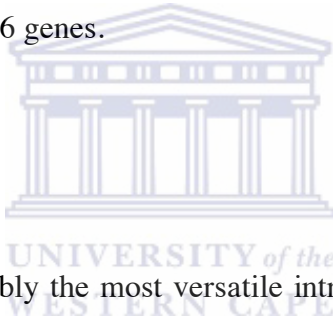
A search for known protein motifs in Mpe1p revealed a zinc knuckle (CX₂CX₄HX₄C) between amino acids 182 and 195. This motif has been implicated in the interactions between proteins and single-stranded nucleic acids (Shi and Berg, 1996). A homology search based on the zinc knuckle identified several other genes. These included *Saccharomyces pombe*, *Arabidopsis thaliana* and *Drosophila melanogaster* in which the Mpe1p domain between amino acids 176 and 216 is conserved.

When these protein sequences were aligned with the Mpe1p sequence, two more regions, A and B, were found to contain similarities. The A region consists of amino acids 5 to 78 of Mpe1p and does not contain any known motifs. The B domain extends from amino acids 284 to 343 of Mpe1p and was shown to be cysteine-rich and presents some of the characteristics of a RING finger. RING fingers are often implicated in protein-protein interactions, notably in the ubiquitination pathway (Aravind and Koonin, 2000).

These three conserved domains were also found in non-overlapping human cDNAs, which all mapped to the same region on chromosome 16. One of these cDNAs contains a domain conserved in Mpe1p that codes for the Rppb6 protein. Rppb6 protein has been shown to interact with pRb1 (Sakai *et al.*, 1995). The pRb1 protein is involved in cell differentiation and is localized to centres of mRNA processing in the nucleus (Durfee *et al.*, 1994). This supports the idea that the human Mpe1p homolog could participate in 3' end processing.

1.7.7 Other RBBP6 homologues

The UniGene and GeneCard databases show evidence for the presence of other RBBP6 homologues, including *Arabidopsis thaliana* (accession number NM124114), *Drosophila melanogaster* (accession number CG3231), *Danio rerio* (BG 737479), *Xenopus laevis* (BJ614254), *Rattus norvegicus* (XP219296), *Pan troglodytes* (XM001164058), *Bos taurus* (XM001254138), *Macaca mulatta* (XM001097526), *Canis lupus familiaris* (XM536929), *Arabidopsis thaliana* (emblZ97343) and *Encephalitozoon cuniculi* (NC003238). No work has been undertaken in these organisms, as compared to the human, mouse and yeast RBBP6 genes.



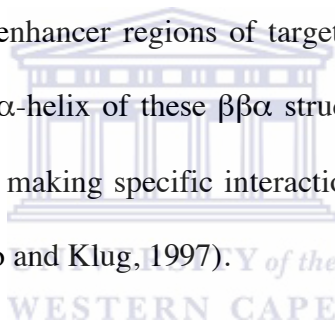
1.8 Zinc fingers

The zinc finger (ZnF) is probably the most versatile intracellular protein domain and is certainly a commonly used one. ZnF-containing proteins form one of the most prevalent structural families in eukaryotes, comprising, for example, ~2 % of the proteins encoded by the human genome (reviewed by Matthews and Sunde, 2002).

The term zinc finger was first used to describe a 30-residue, repeated sequence motif found in an unusually abundant *Xenopus* transcription factor TFIIIA (Zang *et al.*, 1995). It was proposed that each motif is folded around a central zinc ion to form an independent minidomain and that adjacent zinc fingers are combined as modules to make up a DNA-binding domain with the modules “gripping” the DNA (hence the term finger).

Different classes of ZnFs differ largely by function, as well as the identity and spacing of their zinc-binding domains. There are 14 different well-characterized classes known (reviewed by Matthews and Sunde, 2002). These classes have a variety of different roles within the cell, but they share a common feature of being able to mediate the interaction of proteins with other biomolecules, including DNA, RNA other proteins, or lipids.

TFIIIA contains classical or C₂H₂ ZnFs, which ligate zinc via pairs of cysteine and histidine residues. Many proteins that contain classical ZnFs are involved in the regulation of gene expression, with the ZnF often interacting with specific DNA sequences in the promoter or enhancer regions of target genes. Basic and hydrophobic residues that are found in the α -helix of these $\beta\beta\alpha$ structures appear to be the primary determinants of DNA-binding, making specific interactions with 2-4 bases in the major groove of the DNA helix (Choo and Klug, 1997).



1.9 Role of RING fingers in ubiquitin pathway

1.9.1 DWNN ubiquitin homology

RING fingers are typically found in E3-ubiquitin ligases and have been shown to play an essential role in the conjugation of ubiquitin and ubiquitin-like moieties to protein substrates (Joazeiro and Weissman, 2000). The RBBP6 RING domains have a C-X₂-C-X₁₁-C-C-X-[NS]-X₂-C-X₂-C-X₁₂-C-X₂-C rather than the classical C₃H₄ consensus, which means they are either C₄C₄ or C₃NC₄-type RING fingers, depending on which residues are involved in coordinating the two zinc ions. C₄C₄ RING-like domains have

been found in the transcription-associated proteins CNOT4 (Albert *et al.*, 2000) and p44 (Fribourg *et al.*, 2000) and despite its non-typical consensus CNOT4 has also been shown to have ubiquitin-ligase activity (Albert *et al.*, 2002).

In addition to the conserved cysteines, RBBP6 RING domains share the wider set of conserved hydrophobic residues characteristic of U-box domains (Aravind and Koonin, 2000). These are even stronger predictors of ubiquitin-conjugating function than the metal-chelating residues, since they are shared by a wider set of domains that adopt the same fold and participate in ubiquitination even in the absence of zinc ions.

1.9.2 Ubiquitin



Ubiquitin is a highly conserved 76 residue protein found in all eukaryotes either free or covalently attached to cellular proteins (reviewed by Liakopoulos *et al.*, 1998). When a protein is covalently linked to ubiquitin, the process is referred to as ubiquitination. During this process an isopeptide bond between the C-terminal glycine residue of ubiquitin and the amino group of a lysine residue of the target protein is formed. Ubiquitinated proteins are subsequently targeted for degradation by the 26S proteasome, a major protease of the cytosol and the nucleus of eukaryotes, with ubiquitin being recycled. The 26S proteasome degrades the tagged proteins into small peptides, Ubiquitination can also target certain cell surface proteins to lysosomal degradation via the endocytic route (Jentsch and Pyrowolakis, 2000). Conjugated ubiquitin can act as a substrate for further ubiquitination reactions to form polyubiquitin.

1.9.3 The ubiquitin pathway

The ubiquitin pathway occurs via two steps: (1) the covalent attachment of multiple ubiquitin molecules to the target protein and (2) the degradation of the tagged protein by the 26S proteasome (Fig 1.14). Conjugation of ubiquitin to the target protein occurs via three steps involving ubiquitin activating enzyme (E1), ubiquitin-conjugating enzyme (E2) and ubiquitin-protein ligases (E3) (Huibregste *et al.*, 1995). E1 activates ubiquitin in an ATP-dependent manner, forming a thiol ester linkage (Haas and Siepmann, 1997). E2 then transfers the activated ubiquitin from E1 to a target protein that is specifically bound to E3 via a thiol ester linkage.

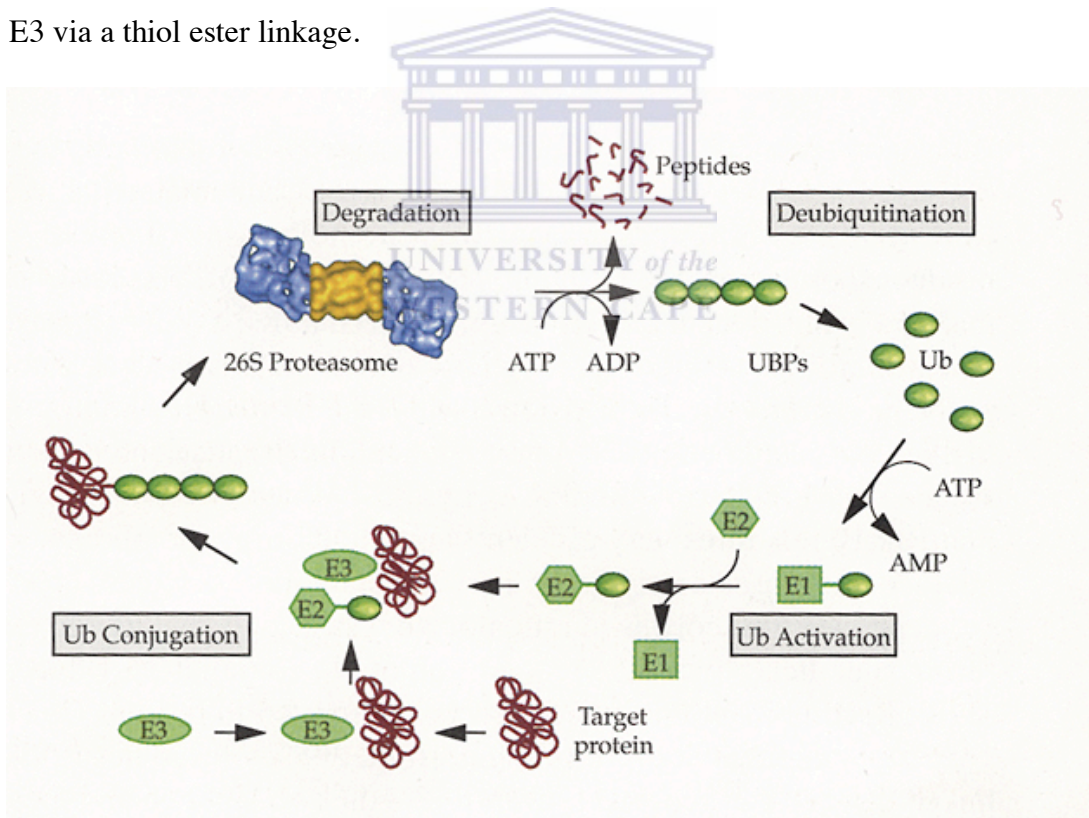


Figure 1.14 Diagrammatic representation of the ubiquitination pathway (taken from [www.hgu.mrc.ac.uk/ Research/Gordon/anre.jpg](http://www.hgu.mrc.ac.uk/Research/Gordon/anre.jpg), 3 April 2008)

There are different classes of E3 enzymes. For the HECT (homologous to the E6-AP COOH terminus) domain E3s, the activated ubiquitin is transferred to E3, generating a third thiol ester intermediate, before being transferred to an E3-bound substrate.

RING finger-containing E3s catalyse the direct transfer of the activated ubiquitin to the E3-bound substrate. E3 is then responsible for the covalent attachment of ubiquitin to the substrate. The ubiquitin molecule is generally transferred an amino group of an internal lysine residue in the substrate to generate an isopeptide bond. This resultant monoubiquitin substrate is usually not targeted for degradation by the 26S proteasome. However, in other cases, ubiquitin is conjugated to the N-terminal residue of the substrate (Breitschopf *et al.*, 1998). In successive reactions, the polyubiquitin chain is synthesised by the transfer of additional ubiquitin to the Lys 48 of the previously conjugated molecule. The polyubiquitin chain serves as a recognition marker for the 26S proteasome complex. The proteasome degrades the ubiquitin-tagged substrate into short peptides, which are released, as well as ubiquitin, which is recycled (Fig 1.14).

1.9.4 Functional relationship between DWNN and the RING finger

Ubiquitin-like proteins typically share the C-terminal GG motif, which acts as a recognition motif for a protease that cleaves between the two glycines, initiating the process of conjugation. Pugh *et al.*, 2006, using NMR to determine the structure of DWNN showed the occurrence of the GG motif in the structurally identical position in human and mouse DWNN domains (highlighted in pink in Figure 1.13D) suggests that the domain may be involved in a similar process of conjugation, which can possibly be

referred to as "DWNylation". The GG lies outside of the structured region as in the case of ubiquitin (see figure 1.13). The absence of the GG in lower organisms is more difficult to rationalize. Preliminary EST analysis however suggests that organisms, in which the GG motif is absent, also do not contain the UBL form of the DWNN domain (unpublished data). This raises the possibility that the DWNN domain does not act as a covalent modifier in lower organisms. In the yeast protein Hub1, which has also been shown to be involved in pre-mRNA splicing (Wilkinson *et al.*, 2004), the role of the diglycine motif is taken by an YY motif (Ramelot *et al.*, 2003). The structurally equivalent position in DWNN is taken by a highly conserved RR motif (see Figure 1.9), which may therefore act as the activation signal. A number of lines of evidence suggest a role for RBBP6 in both mRNA processing and ubiquitin-like protein modification. The close association between domains involved in RNA metabolism and ubiquitination has previously been pointed out in a number of proteins, including MDM2 (Anantharaman *et al.*, 2002). In yeast, the RBBP6 homologue Mpe1p (discussed in section 1.76) has been shown to be a component of the CPF complex (Vo *et al.*, 2001).

Mammalian RBBP6 has been identified as an SR protein on the basis of an SR domain (residues 477–570) (Simons *et al.*, 1997), the CCHC RNA binding domain, its localisation within nuclear speckles (Scott *et al.*, 2003) and its association with heterogeneous nuclear ribonucleoproteins (hnRNPs) (Witte and Scott, 1997). SR proteins are involved in splicing, whereas hnRNPs are thought to play a central role in organizing the polyadenylation, splicing and export of mRNA transcripts (Reed and Magni, 2001). A number of SR proteins are known to interact directly with the C-terminal domain of the

RNA Polymerase II complex. A role for RBBP6 in mRNA processing therefore seems highly probable.

The presence of a RING finger domain in all eukaryotes, combined with the ubiquitin-like structure of the DWNN domain, makes it highly probable that RBBP6 also has ubiquitin-ligase activity, possibly involving modification of hnRNPs with an ubiquitin-like moiety. Several hnRNPs have recently been shown to be SUMOylated (Li *et al.*, 2004), which resulted in a decreased affinity of the hnRNP for mRNA.

Furthermore, since p53 and Rb have both been shown to bind to mammalian RBBP6, it is possible that RBBP6 plays a role in the regulation of these two proteins similar to that played by MDM2 (Hsieh *et al.*, 1999), suggesting a possible model for the integration of the regulation of transcription, cell cycle control and apoptosis. Given the fact that the DWNN domain can be independently expressed in vertebrates, an interesting possibility is that the function of RBBP6 is to DWNNylate other proteins. Furthermore Li *et al.* (2007) showed that PACT/RBBP6 promotes ubiquitination of p53 mediated by Hdm-2.

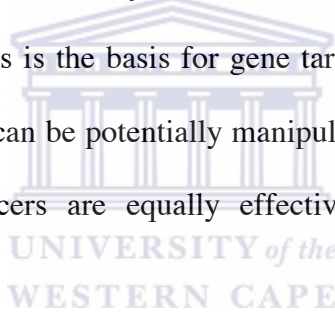
1.10 Gene targeting

Genes were first identified through the description of their mutant phenotype. These mutant phenotypes gave a clue to the function of the gene. With the advent of large-scale genome sequencing, literally thousands of genes have been identified. Reverse genetics is now the most effective way to assess the function of a gene. With a human gene sequence

in hand, it is possible, by gene targeting, to generate a mutation in the homologous mouse gene and thus determine the physiological consequences of this mutation. Since many human diseases have a genetic basis, mouse models generated using a gene targeting strategy should greatly enhance our understanding of the pathophysiology of diseases and consequently lead to the design of new therapies.

1.10.1 Homologous recombination

Foreign DNA are integrated into mammalian cells by either a process of non-homologous or homologous recombination. The ability of mammalian cells to mediate recombination between homologous sequences is the basis for gene targeting technology (Volarevic *et al.*, 1999). The entire genome can be potentially manipulated, such that intron sequences or gene promoters or enhancers are equally effective and useful targets as exon sequences.



The first experimental evidence for the occurrence of gene targeting was observed in a fibroblast cell line with a selectable artificial locus by Lin *et al.* (1985) and was subsequently demonstrated to occur at the endogenous β -globin gene by Smithies *et al.*, (1985) in Erythroleukemia cells. In mammalian cells, non-homologous recombination is orders of magnitude more frequent than homologous recombination. The low frequency of homologous recombination can be related to, at least in part, a competing pathway. This pathway effects the efficient integration of the transfected DNA into random chromosomal sites.

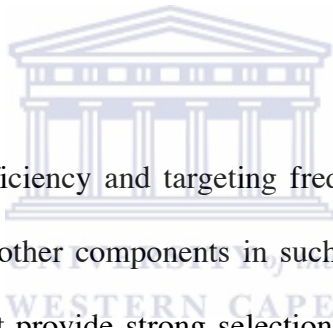
1.10.2 Embryonic Stem (ES) cells

The introduction of DNA by viral transduction or transfection into embryonic stem (ES) cells by Bradley and Robertson, (1986) opened the door to countless possibilities in studying gene function as these cells are able to contribute to the germ line when integrated into the host blastocysts (Jaenisch, 1988). Murine embryonic stem cells are permanent cell lines, established from blastocysts of the inner cell mass of preimplantation mouse embryos. The pluripotent state of ES cells can be maintained *in vitro* by culturing in medium supplemented with a soluble factor called Leukaemia inhibitory factor or differentiation inhibiting factor, or by co-culturing with mitotically inactivated feeder cells, such as embryonic fibroblasts or the fibroblastic STO cell line (Amano *et al.*, 2006). When ES cells are returned to the embryonic environment, they can resume normal development and contribute to all cell lineages including the germ line and the resulting chimeric mice. All the existing ES cell lines are derived from male embryos because the XY karyotype appears to be more stable in culture than the XX karyotype. Also, male mice are hemizygous for X- or Y- chromosome linked genes and only a single copy of these genes needs to be inactivated for phenotype analysis (Fung-Leung and Mak, 1992).

1.10.3 Designing of HR vectors

The first step in the targeting strategy begins by generating a targeting vector, containing the desired gene mutation and homologous flanking sequences. The targeting vector is

subsequently introduced into ES cells by electroporation. In most cells the targeting vector inserts randomly into the embryonic stem cell genome. However, in a few cells homologous DNA sequences in the targeting vector pair with homologous sequences in the embryonic stem cell chromosomal DNA and recombine, introducing the mutation into the genome. After introduction into ES cells, rare integration events are selected for and enriched to form a homogenous population. The selected cells are subsequently injected into a blastocyst and implanted into a foster mother. The offspring is screened for the desired gene followed by the crossing of homologous F1 generation. This leads to the germline transmission of the ES cell genome containing the desired gene modification (see figure 1.15).



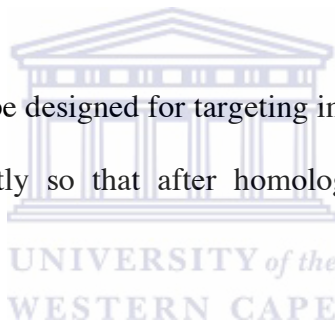
Since both the transfection efficiency and targeting frequency of such a vector can be low, it is desirable to include other components in such a vector, such as positive and negative selection markers that provide strong selection for the targeted recombination product. The positive selection marker may serve a dual function. Firstly, its primary purpose is a selection marker to isolate rare transfected cells that have stably integrated DNA, which occurs at a frequency of about one in every 10^4 cells. Secondly, to serve as a mutagen, disrupting a gene sequence if it is inserted into the coding exon of a gene or replacing a coding exon.

Apart from targeting frequency and targeting efficiency, fidelity of targeted recombination raises several concerns. In contrast to intrachromosomal recombination, which seems very accurate in mammalian cells (Stachelek and Liskay, 1988) several

lines of evidence suggested that targeted recombination may induce additional mutations with high frequency (Thomas and Capecchi, 1987 and Doetschman *et al.*, 1987).

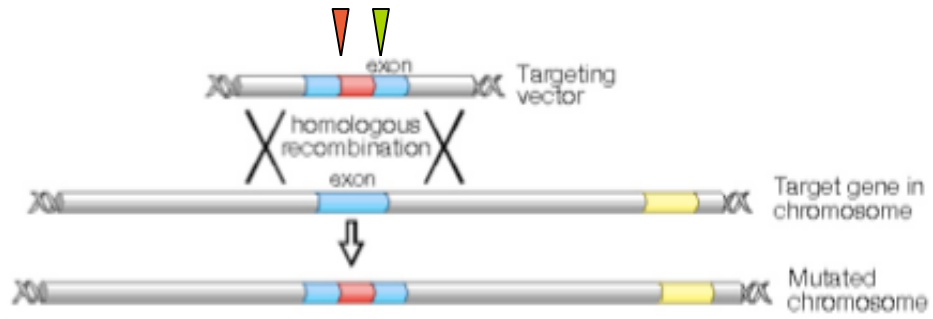
Zheng *et al.* (1991) tested the accuracy of gene targeting by analysing 44 independent targeted recombinants at the hypoxanthine phosphoribosyl transferase (HPRT) locus in a human fibroblast cell line and in mouse embryonic stem cells. They surveyed 80 kilobases around the sites of recombination by using chemical cleavage of mismatches and found only 2 mutations, one in each cell type. Thus, gene targeting in mammalian cells can be extremely accurate.

Different types of vectors can be designed for targeting in mammalian cells. These vector types are configured differently so that after homologous recombination they yield different integration products.



1.10.3.1. Replacements vectors

The principal consideration in the design of a replacement vector is the type of mutation generated. Secondary, yet importantly, considerations relating to the selection and screening techniques to isolate recombinant clones. The recombinant alleles generated by a replacement vectors typically have a selection cassette inserted into a coding exon or replacing part of the locus. Exon interruption and small deletions will not necessarily ablate the function of the target gene to generate a null allele. Consequently, it is necessary to confirm that the allele, which has been generated, is null by RNA and/or protein analysis.

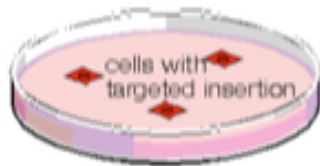


Design principle of promoterless targeting vector. *Neomycin phosphotransferase* gene (red) is used as an example of a positive selectable gene. The *Neo* open reading frame (ORF) is inserted in frame into a downstream coding exon (blue) of the target gene. This strategy results in the expression of a hybrid target-*Neo* fusion.

▼ ATG

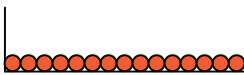
▼ Polyadenylation signal

ES Cells transfected with a targeting vector

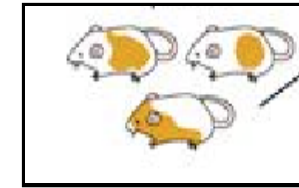
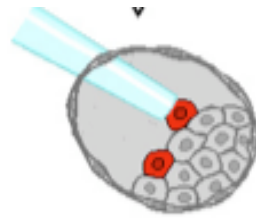


Enrichment of rare targeted ES cells

Pure population of targeted ES cells



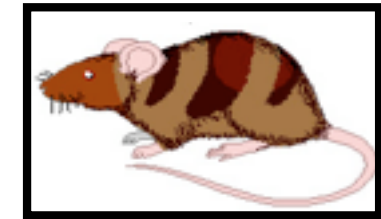
Injection of ES cell into blastocyst



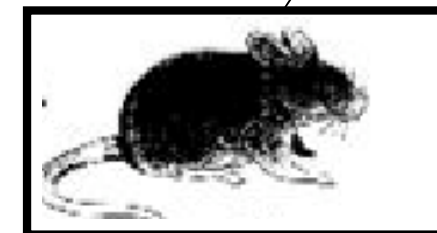
Germline transmission of ES cell genome containing targeted modification

Breed with +/+ animals

Test offspring for presence of gene



Chimeric mouse



Implantation into foster mother



Figure. 1.15 Schematic representation of the steps involved in producing a 'knock-out' mouse

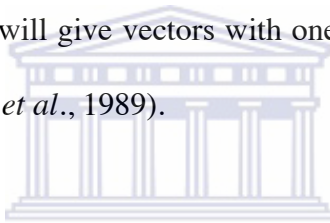
Disruption or deletion of the coding sequences by the positive selection marker will in most instances ablate a gene's function. However, in some situations a truncated protein may result which retains some biological activity. Null alleles are more likely to be generated by deleting or recombining a selection cassette into more 5' exons rather than exons that encode the C-terminus of the protein, since under these circumstances minimal portions of the wild-type polypeptide would be made.

A consideration when a selection marker is to be inserted into an exon is that the length of an exon can influence RNA splicing (Robberson *et al.*, 1990). An artificially large exon created by the insertion of a selectable marker may not be recognized by the splicing machinery and could be skipped. Thus, transcripts initiated from the endogenous promoter may delete the mutated exon from the mRNA species or even additional exons. If a skipped exon is a coding exon whose nucleotide length is not a multiple of three (codon) the net result will be both a deletion and a frame-shift mutation of the gene, which will often generate a null allele. However, if spliced out, this would result in a protein with a small in-frame deletion, which may retain partial or complete function. For most purposes it is advisable to delete portions or the entire target gene so that the genetic consequences are not ambiguous.

1.10.3.1.1 Screening for targeted events

One common screening tool for targeted clones is based on the Polymerase Chain Reaction (PCR), which can be designed to detect the juxtaposition of the vector and the target locus (Joyner *et al.*, 1989). This is accomplished by using one primer, which

anneals to the positive selection marker in the targeting vector and a second primer, which primes from the target chromosomal sequences just beyond the homologous sequences used in the vector. The efficiency of such a PCR reaction is related to the distance between the unique primer site in the vector (usually in the positive selection marker) and the sequences external to the homologous elements of the vector as well as the specific composition of the DNA sequence to be amplified. The amplified product should be in the 0.5 to 2.0 kb range. Thus replacement vectors configured for screens by PCR require the positive selection marker to be inserted at an asymmetric location near one end of the homologous sequence while still leaving sufficient homology for the formation of a crossover. This will give vectors with one long arm and one short arm of homologous sequences (Joyner *et al.*, 1989).

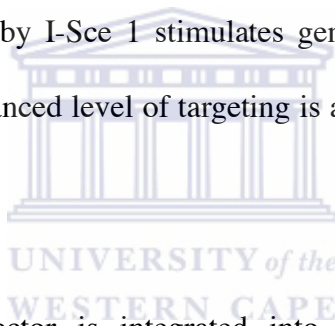


Another common screen for clones targeted with gene replacement vectors is by Southern blot analysis. It is important to design the vector and identify unique probes flanking the homologous sequences in the vector and restriction sites so that the analysis is both unambiguous and can discriminate the various categories of recombinant clones. Since a replacement vector should be linearized before transfection into the cells at a site outside the homologous sequences, the cloning steps must incorporate at least one unique site outside the homologous sequences.

1.10.3.2. Insertion Vectors

The basic elements of an insertion vector are the same as those in a replacement vector. The major difference between the two vector types is that the linearization of an insertion

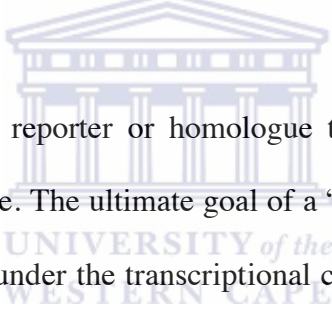
vector is made in the homologous sequences. An insertion vector undergoes single reciprocal recombination, vector insertion with its homologous chromosomal target, which is stimulated by double-strand break or gap in the vector. The repair of DNA double-strand breaks (DSBs) is necessary for the maintenance of genomic integrity in all organisms. In *S. cerevisiae*, repair of DSBs occurs primarily by homologous recombination and requires members of the Rad52 epistasis family (Smith and Rothstein, 1995) and in *E. coli* the RecBCD enzyme (Smith *et al.*, 1995). Studies by Smith *et al.*, 1995, in mammalian cells utilizing the I-Sce 1 endonucleases have demonstrated that in some immortalized cell lines DSBs in chromosomal DNA are recombinogenic. They also found that a DSB introduced by I-Sce 1 stimulates gene targeting at a selectable neo locus at least 50-fold. The enhanced level of targeting is achieved by transient expression of the I-Sce 1 endonuclease.



Since the entire insertion vector is integrated into the target site, including the homologous sequences of the vector, the recombinant allele generated by such a vector becomes a duplication of the target homology separated by the heterologous sequences in the vector backbone. Since insertion vectors duplicate the homologous sequences in the vector, the position of the selectable cassette may not play a critical role in mutating the gene. However, if the selection cassette is cloned into the only exon of the gene, after vector insertion the targeted allele will contain one normal and one artificially large exon. Skipping of this exon may result in normal transcripts being generated from such a recombinant locus at a low frequency (Moens *et al.*, 1992).

1.10.3.3. ‘Knock-in’ targeting vectors

“Knock-in” has been defined by the use of gene targeting to replace an endogenous gene with another, such as a homologue or a marker for gene expression (Hanks *et al.*, 1995). In mouse ES cells, “knock-in” experiments are used to place a transgene (cDNA) contained in a targeting vector, under the transcriptional control of an endogenous gene. When the endogenous gene is replaced with a homologue, it can be used to assess whether members of the same gene family have an identical biological function when expressed in the same spatial and temporal pattern. This can be achieved with the use of reporter genes, such as *Lac Z* or GFP (Stacey *et al.*, 1994).



The effect of a “knocking-in” reporter or homologue typically results in the loss-of-function of the endogenous gene. The ultimate goal of a “knock-in” targeting experiment is to place the gene of interest under the transcriptional control of the endogenous locus. Optimally knock-in constructs should be designed so that no endogenous sequences are deleted so that regulatory sequences associated with positive selectable markers can be deleted after the targeting event. Subsequently “knock-in” experiments have been performed using conventional gene targeting approaches, usually in combination with *Cre-loxP* system to remove the selectable cassette (Hanks *et al.*, 1995).

1.10.4 The use of site-specific recombinases

A number of bacterial and yeast elements encode recombinase enzymes that cleave DNA at specific target sequences, and then cleave it to DNA of a second site. This simple but

elegant reaction results in a precisely defined recombination between two appropriate target sequences. Three principal site-specific recombinases have been used to manipulate DNA in heterologous environments, *Cre*, *FLP* and *R*. *Cre*, *FLP* and *R* all belong to the λ integrase family of recombinases and show striking similarities, not only in the types of reaction they can carry out, but also in their target sites and mechanism of recombination.

The use of site-specific recombinase systems has revolutionized our ability to genetically manipulate ES cells and mice. Recent advances using the *Cre-LoxP* and *FLP-FRT* systems have now made it possible to generate ‘clean’ germline mutations following a single gene targeting event, as well as to activate or inactivate genes in a conditional manner in the living mouse (Feil, 2007). Not only can target gene mutations be induced in a spatially and temporally restricted fashion, but also lineage tracers can be activated in a specific progenitor population to chart cell fate directly in the wild type and mutant mouse (Joyner and Zervas, 2006).

1.10.5 Applications of gene targeting

Animal models are required for an effective drug development program, evaluation of the gene therapy approach, studying the molecular basis of inherited and acquired diseases and understanding the functions of genes during development. Such models can be developed by standard transgenic techniques in which a cloned DNA fragment is injected into a fertilized mouse egg. This standard technique is limited to gain-of-function only

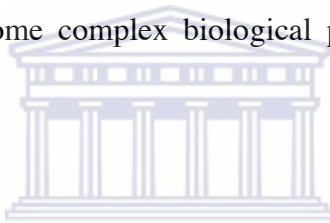
and has two drawbacks: (i) random integration of the injected DNA and (ii) variability in copy numbers. These drawbacks may result either in poor, or no expression or over-expression of a transgene and hence the interpretation of the experiments may become difficult. On the other hand, the gene targeting technology in mice by homologous recombination results in generation of loss-of-function of genes in a pre-selected locus.

In general, mice with single locus disruption show a wide range of phenotypes ranging from normal or less severe to phenotypes lethal for embryonic development. It was surprising that cyclin D1 which is essential for G1 progression when inactivated did not arrest most cells, since these mice are able to produce viable offspring (Baldin *et al.*, 1993). The unexpected result, however, was that they showed severe retinopathy, malformation of the jaw and impaired mammary gland development. Although cyclin D1 is predominantly expressed in kidney and salivary glands this suggests that cyclin D1 is not essential for their development.

Several knockout mice carrying a single disrupted gene produced a minimal phenotype even though the gene in question is abundantly expressed or found to be essential. To explain this unexpected result, a gene function redundancy theory was proposed. The theory is now amply supported by double or triple knockout experiments. For instance, the abnormalities resulting from knocking out either p130 or p137 protein alone (which are expressed in a wide variety of cell types and inhibit cell proliferation) were surprisingly limited. However the compound mice lacking p130 and p107 exhibited severe abnormalities in bone and limb development and neonatal lethality (Cobrinik *et*

al., 1996). Similarly, either retinoblastoma gene or p107 genes produced more pronounced effects in the central nervous system and the liver (Lee *et al.*, 1996).

Similar to any other field of science, there are many more questions than answers in gene disruption techniques. Of course the differences between man and mouse cannot be ignored. For instance, some Xeroderma pigmentosum patients show progressive neurological degeneration (XPA), whilst in mice carrying the disrupted gene no sign of the disease was visible (Marchetto *et al.*, 2006). Recently, there have been also some concerns or criticisms raised about the validity and interpretations of the null mutation experiments, particularly in some complex biological processes such as memory and learning.



Since it is well known that a single gene alteration affects the expression of many other genes, it is possible that a simple gene “knock-out” may alter the entire developmental program of an organism. The “knock-out” mice do not reveal which of these genes are affected and hence the interpretation could be misleading. Although some of these questions cannot be answered, it is clear that more modified methods and additional experiments are required to address complex biological processes.

Whatever the limitations could be, “knock-out” mice are a useful tool which eventually give us new insights into immunology, cancer, development, aging, psychiatric disorders and the complex central nervous system. Further modification of the conditional or tissue

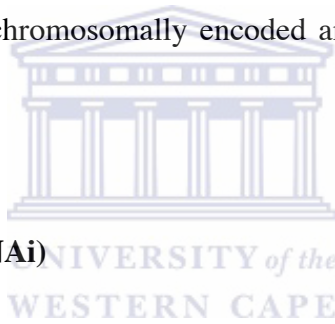
specific knockout technique may provide a better opportunity for the gene therapy approach to correct genetic as well as sporadic human disorders.

1.11 Antisense RNAs

The first natural antisense RNAs were discovered in 1981 independently in two different laboratories. Tomizawa and Nordstrom both found that small plasmid-encoded RNA regulators control the copy number of the *E. coli* plasmids ColEI and RI respectively (Tomizawa *et al.*, 1981 and Stougaard *et al.*, 1981). Antisense RNAs are small, diffusible, highly structured RNAs that act via sequence complementarity on target RNAs called sense RNAs. In eukaryotes, some processes like splicing or editing also make use of complementary small RNAs, however, these RNAs are not independent regulators, and are therefore not regarded as *bona fide* antisense RNAs. In the classical sense, antisense RNAs are encoded in *cis*, i.e. they are transcribed from a promoter located on the opposite strand of the same DNA molecule, and are therefore fully complementary to their target RNAs (reviewed in Werner, 2005).

Over the past years a number of antisense RNAs were detected that are encoded in *trans*. These molecules reveal only partial complementarity to their target RNA and have more than one target. The sense RNAs is mostly mRNAs encoding proteins of important/essential functions. In the majority of cases, antisense RNA action entails post-transcriptional inhibition of the target RNA function.

Naturally occurring antisense RNAs are between 35 and 150 nt long and comprise between one and four stem loops. Efficient antisense RNAs have 5-8 nt GC-rich loops. Stems that are important for metabolic stability are often interrupted by bulges that prevent dsRNase degradation and facilitate melting upon antisense/sense RNA interaction (Hjalt and Wagner, 1992). Recognition loops of the antisense RNA or complementary sense RNA often contain a YUNR motif forming a U-turn structure; a sharp bent in the RNA phosphate backbone, thus providing a scaffold for the rapid interaction with the complementary RNA (Franch *et al.*, 1999). Some antisense RNAs (those involved in plasmid copy number control and post-segregational killing) are unstable, whilst others (most chromosomally encoded and a few phage and transposon antisense RNAs) are stable.



1.12 Interference RNA (RNAi)

The term RNA interference (RNAi) was originally used to describe antisense RNA inhibition of gene expression. RNAi assumed a more specialized definition when it was shown that dsRNA molecules are potent homology-dependent inhibitors of gene expression (Fire *et al.*, 1998).

RNAi (RNA interference) refers to the introduction of homologous double stranded RNA (dsRNA) to specifically target a gene's product, resulting in a null or hypomorphic phenotype. Introduction of dsRNA has recently been showed to produce specific phenocopies of null mutations in such phylogenetically diverse organisms as plants

(Hamilton & Baulcombe, 1999), nematodes (Bosher *et al.*, 1999), *Drosophila* (Kennerdell and Carthew, 2000) trypanosomes (Ngo *et al.*, 1998) and mice (Wianny & Zernicka-Goetz, 2000). The discovery of RNAi was followed by studies of its mechanisms.

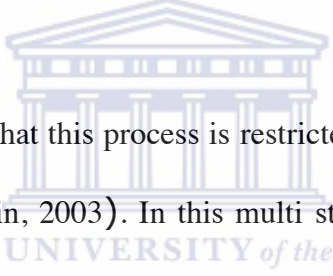
Work in *C. elegans* indicated that RNAi involved at least two important steps. The first step involved the generation of a sequence specific silencing agent. A strong candidate for this agent was a special class of short RNAs that was originally reported by Baulcombe, 1999. They found that Arabidopsis plants that are undergoing transgene- or virus induced post-transcriptional gene silencing (PTGS) contained 21-25-nucleotide (nt) long RNAs that were complementary to both strands of the silenced gene and that have been processed from a long dsRNA precursor. Other investigators revealed that small 21-23-nt dsRNA were associated with silencing in *C. elegans* (Bosher *et al.*, 1999) and *Drosophila* (Kennerdell and Carthew, 2000).

The cloning and sequencing of these RNAs revealed that they had a very specific structure: 21-23-nt dsRNA duplexes with symmetric 2-3-nt 3'-end overhangs and 5'-phosphate and 3'-hydroxyl groups (Elbashir *et al.*, 2001). This structure is reminiscent of an RNase like enzymatic cleavage pattern, which led to the identification of the highly conserved Dicer family of RNase III enzymes as the mediators of the dsRNA cleavage.

The evidence that these short RNAs determined RNAi specificity came from studies in *Drosophila*, in which small RNAs that were isolated from cells undergoing silencing

were shown to be efficient to induce specific silencing in naïve *Drosophila* Schneider-2 (S2) cells (Ishizuka *et al.*, 2006). In addition, when synthetic 21- and 23-nt RNA duplexes were added to the lysate they were able to guide efficient sequence-specific mRNA degradation. These RNAs were named short interfering RNAs (siRNAs). When RNAi was first discovered in the worm, researchers immediately began using the technology to analyse the function of genes. A similarly rapid adoption of siRNA technology followed the definition of the structure of the siRNAs and their ability to silence genes in mammalian cells.

1.12.1 Mechanism of RNAi



Several studies have indicated that this process is restricted to the cytoplasm (Agrawal *et al.*, 2003, Dudley and Goldstein, 2003). In this multi step process, Dicer cleaved long dsRNA to produce siRNAs. These siRNAs are incorporated into a multiprotein RNA inducing silencing complex (RISC) (Nykanen *et al.*, 2001). There is a strict requirement for the siRNAs to be 5' phosphorylated to enter into RISC, whilst siRNAs that lack a 5' phosphate are rapidly phosphorylated by an endogenous kinase. The duplex siRNA is unwound, leaving the antisense strand to guide RISC to its homologous target mRNA for endonucleolytic cleavage. The target mRNA is cleaved at a single site in the centre of the duplex region between the guide and the target mRNA, 10 nt from the 5' end of the siRNA (see figure 1.16). Endogenously expressed siRNAs have not been found in mammals. However, the related micro (mi) RNAs have been cloned from various organisms and different cell types (Pasquinelli, 2002). These short RNA species (22 nt)

are produced by Dicer cleavage of longer (70 nt) endogenous precursors with imperfect hairpin RNA structures.

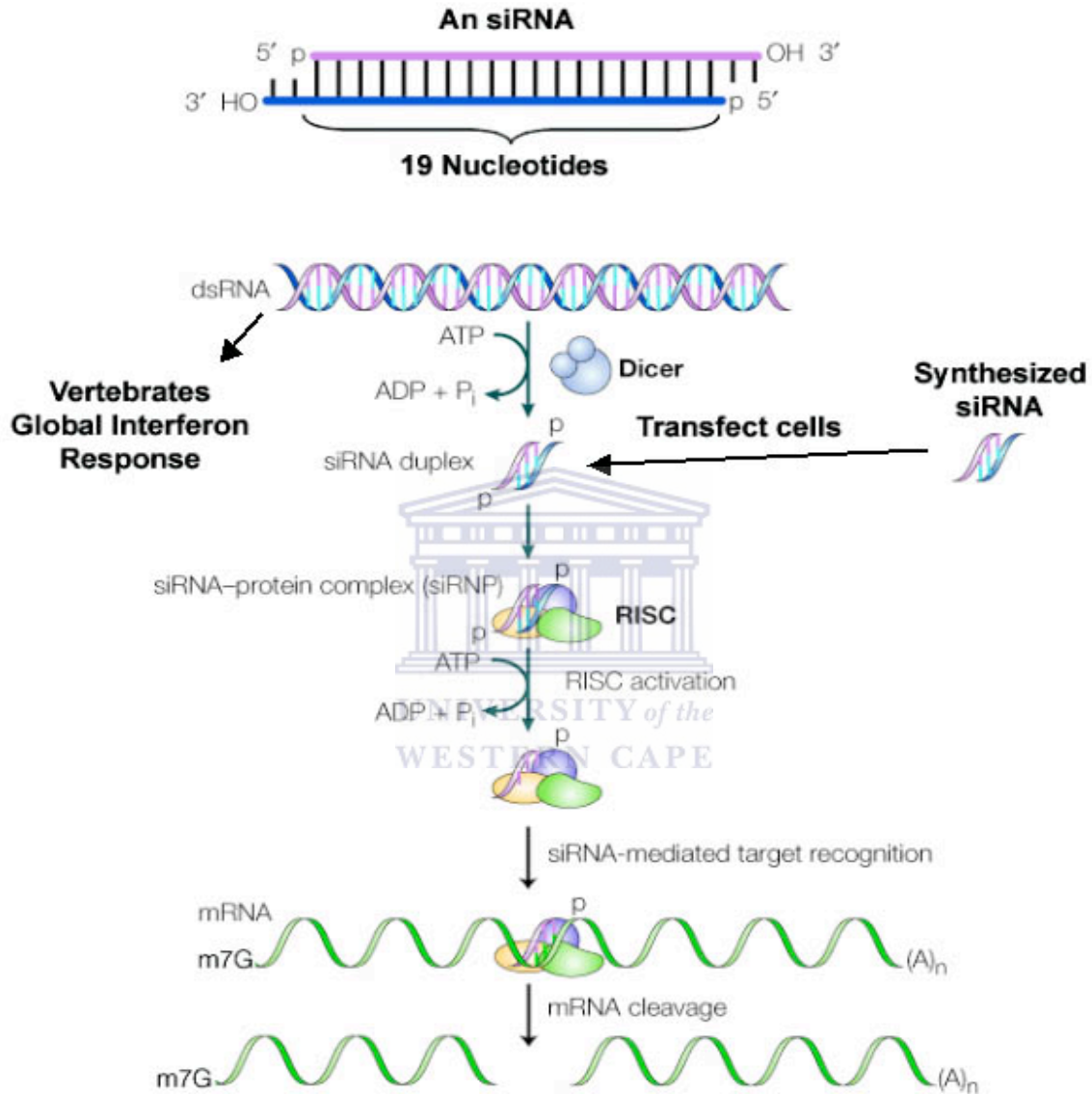


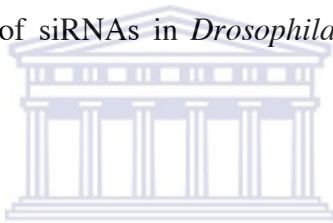
Figure 1.16 Represents a working model of the RNA interference mechanism (taken from Dykxhoorn *et al.*, 2003).

The miRNA are believed to bind to sites that have partial sequence complementarity in the 3' untranslated region (UTR) of their target mRNA, causing repression of translation

and inhibition of protein synthesis (Pasquinelli, 2002). In addition to Dicer, other PAZ/PIWI Domain Proteins (PPD) is likely to function in both pathways (Grishok *et al.*, 2001).

1.12.2 Dicer

From the similarity between the siRNA and the products of RNase III, which cleaves double-stranded RNA into discrete sizes, Bass, (2000), predicted that an RNase III enzyme were involved in the generation of siRNAs. Such an enzyme was indeed found to have a role in the generation of siRNAs in *Drosophila* named Dicer Bernstein *et al.*, (2001).

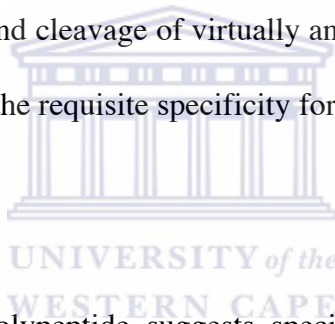


Dicer may be most accurately regarded as a RNA maturation nuclease rather than a degradative nuclease. In its first role, Dicer carries out the maturation of small regulatory RNAs, secondly, Dicer cleaves virtually any dsRNA to provide a small, precisely sized duplexes that are incorporated into a complex that is responsible for homology-dependent RNA degradation.

Dicer is also an important participant in developmental processes through its processing of precursors to small regulatory RNAs. An initial indication of Dicer involvement in development was provided by the affect of a mutation (*Caf*) in one of the *A. thaliana* Dicer genes, which causes defects in flower development and unregulated proliferation of

floral meristem tissue (Jacobsen *et al.*, 1999). Other studies established an essential role for Dicer in germ-line development in *C. elegans* (Grishok *et al.*, 2001).

Dicer is similar to bacterial RNase III in that it can cleave dsRNA in an apparent non-specific manner. The siRNA products possess two nucleotide 3' overhangs, with 5' phosphate, 3'-hydroxyl termini. On the basis of common domain features, the type of product termini, and the divalent metal ion requirement, it is expected that the chemistry of the phosphodiester hydrolysis is the same as that used by bacterial RNase III (Carmell and Hannon, 2004). The sequence non-specificity would be a requirement of the RNAi pathway to allow recognition and cleavage of virtually any dsRNA. The 21 bp size of the siRNA is sufficient to provide the requisite specificity for a unique target sequence within the eukaryotic cytoplasm.



The structure of the Dicer polypeptide suggests specific functional behaviours. The existence of two catalytic domains, coupled with the observation that the dimer interface of the bacterial holoenzyme involves extensive catalytic domain contacts, predicts a dimeric structure for the holoenzyme. A double-stranded ribonuclease purified from *Dictyostelium*, which is likely to be Dicer, exhibits a native gel electrophoretic mobility of about 450 kD (Novotny *et al.*, 2001). Assuming the absence of unusual structural features and/ or associated polypeptides, the size is consistent with a homodimeric structure. However, another scenario is possible, where intramolecular association of the two catalytic domains would provide a dsRNA-binding cleft, thus obviating the need for intermolecular association.

Crystallographic data and molecular modelling suggest how two bacterial RNase III catalytic domain homodimers, bound to adjacent positions on a dsRNA, can provide precisely sized products (Blaszczyk *et al.*, 2001). It has been proposed that one of the two catalytic domains in ~Dicer is disabled through mutation of a conserved residue (Blaszczyk *et al.*, 2001). If so, then it can be argued that the selective inactivation would allow production of 21 bp dsRNA instead of approximately 11 bp species. As mentioned earlier, the longer product size ensures that the siRNA containing RISC complex would have the requisite specificity for the RNA targets.

The biochemical properties of purified recombinant human Dicer have been studied. Human dicer requires a divalent metal ion (Mg^{2+} , Mn^{2+} , or Co^{2+}) for activity, with cleavage of dsRNA directly providing the mature approximately 21-23 bp siRNA species (Provost *et al.*, 2002). Prior treatment with proteases enhances Dicer catalytic activity for reasons that are not clear at this point (Zhang *et al.*, 2002). Similar to other RNase III orthologs, Dicer can bind dsRNA without concomitant cleavage in the absence of divalent metal ion, or alternatively, at lowered temperature or elevated salt concentrations (Provost *et al.*, 2002, Zhang *et al.*, 2002). Human Dicer does not require ATP to cleave dsRNA (Provost *et al.*, 2002), which is consistent with the ATP independence of *E. coli* RNase III, which nonetheless can bind ATP (Chen *et al.*, 1990).

Immunofluorescence analysis has localized Dicer to the endoplasmic reticulum (ER), with no evident nuclear staining (Provost *et al.*, 2002). The ER location would place Dicer in proximity to the RISC complex (see figure 1.17), which is associated with the

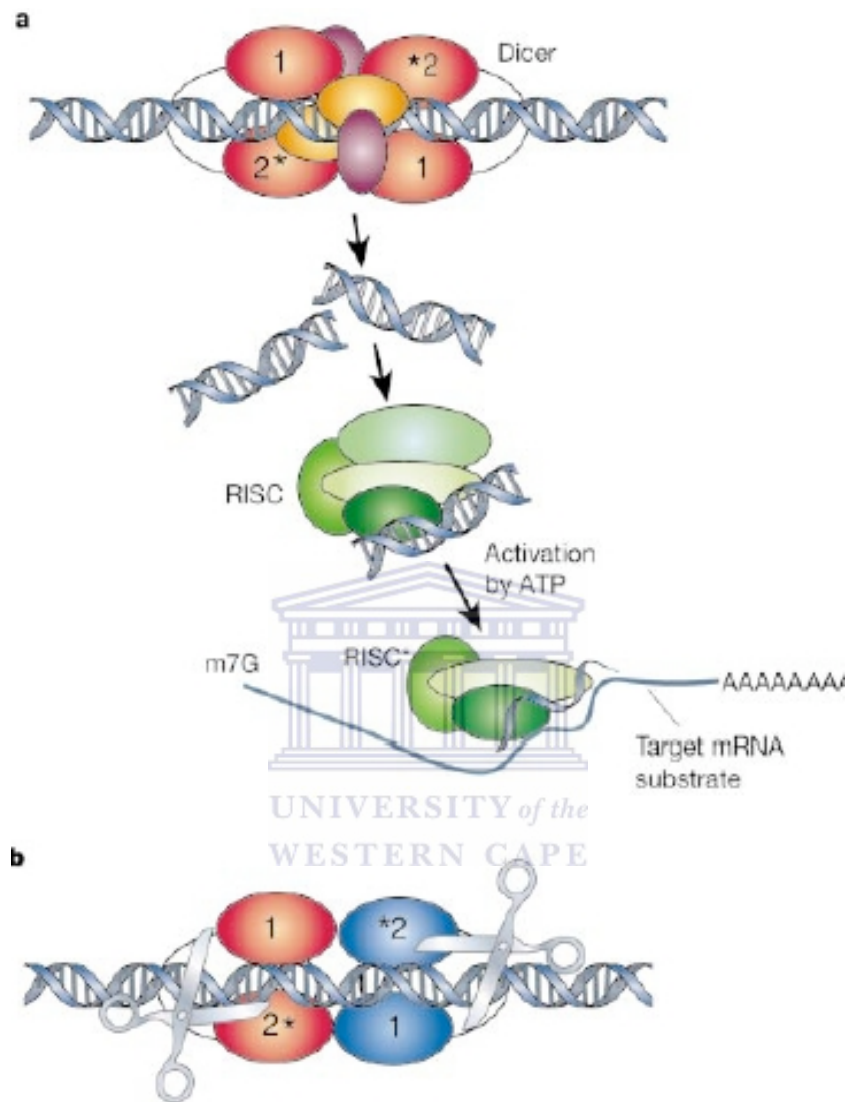


Figure 1.17 Represent the interaction of Dicer and RISC (RNA-induced silencing complex) (a) RNAi is initiated by the Dicer enzyme which processes double-stranded RNA into 22-nucleotide small interfering RNAs. The siRNAs are incorporated into a multi-component nuclease, RISC (green). RISC then uses the unwound siRNA as a guide to substrate selection (b) Diagrammatic representation of Dicer binding and cleaving dsRNA (taken from Dykxhoorn *et al.*, 2003).

translational machinery (Hammond *et al.*, 2000). The apparent lack of nuclear localization suggests that the microRNA precursors may be processed in the cytoplasm.

In addition to having two RNase III domains, Dicer has a helicase domain and a PAZ domain. The function of the amino-terminal helicase domain of Dicer has not yet been defined. Purified human Dicer lacks a demonstrable ATPase activity characteristic of helicases (Zhang *et al.*, 2002). The introduction of a K70A mutation in the conserved loop of the ATPase/ helicase domain of human Dicer, which is expected to inactivate nucleotide binding, has no effect on dsRNA cleavage (Zhang *et al.*, 2002).

1.12.3 Role of RNA pol III



Plasmid based expression systems using RNA polymerase III (pol III) promoters that produce short RNA species and that do not trigger significant interferon responses have been developed by several groups (Wadhwa *et al.*, 2004, Amarzguioui *et al.*, 2005, Timmons, 2006). Two pol III promoters have been used predominantly, the U6 promoter and the H1 promoter. Both of these promoters belong to the type III class of pol III promoters.

Most RNA pol III promoters have sequences downstream of the transcription start site that are essential for transcription (class I and class II), Several class III promoters lack downstream transcription elements. Paule and White. (2000), showed that the deletion of the sequences downstream of the +1 transcription start site in the mouse and the human

U6 promoters has no affect on the level of transcription. Although the U6 and H1 promoters contain the same set of cis-acting elements (octamer motif, Staf-binding site, proximal sequence element (PSE) and TATA motif), the H1 promoter has a more compact organization. The U6 promoter has a requirement for a guanosine in the +1 position, whereas the H1 promoter is much more permissive. In addition, RNA pol III recognizes a simple cluster of four or more T residues as a termination site in the absence of other factors (Dykxhoorn *et al.*, 2003).

Typically, the objective of using siRNAs is to silence a specific gene in a mammalian cell, therefore the base-pairing region for a siRNA must be selected carefully to avoid chance complementarity to an unrelated mRNA (Svoboda, 2007). BLAST sequence analysis programs should be used to screen candidate siRNA sequences for specificity, although this recommendation is based on the assumption that the sequence database is complete. To a certain degree RNAi can tolerate siRNA-mRNA mismatches with 1- and 2-bp mismatches that only partially reduce the rate and extent of cleavage, particularly if the mismatches occur near the end of the duplex. It has been suggested that the first 50-100 nt of a cDNA sequence downstream of the translation start site should be used to target a gene, and that 5' or 3' UTRs, as well as the region around the start site should be avoided, as they might be too rich in protein binding sites (Qiu *et al.*, 2005). However, it is not yet known if any mRNA region is most optimal for siRNA targeting.

McManus and Sharp, 2002, summarized in table form a list of genes that have been successfully targeted by RNAi in regions that are distributed throughout the mRNA,

including the 3'UTR. However, targeting different regions of a given mRNA might give different results. Holen *et al.*, 2002, carried out limited tiling of different siRNA across a region of the human coagulation trigger factor gene (TF). This study indicated positional effect at the level of codon resolution; that is, shifting the siRNA target site by only three nucleotides at a time resulted in different degrees of silencing. This study indicated that mRNA structure might govern accessibility to the siRNA. Alternatively, the sequence composition of siRNA could influence its activity *in vivo*.

Conventional methods of gene targeting like homologous recombination and antisense oligonucleotides are fast making way for siRNAs Bertrand *et al.*, 2002, compared the efficiency of a nuclease resistant antisense oligonucleotide and of siRNA both being targeted against the Green Fluorescent Protein (GFP) in cell culture and *in vivo*. Using Cytfectin GSV to deliver both inhibitors, the siRNAs appear to be quantitatively more efficient and its effect longer lasting in cell culture. In mice only activity of siRNA was observed but not of antisense oligonucleotides. The absence of efficiency of antisense oligonucleotides was probably due to their lower resistance to nuclease degradation.

The most interesting aspects of RNAi are the following; dsRNA, rather than single-stranded antisense RNA, is the interfering agent, it is highly specific and remarkably potent. Only a few dsRNA molecules per cell are required for effective interference and also the interfering activity (and presumably the dsRNA) can cause interference in cells and tissues far removed from the site of introduction.

1.12.4 Applications of RNAi

Many viruses have a genetic blueprint made from RNA, rather than DNA. Upon infection of a cell, they make double-stranded copies of their genetic material. In response the RNAi pathway strikes back. An enzyme known as Dicer first degrades the double-stranded viral RNA into small segments, each around 22 bases long. These segments known as small interfering RNAs or siRNAs then separate into single strands and some bind to intact stretches of single-stranded viral RNA. Finally, proteins target this tagged viral RNA and destroy it (Silva *et al.*, 2002). As a result, RNAi shuts off the key viral genes, potentially stopping infection. Biologists are exploiting RNAi as an experimental tool to find out what genes do. When a gene is activated, its sequence is read to produce messenger RNA (mRNA), which contains the information necessary to manufacture a particular protein. So by using siRNA or double-stranded RNAs that correspond to a specific mRNA sequence, researchers can “trick” a cell into destroying this mRNA and silencing the gene in question.

In theory, RNAi could be used to treat any disease—forms of cancer, for instance cancers that is linked to an overactive gene or genes. At present, most of the clinical interest lies in applying RNAi in its natural role, as a means of combating pathogenic viruses by disabling their RNA. One of the obvious targets is HIV, a virus for which there is no cure and no vaccine. Coburn and Cullen, 2002, introduced siRNAs against two HIV genes into the human immune cells that are destroyed by the virus. The siRNAs allowed these cells to resist viral replication better than those that had not been triggered to undergo RNAi.

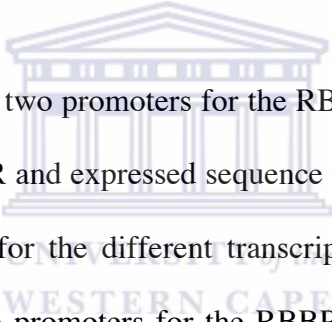
Meanwhile, other researchers have shown that, in culture of human cells, RNAi can similarly combat viruses as diverse as respiratory syncytial virus (Bitko and Barik, 2001) and those that cause influenza (Ge *et al.*, 2003) and polio (Gitlin *et al.*, 2002).

Kapadia *et al.*, (2003) generated multiple siRNAs targeting various regions of the hepatitis C virus (HCV) subgenomic replicon sequence. These siRNAs were transfected into a Huh-7 cell line that stably expressed the HCV RNA replicon. Two of these siRNAs showed the greatest specific inhibition of HCV RNA replication. These two were further tested for their ability to suppress HCV RNA and protein expression. HCV protein expression level was shown to be significantly reduced whilst similar results were seen at the mRNA level. Viral replication was also inhibited. These results suggest that RNAi might represent a new approach for the treatment of HCV infection. In the current study the RNAi technology will be used to target the expression of the RBBP6 gene using a plasmid based system. Following the identification of suitable siRNAs to silence the expression of RBBP6, the effect on RBBP6 expression will be investigated using primary cell lines. Once it has been established that the expression of the gene has been silenced, the physiological outcome of this silencing will be investigated in terms of apoptosis and the cell cycle.

1.13 AIMS

The DWNN gene was isolated from a genetic screen to identify novel components of the antigen processing and presentation pathway via MHC class I using a promoter-trap

strategy and was later found to be located on human chromosome 16p12.2, upstream of the previously identified RBBP6/PACT/P2P-R gene. Previous work showed that the CHO cell line 16(3xHA8)3.5hr, from which DWNN was identified, to be resistant to staurosporine induced apoptosis (Pretorius, 2000, MSc thesis). Recent work done by Gao and Scott, 2002, showed that over-expression of P2P-R results in cell cycle arrest at prometaphase and similarly promotes camptothecin-induced apoptosis in a p53 independent manner Gao and Scott, 2003. Li *et al.*, 2007, showed that by ablating expression of the PACT gene, increased apoptosis in mice and similarly increased ubiquitination of p53 mediated by Hdm-2.



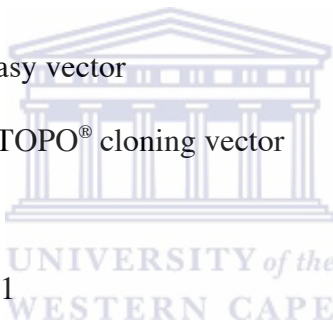
Genetic analysis also identified two promoters for the RBBP6 gene, Promoter 0 (P0) and Promoter 1 (P1). From RT-PCR and expressed sequence tags (EST) data both the P0 and P1 promoters are responsible for the different transcripts of RBBP6. This thesis will investigate the presence of two promoters for the RBBP6 gene and study the effect on apoptosis induced by camptothecin and the cell cycle following the silencing of RBBP6 using RNAi.

The aims of this thesis are as follows

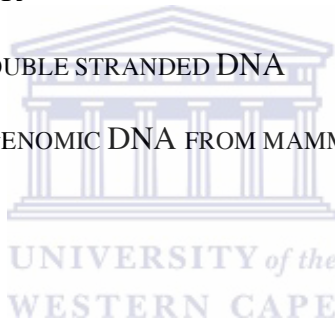
- To investigate the activity of the RBBP6 promoters *in vivo* before and after camptothecin-induced apoptosis.
- To construct several siRNA vectors targeting the RBBP6 gene
- Investigate the effect on RBBP6 expression as mediated by the siRNA vectors.
- Investigate the physiological role of RBBP6 in apoptosis and the cell cycle.

CHAPTER 2: MATERIALS AND METHODS

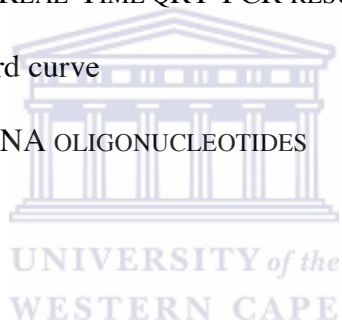
- 2.1 MATERIALS AND SUPPLIERS
- 2.2 GENERAL STOCK SOLUTIONS AND BUFFERS
- 2.3 BACTERIAL CULTURE
 - 2.3.1 Strains
 - 2.3.2 Selection
 - 2.3.3 Storage of bacterial strains
- 2.4 CLONING VECTORS
 - 2.4.1 pGEM-T Easy vector
 - 2.4.2 pCR[®]-XL-TOPO[®] cloning vector
 - 2.4.3 pEGFP-C1
 - 2.4.4 pDsRed1-C1
- 2.5 PREPARATION OF COMPETENT *E. COLI* CELLS FOR TRANSFORMATION
- 2.6 TRANSFORMATION OF *E. COLI* CELLS
- 2.7 PREPARATION OF PLASMID DNA
 - 2.7.1 Small-scale preparation (minipreps)
 - 2.7.2 Large-scale preparation
 - 2.7.3 Double CsCl/ethidium bromide fractionation
- 2.8 MANIPULATION OF PLASMID DNA
 - 2.8.1 Ethanol precipitation
 - 2.8.2 Phenol/chloroform extraction



- 2.8.3 Restriction enzyme digests
- 2.8.4 Ligation of DNA
- 2.9 AGAROSE GEL ELECTROPHORESIS OF DNA
 - 2.9.1 DNA molecular weight markers
 - 2.9.2 Purification of DNA fragments from agarose gels
- 2.10 POLYMERASE CHAIN REACTION (PCR) AMPLIFICATION
 - 2.10.1 Standard PCR
 - 2.10.2 PCR amplification of plasmid DNA
 - 2.10.3 Colony PCR
- 2.11 SEQUENCING OF DOUBLE STRANDED DNA
- 2.12 PREPARATION OF GENOMIC DNA FROM MAMMALIAN CELL LINES
- 2.13 CELL CULTURE
 - 2.13.1 Cell lines
 - 2.13.2 Tissue culture media
 - 2.13.3 Propagation and storage of cell lines
 - 2.13.4 Transfection of cell lines
- 2.14 IMMUNOFLUORESCENCE
 - 2.14.1 Fixation and permeabilization of cells
 - 2.14.2 Immunostaining of cells
- 2.15 FACS ANALYSIS
- 2.16 APOPTOSIS ASSAYS
 - 2.16.1 The screening of camptothecin as an inducer of apoptosis



- 2.16.2 APOPercentage™ apoptosis assay
- 2.16.3 Annexin V-PE assay
- 2.16.4 APO-Direct/TUNEL assay
- 2.17 CELL CYCLE ANALYSIS
- 2.18 RNA ISOLATION
- 2.19 AGAROSE GEL ELECTROPHORESIS OF RNA
- 2.20 cDNA SYNTHESIS
- 2.21 REAL-TIME QUANTITATIVE RT-PCR
- 2.22 QUANTITATION OF REAL-TIME QRT-PCR RESULTS
 - 2.22.1 The standard curve
- 2.23 ANNEALING OF siRNA OLIGONUCLEOTIDES



CHAPTER 2: MATERIALS AND METHODS

2.1 Materials and suppliers

40 % 19:1 Acrylamide: bis-acrylamide	Biorad
Agarose	Promega
Alexa Fluor 488 goat anti-rabbit IgG antibody	Molecular Probes
Alexa Fluor 594 goat anti-rabbit IgG antibody	Molecular Probes
Ammonium acetate	Merck
Ampicillin	Roche
AMPS (Ammonium persulphate)	Merck
Annexin V-PE apoptosis detection kit	BD Biosciences
APOPercentage™ assay kit	Bicolor Ltd
APO-Direct/TUNEL assay kit	BD Biosciences
Bacteriological agar	Merck
Big Dye v3.1 sequencing kit	Applied Biosystems
Boric acid	Merck
BSA (Bovine serum albumin)	Roche
Bromophenol blue	Sigma
Buffer saturated phenol	Invitrogen
Camptothecin	Sigma
Cell culture media and reagents	Gibco Life Technologies
Caesium chloride	Roche Diagnostics
Calcium chloride	Merck



Chloroform	BDH
DAPI (4', 6' -diamidino-2-phenylindole)	Sigma
DEPC (Diethyl Pyrocarbonate)	Sigma
DMSO (Dimethyl Sulphoxide)	Sigma
EDTA (Ethylene diamine tetra acetic acid)	Merck
Ethanol	BDH
Ethidium bromide	Sigma
First strand cDNA synthesis kit (AMV)	Roche
G418 (Neomycin sulphate)	Roche
GFX DNA purification kit	Promega
Glacial acetic acid	Merck
Glucose	Merck
Glycerol	BDH
Hydrochloric acid	Merck
Isoamyl alcohol	BDH
Kanamycin mono-phosphate	Roche Diagnostics
LightCycler FastStart DNA Master ^{PLUS} SYBR Green 1	Roche Applied Science
Lipofectamine 2000 transfection reagent	Invitrogen
Magnesium chloride	Merck
Manganese chloride	Sigma
Metafectene TM transfection reagent	Biontex
MOPS (4-Morpholine propanesulphonic acid)	Roche
pCR [®] -XL-TOPO [®] cloning kit	Invitrogen



pGEM [®] -T Easy cloning kit	Promega
Paraformaldehyde	Sigma
Potassium acetate	Merck
Potassium chloride	Merck
Propan-2-ol	Merck
Propidium iodide	Sigma
Proteinase K	Roche
Restriction enzymes	Inqaba Biotechnologies
RNase A	Roche
SDS (Sodium dodecyl sulphate)	Promega
Shrimp alkaline phosphatase (SAP)	Roche
Sodium acetate	Merck
Sodium chloride	Merck
Sodium hydroxide	Merck
T4 ligase	Inqaba Biotechnologies
TEMED (N, N, N', N'-Tetra methylethylene-diamine)	Promega
Tris [hydroxymethyl] aminomethane	BDH
TRIzol reagent	Gibco Life Technologies
Tryptone	Merck
Urea	Amersham Pharmacia
Vectorshield Hard Set mounting medium	Vectorshield
Xylene cyanol	BDH
Yeast extract	Merck



The chemicals used were all of AnalaR or equivalent grade.

2.2 General stock solutions and buffers

AMPS:	10 % ammonium persulphate.
10x TBE:	0.9 M Tris (pH 8.3), 0.89 M boric acid and 25 mM EDTA. This stock solution was diluted 10 fold for the running of agarose and polyacrylamide gels.
40 % acrylamide mix:	(19:1 acrylamide: bis-acrylamide) obtained from Biorad.
10x MOPS:	0.2 M Na-MOPS, 50 mM Na-Acetate, 10 mM EDTA (pH 7.0) adjusted with acetic acid. This stock solution was diluted 10 fold for the running of agarose gels to resolve RNA.
10x Ligase Buffer:	660 mM Tris-Cl, 50 mM MgCl ₂ , 10 mM DTT, 10 mM ATP and 10 % polyethylene glycol (pH 7.5).
10x PCR Buffer:	100 mM Tris-Cl, 500 mM KCl and 0.1 % gelatin (pH 8.3).
5x Sequencing Buffer:	1 M Tris-Cl and 25 mM MgCl ₂ . This buffer was stored at –20 °C and used at a 2.5x concentrate.
Ampicillin:	A 100 mg/ml stock solution was prepared in deionised water and stored at –20 °C.
Digestion buffer:	100 mM NaCl, 10 mM Tris-Cl (pH 8.0), 25 mM EDTA, (pH 8.0), and 0.5 % SDS. Proteinase K (to a final concentration of 0.1 mg/ml) was added just before use.

FACS buffer: 1 % foetal calf serum in PBS

Glycerol BPB: 30 % glycerol (v/v), 15 mM EDTA (pH 8.0) and 0.5 % bromophenol blue (w/v).

GTE Buffer: 10 mM EDTA, 50 mM glucose, 25 mM Tris-Cl (pH 8.0) stored at 4 °C, a 0.2 M stock solution of glucose was prepared and filter sterilized before addition of the rest of the chemicals.

Kanamycin mono-phosphate: A 50 mg/ml stock was prepared in deionised water and stored at -20 °C.

L-agar; 1 % tryptone, 0.5 % yeast extract, 0.5 % NaCl, 0.2 % glucose and 1.2 % bacteriological agar, antibiotic as required.

L Broth: 1 % tryptone, 0.5 % yeast extract, 0.5 % NaCl and 0.2 % glucose.

Lysis Solution: 200 mM NaOH, and 1 % SDS (w/v).

Neutralisation Solution: 3 M potassium acetate (pH 5.0).

Paraformaldehyde Fixative: 16 g paraformaldehyde was dissolved in 80 ml of deionised water by stirring at 70 °C in a fume cupboard. One drop of 2 M NaOH was added. The solution was cooled down slowly to room temperature and the volume adjusted to 100 ml with deionised water. The solution was filter sterilised through a 0.45-micron filter and a 100 ml of 2x PBS added.

The paraformaldehyde solution was stored at 4 °C wrapped in foil.

Phenol/chloroform:	25 parts buffer saturated phenol and 24 parts chloroform.
RNase A (DNase free):	A 20 mg/ml stock solution was prepared in a buffer containing 0.1 M sodium acetate and 0.3 mM EDTA (pH adjusted to 4.8 with acetic acid). This solution was boiled for 15 min and cooled quickly by placing it in ice water and stored at -20 °C.
TE Buffer:	10 mM Tris, 1 mM EDTA adjusted to pH 7.4 with HCl.
Transformation buffer 1 (Tbf1):	30 mM KOAc, 50 mM MnCl ₂ , 0.1 M KCl, 10 mM CaCl ₂ and 15 % glycerol (v/v).
Transformation buffer 2 (Tfb2):	9 mM Na-MOPS, 50 mM CaCl ₂ , 10 mM KCl and 15 % glycerol (v/v).
TYM:	20 % tryptone, 0.5 % yeast extract, 0.1 m NaCl, 0.2 % glucose and 10 mM MgCl ₂ .

All solutions were made using deionised water unless otherwise stated.

2.3 Bacterial culture

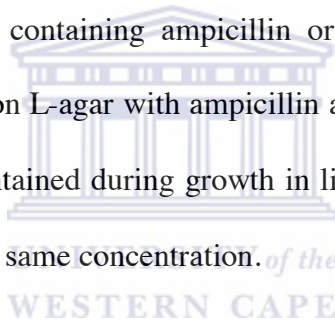
2.3.1 Bacterial strains

Escherichia coli strain MC1061 (Casadaban & Cohen, 1980).

F^- *araD139* Δ (*ara-leu*) 7696-*galE15 galK16* Δ (*lac*) X17 *rpsL* (Str^r) *hsdR2* (r_K^- m_K^+) *mcrA mcrB1* was used to produce plasmid DNA.

2.3.2 Selection

For experiments with *E. coli* containing ampicillin or kanamycin resistant plasmids, transformed cells were plated on L-agar with ampicillin at 100 $\mu\text{g}/\text{ml}^{-1}$ and kanamycin at 25 $\mu\text{g}/\text{ml}^{-1}$. Selection was maintained during growth in liquid culture by the inclusion of the appropriate antibiotic at the same concentration.



2.3.3 Storage of bacterial strains and clones

Overnight cultures were diluted by the addition of an equal volume of sterile glycerol and stored at -70°C .

2.4 Cloning vectors

2.4.1 pGEM[®]-T Easy Vector (Promega)

The pGEM[®]-T Easy vector is used for the cloning of PCR products. The vector which is 3.0 kb in size is designed by digestion with the restriction enzyme Eco RV and the addition of 3' terminal thymidine to both digested ends. The single 3'-T overhangs at the insertion site improves the efficiency of ligation of a PCR product (which has an extra dA residues added to the PCR product by *Taq* polymerase). The high copy number vector contains T7 and SP6 RNA polymerase promoters flanking a multiple cloning site (MCS) within the α -peptide coding region of the enzyme β -galactosidase allowing for selection of recombinant clones by colour screening on indicator plates. The vector also contains the origin of replication of the filamentous phage f1 for the preparation of single-stranded DNA and allows for selection with ampicillin in prokaryotes.

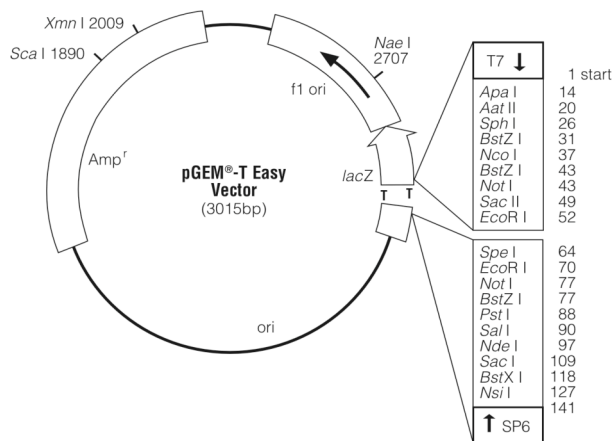


Fig 2.1 Represents the circular map of pGEM[®]-T Easy cloning vector indicating unique restriction recognition sequences in the multiple cloning site (MCS).

2.4.2 pCR[®]-XL-TOPO[®] Cloning Vector (Invitrogen)

The pCR[®]-XL-TOPO[®]-cloning vector provides a highly efficient, 5 minute; one-step cloning strategy for the cloning of long PCR products (3-10 kb). The 3.5 kb linearized vector supplied in the kit has single overhanging 3' deoxythymidine residues. This allows PCR inserts to ligate efficiently with the vector. The vector contains the *ccdB* gene fused to the C-terminus of the *LacZα* fragment. Ligation of a long PCR product disrupts the expression of the *LacZα-ccdB* gene fusion permitting growth of only positive recombinants upon transformation. Cells that contain non-recombinant vector are killed upon plating. The vector confers Kanamycin resistance in prokaryotic cells and Zeocin resistance in eukaryotic cells.

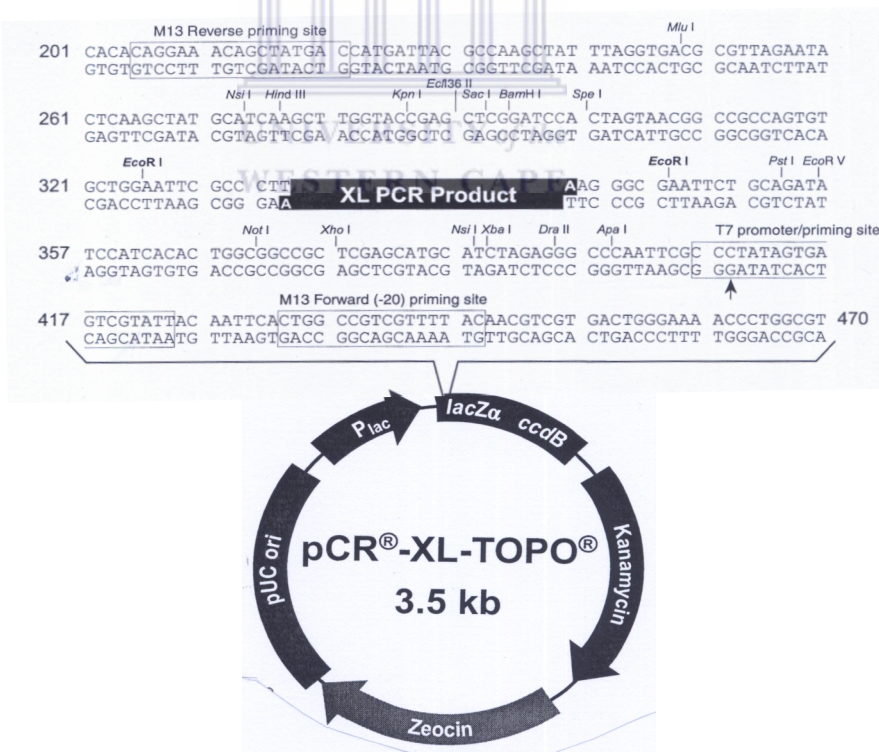


Fig 2.2 Shows the sequence surrounding the TA cloning site and the diagrammatic representation of the pCR[®]-XL-TOPO[®] cloning vector map.

2.4.3 pEGFP-C1 (Clontech)

This vector was used to construct fusions to the C-terminus of the green fluorescent protein (GFP). If a fusion construct retains the fluorescent properties of the native protein, its expression and localization *in vivo* can be monitored by fluorescence microscopy or flow cytometry. pEGFP-C1 encodes a red-shifted variant of wild-type GFP, which has been optimised for brighter fluorescence and higher expression in mammalian cells (excitation maximum = 498 nm; emission maximum = 509 nm). Sequences flanking EGFP have been converted to a Kozak consensus translation initiation site to further increase the translation efficiency in eukaryotic cells. The vector backbone contains an SV40 origin of replication in mammalian cells expression the SV40 T antigen. A neomycin resistance cassette (Neo^r) consisting of the SV40 early promoter, the neomycin/kanamycin resistance genes of Tn5, and polyadenylation signals from the herpes simplex virus thymidine kinase (HSV TK) gene, allows a stably transfected eukaryotic cells to be selected using G418.

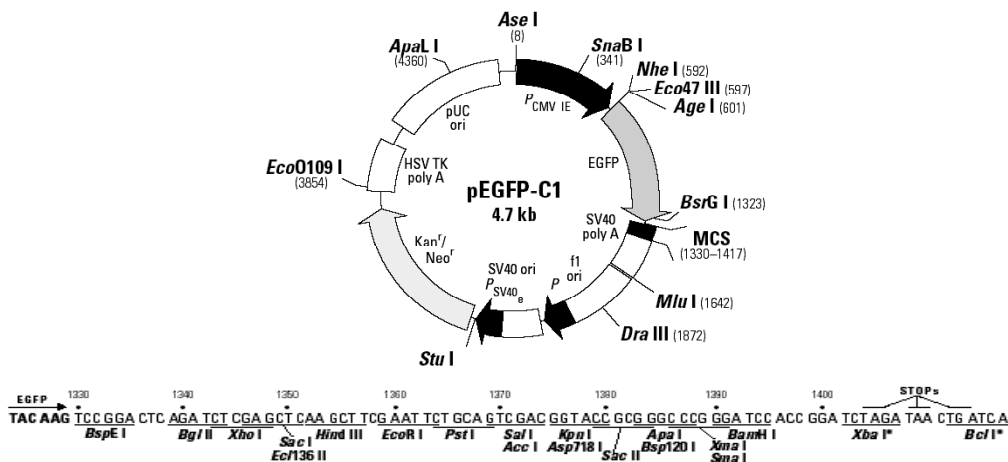


Fig 2.3 Represents the circular map and MCS of the pEGFP-C1 vector.

2.4.4 pDsRed1-C1 vector (Clontech)

The pDsRed1-C1 vector encodes a novel red fluorescent protein (DsRed1) that has been optimized for expression in mammalian cells (excitation maximum = 558 nm; emission maximum = 583 nm). DsRed 1's coding sequences contain 144 silent base pair changes, which correspond to human codon-usage preference for high expression in mammalian cells. A nucleotide sequence upstream of DsRed has been converted to a Kozak consensus translation initiation site to further increase the translation efficiency in eukaryotic cells. The vector backbone contains an SV40 origin of replication in mammalian cells expression the SV40 T antigen. A neomycin resistance cassette consisting of the SV40 early promoter, the neomycin/kanamycin resistance genes of Tn5, and polyadenylation signals from the herpes simplex virus thymidine kinase (HSV TK) gene, allows a stably transfected eukaryotic cells to be selected using G418.

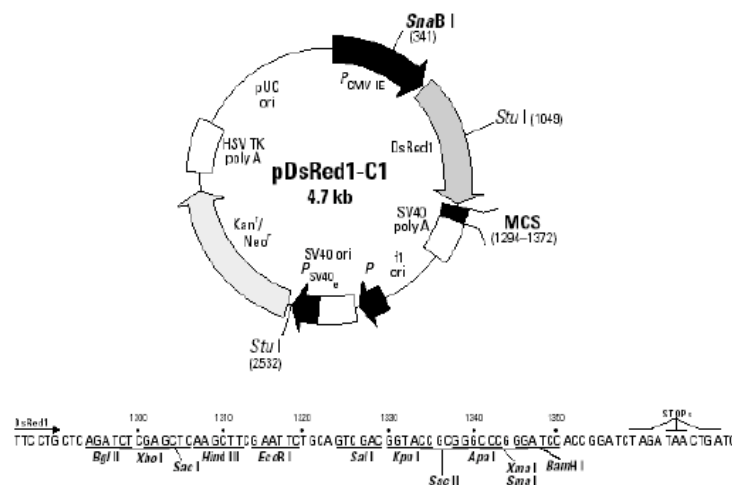


Fig 2.4 Represents the circular map of the pDsRed1-C1 vector and the MCS.

2.5 Preparation of competent *E. coli* cells for transformation

The desired bacterial strain was streaked out on a L.B agar plate that contained 10 mM MgCl₂ or MgSO₄ and incubated overnight at 37 °C. Following incubation a single colony of the strain was taken and inoculated into 20 ml of TYM broth and grown with vigorous shaking at 37 °C until the optical density (OD) at 550 nm reached 0.2. The cells were transferred to 100 ml of TYM broth and grown at 37 °C until the optical density at 550 nm reached 0.2. To this culture 400 ml of fresh TYM broth was added and the cells grown under the same conditions until optical density at 550 nm was between 0.4-0.6. The cells were rapidly chilled in ice water, with swirling, transferred to a 250 ml tube and pelleted by centrifugation at 6000 g for 10 min in a pre-cooled Beckman J2-14 rotor. After removing the supernatant the cells were re-suspended in 250 ml ice cold Tfb1 and allowed to incubate at 0 °C for 30 min. The cells were recovered by centrifugation at 6000 g for 8 min. The supernatant was removed and the pellet was resuspended in 50 ml of ice cold Tfb2. Cells were frozen in liquid nitrogen as 300 µl aliquots and stored at – 80 °C.

2.6 Bacterial transformations (Cohen *et al.*, 1972)

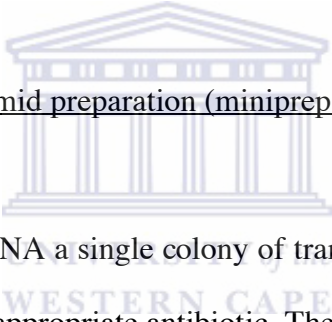
For DNA transformations competent cells (prepared as described in the section 2.5) were thawed on ice and 100 µl were added to 20 µl (1.0 – 10 ng) of the plasmid DNA solution, gently mixed and incubated for 30 min at 0 °C. The mixture was heat shocked by transfer to a 42 °C water bath for 45 sec, after which 500 µl of pre-warmed L.B was added and the

mixture incubated at 37 °C for an hour to allow for the expression of the antibiotic resistance marker. The transformed cells (100-200 µl) were then plated onto pre-warmed nutrient agar plates containing the appropriate antibiotic and the plates incubated at 37 °C for 16 hrs.

2.7 Preparation of plasmid DNA

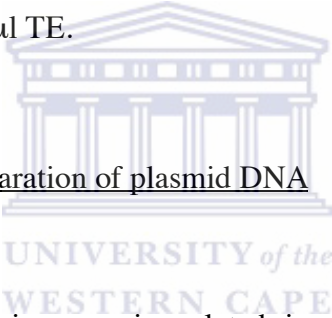
The preparation of plasmid DNA on both a small and large scale was based on an alkaline lysis procedure (Birnboim and Doly, 1979).

2.7.1 Small-scale plasmid preparation (minipreps)



In the preparation of plasmid DNA a single colony of transformed *E. coli* was inoculated into 5 ml of LB containing the appropriate antibiotic. The inoculated broth was incubated at 37 °C with vigorous shaking for 16 hrs after which 1 ml of this saturated culture was transferred to a 1.5 ml eppendorf tube and the cells pelleted by centrifugation at 5000 g for 5 min in a Beckman bench top centrifuge with a fixed angle rotor. The supernatant was aspirated off and the pellet completely resuspended in 200 µl of ice cold GTE followed by incubation at room temperature for 5 min. The cells were lysed by the addition of 400 µl of a 0.2 M NaOH and 1 % SDS (w/v) solution. The solution was gently mixed by inversion 4-5 times and incubated on ice for an additional 5 min, after which 300 µl of ice cold 3.5 M KOAc (pH 5.5) was added to neutralize the alkali. This solution was further incubated on ice for 5 min. The cell debris was pelleted at 14 000 g

for 10 min and the plasmid containing supernatant transferred to a clean eppendorf containing 0.6 volumes of propan-2-ol. Plasmid DNA was left at -20°C for 30 min to precipitate and pelleted at 14 000 g for 15 min. The resulting pellet was washed with 500 μl of 70 % EtOH, briefly dried and resuspended in 500 μl of TE. RNA was removed from the solution by the addition of 100 $\mu\text{g/ml}$ RNase A solution followed by incubation at 37°C for an hour. The RNase treated DNA was extracted with phenol/chloroform and the upper aqueous phase recovered. The DNA from the recovered phase was precipitated by the addition of 0.3 M sodium acetate and 2.5 volumes of ethanol and incubated at -20°C for 30 min. The precipitate was centrifuged at 10 000 g for 10 min, washed with 70 % ethanol and redissolved in 100 μl TE.



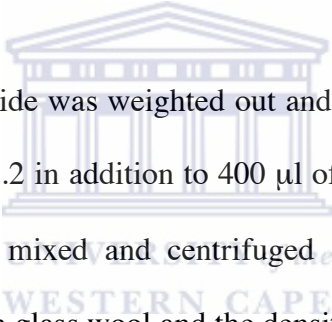
2.7.2 Large-scale preparation of plasmid DNA

The plasmid containing bacteria were inoculated in 500 ml of LB containing the appropriate antibiotic and grown overnight. The cells were harvested by centrifugation at 5 000 g for 10 min in a Beckmann JA14 rotor. The supernatant was discarded and the pellet resuspended in 15 ml of GTE buffer and incubated on ice for 10 min. To the cell suspension 15 ml of 0.2 M NaOH, 0.1 % SDS was added to lyse the cells. This solution was gently mixed by inversion 6-8 times and incubated on ice for 5 min. Subsequent to this incubation period 15 ml of 3.5 M KOAc (pH 5.5) was added to neutralize the alkali, and the mixture incubated on ice for an additional 10 min. The precipitate of cell debris, chromosomal DNA and SDS was removed by centrifugation at 10 000 g for 30 min at 4°C . The resulting supernatant was removed and filtered through glass wool to remove

particulate material and the nucleic acid precipitated by the addition of 0.6 volumes of propan-2-ol. The DNA solution was incubated at -20 °C for 30 min and recovered by centrifugation at 10 000 g for 10 min. Plasmid DNA was separated from RNA by double CsCl/ethidium bromide fractionation (section 2.7.3).

2.7.3 Double CsCl/ethidium bromide fractionation

This method was used to produce high quality plasmid DNA for transfection of eukaryotic cell lines.



A total of 5.75 g caesium chloride was weighted out and added to the propan-2-ol pellet solution prepared in section 2.7.2 in addition to 400 µl of ethidium bromide [10 mg/ml]. This solution was thoroughly mixed and centrifuged at 10 000 g for 10 min. The supernatant was filtered through glass wool and the density adjusted to 1.61 gml⁻¹ using a caesium chloride saturated TE solution. This solution was transferred to a Beckman Quickseal tube and centrifuged at 55 000 g for 16 hrs at 20 °C in a Beckman L7-80 ultracentrifuge using an NVi 65 rotor. Following centrifugation the different DNA conformations were visualized using a handheld UV lamp and the desired band extracted using a 14-gauge 5 ml syringe.

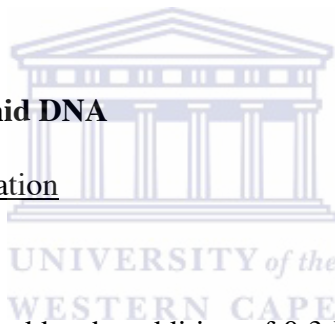
For double caesium chloride gradients the extracted DNA was made up to 5 ml with TE to which 5.75 g of caesium chloride and 400 µl of ethidium bromide was added followed by centrifugation at 10 000 g for 10 min. The supernatant was filtered through glass wool

and the density adjusted to 1.61 gml^{-1} with a caesium chloride saturated TE solution. The solution was subjected to centrifugation at 55 000 g overnight in a Beckman L7-80 ultracentrifuge. After removing the desired band the solution was extracted three times with a NaCl saturated iso-propan-2-ol solution to remove the ethidium bromide. Two volumes of water and three volumes of propan-2-ol was added, mixed and incubated at $-20 \text{ }^{\circ}\text{C}$ for 30 min. The DNA was pelleted by centrifugation at 10 000 g for 10 min and the resulting pellet washed twice with 500 μl of 70 % ethanol. The final pellet was air-dried and re-suspended in 500 μl of TE and the concentration determined by taking an absorbance reading at $\lambda 260 \text{ nm}$.

2.8 Manipulation of plasmid DNA

2.8.1 Ethanol precipitation

DNA in solution was precipitated by the addition of 0.3 M NaOAc, pH 7.4, followed by the addition of 2-3 volumes of absolute ethanol. The solution was mixed well and incubated at $-20 \text{ }^{\circ}\text{C}$ for 30 min. DNA was recovered as a pellet by centrifugation at 12 000 g for 10 min. The resulting pellet was washed twice with 500 μl of 70 % ethanol and air-dried for 5 min at room temperature. The pellet was re-suspended in 100 μl of TE and stored at $4 \text{ }^{\circ}\text{C}$ (short term) and $-20 \text{ }^{\circ}\text{C}$ (long term).



2.8.2 Phenol/chloroform extraction

This method was generally used to remove proteins from DNA solutions such as restriction enzymes. Generally, 200 µl of DNA was vortexed with an equal volume of buffered phenol and centrifuged at 12 000 g for 5 min. The supernatant was recovered and re-extracted with an equal volume of phenol. After centrifugation the supernatant was removed and extracted with an equal volume of chloroform. This resulting supernatant was ethanol precipitated as described in section 2.8.1 to recover the DNA and to remove trace amounts of organic solvents.

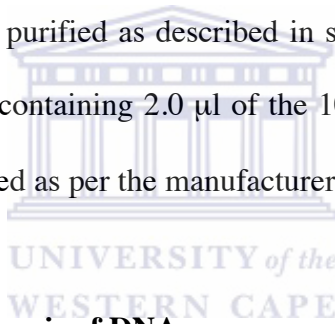
2.8.3 Restriction enzyme digests



Restriction enzymes were used according to the manufacturers instructions with the supplied 10x reaction buffer. Generally, 0.5 µg of plasmid DNA was digested with 10 units of the desired restriction enzyme. Digestion volumes ranged from 0.5-1.0 ml to ensure complete digestion. Reactions were incubated at the appropriate temperature for 2 hours. The reaction was inactivated by incubation at 65 °C for 20 min or extraction with phenol/chloroform followed by ethanol precipitation as described in section 2.8.1. Where multiple digests were performed, the buffer conditions were selected to be compatible with both enzymes. When this was not possible, after the completion of the first digest, the enzyme was removed by phenol/chloroform extraction and the DNA recovered by ethanol precipitation, the buffer conditions adjusted accordingly and the second digest performed.

2.8.4 Ligation of DNA

Vectors used for cloning were prepared using the large-scale plasmid preparation as described in section 2.7.2. The plasmid DNA was digested with the appropriate restriction endonuclease as described in section 2.8.3. If vectors were digested with a single enzyme that left compatible ends, the vectors were subsequently treated with SAP (Shrimp Alkaline Phosphatase) to remove the 5' phosphates. When vectors were digested with different enzymes leaving non-compatible ends, the vectors were used directly in a ligation reaction. All cloning vectors were used at a concentration of 10 ng/ μ l. Both the cloning vector and insert were purified as described in section 2.9.2. Ligations were set up in a 20 μ l reaction volume containing 2.0 μ l of the 10x buffer and 1.0 Weiss unit of T4 ligase. Cloning kits were used as per the manufacturers instructions.



2.9 Agarose gel electrophoresis of DNA

DNA was size fractionated by agarose gel electrophoresis on 1 or 2 % gels containing 0.5 μ g/ml ethidium bromide and electrophoresed in 1x TBE buffer. Generally, 1/10th of the DNA sample to be resolved was mixed with glycerol BPB before loading onto the gel. DNA size markers were loaded alongside the samples to estimate the size of DNA fragments. Two gel sizes were used: “mini” gels (6.5 x10 x 1 cm, 8 wells) and “slab” gels (18 x 20 x 1 cm, 2 x 25 wells). After electrophoresis the DNA was visualised with short wave UV light on a transilluminator and photographed using the Sony UVP Image Store 5000 photographic system. When DNA was to be recovered from the gel, a hand-

held long wavelength lamp was used to avoid damage to the DNA and a sterile blade used to excise the desired band. DNA was purified from agarose gels as described in section 2.9.2.

2.9.1. DNA molecular weight markers

Two DNA molecular weight markers were used pTZ and pKG 2. pTZ was used to estimate DNA sizes of 1.2 kb and less, whilst pKG 2 was used to estimate DNA sizes of between 6.0 kb and 1.6 kb. pTZ marker was made by digesting pTZ 18R vector with Hinf 1 and pKG 2 was made by digesting pKG-IX with Bam HI and Hind III at 37 °C for an hour.

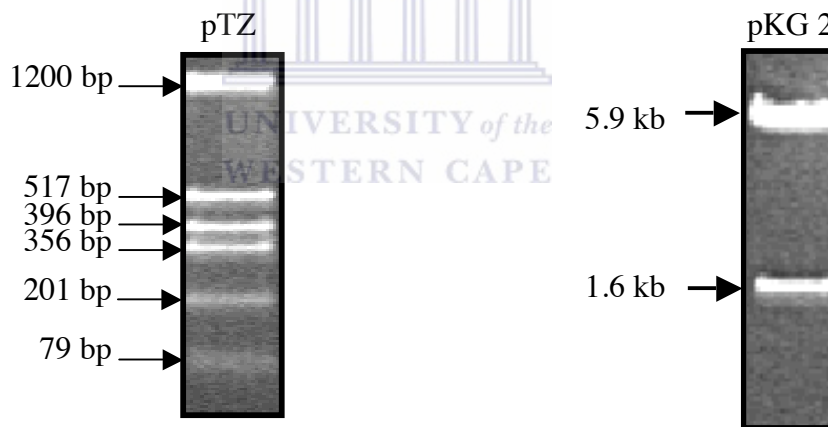


Fig 2.5 Agarose gel showing the sizes of the molecular weight markers pTZ and pKG 2.

2.9.2 Purification of DNA fragments using the GFX- purification kit

This protocol was used to purify both PCR fragments and digested cloning vectors. The DNA sample to be purified was electrophoresed on an agarose gel as described in section 2.9. The fragments were viewed with a long wave hand held UV lamp and excised using a sterile blade. The agarose embedded fragment was weighed and 100 µl of capture buffer was added for every 10 mg of agarose and vigorously mixed. The tube was placed at 60 °C for 5-15 min to melt the agarose. After incubation the sample was transferred to a GFX column within a collection tube and centrifuged for 30 sec at 13 000 g. The flow through was discarded and the column placed back in the collection tube. 500 µl of wash buffer was added to the column and the tube centrifuged for 1 min at 13 000 g. The collection tube was removed and placed in a 1.5 ml eppendorf. 20 µl of elution buffer was placed directly on the matrix of the column and allowed to incubate at room temperature for 1 min. The tube was centrifuged for 1 min at 13 000 g to collect the DNA.

2.10 Polymerase Chain Reaction (PCR) amplification

2.10.1 Standard PCR

The standard PCR was used to amplify genomic DNA. The reaction consisted of 50-100 ng genomic DNA, 1x PCR buffer, 50 µM of each dNTP, 1 U Taq DNA polymerase and 0.5 pmol of reverse and forward gene specific oligonucleotides in a final volume of 50 µl.

In amplification with Taq DNA polymerase the reaction contained titrated amounts of $MgCl_2$.

The reaction mixture was cycled through the following parameters:

95 °C for 2 minutes (Initial denaturation)

95 °C for 1 min (Denaturation)

($T_m - 5$ °C) for 1 min (Annealing)

72 °C for 2 min (Extension)

72 °C for 5 min (Final extension)

} 35 cycles

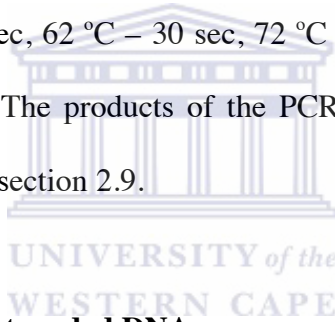
PCR reactions were analysed by electrophoresis in 1 % agarose run with 1x TBE as described in section 2.9.

2.10.2. PCR amplification of plasmid DNA

50 ng of plasmid DNA was used as template in a PCR amplification reaction and was prepared as follows, 1x PCR buffer, 50 μ M dNTPs, 1 U Taq DNA polymerase and 1.0 pmol of reverse and forward gene specific oligonucleotides in a final volume of 50 μ l. In amplification with Taq DNA polymerase the reaction contained titrated amounts of $MgCl_2$. The reaction was cycled through the parameters as described for the standard PCR (See section 2.10.1).

2.10.3 Colony PCR

This technique was routinely used to screen bacterial cells for recombinant clones. Following transformations a single colony was removed from an L-agar plate and re-suspended in 20 μ l of sterile deionised water with 1 μ l of this solution serving as template in a PCR with a 25 μ l final volume. PCR reactions were carried out as described in section 2.10.1 using the M13 forward and reverse oligonucleotides at a concentration of 10 pmol. A negative control, substituting 1 μ l of deionised water for the bacterial suspension was also performed. The cycling PCR conditions were as follows: 95 °C - 2 min, followed by 94 °C – 30 sec, 62 °C – 30 sec, 72 °C – 1 min repeated for 35 cycles, followed by 72 °C – 10 min. The products of the PCR were analysed by agarose gel electrophoresis as described in section 2.9.



2.11 Sequencing of double stranded DNA

DNA sequencing using the ABI 310 DNA Sequencer was employed. The BigDye Terminator Ready Reaction Kit version 3.0 (ABI) was used and this kit includes AmpliTaq DNA Polymerase, the BigDye terminators and all the required components for the sequencing reaction. Sequencing reaction consisted of the following:

REAGENT	QUANTITY
Terminator Ready Reaction Mix	2 μ l
Double-stranded DNA	200-500 ng
Primer	3.2 pmol
Deionised water	To a final volume of 10 μ l

Table 2.1 The sequencing reaction protocol.

The sequencing reactions were placed in a GeneAmp 9700 thermal cycler and cycled through the following parameters:

STEP	ACTION
1	96°C for 10 sec. Repeat for 25 cycles: 60°C for 4 min.
2	Hold at 4°C

Table 2.2 PCR cycles for sequencing.

Precipitation of extension products: UNIVERSITY of the WESTERN CAPE

The contents of each extension reaction were transferred to a 1.5 ml eppendorf tube to which 8 μ l deionised water and 32 μ l of 95 % ethanol were added. The tubes were vortexed briefly and incubated at room temperature for 30 min. Tubes were centrifuged for 20 min at 15 000 g. Supernatants were carefully aspirated. 250 μ l of 70 % ethanol was added to the tubes and vortexed briefly. Tubes were centrifuged at 15 000 g for 20 min. This step was repeated twice and the pellets were dried and either stored at -20°C or loaded immediately onto the ABI 310 Genetic Analyser. 12.5 μ l of Template Suppressor Reagent (TSR) was added and tubes were vortexed briefly. The samples were denatured at 95°C for 2 min and tubes were placed on ice immediately. The samples were loaded onto the ABI 310 PRISM™ Genetic Analyser (Applied Biosystems) and the data

collected using the ABI 310 PRISM™ Collection Software and analysed using the Sequencing Analysis 3.4.1 Software.

Subsequent constructs were sequenced at the Inqaba Biotech core sequencing facility. Clones to be sequenced were plated on LB agar with the appropriate antibiotic and submitted to Inqaba Biotech core sequencing facility for analysis.

2.12 Isolation of genomic DNA from cultured cells

Cells were cultured until confluent as described in section 2.13.3. The cells were washed with 10 ml of ice cold PBS and dissociated from the flask by scraping with a Falcon 3085 cell scraper. The dissociated cells were resuspended in 1 ml digestion buffer and shaken for 16 hrs at 55 °C. The samples were extracted with an equal volume of phenol/chloroform/isoamyl alcohol and centrifuged at 3000 g for 10 min in a Beckman fix angle bench top centrifuge. The top (aqueous) layer was then transferred to a clean tube and the DNA precipitated as described in section 2.8.1. The DNA was recovered by centrifugation at 3000 g for 10 min and the pellet washed with 500 µl of 70 % ethanol and air-dried. The pellet was resuspended in 50 µl of TE and incubated at 65 °C for 4 hours to facilitate solubilization. The isolated DNA was resolved on 0.8 % agarose as described in section 2.9 to determine the integrity of the DNA isolated. The DNA concentration was determined at 260 nm, given that 40 mg DNA/ml has an absorbance of 1.0 at 260 nm.

2.13 Cell Culture

2.13.1 Cell lines

The following adherent cell lines were used in this project.

(i) NIH 3T3

Fibroblast line established from a NIH Swiss mouse embryo. NIH 3T3 cells are non-tumourigenic and are highly contact inhibited. NIH 3T3 cells are also sensitive to sarcoma virus focus formation and leukaemia virus propagation. NIH 3T3 were cultured in DMEM containing 10 % FCS.

(ii) 293T (Hek 293T)

This line was established from a human primary embryonal kidney transformed by an type 5 adenovirus. Hek 293T cells are an adherent fibroblastoid line growing as a monolayer. Cells were cultured in RPMI containing 10 % FCS.

2.13.2 Tissue culture media

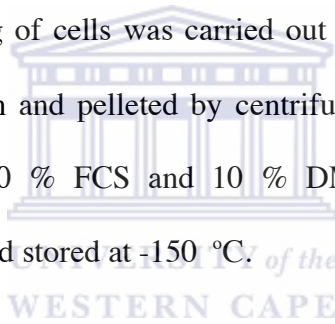
The following tissue culture media and supplements were supplied by Gibco BRL; DMEM and RPMI 1640 with Glutamax-L, 100x penicillin-streptomycin (P/S), foetal calf serum (FCS) and phosphate buffered saline (PBS) (pH 7.0). Working solutions of 0.125 % trypsin and 10x P/S were prepared using sterile PBS.

The following antibiotic was prepared for selection of stable cell lines:

Geneticin (G418): A 100 mg/ml stock solution was prepared in PBS containing 0.5 mM EDTA. The solution was filtered through a 0.45 micron filter and stored at $-20\text{ }^{\circ}\text{C}$.

2.13.3 Propagation and storage of cell lines

Cells were grown in complete media, 1x P/S and 10 % (v/v) FCS and were maintained at subconfluent levels in a $37\text{ }^{\circ}\text{C}$ incubator in 5 % CO_2 atmosphere and passaged when confluency was reached. Cells were removed for passage using sterile trypsin pre-equilibrated to $37\text{ }^{\circ}\text{C}$. Freezing of cells was carried out when they reached confluency. Cells were treated with trypsin and pelleted by centrifugation at 300 g for 3 min. The pellet was re-suspended in 90 % FCS and 10 % DMSO. Resuspended cells were aliquoted into 1 ml fractions and stored at $-150\text{ }^{\circ}\text{C}$.



2.13.4 Transfection of cell lines

2.13.4.1. Transient transfection of cell lines

Plasmid DNA prepared by double CsCl/ethidium bromide fractionation as described in section 2.7.2 and the ultra pure yield midi plasmid extraction kit (Qiagen) was used for all transfections. The transfection reagent was TransFectin™ Lipid Reagent (Biorad) and Metafectene™ (Biontex), used according to the manufacturers instructions. Confluent cell were passaged one or two days prior to transfection, to allow cells to grow to 70 % confluence on the day of the experiment. DNA was mixed gently with the transfection reagent at a ratio determined by the experiment to give the maximum number of

transfectants. For 6 well plates 1 μg of DNA was mixed with 250 μl of serum free media and 5 μl of the transfection reagent was mixed with 250 μl of serum free media. The two solutions were mixed and incubated at room temperature for 20 min to allow the DNA/lipid complexes to form. The mixed solution were added directly to the cells in the 6 well plates and mixed gently to distribute the DNA/lipid complexes. Cells were further treated depending on the specific analysis to be carried out.

2.13.4.2 Stable transfection of cell lines

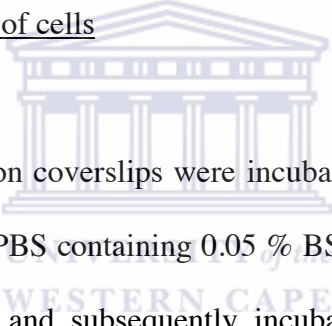
Stable transfections were carried out in 25 cm^3 tissue culture flasks. For 25 cm^3 flasks 4 μg of DNA was mixed with 1 ml of serum free media and 20 μl of the transfection reagent was mixed with 1 ml of serum free media. The two solutions were mixed and incubated at room temperature for 20 min to allow the DNA/lipid complexes to form. The mixed solution were added directly to the cells in the 25 cm^3 flask and mixed gently to distribute the DNA/lipid complexes. After 24 hours, the cells were passaged at a 1:10 dilution with fresh growth medium containing the appropriate antibiotic. For selections with G418, 800 $\mu\text{g}/\text{ml}$ was used for 3 to 4 weeks until resistant colonies were visible, after which cells were maintained in 500 $\mu\text{g}/\text{ml}$ of the antibiotic.

2.14 Immunofluorescence

2.14.1 Fixation and permeabilization of cells

Cells grown on coverslips were removed from 6 well plates and washed twice in cold PBS followed by fixation in 4 % paraformaldehyde in PBS at room temperature for 5 min, Following fixation cells were permeabilized by incubation with permeabilization buffer for an additional 5 min. The cells were washed twice for 5 min in PBS containing 0.05 % BSA.

2.14.2 Immunostaining of cells



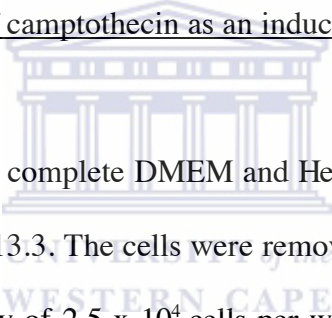
Fixed and permeabilized cells on coverslips were incubated at room temperature for 1 h in primary antibody diluted in PBS containing 0.05 % BSA. The cells were washed with PBS containing 0.05 % BSA and subsequently incubated in diluted dye conjugated secondary antibody for 1 h and washed again. For nuclei staining, cells were incubated with DAPI for 30 min and washed with PBS. At this point cells were either prepared to be FACS analyzed or mounted on microscope slides. Cover slips were placed on microscope slides containing a drop of VECTASHIELD hard set™ mounting medium. Cells were viewed using a Zeiss fluorescent microscope.

2.15. FACS analysis

Cells that were FACS analysed were trypsinized as described in section 2.13.3 and resuspended in 1 ml of ice-cold FACS buffer. Cells were FACS analysed using a three colour FACScan (Becton Dickinson). A minimum of 10 000 cells per sample were acquired using the Becton FACScan and the data analyzed using the CELLQuest PRO software (BD Biosciences).

2.16 Apoptosis Assays

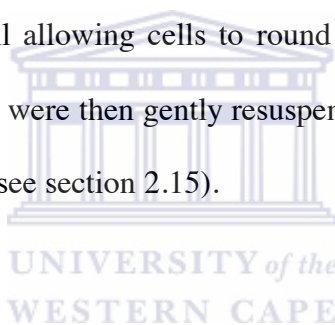
2.16.1 The screening of camptothecin as an inducer of apoptosis



NIH 3T3 cells were cultured in complete DMEM and Hek 293T cells in complete RPMI 1640 as described in section 2.13.3. The cells were removed by trypsinization and plated in 6 well plates at a cell density of 2.5×10^4 cells per well. After 24 hrs the media was removed and the cells washed with PBS, and fresh media containing camptothecin was added. The final concentration of camptothecin varied between 0 and 25 $\mu\text{g/ml}$. The cells were exposed for 24 hrs during which time the cells were monitored for morphological changes. After the incubation period the cells were harvested and assayed using different apoptosis assays.

2.16.2 APOPercentage™ Apoptosis Assay

The APOPercentage™ assay is a detection and measurement system to monitor the occurrence of apoptosis in mammalian cells. Cells were grown in six well plates until confluent. Cells were treated with a concentration of camptothecin determined for each cell line as the optimum concentration to cause maximum apoptosis (see section 2.16.1). The treated cells were washed twice with PBS and 1 ml of the APOPercentage™ dye was added to each well and incubated at 37 °C for an hr. The dye was removed and the cells were washed twice with PBS. The PBS was removed from each well and 0.5 ml of trypsin was added to each well allowing cells to round up (and not detach) before the trypsin was removed. The cells were then gently resuspended in 2 ml of complete culture media and analysed by FACS (see section 2.15).



2.16.3 Annexin V-PE assay

The assay was performed using the Annexin V-PE Apoptosis Detection Kit (BD Pharmingen™). The cells were plated in 6 well plates at a cell density of 2.4×10^4 and incubated for 24 hrs. Following the incubation period cells were treated with camptothecin for 24 hour and subsequently removed by trypsinization and re-suspended in 1x binding buffer at a concentration of 1×10^6 cells. From this cell suspension 100 μ l was removed to a 5 ml Falcon tube and 5 μ l of both Annexin V-PE and 7-AAD (7-amino-actinomycin D) was added to each sample. The cells were gently vortexed and incubated at room temperature for 15 min in the dark. After incubation 400 μ l of 1x

binding buffer was added to each tube and the samples analyzed by FACS (see section 2.15).

2.16.4 APO-Direct/TUNEL assay

This assay was performed using the APO-Direct™ Kit from BD Biosciences. The cells were plated in 6 well plates at a cell density of 2.4×10^4 . The cells were treated with camptothecin at the concentrations determined to induce maximum apoptosis and further incubated for 48 hrs to allow DNA fragmentation. Following the induction period cells were harvested by trypsinization and washed in 2 ml of PBS. The cells were re-suspended in 1 % (w/v) paraformaldehyde in PBS (pH 7.4) and incubated for 30 min on ice. The cells were washed twice with 5 ml of PBS and subsequently re-suspended in the residual PBS to which 4 ml of 70 % ethanol was slowly added with regular mixing. The cells were incubated at $-20\text{ }^{\circ}\text{C}$ for at least 48 hrs. Following this incubation period the cells were harvested by centrifugation for 10 min at 4000 g and washed twice with 1 ml of wash buffer. After removal of the wash buffer the pellet was re-suspended in 50 μl of DNA labelling solution and incubated at $37\text{ }^{\circ}\text{C}$ for an hour with regular shaking. Following this incubation period the cells were rinsed twice in rinsing buffer and pelleted by centrifugation. The final cell pellet was re-suspended in 0.5 ml of Propidium iodide (PI)/RNase A solution and incubated for 30 min in the dark. The cell were subsequently analysed by FACS (see section 2.15).

2.17 Cell cycle analysis

NIH 3T3 cells to be analysed for the cell cycle was cultured in 25 cm³ flasks till confluent. The cells were trypsinized and re-plated in 6 well plates at a density of 2 x 10³ cells per well. The cells were incubated at 37 °C and harvested at the following time intervals 12 hrs, 18 hrs, 24 hrs, 48 hrs and 72 hrs. Cells were removed by trypsinization and pelleted by centrifugation at 2000 g for 2 min. The cells were washed with PBS and resuspended in 200 µl of PBS. 4 ml of 70 % ethanol was added to the cells drop wise and thoroughly mixed to prevent the cells from clumping. The cells were incubated at -20 °C for 48 hrs to fix the cells. After fixing the cells it was harvested by centrifugation at 4000 g for 2 min. The cells were washed twice in 2 ml PBS and recovered by centrifugation at 4000 g for 2 min. A 1 ml PI solution was added to each sample to be analyzed. The PI solution was prepared at a stock concentration of 3 mg/ml in sodium acetate. The working PI solution was prepared by diluting 400 µl of the PI stock solution in 9.5 ml of PBS and 100 µl of RNase A [10 mg/ml}. 1 ml of the working PI solution was used to resuspend the cells before assaying the cells on a FACScan (Becton Dickinson) (see section 2.15).

2.18 RNA isolation

Total RNA was isolated from cultured cells using the TRIzol LS protocol from Gibco life technologies. Cells grown in monolayer were homogenised by the addition of 0.3-0.4 ml per 10 cm³ culture flask TRIzol LS reagent. The homogenate was transferred to a 15 ml

falcon conical tube and 0.2 ml of chloroform per 0.75 ml of TRIzol LS reagent was added. The solution was vigorously shaken for 15 sec and allowed to incubate at room temperature for 10 min. The sample was centrifuged for 30 min at 3000 g at 4 °C to allow phase separation. The top aqueous phase was transferred to a fresh conical tube and mixed with 0.5 ml of propan-2-ol per 0.75 ml of TRIzol LS reagent to allow for RNA precipitation. The sample was incubated at room temperature for 15 min and centrifuged for 30 min at 3000 g at 4 °C. The resulting pellet was washed with 1 ml of 70 % ethanol per 0.75 ml of TRIzol LS reagent. The pellet was allowed to dry at room temperature and resuspended in 100 µl DEPC treated water. The isolated RNA was stored as 20 µl aliquots at -80 °C.

2.19 Agarose gel electrophoresis of RNA



Total RNA was size fractionated by electrophoresis in 1.2 % agarose gel containing 1.27 % formamide and 0.5 µg/ml Ethidium Bromide and electrophoresed with 1x MOPS. The RNA sample to be electrophoresed was mixed with formamide buffer before loading onto the gel. "Mini" gels were used for the electrophoresis of RNA. RNA was visualised with short wave UV light on a transilluminator and photographed using the Sony UVP Image Store 5000 photographic system.

2.20. cDNA synthesis

For first strand cDNA synthesis the AMV kit for reverse transcription (Roche Applied Science) was used. The reaction for the first strand cDNA synthesis consisted of the following reagents:

REAGENT	VOLUME/ 1 SAMPLE	FINAL CONCENTRATION
10x reaction buffer	2 μ l	1x
25 mM MgCl ₂	4 μ l	5 mM
10 mM dNTPs	2 μ l	1 mM
Primer	Variable	0.75-1.0 μ M
RNase inhibitor	1 μ l	50 units
AMV reverse transcriptase	0.8 μ l	20 units
Sterile water	To final volume of 20 μ l	
RNA	1 μ g	

Table 2.3 Represents the reagents used for the first strand cDNA synthesis reaction.

The mixture was vortexed and centrifuged briefly. The reaction was incubated at 25 °C for 10 minutes and then at 42 °C for 60 minutes. Following the 42 °C incubation, the AMV reverse transcriptase was denatured by incubating at 99 °C for 5 minutes and then cooled to 4 °C for 5 minutes and the resultant first strand cDNA preparation was stored at -20 °C. The cDNA synthesised was used for amplification using the standard PCR protocol (section 2.10.1).

2.21 Real-Time Quantitative RT-PCR

A standard PCR mix contained 4 µl of LightCycler FastStart DNA Master^{PLUS} SYBR Green Reaction Mix (Roche Applied Science) 200 ng of the pre synthesized cDNA was used as template and 0.5 µM of each primer in a final volume of 20 µl. A negative control was included which contained the same mix with the cDNA replaced by water. The PCR mixed was subsequently transferred to capillary tube in a pre-cooled adapter block and centrifuged at 700 g for 5 sec. The capillaries were placed into the LightCycler instrument and cycled through the following parameters

Program	Step	Temp.	Time	Temperature Transition Rate	Fluorescence acquisition
Pre-incubation		95°C	10 min	20°C/sec	None
Amplification	Denaturation	95°C	10 sec	20°C/sec	None
Amplification	Annealing	Primer dependant	10 sec	20°C/sec	None
Amplification	Extension	72°C	5 sec	20°C/sec	Single
Melting curve	Denaturation	95°C	0	20°C/sec	None
Melting curve	Annealing	65°C	10 sec	20°C/sec	None
Melting curve	Melting	95°C	0	0.1°C/sec	Continuous
cooling		40°C	30 sec	20°C/sec	None

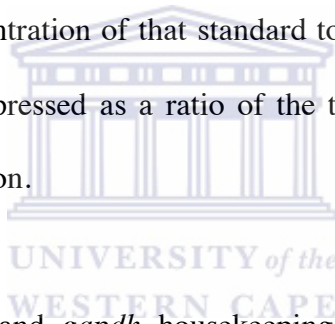
} 35 cycles

Table: 2.4 Represents the PCR conditions used in Real-Time Quantitative PCR

2.22 Quantitation of Real-Time qRT-PCR results

2.22.1 The standard curve

The default (fit point/arithmic) method of Real-Time Quantitative Software version 3 was used to determine the relative starting copy numbers of target in each reaction. The Real-Time Quantitative Software generates a standard curve by plotting the logarithm of fluorescence versus the cycle number for each serial dilution of the standard template and then identifies the crossing point (cycle number) where the fluorescent signal emerges from background and enters the log-linear phase. Each crossing point is then plotted against the user-defined concentration of that standard to produce a standard curve. The relative gene expression is expressed as a ratio of the target gene concentration to the housekeeping gene concentration.



PCR amplifications for *hprt* and *gapdh* housekeeping genes were performed, using published data from PrimerDB, producing fragments of 260 and 280 bp, respectively. Quantification of the molecular concentration of template cDNA was performed with the standard curve method for relative quantification. The template concentrations were given arbitrary values of 1 (for 10 fold-dilution of synthesized cDNA), 0.1 (for 100 fold dilution) and 0.01 (for 1000 fold dilution).

Data on expression levels for the housekeeping genes (HKG) were obtained in the form of crossing points/cycle threshold (CP/ C_T) (Larionov *et al.*, 2005). The data acquisition was done employing the 'second derivative maximum' method as computed by the LightCycler Software 3.5 (Roche Diagnostics).

	<i>GAPDH</i>	<i>HPRT</i>
n	10	10
GM [CP]	21.68	25.20
AM [CP]	21.68	25.20
Min [CP]	21.40	25.00
Max [CP]	22.00	25.60
SD [\pm CP]	0.18	0.20
CV [% CP]	0.83	0.79
SE [CP]	± 0.19	± 0.254
p-value	0.120	0.431
Power [x-fold]	1.12	1.08

Table 2.5 Descriptive statistics of two candidate housekeeping genes (HKG) based on their crossing point (CP/ C_T) values.

N: number of samples; GM [CP]: the geometric mean of CP; AM [CP]: the arithmetic mean of CP; Min [CP] and Max [CP]: the extreme values of CP; SD [\pm CP]: the standard deviation of the CP; CV [% CP]: the coefficient of variance expressed as a percentage on the CP level; SE [CP]: standard error of the CP; Power [x-fold]: the extreme values of expression levels expressed as an absolute x-fold over- or under-regulation coefficient.

The Real-Time PCR efficiencies (E) were calculated from the resulting slopes provided by the Real-Time Quantitative PCR software and was calculated according to the equation.

$$R = \frac{(E_{\text{target}})^{\Delta CP_{\text{target}}^{\text{(control-sample)}}}}{(E_{\text{ref}})^{\Delta CP_{\text{ref}}^{\text{(control-reference)}}}} \quad (\text{Pfaffl, 2001})$$

The expression levels of all genes were determined relative to *hprt* and *gapdh* using the geNORM excel spreadsheet (Vandesompele *et al.*, 2002).

2.23 Annealing of siRNA oligonucleotides

Equimolar quantities of sense and antisense siRNA oligonucleotides were mixed in the annealing buffer (10mM Tris pH7.4, 0.1mM EDTA) at a concentration of 1.0 μ M. The mixture was heated at 95 °C for 10 min and allowed to cool down to room temperature to allow for the formation of double-stranded DNAs.



CHAPTER 3: EXPRESSION ANALYSIS OF THE RBBP6 PROMOTERS IN CELL CULTURE

- 3.1 INTRODUCTION
- 3.2 CLONING OF P0 AND P1 INTO pGEM-T EASY
 - 3.2.1 PCR amplification of promoters
 - 3.2.2 Cloning of P0 and P1 PCR products
- 3.3 PREPARATION OF pEGFP-C1 AND pDsRed1-C1 PROMOTER CONSTRUCTS
 - 3.3.1 Preparing pEGFP-C1 and pDsRed1-C1 cloning vectors
 - 3.3.2 Digestion and purification of inserts
 - 3.3.3 Cloning of P0 and P1 into pEGFP-C1 and pDsRed1-C1
- 3.4 EVALUATION OF THE EXPRESSION OF EGFP AND DSRED1 *IN VIVO*.
 - 3.4.1 Transfection of constructs
 - 3.4.2 Fluorescence microscopy
 - 3.4.3 Quantification of fluorescence
- 3.5 THE EFFECT OF APOPTOSIS ON PROMOTER EXPRESSION
 - 3.5.1 Induction of Apoptosis
 - 3.5.2 The effect of apoptosis on promoter activity
- 3.6 SUMMARY

CHAPTER 3: EXPRESSION ANALYSIS OF THE RBBP6 PROMOTERS IN MAMMALIAN CELL CULTURE

3.1 Introduction

To turn a gene into a protein at least two general steps are required. Firstly, the gene is transcribed, spliced and processed to form mRNA and secondly, the mRNA is translated into a polypeptide. Transcription is a controlled process. Whilst multiple DNA regions are involved, the promoter is the main determinant for the initiation of transcription and modulation of levels and timing of gene expression. The promoter region is the key cis-acting regulatory region that controls the transcription of adjacent coding region(s) into mRNA, which is then directly translated into proteins. Higher eukaryotes generally utilize extensive promoter/enhancer/locus control regions spanning many kilobases of DNA, and encompass multiple discrete binding sites for transcription factors that combinatorially encode specificity of gene transcription.

The ability of each cell to program its genome and determine which genes are to be expressed at a given time and under specific stimuli is central to tissue differentiation, organogenesis, organismal development, and disease. The problem is that the same genetic information is contained within every cell, and many proteins that regulate gene activity can function non-discriminately on DNA elements that control gene expression. Fortunately, a number of diverse mechanisms have evolved to ensure that the expression of our genome is a highly regulated process. A wealth of studies have shown that

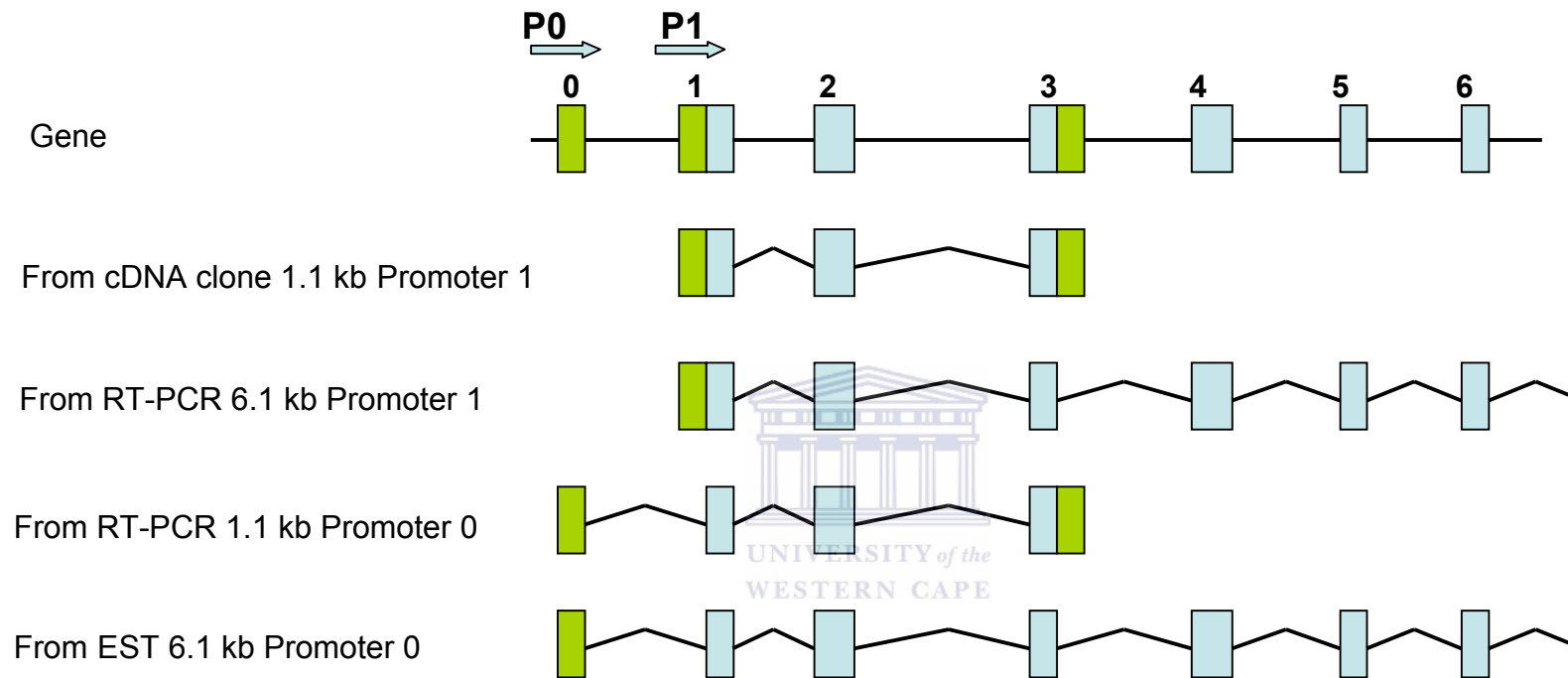
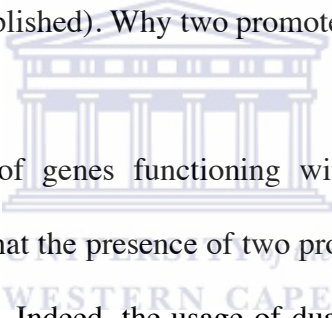


Figure 3.1. Diagrammatically represents the different RBBP6 transcripts resulting from the activity of Promoter 0 (P0) and Promoter 1 (P1) using EST data and RT-PCR analysis.

transcriptional activation occurs in discrete and controlled stages, from the packaging of a gene into chromatin and its localization within the nucleus to the recruitment of multiprotein complexes whose conformation and activity results from specific protein-protein or protein-DNA interactions to genes with complex (dual) promoters (reviewed in Emerson, 2002).

Genetic analysis of the RBBP6 gene showed the activity of two promoters for the gene, Promoter 0 (P0) and Promoter 1 (P1). RT-PCR analysis and EST data showed the activity of both promoters to be responsible for the 1.1 kb and the 6.1 kb transcripts of RBBP6 (see figure 3.1) (Dlamini, unpublished). Why two promoters?



Previously published reports of genes functioning within the immune system with multiple promoters illustrated that the presence of two promoters is not unique (Wildin *et al.*, 1995, Gessner *et al.*, 1996). Indeed, the usage of dual promoters has been described for several of the *Ly-49* genes. The Ly49A NK cell receptor interacts with MHC class I molecules on target cells and negatively regulates NK cell-mediated target cell lysis. The distal promoter of some *Ly-49* genes was shown to have promoter activity in fetal cells and in bone marrow cells, possibly linking its usage to the initiation of *Ly-49* expression in NK cells (Saleh *et al.*, 2002). In addition, the mouse *NKR-P1C* gene has also recently been shown to have a novel upstream non-coding exon that is differentially used during NK cell development, as well as a DNase I HSS (hypersensitive site) upstream of the gene (Ljusic *et al.*, 2003).

Studies have also indicated that in dual promoter systems the activity of the one promoter can control the activity of the other one during preferential promoter usage (Wilhelm *et al.*, 2003). Thus the presence of two promoters for RBBP6 can possibly be an indication of various functions for the gene with differential usage of its promoters under different cellular conditions.

The aims of this chapter were as follows:

- The construction of promoter vectors placing the reporter genes EGFP (Enhanced Green Fluorescent Protein) and DsRed1 (Red Fluorescent Protein) under the transcriptional control of RBBP6 promoters P0 and P1 using the CMV promoter as control.
- To evaluate the expression of the reporter genes using fluorescence microscopy, FACS analysis and Real-Time qRT-PCR.
- To evaluate the expression of the reporter genes after the induction of apoptosis using the aforementioned techniques.

3.2 Cloning of P0 and P1 into pGEM®-T Easy

3.2.1 PCR amplification of promoters

3.2.1.1 Primer design

Gene specific oligonucleotides were designed for the amplification of P0 and P1 (see table 3.1 for sequences). The oligonucleotides were engineered to include a recognition site for the restriction endonucleases Ase I at the 5' end and Nhe I at the 3' end. The

	PRIMER NAME	PRIMER SEQUENCE	POSITION
PCR	P0F1	5' GCGATTAATCAGAGCAAGACCCGGACTCC 3'	264-283
	P0R1	5' CTAGCTAGCGCTGCCAGGTCCTCTTCAGG 3'	1247-66
	P1F1	5' GCGATTAATGATCCAACCCAGACAACGTGG 3'	263-283
	P1F2	5' GCGATTAATTTACAGCCAAGGAGACCCAGG 3'	320-340
	P1R1	5' CTAGCTAGCCGGGGTCAGGGGTCCATAGC 3'	1587-606
	P1R3	5'CTAGCTAGCCACTCAAAGACACCGAAGGACC 3'	1870-1891
Cloning and Sequencing	M13F pGEM-T Easy	5' GTTTTCCCAGTCACGACGTTGTA 3'	2949-2957
	M13R pGEM-T Easy	5' TTGTGAGCGGATAACAATTTTC 3'	176-192
	M13F pCR®-XL-TOPO®	5' CTGGCCGTCGTTTTAC 3'	433-448
	M13R pCR®-XL-TOPO®	5' CAGGAAACAGCTATGA	205-222
	P0Seq	5' CTCATTCGGACTTCCTGAGC 3'	342-361
	P1Seq	5'AAATCTAGAGCCCCACAGC 3'	296-315
	Forward common (Fc)	5' ACTACTACGTGGACTCCAAGC 3'	1190-1211
	GFP-R	5' TAGGTGGCATCGCCCTCG 3'	501-517
	RFP-R	5' TCGTAGGGGCGGCCCTC 3'	501-517
Real-Time qRT-PCR	LC-RFP-F1	5' CCCAGTTCCAGTACGG 3'	1217-1232
	LC-RFP-R1	5' GGTCTTCTTCTGCATTACG 3'	1017-1035
	LC-GFP-F1	5' ACGTCTATATCATGGCCG 3'	1061-1078
	LC-GFP-R1	5' TGTGATCGCGCTTCTT 3'	1260-1276
	hGAPDH F	5'ACCCACTCCTCCACCTTTG 3'	970-988
	hGAPDH R	5'CTCTTGTGCTCTTGCTGGG 3'	1129-1147

Table 3.1 Oligonucleotides used in this chapter. The Ase I restriction sequence shown in red, and the Nhe I restriction sequence shown in blue



incorporation of these restriction sites into the resulting PCR fragments would allow for the directional cloning of the two promoters into pEGFP-C1 and pDsRed-C1 respectively. A 1.3 kb nucleotide sequence was used for the design of oligonucleotides to amplify P0 (see figure 3.2) and a 2.0 kb nucleotide sequence to amplify P1 (see figure 3.3). For the amplification of P1 two sets of oligonucleotide pairs were designed to amplify different sized fragments of the promoter. Oligonucleotides were positioned to include all possible predicted transcription start sites as determined using TRANSFAC (Schug and Overton, 1997) and the Promoter 2.0 software (Knudsen, 1999).

3.2.1.2 PCR amplification of promoters

The human BAC clone CIT DM210 was used as template in a 50 µl standard PCR reaction as described in chapter 2.10.1. Long-range, high fidelity *Taq* (Southern Cross Biotechnologies) was used to amplify P0 and P1 resulting in specific PCR products of the expected size.

PCR products for P0 and P1 were resolved on a 1 % agarose gel as described in section 2.9. From figure 3.4 PCR results showed the expected fragment of 1.0 kb for P0 compared to the size marker pTZ. Figure 3.5 shows several PCR fragments for P1 with sizes ranging from 1.0 to 1.6 kb. However smaller fragments than the expected sizes are also observed in lanes 6 and 8. These are probably PCR artefacts caused by mispriming. Furthermore, amplicons for P1 resulting from P1F1/P1R1 seems to differ in size. This can be a consequence of overloading of the sample in lanes 4 and 6 causing slower

1

GGACCAGGCACAAGCTCAGTCCTGTAACCCCAGCACTTTGGGAGGCC
AAGGCGGGAGGACTGCTTGAGGCCGTGAGTTTGAGACCAGGGTGGG
TAGCATAGTGAGGCTCTGACACTACTGAAAAAACTAAAAATTAGCTG
AGCATGTTGGCACAAGCCTATAGTCCCAGCTACTCAGGAGCCTGAAG
CAGGAGGATTACTTGATCCCAGGAGTTCAAAGTTACAGTGAAGTGTG
ATTGCACCACTGCACTCCAGCCTGGGTGA

P0F1

CAGAGCAAGACCCGGACTCCAAAATAATACTACTAATAATTAACA
AACAAAAAGAGAACAGCCTCCATGAAATAGATCTCATTCCGACTTCC
TGAGCTTGAGTAGTTCACTACAGACAGCAGGCAGGCAGAGCTCCTTG
GATCTCCCAATCCGCTTGCTGGAAGTGAATTTTGACATAAGAAAAT
AAGTTAAGGGGTTTACTAACTGTCTATGGTCAATGGTATGAGGCTAT
ACTGGGTTTGAGAATGACAAAGGTTTGAAATCCTGGGACATGGGAG
CTCCAGAATTGTTACATTATGAGAAGCTTAGACAGGAATGCTTCATT
CACTGTAGGATAGTACAAAAGGCTTTTTTCAGGGCTTACAAAATATT
GGTAGGGAGAGAAGCGTCAGGGAGACCAGCTCCATATTACCCAAAG
AAAACGGCAAAATTTACAATTCAGCTCACTGAAGAAAAAAGAAAAT
AAAAAGTTTTTTTTTAAAAAAGAAAAGTCAAAATGAAGATTAGT
AAAGGAATTCAGTGAAATGGACCAAATGTAGCATTGTGTCAATTAGT
CAGGCAACTCAAGTCATAGGCTTATTGCAGGTGGTGAATGCATTTTG
ACCTGTTTGATGTGATATGAAGTGAGGCCTCTGTAAGTGAGAATATC
AAGGTTGAACAAAGTTTTTGGCAGATGAGAACGGTTGGACCAATAG
ACAACATTCTTTCCAAGGACATCCCCCCTGCAGATTAGGTTATGAT
CCACTCTGTCATATCCTGAGGGTGTGGCCCACTTTGAGATCCCATGA
TGCACCACGCTGATTAAATTAGGCATTCAGTATATAAAGGGGTTCGGC
CACAGACGGGCAAAAGGAACAGATTCACCGCTTCGGAGTGAATTCC
ATGACGGCTTGCAATTTTCTCGTCGAGTTTTTCTTTCACTAGAGATAG
CCCTCGCCCTTTCATTACACAGAGGCTTTTAAGAAAAAAGCAACCA

P0R1

ACCTGAAGAGGACCTGGCAGCAATAAGTTTTTGGTGAAATAACAAA
GAGGTAAAA

1320 bp

Figure 3.2 Nucleotide sequence for the human RBBP6 Promoter 0 gene.

The position of the P0F1 (forward primer) are shown in blue and the P0R1 (reverse primer) are shown in red.

1

CGGGACCCTGCCACTGAGCAGGCATCCCCTTCTGCAAATTCAGAAAGTACATGATTGC
TAGCTTCAGTTCCATCATCTATAAATCGGAAATAATGTCATGTTGACCACGTAGGGTTT
TTGTTGTTAAATTGACATTTATTGAGCTACAGCTATTAATATTTTCGGTGCATTGAGCCA
CGTCAATGCACCGGCATGGTCTTAGACTATGGATTTATGTGCATTTATTTAATCCAAGT

P1F2

AAACCAAGTACTATTTTAAATGGCATT**TACAGCCAAGGAGACCCAGG**CACAGAGGG

P1F1

GATAAATCTAGAGCCCCACAGCCAGG**GATCCAACCCAGACAACGTGG**CTGCTGAG
CCTGGCAATGTTGTTATGCGATCAGCCCTGTGCCTAGCACATAGTAAGAGCTCAATAA
ATCTGTATGGTGTGGTGGCTGTTATCAGTTCTTGGCAGCGGCTGCTCCACGATTTCCA
CTTGTC AAGAGTATAGGGTAGCCAGTTTATTGGAAGCAGCAGCTAGGGAGCGCTTGCA
TAGCAACCATAGTTTTCTGCGTAGCAACCATAATGCTCACTTAAATTGGGAGGCTTAG
AGGAGCTGACGGGGCCTGTGGGAAGGGGGAGTTAGCCGGCCACCCCTAGGCAAGCC
ACTTTGCAGTGAAACTGCACGCAGCCCCTGCAAGGCGAGCTCTCCCCACCGAGCCTC
CCTGTGAGCCGGTCTCTGACGCGCAACCCCCCTCCCTTTTGAAGCAGATGGTTCTTC
CCGTTGTCCCTGCTCTTTCAGTTTCCGCGCTTTGGAGTCAAAAGCGCGGGGTCACGTG
GGCGGGCCGTGCGCTTTGTGACGTCAGCCGCCCGCCTCTCGGCCCGCCTATCCGCGC
ACGCCAGCCCCGCTCGCGCGCGCCGCCGTGCAATCCCTGCTTAAGAGACCCCGCAG
TGGGGCGCTCGTCCGAAGCCAGGCCGCGTCCGCCATAGTACCTGGCTTGGAGGTGTCG
CCGCCGCTCGGTGAGAGCCCCGAGCGGCAGGGGGCCAACACAAAAAGGGAGCCGGA
GAAGCCCTAGCCGCTGCCAGCAGCTTTCGGGCGTGTCTCGCGGTTCCGGCCTCAA
GGCGACGGAACGAAAGGCGAGCGAAGCGCGGAGGATCCGGCGAGAAGAAGCGTCA
GGGAGCCTCGGCGGTGTCCCCGGGGTCCGCCGAAGCCACCCGGCCCGCGGCTGGGGC
CCGGGGTGGTGAGGAAGTGCTCCGAGGCCTCGCCGAGGCCTAGCGCCGGCTTTGTGTC
CGAGGCGGCGGCGGGCGGGGGAGGCGGAGCCGGGGGCGGCCTGCGGGAAGGCC
TCTCCTCCGCCGACCGCGGTTTTTCGGCCTAGGCCGTGGGGCCGCTCGTGGCCTCCGGG
GAGCAGGCGCCAGGGGTTTGTGTGCGGTGGGGGCTGGGCCTGGGCCTGGGGAAGCT
GACGCCGGTCTCGGAAGCCAGGAGGAGGCGTGAGGCCGCTCGTGGACTCCGGGCC
TAGGCCCTCTCCCCTCAACCTTCTCCCGGGGCCTGGGTCACCCAATCCACGGAGAGA

P1R1

GAGACCCGCGGGAGGTGCGGCCG**GCTATGGACCCCTGACCC**CGTGGGGTTCGCTC
GGACTCTTAACGTGTGGACTGACCGCTACTGACTGCACCGCCAATCCCCCGTCTCTGC
CGGCCCTTAGCATGAGCGAGGGGACCCAGCCGGGTGACATTGTGCCCGTTGGCGGA
TTCTCGATTTCCCCTCTTCCCGTCTCGTCCTCCTCCTCCCCATGAAGTGATTCTGAG
TATCGGGGGTCTCTGGATTATTGTTCTGACGAACCCCTGCTTGTGGTTGGGGGTATT

P1R3

TAATCTGAGGCCTTAGGGT**CCTTCGGTGTCTTTGAGT**GTTTTGTGTGTACATATTTG
CTCTTAAAGTTTATAAATATACGTATATTGAGAGTGTC

1900 bp

Figure 3.3 Nucleotide sequence for the human RBBP6 Promoter 1 gene.

The position of P1F1 is shown in red and the P1F2 is shown in green. The P1R1 primer is shown in blue and the P1R3 primer in bold text.

migration of the sample through the agarose gel. The expected size fragments for P0 and P1 resulting from PCR was calculated based on the position of the forward and reverse oligonucleotides.

3.2.2. Cloning of P0 and P1 PCR products

3.2.2.1 Purification and cloning of PCR products

All PCR fragments were purified using the GFX-purification kit as described in section 2.9.1. PCR fragments were first cloned using the pGEM[®]-T Easy cloning vector (see figure 2.1 for map of pGEM[®]-T Easy) for the P0 fragment and the pCR[®]-XL-TOPO[®] cloning system (see figure 2.2 for map of pCR[®]-XL-TOPO[®]) for the P1 fragments as per the manufacturers instructions. This first cloning step would ensure sufficient digestion of the promoters before cloning into the pEGFP-C1 and pDsRed1 vectors.

3.2.2.2 Screening for recombinants

Colonies were screened for recombinant clones using the M13 universal oligonucleotides in a colony PCR as described in section 2.10.3 (see table 3.1 for primer sequences). Amplicons resulting from the colony PCR reactions were resolved on a 1 % agarose gel as described in chapter 2.9. Figure 3.6 shows the PCR result for the identification of pGEM[®]-T Easy P0 recombinant. The expected size fragment of 1.2 kb is observed in lanes 6 and 7. Since the positions of the M13 universal oligonucleotides are 100 bp

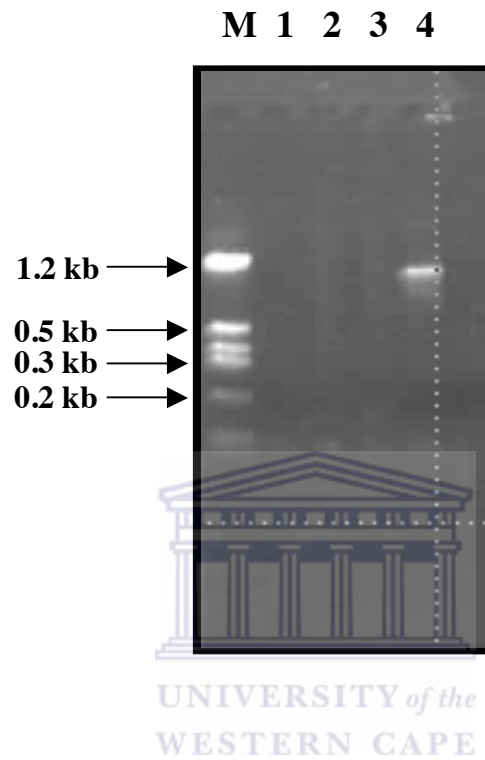


Figure 3.4 PCR amplification of the human RBBP6 Promoter 0 (P0) gene.

P0 was PCR amplified with POF1 and POR1 using the BAC clone CIT DM210 as template. **Lane M.** represents the marker pTZ **Lane 1.** the water blank, **Lane 2.** 1 in 10 dilution of the template DNA, **Lane 3.** a 1 in 100 dilution of the template DNA and **Lane 4.** a 1 in 1000 dilution of the template DNA The expected size of the amplicon equals 1.0 kb. PCR fragments were resolved on a 1 % agarose gel.

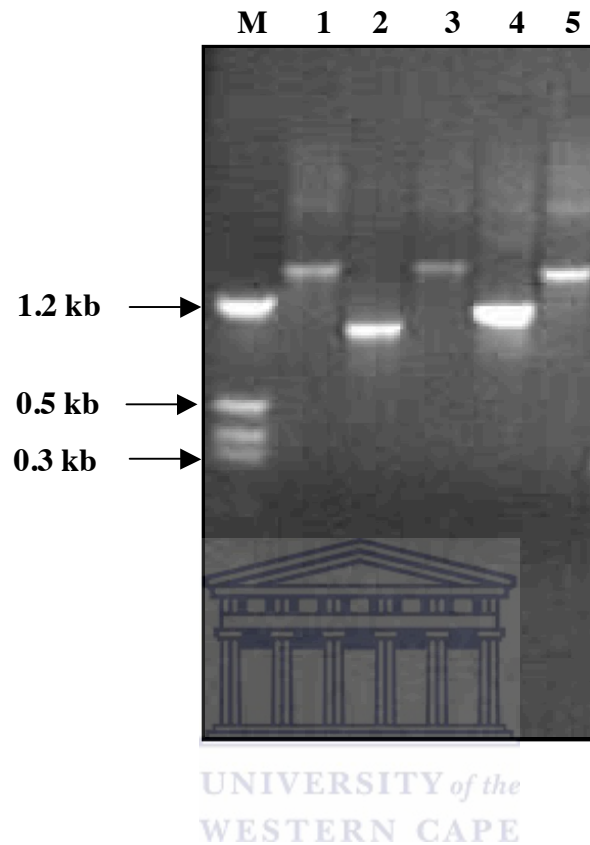
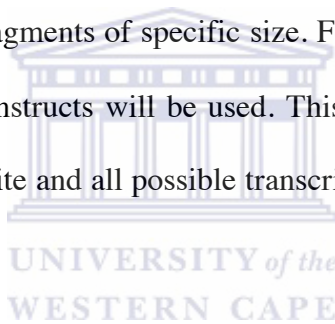


Figure 3.5 PCR amplification of the human RBBP6 Promoter 1 (P1) gene.

Different oligonucleotide sets were designed to amplify P1 using PCR. The BAC clone CIT DM210 was used in a standard PCR. **Lane M.** represents the size marker pTZ, **Lanes 1, 3 and 5** represent primer pair P1F2 and P1R3 (1.6 kb), **Lanes 2 and 4** represent primer set P1F1 and P1R1 (1.2 kb). PCR fragments were resolved on a 1 % agarose gel.

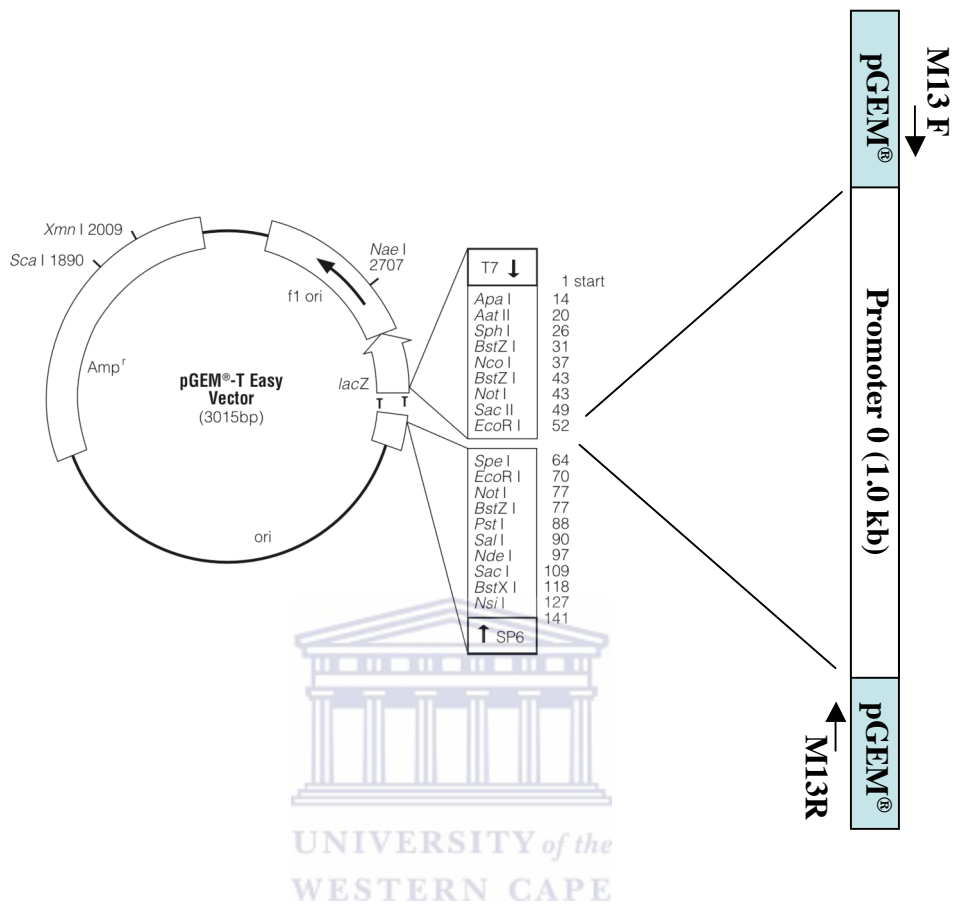
upstream and 100 bp downstream from the cloning site, the initial cloned PCR product will be increased by an additional 200 bp following colony PCR.

From figure 3.7 several fragments are observed. The expected sizes for P1 and pCR[®]-XL-TOPO[®] recombinant clones range from 1.6 kb to 1.8 kb. The M13 oligonucleotides are similarly positioned on this cloning vector as with the pGEM[®]-T Easy vector, thus PCR fragments increased by an additional 200 bp. Several low molecular weight fragments are also observed. This can possibly be explained as the PCR artefacts that were cloned alongside the expected fragments since the entire P1 PCR reaction was purified and cloned without selection for fragments of specific size. For further analysis only the full-length P0 and P1 promoter constructs will be used. This will ensure that the sequences include the transcription start site and all possible transcription factors that can determine promoter activity.



3.2.2.3. Isolation of plasmid DNA

Presumptive positive recombinant clones identified by colony PCR were cultured using the appropriate antibiotic and subjected to small-scale plasmid DNA isolation using the alkaline lysis procedure as described in chapter 2.7.1. The extracted plasmid DNA was electrophoresed on a 1 % agarose gel as described in chapter 2.9 to determine the quality of the DNA and the concentrations determined by taking an absorbance reading at 260 nm.



(a)



(b)

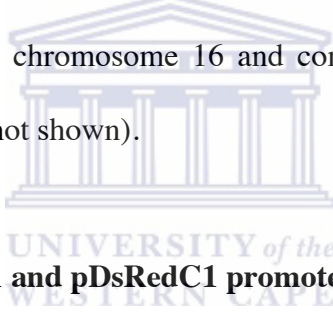
Figure 3.6 PCR based screening method to identify P0 pGEM[®]-T Easy recombinants.

(a) Diagrammatical representation of the PCR strategy used to identify pGEM[®]-T Easy Promoter 0 recombinant clones indicating the position of the M13 forward and reverse oligonucleotides.

(b) Represents the PCR results obtained for pGEM[®]-T Easy-P0 recombinants clones. **M.** pTZ size marker with the 1.2 kb fragment indicated. **B.** the water blank. **Lanes 1 to 6.** background colonies **Lane 7 and 8.** represents pGEM[®]-T Easy/P0 recombinants with the expected size of 1.2 kb indicated. PCR fragments were resolved on a 1% agarose gel.

3.2.2.4 Sequencing of recombinants

A number of clones representing pGEM[®]-T Easy/P0 and pCR[®]-XL-TOPO[®]/P1 recombinants were selected for sequencing analysis. Sequencing reactions using the Big Dye v3.0 cycle sequencing kit were carried out as described in section 2.11. Both the M13 universal and gene specific oligonucleotides designed for sequencing were used in sequencing reactions (see table 3.1 for sequences). The sequence data obtained were compared to the human genome sequence using BLASTn (Altschul *et al.*, 1990) and also aligned with the known sequences for P0 (figure 3.2) and P1 (figure 3.3) using BLAST (bl2seq) (Tatiana *et al.*, 1999) The results showed complete matches with the human BAC clone CTD-2450M10 on chromosome 16 and complete alignment to the known sequences for P0 and P1 (data not shown).



3.3 Preparation of pEGFP-C1 and pDsRedC1 promoter constructs

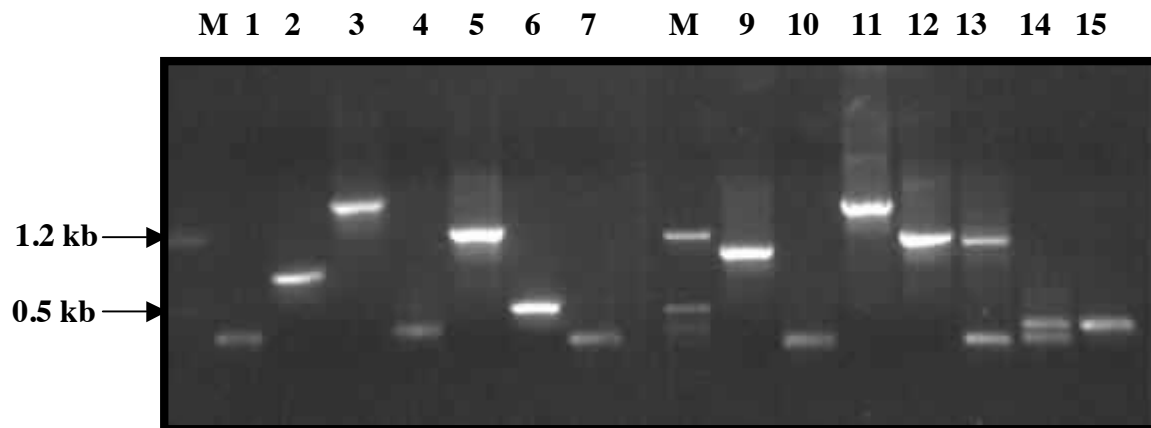
3.3.1. Preparing pEGFP-C1 and pDsRed-C1 cloning vectors

The next step in preparation of the promoter constructs was to place EGFP and DsRed1 under the transcriptional control of P0 and P1 respectively. The CMV promoter in both vectors had to be replaced. This would be achieved by digesting the pEGFP-C1 and pDsRed-C1 vectors with the Ase I and Nhe I restriction endonucleases that flank the CMV promoter, thus releasing it.

The equivalent volume of 1 µg representing pEGFP-C1 and pDsRed-C1 respectively were digested with Ase I and Nhe I as described in section 2.8.3 to release the CMV



(a)



(b)

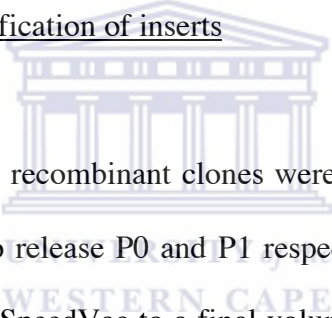
Figure 3.7 PCR based screening method to identify P1 pCR[®]-XL-TOPO[®] recombinants.

(a) Diagrammatical representation of the PCR strategy used to identify pCR[®]-XL-TOPO[®] Promoter 1 recombinant clones indicating the position of the M13 forward and reverse oligonucleotides.

(b) Represents the PCR results obtained for the pCR[®]-XL-TOPO[®] P1 recombinants clones. All PCR fragments representing P1 was cloned using the pCR[®]-XL-TOPO[®] cloning system and recombinant clones screened using colony PCR M. pTZ size marker with the 1.2 kb fragment indicated **Lanes 1 to 15.** represent pCR[®]-XL-TOPO[®]/P1 recombinants. PCR fragments were resolved on a 1 % agarose gel.

promoter. Reactions volumes were reduced to 50 μ l using a Savant SC100 SpeedVac and resolved on a 1 % agarose gel as described in section 2.9. Figure 3.8 shows the digestion of pEGFP-C1 with Ase I and Nhe I. From figure 3.8, lane 1 represents a single digest with Ase I and lane 2, a single digest with Nhe I. Lane 3 represents the double digestion of the vector showing the release of the CMV promoter, bottom band. The top band corresponding to pEGFP-C1 was excised using a sterile blade under long wave UV light and purified using the GFX-purification protocol as described in section 2.9.2. The same were done for the pDsRed-C1 vector (data not shown).

3.3.2 Digestion and purification of inserts

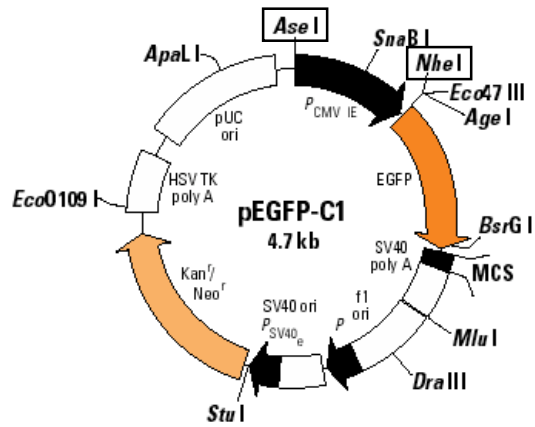


Sequence confirmed P0 and P1 recombinant clones were digested with Ase I and Nhe I as described in chapter 2.8.3 to release P0 and P1 respectively. Reaction volumes were reduced using a Savant SC100 SpeedVac to a final volume of 50 μ l and resolved on a 1 % agarose gel as described in chapter 2.9 and the fragments excised using a sterile blade under long wave UV light and purified using the GFX-purification protocol as described in section 2.9.2.

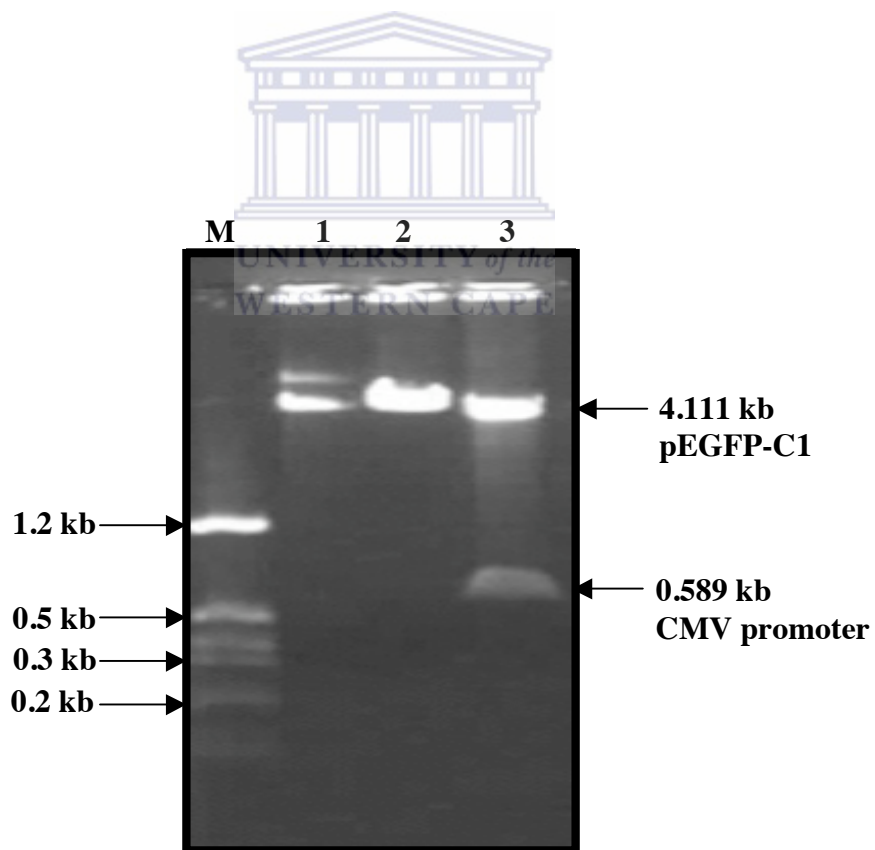
3.3.3. Cloning of P0 and P1 into pEGFP-C1 and pDsRed-C1

3.3.3.1 Cloning and screening

Purified fragments corresponding to P0 and P1 were ligated into pEGFP-C1 and pDsRed-C1 (prepared in section 3.3.1) respectively. Cloning reactions were set up at a vector to insert ratio of 1:3 as described in section 2.8.4. A forward common oligonucleotide (Fc)



(a)



(b)

Figure 3.8 Restriction digestion of the pEGFP-C1 vector deleting the CMV promoter.

(a) Represents the graphical map of pEGFP-C1. The position of the Ase I and Nhe I restriction endonucleases, flanking the CMV promoter, are indicated.

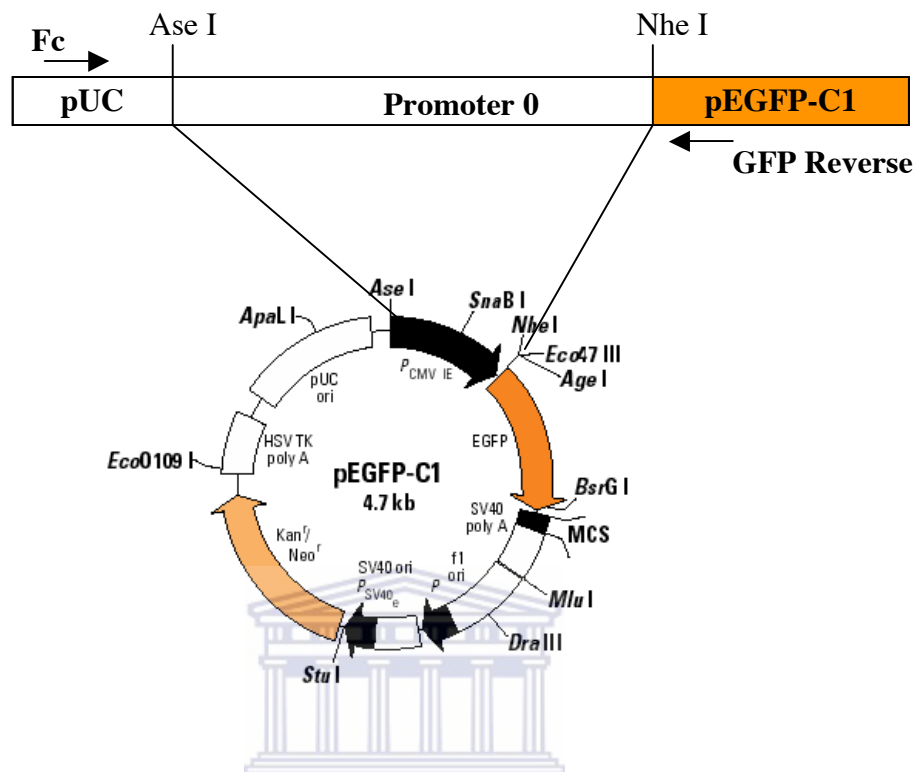
(b) Shows restriction analysis of the pEGFP-C1 vector with Ase I and Nhe I. **Lane M.** represents the size marker pTZ, **lane 1.** represents the pEGFP-C1 vector digested with Ase I **lane 2.** represents the pEGFP-C1 vector digested with Nhe I and **lane 3.** represents the pEGFP-C1 vector digested with both Ase I and Nhe I with the release of the CMV promoter. The results from the restriction analysis were resolved on a 1 % agarose gel.

complementary to the pUC region of both vectors was designed situated a 100 bp upstream of the Ase I recognition site. A reverse oligonucleotide was designed in the 5' region of EGFP (GFP-R) and DsRed1 (RFP-R) respectively, located 100 bp downstream of the Nhe I recognition site (see table 3.1 for sequences).

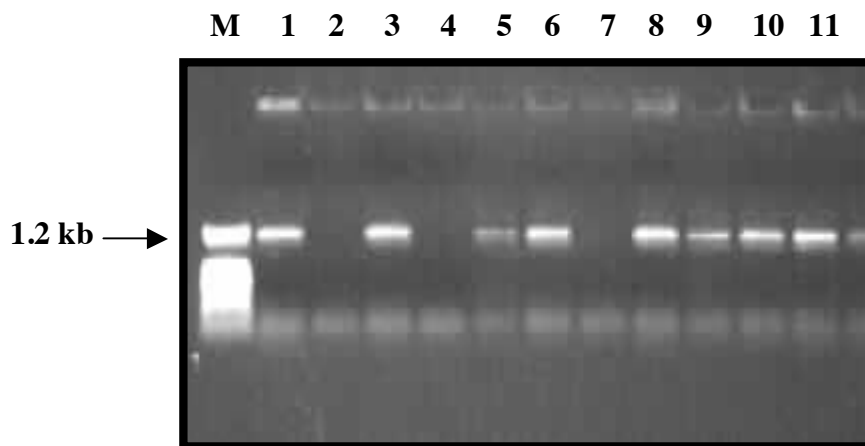
Recombinant clones were identified by colony PCR as described in chapter 2.10.3. PCR reactions were resolved on a 1 % agarose with the appropriate size markers. See figure 3.9 for the screening of pEGFP-C1-P0 recombinant clones. The results show PCR products of the expected size of 1.2 kb. Recombinant clones were also identified for pEGFP-C1-P1, pDsRed-C1-P0 and pDsRed-C1-P1 using colony PCR. Amplicons resulting from colony PCR for pDsRed-C1-P0 recombinant clones were the same as those observed for pEGFP-C1-P0 recombinant clones as observed in figure 3.9. The expected size of 1.8 kb were observed for pEGFP-C1-P1 and pDsRed-C1-P1 recombinant clones.

3.3.3.2. Isolation of plasmid DNA using double CsCl₂ gradients

Recombinant clones were cultured and overnight cultures were subjected to large-scale plasmid DNA isolation using the alkaline lysis method. Double CsCl₂ gradients were performed as described in chapter 2.7.2 to isolate transfection quality plasmid DNA.



UNIVERSITY of the
WESTERN CAPE



(b)

Figure 3.9 PCR identification of the P0-pEGFP-C1 recombinant clones.

(a) Diagrammatical representation of the PCR strategy used to identify P0-pEGFP-C1 recombinant clones indicating the position of Fc (common forward primer) and the GFP primer (EGFP specific reverse primer).

(b) Identification of the P0-pEGFP-C1 recombinants clones using PCR.

Lane M. represents the pTZ size marker, **Lanes 1 to 11** represents the recombinant clones. PCR fragments were resolved on a 1 % agarose gel.

3.3.3.3 Restriction analysis of recombinant clones

Plasmid DNA corresponding to the respective recombinant clones was used in a restriction analysis reaction with Ase I and Nhe I as described in section 2.8.3. From figure 3.10 the digestion of the pEGFP-C1-P0 clone did not show the release of the insert. However, a shift in mobility when compared to pEGFP-C1-P0 singly digested with Ase I was observed, indicating the presence of an insert. Single restriction analysis of the recombinant clone indicated that the Nhe I recognition site was lost. This might have been caused by methylation of the site. Restriction analysis of the pEGFP-C1-P1 recombinant clone showed the release of an insert corresponding to the expected size of 1.6 kb.

3.3.3.4 Sequencing analysis of recombinant clones

Recombinant clones were sequenced at the Inqaba Biotech core sequencing facility. Sequence data obtained for the different clones were compared to the non-redundant database using BLASTn (Altschul *et al.*, 1990). From figure 3.11 the BLAST results for P0 showed a significant match to the Homo sapiens BAC clone CTD-2540M10 on chromosome 16. The sequence obtained for P1, when matched to the non-redundant database showed a significant match to the same BAC clone (see figure 3.12). Also significant matches were shown to the *Pan troglodytes*, *Homo sapiens* and the *Mus musculus* retinoblastoma binding protein 6.

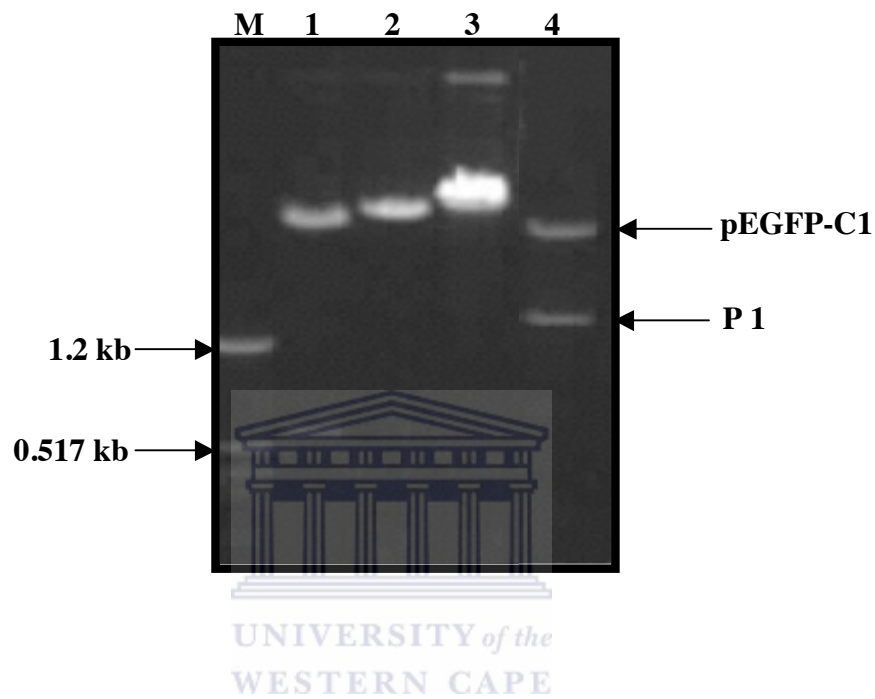


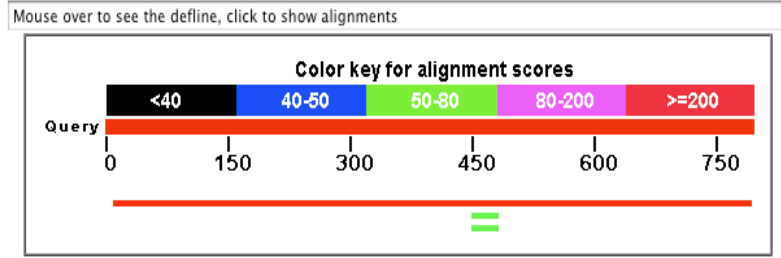
Figure 3.10 Restriction analysis of the pEGFP-C1 promoter constructs.

Lane M represents the size marker pTZ, **lane 1** represents pEGFP-C1 digested with Ase 1 and Nhe 1 **lane 2** represents the digestion of pEGFP-C1 with Ase 1, **lane 3** represents the digestion of pEGFP-C1-P0 with Ase I and Nhe I and **lane 4** represents the digestion of pEGFP-C1-P1 with both Ase 1 and Nhe 1.

Sequence data obtained were also aligned with the sequences used to design the PCR oligonucleotides to amplify P0 and P1 using BLAST (bl2seq) (Tatiana *et al.*, 1999). Sequence data were obtained from different sets of oligonucleotides since the recombinant clones were sequenced with the M13 universal oligonucleotides as well as gene specific oligonucleotides for each promoter. The sequence data for each promoter was aligned and the resulting consensus sequences used for BLAST analysis.

Figure 3.13 shows the alignment of P0 sequence to that in figure 3.2 and figure 3.14 shows the alignment of P1 to that in figure 3.3. Both query sequences showed complete match to the subject sequences. The sequence results for P0 showed two mismatches at the beginning of the sequence and can possibly be attributed to the efficiency of the sequencing reactions. The sequence traces for P0 showed some level of background (noise) causing two nucleotides to be unresolved. From the sequence data it was concluded that the correct sequences corresponding to the RBBP6 P0 and P1 promoters were successfully amplified and cloned. Table 3.2 shows the list of constructs sequenced and the nomenclature that will be used in subsequent sections of this chapter to describe the different constructs.

Distribution of 3 Blast Hits on the Query Sequence



(a)

[Distance tree of results](#) NEW

Sequences producing significant alignments:	Score (Bits)	E Value
gi 17921202 qb AC010321.8 Homo sapiens chromosome 16 clone CTD-	1380	0.0
gi 78214466 qb AC122309.5 Mus musculus BAC clone RP23-293G2 ...	58.4	4e-05
gi 78190347 qb AC163358.3 Mus musculus BAC clone RP23-11M14 ...	58.4	4e-05

(b)

> [gb|AC010321.8](#) | **D** Homo sapiens chromosome 16 clone CTD-2540M10, complete sequence
Length=207256

Score = 1520 bits (823), Expect = 0.0
Identities = 827/829 (99%), Gaps = 0/829 (0%)
Strand=Plus/Minus

```

Query 1      CTGaaaaaaactaaaaaTTGGCTGAGCATGTTGGCACAAGCCTATATCCAGCTACTCAG 60
Sbjct 123952  CTGAAAAAACTAAAAATTAGCTGAGCATGTTGGCACAAGCCTATAGTCCCAGCTACTCAG 123893

Query 61     GAGCCTGAAGCAGGAGGATTACTTGATCCCAGGAGTTCAAAGTTACAGTGAAGTGTGATT 120
Sbjct 123892  GAGCCTGAAGCAGGAGGATTACTTGATCCCAGGAGTTCAAAGTTACAGTGAAGTGTGATT 123833

Query 121    GCACCACTGCACTCCAGCCTGGGTGACAGAGCAAGACCCGGACTCCAAAATAATACTACT 180
Sbjct 123832  GCACCACTGCACTCCAGCCTGGGTGACAGAGCAAGACCCGGACTCCAAAATAATACTACT 123773

Query 181    AATAATTAACAAACAAAAGAGAACAGCCTCCATGAAATAGATCTCATTCGAGTTCCCT 240
Sbjct 123772  AATAATTAACAAACAAAAGAGAACAGCCTCCATGAAATAGATCTCATTCGAGTTCCCT 123713

Query 241    GAGCTTGAGTAGTTCACACAGCAGCAGGCAGGCTCCTTGGATCTCCCAATTCC 300
Sbjct 123712  GAGCTTGAGTAGTTCACACAGCAGCAGGCAGGCTCCTTGGATCTCCCAATTCC 123653

Query 301    GCTTGCTGGAAGTGAATTTGACATAAGAAAATAAGTTAAGGGGTTTACTAAGTGTCTAT 360
Sbjct 123652  GCTTGCTGGAAGTGAATTTGACATAAGAAAATAAGTTAAGGGGTTTACTAAGTGTCTAT 123593

Query 361    GGTCAATGGTATGAGGCTATAGTGGTGTGAGAATGACAAAGGTTTGAATCCTGGGACA 420
Sbjct 123592  GGTCAATGGTATGAGGCTATAGTGGTGTGAGAATGACAAAGGTTTGAATCCTGGGACA 123533

Query 421    TGGGAGCTCCAGAATTGTTACATTATGAGAAGCTTAGACAGGAATGCTTCATTCAGTGA 480
Sbjct 123532  TGGGAGCTCCAGAATTGTTACATTATGAGAAGCTTAGACAGGAATGCTTCATTCAGTGA 123473

Query 481    GGATAGTACAAAAGGCTTTTTCAGGGCTTACAAAAATATTGGTAGGGAGAGAAGCGTCAG 540
Sbjct 123472  GGATAGTACAAAAGGCTTTTTCAGGGCTTACAAAAATATTGGTAGGGAGAGAAGCGTCAG 123413

Query 541    GGAGACCAGCTCCATATTACCCAAAGAAAACGGCAAAATTTACAATTCAGCTCACTGAAG 600
Sbjct 123412  GGAGACCAGCTCCATATTACCCAAAGAAAACGGCAAAATTTACAATTCAGCTCACTGAAG 123353

Query 601    aaaaaagaaaaataaaaagttttttttttaaaaaaagaaaaCTGCAAAATGAAGATTAGTA 660
Sbjct 123352  AAAAAAGAAAATAAAAAGTTTTTTTTTAAAAAAGAAAACCTGCAAAATGAAGATTAGTA 123293

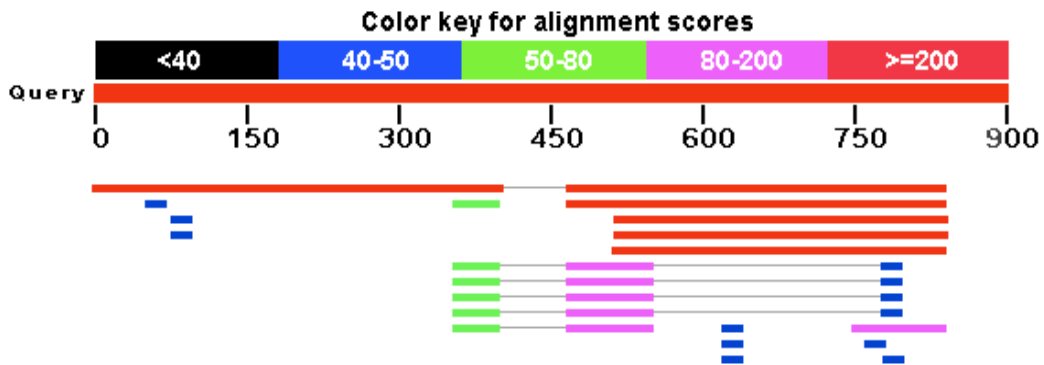
Query 661    AAGGAATTCAGTGAATGGACCAAAATGTAGCATTGTGTCAATTAGTCAGGCAACTCAAGT 720
Sbjct 123292  AAGGAATTCAGTGAATGGACCAAAATGTAGCATTGTGTCAATTAGTCAGGCAACTCAAGT 123233
    
```

(c)

Figure 3.11 BLAST search results for the pEGFP-C1 P0 construct.

- (a) Shows the alignment of the P0 gene sequence with the non-redundant (nr) database using BLASTn.
- (b) the best matches
- (c) the sequence for the best match Homo sapiens chromosome 16 clone CTD-2540M10.





(a)

Sequences producing significant alignments:	Score (Bits)	E Value	
gi 17921202 gb AC010321.8 Homo sapiens chromosome 16 clone CTD-	803	0.0	
gi 55643596 ref XM_510882.1 PREDICTED: Pan troglodytes simil...	688	0.0	G
gi 38683864 ref NM_032626.5 Homo sapiens retinoblastoma bind...	654	0.0	U E G
gi 38683863 ref NM_018703.3 Homo sapiens retinoblastoma bind...	654	0.0	U E G
gi 38683862 ref NM_006910.4 Homo sapiens retinoblastoma bind...	654	0.0	U E G
gi 78675929 gb AC141887.5 Mus musculus BAC clone RP23-478L20...	109	2e-20	
gi 47825187 gb AC125221.4 Mus musculus BAC clone RP23-74N13 ...	109	2e-20	
gi 82907600 ref XM_900847.1 PREDICTED: Mus musculus hypothet...	109	2e-20	G
gi 82914374 ref XM_923116.1 PREDICTED: Mus musculus hypothet...	109	2e-20	G
gi 74148360 dbj AK161332.1 Mus musculus adult male testis cD...	101	4e-18	G
gi 15868597 emb AJ324218.1 HSA324218 Homo sapiens genomic seq...	91.7	4e-15	
gi 12853350 dbj AK015130.1 Mus musculus adult male testis cD...	71.9	3e-09	U E G

(b)

> [gi|17921202|gb|AC010321.8|](#) **D** Homo sapiens chromosome 16 clone CTD-2540M10, complete sequence
Length=207256

Score = 803 bits (405), Expect = 0.0
Identities = 405/405 (100%), Gaps = 0/405 (0%)
Strand=Plus/Minus

```

Query 1      TTC TTGGCAGCGGCTGCTCCACGATTCCACTTGTC AAGAGTATAGGGTAGCCAGTTTAT 60
            ||| ||| ||| ||| ||| ||| ||| ||| ||| ||| ||| ||| ||| ||| ||| ||| |||
Sbjct 121634  TTC TTGGCAGCGGCTGCTCCACGATTCCACTTGTC AAGAGTATAGGGTAGCCAGTTTAT 121575

Query 61     TGGAAGCAGCAGCTAGGGAGCGCTTGCATAGCAACCATAGTTTCTGCGTAGCAACCATA 120
            ||| ||| ||| ||| ||| ||| ||| ||| ||| ||| ||| ||| ||| ||| ||| ||| |||
Sbjct 121574  TGGAAGCAGCAGCTAGGGAGCGCTTGCATAGCAACCATAGTTTCTGCGTAGCAACCATA 121515

Query 121    ATGCTCACTTAAATTGGGAGGCTTAGAGGAGCTGACGGGGCCTGTGGGAAGGGGAGTT 180
            ||| ||| ||| ||| ||| ||| ||| ||| ||| ||| ||| ||| ||| ||| ||| ||| |||
Sbjct 121514  ATGCTCACTTAAATTGGGAGGCTTAGAGGAGCTGACGGGGCCTGTGGGAAGGGGAGTT 121455

Query 181    AGCCGGCCACCCCTAGGCAAGCCACTTTGCAGTGGA AACTGCACGCAGCCCTGCAAGGC 240
            ||| ||| ||| ||| ||| ||| ||| ||| ||| ||| ||| ||| ||| ||| ||| ||| |||
Sbjct 121454  AGCCGGCCACCCCTAGGCAAGCCACTTTGCAGTGGA AACTGCACGCAGCCCTGCAAGGC 121395

Query 241    GAGCTCTCCCCACCGAGCTCCCTGTGAGCCGGTCT CCTCTGACGCGCAACCCCTCCCT 300
            ||| ||| ||| ||| ||| ||| ||| ||| ||| ||| ||| ||| ||| ||| ||| ||| |||
Sbjct 121394  GAGCTCTCCCCACCGAGCTCCCTGTGAGCCGGTCT CCTCTGACGCGCAACCCCTCCCT 121335

Query 301    TTTGAAGCAGATGGTTCTCCCGTTGTCCTGCTCTTTCAGTTTCCGCGCTTTGGAGTCA 360
            ||| ||| ||| ||| ||| ||| ||| ||| ||| ||| ||| ||| ||| ||| ||| ||| |||
Sbjct 121334  TTTGAAGCAGATGGTTCTCCCGTTGTCCTGCTCTTTCAGTTTCCGCGCTTTGGAGTCA 121275

Query 361    CAAAGCGGGGGTACGTGGGCGGGCCGTGCGCTTTGTGACGTCA 405
            ||| ||| ||| ||| ||| ||| ||| ||| ||| ||| ||| ||| ||| ||| ||| ||| |||
Sbjct 121274  CAAAGCGGGGGTACGTGGGCGGGCCGTGCGCTTTGTGACGTCA 121230

```

(c)

Figure 3.12 BLAST search results for the pDsRed-C1 P1 construct.

- (a) Shows the alignment of the P1 gene sequence with the non-redundant (nr) database using BLASTn.
- (b) the best matches
- (c) the sequence for the best match Homo sapiens chromosome 16 clone CTD-2540M10.



Construct	EGFP Enhanced green fluorescent protein	DsRed1 (Red fluorescent protein)	CMV Cytomegalovirus Promoter	P0 RBBP6 Promoter 0	P1 RBBP6 Promoter 1
EGFP- CMV	✓		✓		
EGFP- P0	✓			✓	
EGFP- P1	✓				✓
DsRed- CMV		✓	✓		
DsRed- P0		✓		✓	
DsRed- P1		✓			✓

Table 3.2 List of promoter constructs with the nomenclature used in the subsequent sections of this chapter.



3.4 Evaluation of the expression of EGFP and DsRed1 *in vivo*

3.4.1. Transfection of constructs

The normal human embryonic kidney cell line (Hek 293T) was cultured as described in section 2.13.3 till confluent. Having reached confluency cells were re-plated at a density of 2.5×10^4 on coverslips in 6 well plates and re-cultured to 80 % confluency. The cells were subsequently transiently transfected with 1 μ g of DNA representing the different constructs (see table 3.2 for list of constructs) using the TransFectin™ lipid reagent as described in section 2.13.4.1. EGFP and DsRed1 under the transcriptional control of the CMV promoter were used as reference constructs.



Score = 1112 bits (578), Expect = 0.0
 Identities = 580/581 (99%), Gaps = 0/581 (0%)
 Strand=Plus/Plus

```

Query 20  GCTGAGCATGTTGGCACAAGCCTATACTCCCAGCTACTCAGGAGCCTGAAGCAGGAGGAT 79
          |||
Sbjct 137  GCTGAGCATGTTGGCACAAGCCTATAGTCCCAGCTACTCAGGAGCCTGAAGCAGGAGGAT 196

Query 80  TACTTGATCCCAGGAGTTCAAAGTTACAGTGAAGTGTGATTGCACCACCTGCACTCCAGCC 139
          |||
Sbjct 197  TACTTGATCCCAGGAGTTCAAAGTTACAGTGAAGTGTGATTGCACCACCTGCACTCCAGCC 256

Query 140 TGGGTGACAGAGCAAGACCCGGACTCCAAAATAATACTACTAATAATTAACAAACAAAA 199
          |||
Sbjct 257  TGGGTGACAGAGCAAGACCCGGACTCCAAAATAATACTACTAATAATTAACAAACAAAA 316

Query 200  AGAGAACAGCCTCCATGAAATAGATCTCATTCCGACTTCCTGAGCTTGAGTAGTTCACTA 259
          |||
Sbjct 317  AGAGAACAGCCTCCATGAAATAGATCTCATTCCGACTTCCTGAGCTTGAGTAGTTCACTA 376

Query 260  CAGACAGCAGGCAGGCAGAGCTCCTGGATCTCCAATTCGGCTTGCTGGAAGTGAATTT 319
          |||
Sbjct 377  CAGACAGCAGGCAGGCAGAGCTCCTGGATCTCCAATTCGGCTTGCTGGAAGTGAATTT 436

Query 320  TGACATAAGAAAATAAGTTAAGGGGTTTACTAACTGTCTATGGTCAATGGTATGAGGCTA 379
          |||
Sbjct 437  TGACATAAGAAAATAAGTTAAGGGGTTTACTAACTGTCTATGGTCAATGGTATGAGGCTA 496

Query 380  TACTGGGTTTGAGAATGACAAAGGTTTGAATCCTGGGACATGGGAGCTCCAGAATTGTT 439
          |||
Sbjct 497  TACTGGGTTTGAGAATGACAAAGGTTTGAATCCTGGGACATGGGAGCTCCAGAATTGTT 556

Query 440  ACATTATGAGAAGCTTAGACAGGAATGCTTCATTCCTGCTAGGATAGTACAAAAGGCTTT 499
          |||
Sbjct 557  ACATTATGAGAAGCTTAGACAGGAATGCTTCATTCCTGCTAGGATAGTACAAAAGGCTTT 616

Query 500  TTCAGGGCTTACAAAAATATTGGTAGGGAGAGAAGCGTCAGGGAGACCAGCTCCATATTA 559
          |||
Sbjct 617  TTCAGGGCTTACAAAAATATTGGTAGGGAGAGAAGCGTCAGGGAGACCAGCTCCATATTA 676

Query 560  CCCAAAGAAAACGGCAAAATTTACAATTCAGCTCACTGAAG 600
          |||
Sbjct 677  CCCAAAGAAAACGGCAAAATTTACAATTCAGCTCACTGAAG 717
  
```

Figure 3.13 Sequence alignment of pEGFP-C1 P0.

- (a) Shows the sequence of P0 compared to the human RBBP6 gene sequence as shown in figure 3.2 using BLAST (bl2seq).



Score = 1577 bits (820), Expect = 0.0
Identities = 820/820 (100%), Gaps = 0/820 (0%)
Strand=Plus/Plus

```
Query 1 CGGCATGGTCTTAGACTATGGATTTATGTGCATTTATTTAATCCAAGTAAACCAAGTACT 60
      |||
Sbjct 188 CGGCATGGTCTTAGACTATGGATTTATGTGCATTTATTTAATCCAAGTAAACCAAGTACT 247

Query 61 ATTTTAAATGGCATTTCACAGCAAGGAGACCCAGGCACAGAGGGGTAAATCTAGAGCC 120
      |||
Sbjct 248 ATTTTAAATGGCATTTCACAGCAAGGAGACCCAGGCACAGAGGGGTAAATCTAGAGCC 307

Query 121 CCCACAGCCAGGGATCCAACCCAGACAACGTGGCTGCTGAGCCTGGCAATGTTGTTATGC 180
      |||
Sbjct 308 CCCACAGCCAGGGATCCAACCCAGACAACGTGGCTGCTGAGCCTGGCAATGTTGTTATGC 367

Query 181 GATCAGCCCTGTGCCTAGCACATAGTAAGAGCTCAATAAATCTGTATGGTGCTGGTGGCT 240
      |||
Sbjct 368 GATCAGCCCTGTGCCTAGCACATAGTAAGAGCTCAATAAATCTGTATGGTGCTGGTGGCT 427

Query 241 GTTATCAGTTCCTGGCAGCGGCTGCTCCACGATTTCCACTTGTC AAGAGTATAGGGTAGC 300
      |||
Sbjct 428 GTTATCAGTTCCTGGCAGCGGCTGCTCCACGATTTCCACTTGTC AAGAGTATAGGGTAGC 487

Query 301 CAGTTTATTGGAAGCAGCAGCTAGGGAGCGCTTGCATAGCAACCATAGTTTCTGCGTAG 360
      |||
Sbjct 488 CAGTTTATTGGAAGCAGCAGCTAGGGAGCGCTTGCATAGCAACCATAGTTTCTGCGTAG 547

Query 361 CAACCATAATGCTCACTTAAATTGGGAGGCTTAGAGGAGCTGACGGGGCCTGTGGGGAAG 420
      |||
Sbjct 548 CAACCATAATGCTCACTTAAATTGGGAGGCTTAGAGGAGCTGACGGGGCCTGTGGGGAAG 607

Query 421 GGGGAGTTAGCCGGCCACCCCTAGGCAAGCCACTTGCAGTGGAAACTGCACGCAGCCCC 480
      |||
Sbjct 608 GGGGAGTTAGCCGGCCACCCCTAGGCAAGCCACTTGCAGTGGAAACTGCACGCAGCCCC 667

Query 481 TGCAAGGCGAGCTCTCCCCACCGAGCCTCCCTGTGAGCCGGTCCCTCCTGACGCGCAACCC 540
      |||
Sbjct 668 TGCAAGGCGAGCTCTCCCCACCGAGCCTCCCTGTGAGCCGGTCCCTCCTGACGCGCAACCC 727

Query 541 CCCTCCCTTTTGAAGCAGATGGTTCCTCCCGTTGTCCCTGCTCTTTCAGTTCCGCGCTT 600
      |||
Sbjct 728 CCCTCCCTTTTGAAGCAGATGGTTCCTCCCGTTGTCCCTGCTCTTTCAGTTCCGCGCTT 787

Query 601 TGGAGTCACAAAGCGCGGGGTACGTGGGCGGGCCGTGCGCTTTGTGACGTAGCCGCCC 660
      |||
Sbjct 788 TGGAGTCACAAAGCGCGGGGTACGTGGGCGGGCCGTGCGCTTTGTGACGTAGCCGCCC 847

Query 661 CGCCTCTCGGCCCGCCTATCCGCGCACGCCAGCCCCGCTCGCGCGCGCCCGCCGTGCAA 720
      |||
Sbjct 848 CGCCTCTCGGCCCGCCTATCCGCGCACGCCAGCCCCGCTCGCGCGCGCCCGCCGTGCAA 907

Query 721 TCCCTGCTTAAGAGACCCCGCAGTGGGGCGCTCGTCCGAAGCCAGGCCCGCTCCGCCATA 780
      |||
Sbjct 908 TCCCTGCTTAAGAGACCCCGCAGTGGGGCGCTCGTCCGAAGCCAGGCCCGCTCCGCCATA 967

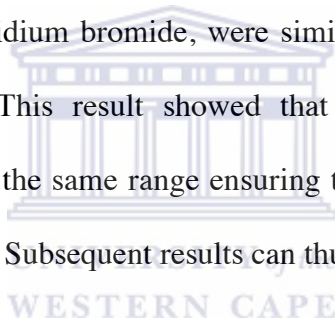
Query 781 GTACCTGGCTTGGAGGTGTCGCCGCCGCTCGGTGAGAGCC 820
      |||
Sbjct 968 GTACCTGGCTTGGAGGTGTCGCCGCCGCTCGGTGAGAGCC 1007
```

Figure 3.14 Sequence alignment of pDsRed-C1 P1.

- (a) Shows the sequence of P1 compared to the human RBBP6 gene sequence as shown in figure 3.3 using BLAST (bl2seq).



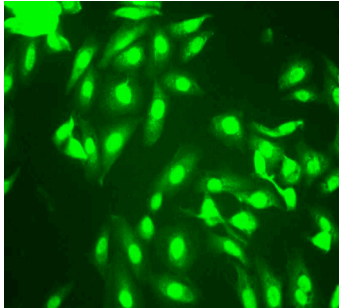
However prior to transfection a standard PCR was first set up using the different constructs as template. This was done to ensure that equal concentration of plasmid DNA representing each construct would be transfected. A 100 ng of plasmid DNA representing the different promoter constructs, as measured on a NanoDrop ND1000 spectrophotometer, was used in a 50 μ l PCR reaction using the gene specific oligonucleotides designed for qRT-PCR against EGFP and DsRed1 as described in section 2.10.2 were carried out. The PCR products were analyzed on a 1 % agarose gel as described in section 2.9 alongside the size marker pTZ. The results indicated amplicons of the expected size of 200 bp as compared to the size marker. The intensities of the amplicons, as stained with ethidium bromide, were similar for all of the different lanes representing each construct. This result showed that the DNA readings using the spectrophotometer falls within the same range ensuring that equal concentration of each construct would be transfected. Subsequent results can thus be seen as comparable.



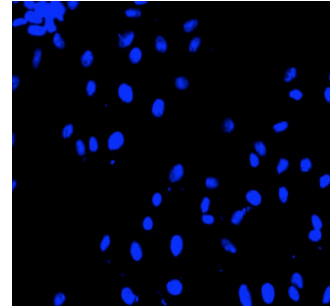
3.4.2 Fluorescence microscopy

Coverslips were removed 48 hours post-transfection and the cells fixed in 4 % paraformaldehyde as described in chapter 2.14. Nuclei were stained using DAPI. The cells were then viewed using a Zeiss fluorescence microscope and photographed. Figure 3.15(i) shows the results of the expression of EGFP driven by the CMV promoter compared to expression driven by P0 and P1 in the Hek 293T cells. The intensity of fluorescence appears to be magnitudes higher in the nucleus compared to the cytoplasm, a result that correlates well with previous observations (Gao *et al.*, 2002). The fluorescent

(a)

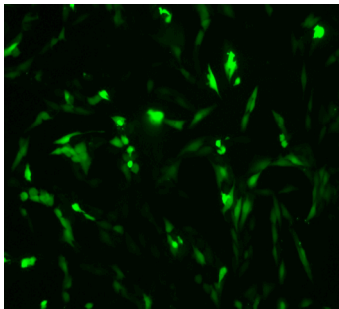


(b)

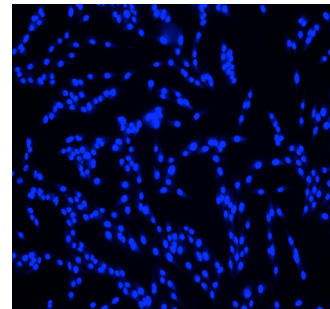


40X magnification

(c)

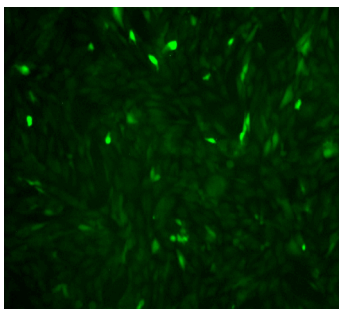


(a)

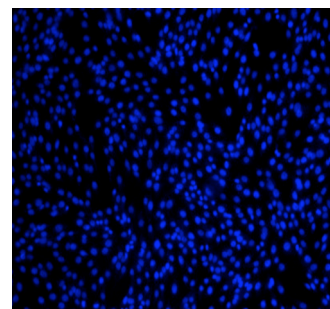


20X magnification

(e)



(f)



20X magnification

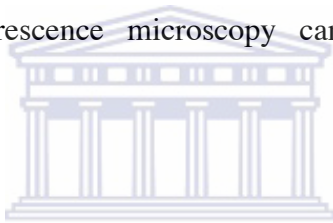
Figure 3.15(i) Fluorescence microscopy analysis of EGFP expression in Hek 293T cells.

The Hek 293T cells were transfected with the different promoter constructs and the expression of EGFP evaluated using a Zeiss fluorescence microscope.

- (a) Hek 293T cells transfected with EGFP-CMV
- (b) Hek 293T cells transfected with EGFP-CMV counterstained with DAPI
- (c) Hek 293T cells transfected with EGFP-P0
- (d) Hek 293T cells transfected with EGFP-P0 counterstained with DAPI
- (e) Hek 293T cells transfected with EGFP-P1
- (f) Hek 293T cells transfected with EGFP-P1 counterstained with DAPI.

intensity observed for CMV driven expression of EGFP was higher compared to that driven by P0 and P1. The expression of EGFP from the P0 promoter appears stronger than that of P1.

Figure 3.15(ii) compares the expression of DsRed1 driven by CMV with that driven by P0 and P1. It is however not clear from the data which of the promoters show stronger activity when related to the fluorescent intensities of DsRed1 under the transcriptional control of the different promoters. It is clear from the fluorescence results that no clear conclusions can be drawn and additional quantitative analysis is needed to determine promoter activity since fluorescence microscopy can be considered to be more qualitative.

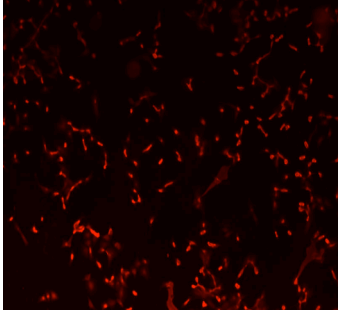


3.4.2. Quantification of fluorescence

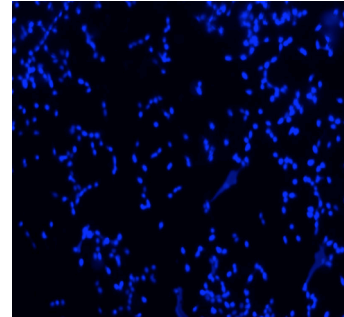
3.4.2.1. FACS analysis

The Hek 293T cell line were transiently transfected as described in section 2.13.4.1 with the different promoter constructs. Cells were FACS analyzed as described in section 2.15. Green and red fluorescence was read using the FL-1 channel on a FACS instrument. From figure 3.16(i), 84 % of cells were positive for EGFP expression driven off the CMV promoter compared to 17 % of cells positive for EGFP driven off P0. Figure 3.16(ii) compares the result obtained for DsRed1 driven off the CMV and P1 promoters. From the results 77 % of cells were positive for DsRed1 expression driven by CMV compared to 9.8 % of cells expressing DsRed1 driven off P1

(a)

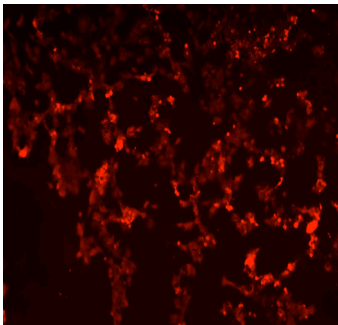


(b)

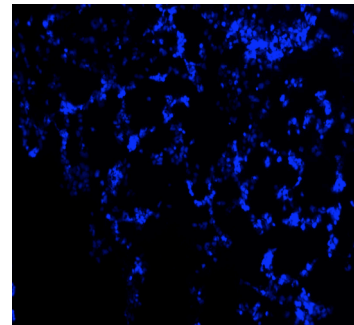


20X magnification

(c)

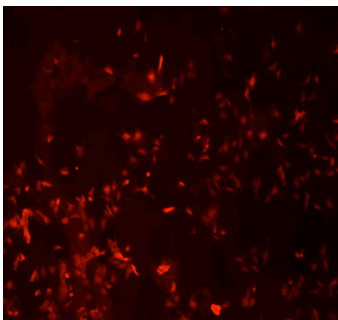


(d)

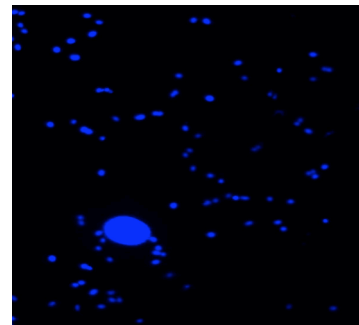


20X magnification

(e)



(f)



20X magnification

Figure 3.15(ii) Fluorescence microscopy analysis of DsRed1 expression in Hek 293T cells.

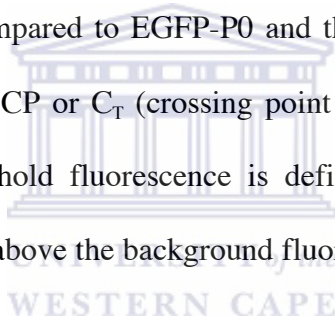
The Hek 293T cells were transfected with the different promoter constructs and the expression of DsRed1 evaluated using a Zeiss fluorescence microscope.

- (a) Hek 293T cells transfected with DsRed1-CMV
- (b) Hek 293T cells transfected with DsRed1-CMV counterstained with DAPI
- (c) Hek 293T cells transfected with DsRed1-P0
- (d) Hek 293T cells transfected with DsRed1-P0 counterstained with DAPI
- (e) Hek 293T cells transfected with DsRed1-P1
- (f) Hek 293T cells transfected with DsRed1-P1 counterstained with DAPI.

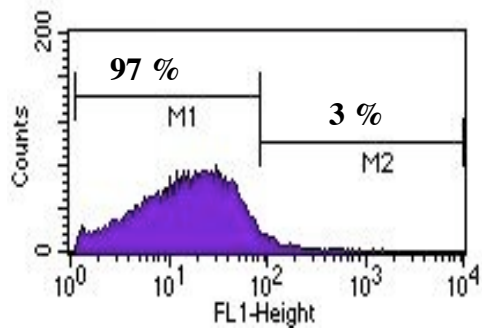
3.4.2.2. Real-Time qRT-PCR

Hek 293T cells were transiently transfected as described in section 2.13.4.1 with the different promoter constructs. Total RNA using the TRIzol reagent was isolated as described in section 2.18 and cDNA synthesized as described in section 2.20. Gene specific oligonucleotides designed against EGFP and DsRed1 (see table 3.1 for sequences) were used in a Real-Time qRT-PCR reaction as described in chapter 2.21.

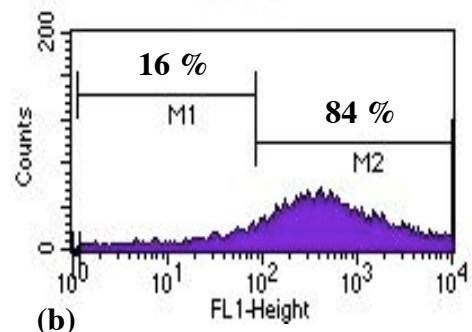
Figure 3.18(i) shows the results obtained following Real-Time qRT-PCR analysis of the expression of EGFP-CMV compared to EGFP-P0 and the expression of DsRed1-CMV compared to DsRed1-P1. The CP or C_T (crossing point threshold) values were used to compare each reaction. Threshold fluorescence is defined as the point at which the fluorescence rises appreciably above the background fluorescence.



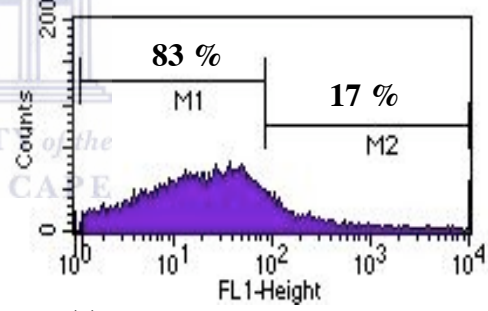
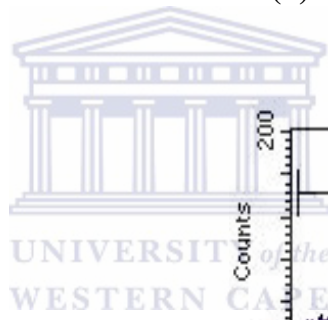
There is an approximate 8-cycle difference between the qRT-PCR curve observed for EGFP-CMV (CP = 23.89) and EGFP-P0 (CP = 31.56). This indicates a higher mRNA copy level of EGFP in cells transfected with EGFP-CMV. This difference is significantly greater between DsRed1-CMV (CP = 23.89) and DsRed1-P1 (CP = 37.65) similarly indicating a higher mRNA copy level in cells transfected with CMV-DsRed1, thus the more copies of the target there are at the beginning of the assay, the fewer cycles of amplification are required to generate the number of amplicons that can be detected reliably. Consequently, fewer amplification cycles are required for the fluorescence to



(a)



(b)

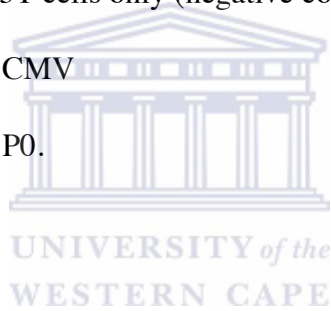


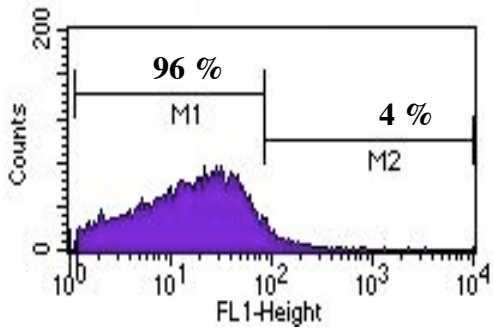
(c)

Figure 3.16(i) FACS analysis of EGFP expression in the Hek 293T cells.

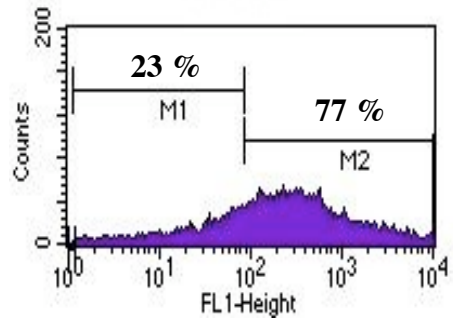
Hek 293T cells were transfected with the different promoter constructs and the EGFP fluorescence measured using the FL-1 channel on a FACS instrument.

- (a) Hek 293T cells only (negative control)
- (b) EGFP- CMV
- (c) EGFP- P0.

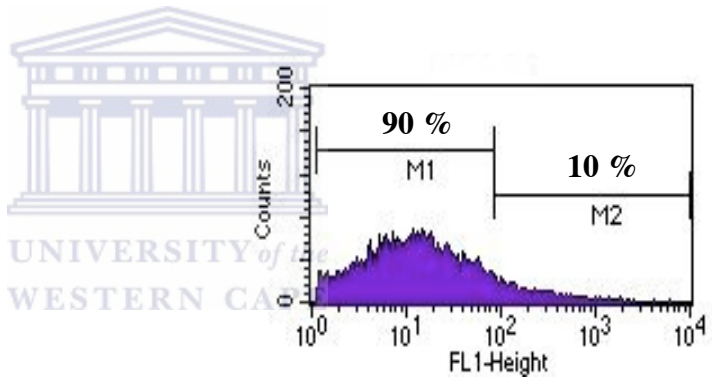




(a)



(b)



(c)

Figure 3.16(ii) FACS analysis of DsRed1 expression in Hek 293T cells.

Hek 293T cells were transfected with the different promoter constructs and the DsRed1 fluorescence measured using the FL-1 channel on a FACS instrument.

- (a) Hek 293T cells only (negative control)
- (b) DsRed1- CMV
- (c) DsRed1- P1

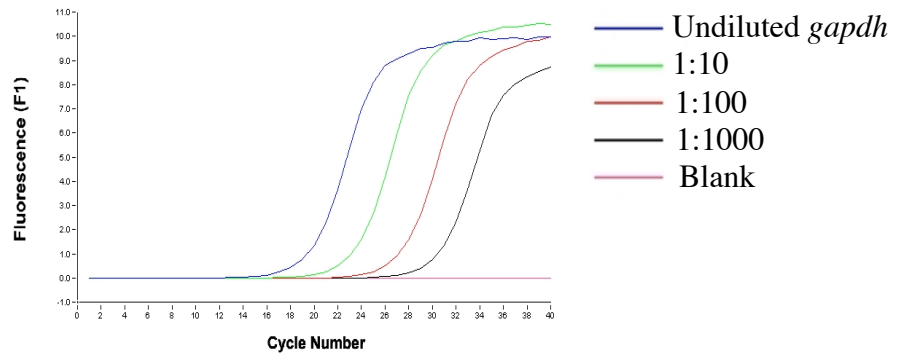


reach the threshold level of detection (CP or a C_T value calculated by a mathematical algorithm).

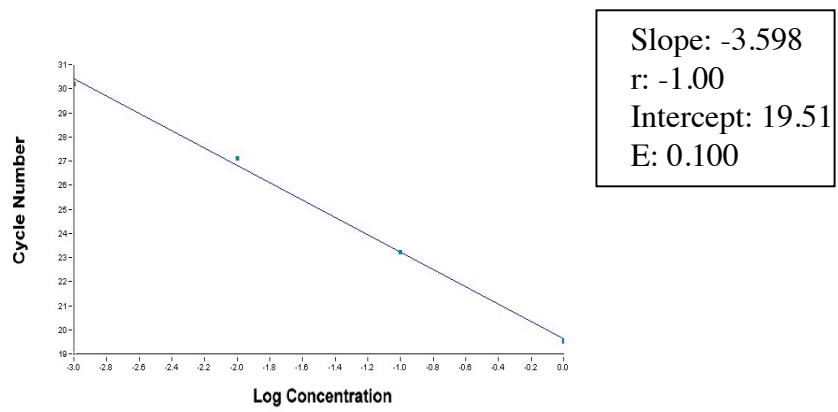
The Real-Time PCR efficiencies (E) were calculated from the resulting slopes provided by the Real-Time Quantitative PCR software and was calculated according to the equation formulated by Pfaffl (2001) as described in section 2.22. A standard curve using the *gapdh* housekeeping gene data was drawn (see figure 3.17) and the expression of EGFP and DsRed1 calculated relative to *gapdh* expression. The expression of EGFP and DsRed1 driven off CMV was calculated as 100 % and the expression of EGFP and DsRed1 driven off P0 and P1 calculated relative to it and represented as the mean \pm SD. From figure 3.18(ii) P0 shows a calculated expression level of 15 % and P1 a calculated expression level of 5 % relative to CMV expression. From the data it can be concluded that the activity of CMV is approximately 7x higher than that of P0 and 20x higher than of P1 with P0 being 3x higher than P1.

3.5 The effect of Apoptosis on promoter activity

The DWNN/RBBP6 gene was isolated in a genetic screen to identify novel components of the MHC class 1 processing and presentation pathway (George, 1995). Further analysis showed the same CTL resistant cell lines, from which it was identified, to be resistant to apoptosis induced by staurosporine as well (Pretorius, 2000). Gao and Scott, 2003, showed that the over-expression of the P2P-R protein promotes camptothecin-



(a)



(b)

Figure 3.17 Represents the *gapdh* standard curve.

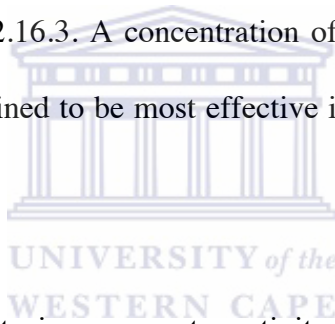
- (a) represents the Real-Time qRT-PCR data using different dilutions of cDNA
- (b) represents the resulting standard curve



induced apoptosis in the human cell line MCF -7. This section will investigate the effect of apoptosis on the expression activity of the human RBBP6 promoters.

3.5.1 Induction of Apoptosis

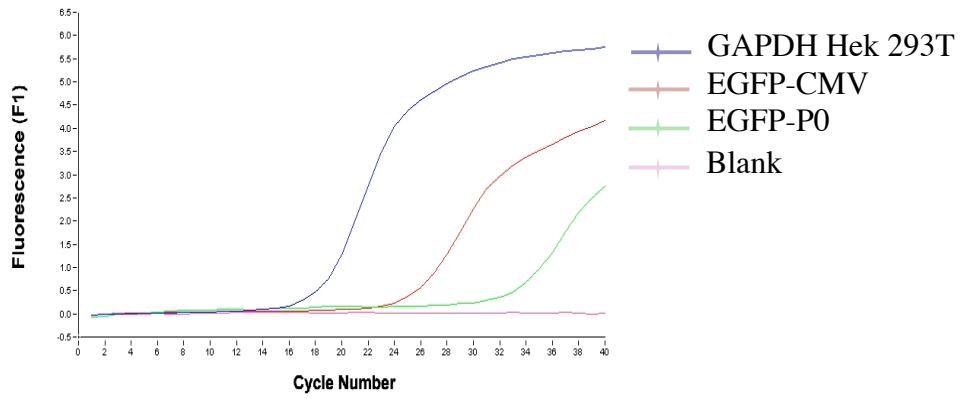
In this section the optimum concentration of camptothecin needed to yield maximum killing of the Hek 293T cells was determined. Hek 293T cells were cultured as described in chapter 2.13.3 and treated with increasing concentrations of camptothecin ranging from 0 to 15 $\mu\text{g/ml}$ and the percentage cell death determined using the Annexin V-PE assay as described in section 2.16.3. A concentration of 10 $\mu\text{g/ml}$ camptothecin over a period of 24 hours was determined to be most effective in inducing maximum cell death in the Hek 293T cell line.



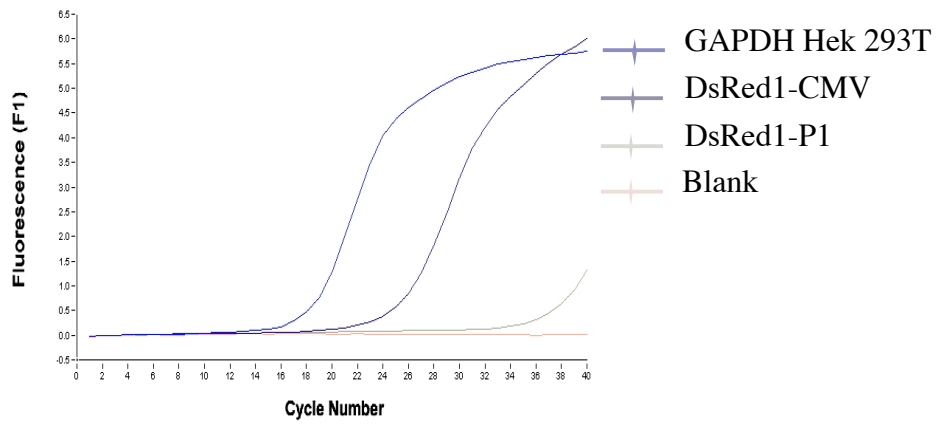
3.5.2 The effect of apoptosis on promoter activity

3.5.2.1 FACS

Hek 293T cells were cultured in 6 well plates as described in section 2.13.3 and transfected with 1 μg of DNA corresponding to the different promoter constructs. After 24 hrs the transfected cells were treated with 10 $\mu\text{g/ml}$ camptothecin and incubated for an additional 24 hrs. Following the induction period cells were FACS analyzed as described in section 2.15. From figure 3.19 an increase in EGFP expression driven off P0 from 17 % to 44 % and a marginal change in DsRed1-P1 expression from 8 to 10 % were observed following camptothecin-induced apoptosis. The FACS results observed



(a)



(b)

Figure 3.18(i) Expression analysis of EGFP and DsRed1 in Hek 293T cells using Real-Time qRT-PCR.

- (a)** represents the Real-Time qRT-PCR data for EGFP-CMV compared to EGFP-P0
- (b)** represents the Real-Time qRT-PCR data for DsRed1-CMV compared to DsRed1-P1.



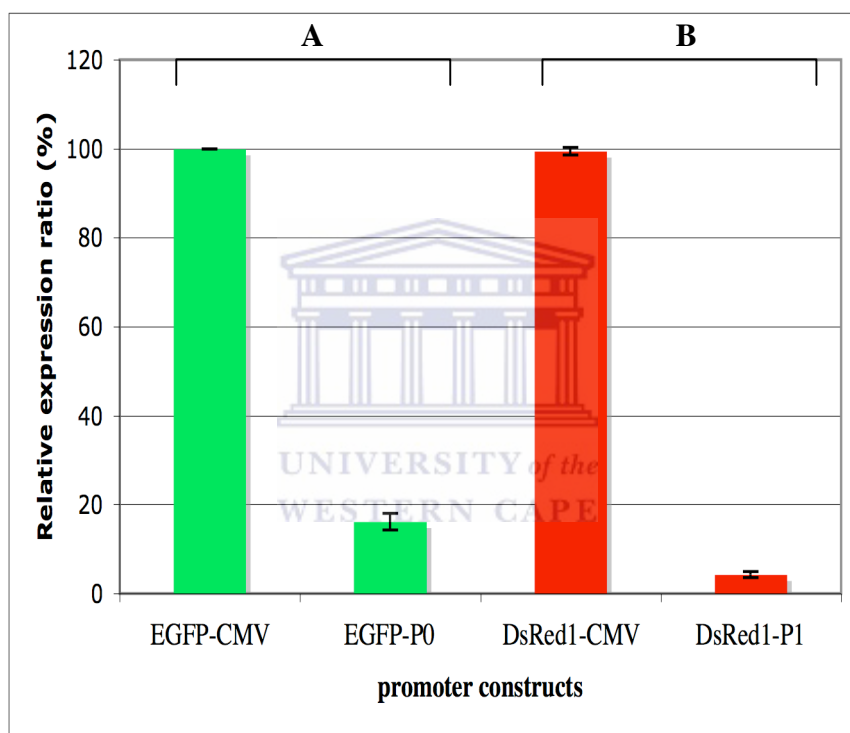
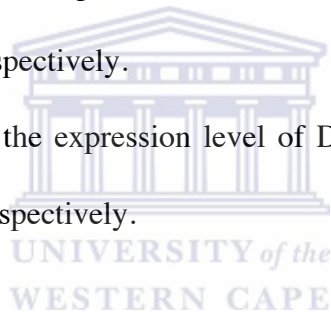


Figure 3.18(ii) Expression analysis of EGFP and DsRed1 using Real-Time qRT-PCR.

The Real-Time qRT-PCR data obtained (see figure 3.17) was analyzed and presented in the graph as the relative expression of EGFP and DsRed1 as the mean \pm SD.

Panel A compares the expression level of EGFP driven of CMV and P0 respectively.

Panel B compares the expression level of DsRed1 driven of CMV and P1 respectively.

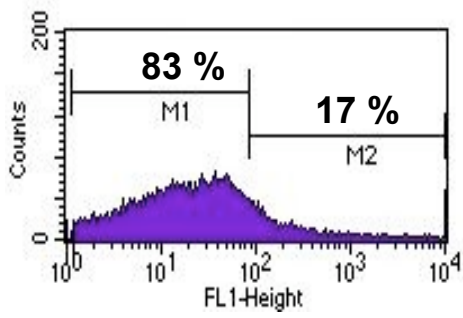


following the induction of apoptosis were compared to that of the two promoters before the induction of apoptosis Both EGFP and DsRed1 driven of CMV showed no increase in expression following treatment with camptothecin (data not shown).

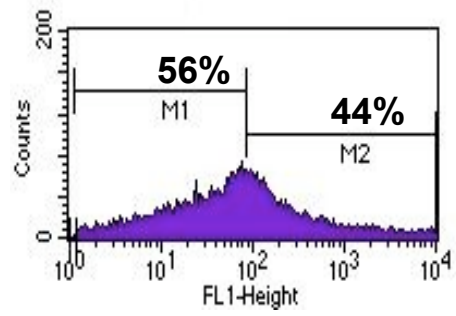
3.5.2.2 Real-Time qRT-PCR

Following induction of apoptosis total RNA was isolated using the TRIzol protocol as described in section 2.18 and cDNA synthesized as described in section 2.20. Real-Time qRT-PCR was performed as described in section 2.21. Figure 3.20(i) shows the data obtained using Real-Time qRT-PCR for the expression of EGFP and DsRed1. Figure 3.20i(a) shows the results of EGFP-CMV and EGFP-P0. There is an upward shift in the qRT-PCR curve representing EGFP-P0 (CP = 26.95) following the induction of apoptosis compared to that observed before the induction of apoptosis (CP = 31.56) showing an increase in the mRNA level of EGFP. Thus the expression activity of the P0 promoter increases following camptothecin-induced apoptosis. An increase in expression activity is also observed for DsRed1-P1 as seen in figure 3.20i(b) with a calculated CP value = 36.42 after induction of apoptosis compared to a CP value = 37.65 before the induction of apoptosis.

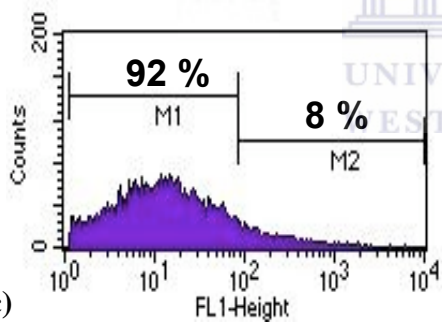
The Real-Time PCR efficiencies (E) were calculated from the resulting slopes provided by the Real-Time Quantitative PCR software and was calculated according to the equation formulated by Pfaffl (2001) as described in section 2.22. The expression of EGFP and DsRed1 calculated relative to *gapdh* expression using the standard curve. The



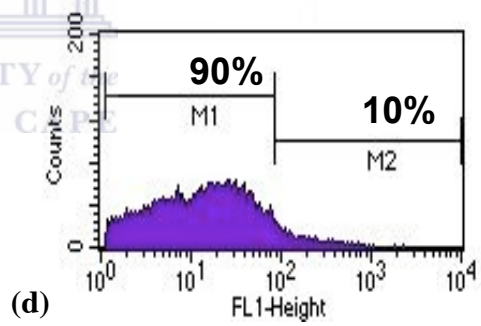
(a)



(b)



(c)

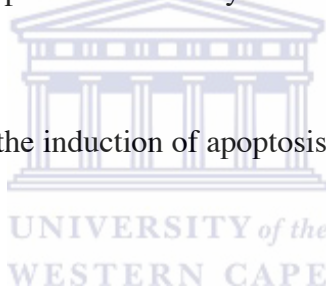


(d)



Figure 3.19 FACS analysis of EGFP and DsRed1 expression in Hek 293T cells following the induction of apoptosis.

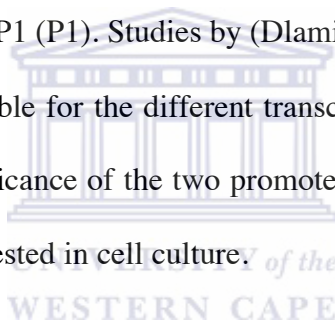
- (a) EGFP expression driven by P0 before the induction of apoptosis
- (b) following the induction of apoptosis using camptothecin.
- (c) DsRed1 expression driven by P1 before the induction of apoptosis
- (d) following the induction of apoptosis using camptothecin.



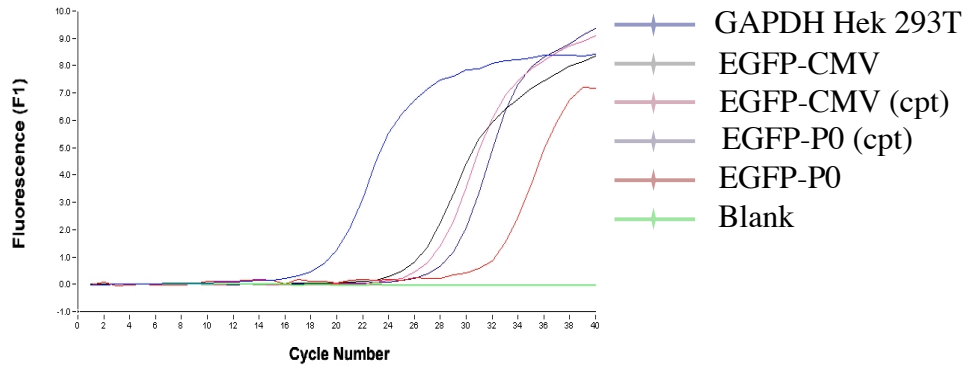
expression of EGFP and DsRed1 driven off CMV was calculated as 100 % and the expression of EGFP and DsRed1 driven off P0 and P1 calculated relative to it and represented as the mean \pm SD of independent repeats of the experiment (see figure 3.21). The results show a 2.0 fold increase in the expression of EGFP driven off P0. The increase in DsRed1 expression driven by P1 was calculated as a 1.4 fold increase.

3.6 Summary

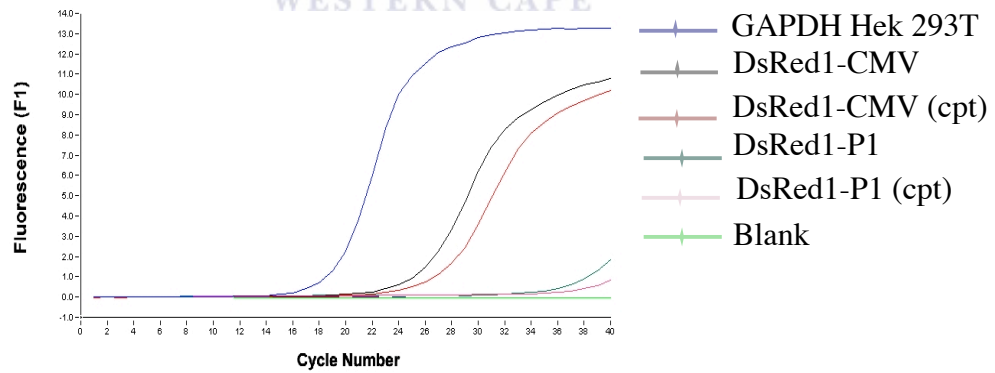
Genetic analysis of the RBBP6 gene showed the presence of two promoters designated Promoter 0 (P0) and Promoter P1 (P1). Studies by (Dlamini in prep.) showed that activity of both promoters are responsible for the different transcripts of the human RBBP6 gene. To better understand the significance of the two promoters for RBBP6, several promoter constructs were designed and tested in cell culture.



The enhanced green fluorescent protein (EGFP) and the red fluorescent protein (DsRed1) were placed under the transcriptional control of P0 and P1 respectively. A PCR based method was used to achieve this. Oligonucleotides were engineered to include an Ase I recognition sequence at the 5' end of both forward oligonucleotides and a Nhe I recognition sequence at the 3' end. Promoters were amplified and cloned into pEGFP-C1 and pDsRed-C1 vectors replacing the CMV promoter. Sequence analysis of the constructs showed complete and correct matches for both promoters when compared to the human genome sequence and existing sequences. EGFP and DsRed1 under the transcriptional control of the CMV promoter were used as reference constructs.



(a)



(b)

Figure 3.20 Expression analysis of EGFP and DsRed1 after camptothecin (cpt)-induced apoptosis using Real-Time qRT-PCR.

- (a) compares the qRT-PCR data obtained for EGFP-CMV to that for EGFP-P0
- (b) compares the qRT-PCR data obtained for DsRed1-CMV to that for DsRed1-P1.



The transcriptional activity of P0 and P1 were evaluated using different methods. Firstly, fluorescence microscopy was used to evaluate the activity of each promoter. EGFP and DsRed1 intensities were evaluated qualitatively following the transfection of the constructs into the Hek 293T cell line using a Zeiss fluorescence microscope. From the data obtained it was shown that the expression of EGFP driven by CMV showed a higher fluorescent intensity when compared to EGFP under the transcriptional control of P0 and P1 with P0 activity higher than that of P1. The result for DsRed1 expression however appeared similar for CMV, P0 and P1 promoters.

A second approach in the evaluation of the activity of the different promoters was FACS analysis. For EGFP expression driven by CMV 84 % of Hek 293T cells showed fluorescence compared with 17 % for EGFP driven by P0. For DsRed1 expression driven by CMV 77 % of Hek 293T cells showed fluorescence compared to 8 % for DsRed driven by P1. However the transfection efficiency of the reagent used should be considered in the Hek 293T cell line. The fluorescence observed are considered to a consequence of the activity of the individual promoters, but if the transfection efficiencies varies amongst the respective constructs, fluorescent intensity becomes a measure of the number of expressing cells and not level of expression. The results thus cannot be taken at face value and should be considered in combination with those observed for Real-Time qRT-PCR.

A third method was Real-Time qRT-PCR. The results were similar as for those obtained for FACS analysis. The activity of the CMV promoter was calculated to be

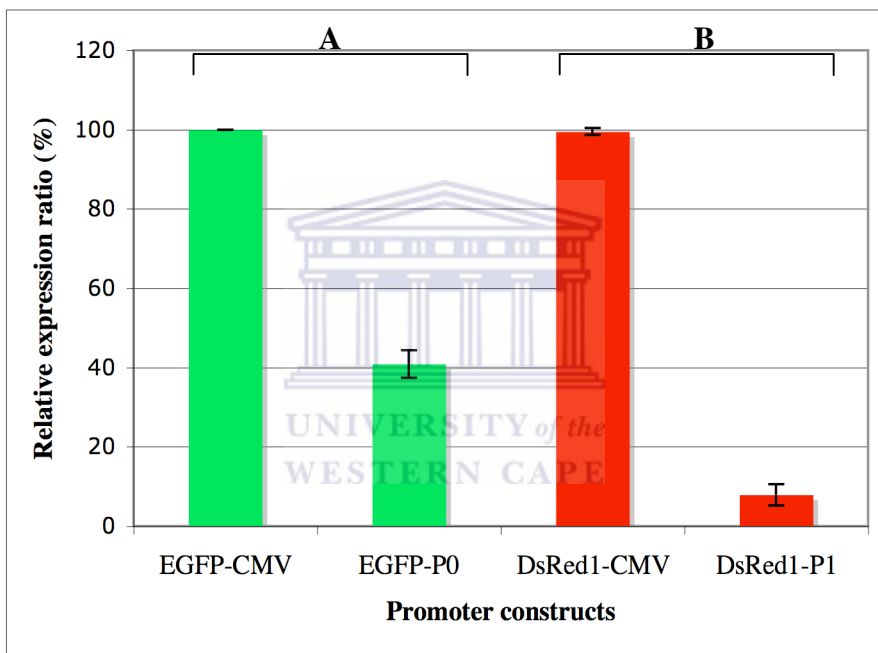
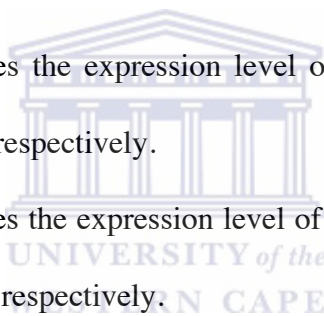


Figure 3.21 Expression analysis of EGFP and DsRed1 following the induction of apoptosis.

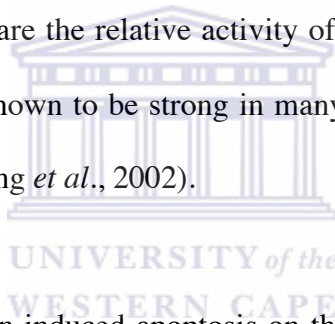
The Real-Time qRT-PCR data (see figure 3.20(i)) was analyzed and presented in the graph as the relative expression of EGFP and DsRed1 following the induction of apoptosis using camptothecin as the mean \pm SD.

Panel A compares the expression level of EGFP driven of CMV and P0 respectively.

Panel B compares the expression level of DsRed1 driven of CMV and P1 respectively.



approximately 20x higher than that of P1 and 7x higher than that of P0 whilst P0 activity was calculated to be 3x higher than that of P1. The Real-Time qRT-PCR technique can be considered an accurate method to measure the concentration of any transcript in the cell. Experimental differences between samples can be accommodated by normalization of qRT-PCR data. A common method for the normalization of qRT-PCR data is the simultaneous amplification of an endogenous reference, or a housekeeping gene (Vandesompele *et al.*, 2002). Maubach *et al.*, (2006) showed that the activity of the hGFAP promoter could be effectively measured by quantification of the expression of the LacZ reporter gene using qRT-PCR. A drawback of this study was using the CMV promoter as reference to compare the relative activity of P0 and P1 since the activity of the CMV promoter has been shown to be strong in many cell lines (Muller *et al.*, 1990) including Hek 293T cells (Chung *et al.*, 2002).



Next the effect of camptothecin-induced apoptosis on the activity of the promoters was investigated. The optimal concentration of camptothecin needed to induce 100 % killing of the Hek 293T cells was firstly determined using the Annexin V-PE apoptosis assay, The Hek 293T cell line were transfected with the different promoter constructs and apoptosis induced using the concentration of camptothecin previously determined. FACS and qRT-PCR analysis were used to evaluate the activity of the promoters following camptothecin-induced apoptosis. No effect was observed on the activity of the CMV promoter following the induction of apoptosis. The activity of P0 showed a 2-fold increase and that of P1 a 1.4 fold increase following the induction of apoptosis. The increase in promoter activity can be considered a significant increase bearing in mind that

these are relative to the activity of CMV. As earlier stated CMV activity has been shown to be strong in many cell lines. A possible solution to this would be to replace CMV with a well-understood and characterized cellular promoter making the results more comparable. From the results it can thus be concluded that the RBBP6 gene plays a possible role in camptothecin-induced apoptosis since there is an increase in the activities of its promoters.



CHAPTER 4: INTERFERENCE RNA – CONSTRUCTION OF MOUSE

RBBP6 siRNA VECTORS

4.1 INTRODUCTION

4.2 AMPLIFICATION OF THE RNA POL III PROMOTERS

4.3 CLONING OF H1 AND U6 PROMOTERS

4.3.1 Deletion of the MCS from pEGFP-C1 and pDsRed-C1 vectors

4.3.2 Preparing pG-MCS and pR-MCS as cloning vectors

4.3.3 Cloning of the U6 and H1 promoters

4.3.4 Screening for recombinant clones

4.4 CLONING OF siRNA OLIGONUCLEOTIDES

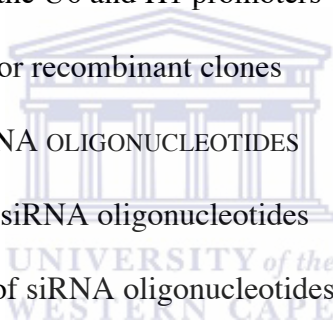
4.4.1 Identifying siRNA oligonucleotides

4.4.2 Annealing of siRNA oligonucleotides

4.4.3 Cloning of siRNA oligonucleotides

4.4.4 Sequencing of recombinant siRNA clones

4.5 SUMMARY



CHAPTER 4: INTERFERENCE RNA – CONSTRUCTION OF MOUSE RBBP6 siRNA VECTORS

4.1 Introduction

The ultimate goal of current genome projects is to identify the biological function of every gene in the genome. Whole genomes of several organisms (including Arabidopsis) have been completely sequenced. The functions of some of the genes have been identified directly by the appropriate assay, or have been inferred by homology to genes of known function in other organisms. Loss-of-function mutants, from insertional mutagenesis or transposable elements, have also been very informative about the role of some of these genes (Martienssen, 1998), particularly in the large-scale analysis of the yeast genome. However, the functions of a large proportion of genes remain unknown.

Injection or ingestion of dsRNA into nematodes can trigger specific RNA degradation, in a process known as RNA interference (Fire *et al.*, 1998). This process facilitates targeted post-transcriptional gene silencing (PTGS) and has recently been harnessed to study the function of over 4000 genes on chromosome III and I in *Caenorhabditis elegans* (Frazer *et al.*, 2000, Gonczy *et al.*, 2000).

The applicability of injecting dsRNA is limited in mammals, because the introduction of dsRNA longer than 30 nt induces a sequence non-specific interferon response (Elbashir *et al.*, 2001). Interferon triggers the degradation of mRNA by inducing 3'-5' oligoadenylate

synthase, which in turns activates RNase I. In addition, interferon, activates the protein kinase PKB, which phosphorylates the translation initiation factor eIF2a leading to a global inhibition of mRNA translation (Stark *et al.*, 1998). To overcome this, Tuschl *et al.*, 1998, introduced chemically synthesized siRNA into mammalian cells. However, unlike plants, fungi and worms, which can replicate siRNAs, there is no evidence of siRNA replication in mammals (Caplen *et al.*, 2002, Wianny and Zernicka-Goetz, 2000). Therefore, siRNA directed silencing by transfection is limited in *Drosophila* and mammals by its transient nature. To overcome the shortcomings of the transfection of chemically synthesized siRNA into cells, several groups have developed DNA vector mediated mechanisms to express substrates that can be converted into siRNA *in vivo* (Kawasaki and Taira, 2003, Miyagishi and Taira, 2002, Yu *et al.*, 2002).

In organisms and cell types with weak or absent interferon responses, constructs that express long hairpins have been used. These constructs make use of RNA Polymerase II (Pol II) promoters that drive the expression of long hairpin RNA that can be cleaved by Dicer into siRNAs. These long hairpin-expression systems have effectively silenced target-gene expression in several different organisms, including mouse oocytes and preimplantation embryos (Wianny and Zernicka-Goetz, 2000).

Plasmid based expression systems using RNA Polymerase III (Pol III) promoters that produce short RNA species and do not trigger a significant interferon response have been developed by several groups (Kawasaki and Taira, 2003, Yu *et al.*, 2002). Two Pol III promoters have been used predominantly, the U6 and the H1 promoters. Both of these promoters are members of the type III class of Pol III family of RNA promoters

	PRIMER NAME	PRIMER SEQUENCE	POSITION
siRNA oligonucleotides	DWNN-A F	5' GATCCC TTATTGCCAGCTGCCGCC TTCAAGAGA GGGCGGCAGCTGGCAATAA TTTTTGAAA GCTT 3'	850-868
	DWNN-A R	5' AGCTTTTCCAAAAA TTATTGCCAGCTGCCGCC TCTCTTGAA GGGCGGCAGCTGGCAATAA GGG 3'	868-850
	DWNN-B F	5' GATCCC TGCAGGGGATCGTCAGGGATT TTCAAGAGA AATCCCTGACGATCCCCTGCA TTTTTGAAA GCTT 3'	2329-2349
	DWNN-B R	5' AGCTTTTCCAAAAA TGCAGGGGATCGTCAGGG ATT TCTCTTGAA AATCCCTGACGATCCCCTGCA GGG 3'	2349-2329
Promoter oligonucleotides	U6 F	5' AC ATTAAT CCA TGG AAT TCA TCC GAC GCC GCC ATC TCT AG 3'	2-22
	U6 R	5' AC ATTAAT CGC AAGCTT GCGCCT AGATCT CAC AAA CAA GGC TTT TCC TTG G 3'	333-352
	H1 F	5' ATTAAT CCA TGG AAT TCG AAC GCT GAC GTC 3'	141-164
	H1 R	5' ATTAAT CGC AAGCTT CGC CTT AGATCT GTG GTC TCA TAC AGA AC 3'	350-366
Cloning and sequencing oligonucleotides	Fc	5' ACT ACT ACG TGG ACT CCA AGC 3'	1190-1211
	Rc	5' ATT ATG ATC AGT TAT CTA GAT CC 3'	1399-1421
	M13F pGEM-T Easy	5' GTT TTC CCA GTC ACG ACG TTG TA 3'	2949-2957
	M13R pGEM-T Easy	5' TTG TGA GCG GAT AAC AAT TTC 3'	176-192

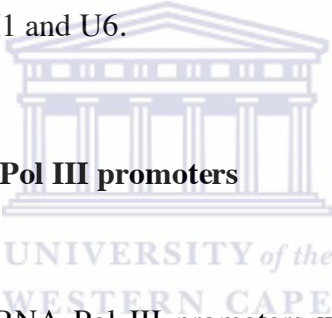
Table 4.1. List of oligonucleotides used in construction of siRNA vectors. The Ase I recognition sequence are indicated in bold text, Hind III in blue text and Bgl II in red text.

(Miyagishi and Taira, 2002). With the advent of vector based siRNA delivery systems it is now possible to make transgenic animals that can silence gene expression stably. This can be achieved by either standard transgene technology, Gordon, 1994, or by the infection of hematopoietic embryonic stem cells (HSC) (Onodera, 2004) or blastocysts with viral based vectors (Kamihira *et al.*, 2005).

Aims of this chapter:

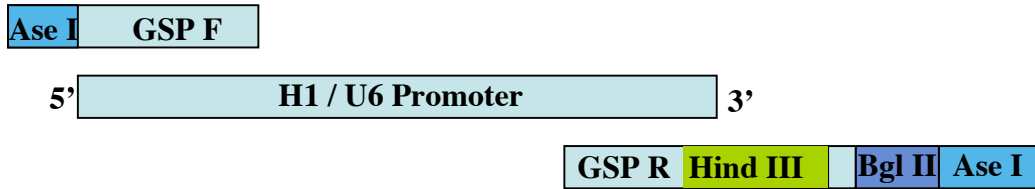
- To identify siRNA oligonucleotides against the mouse RBBP6 gene.
- To construct plasmid based siRNA expression vectors using the RNA Polymerase III (Pol III) promoters H1 and U6.

4.2 Amplification of the RNA Pol III promoters

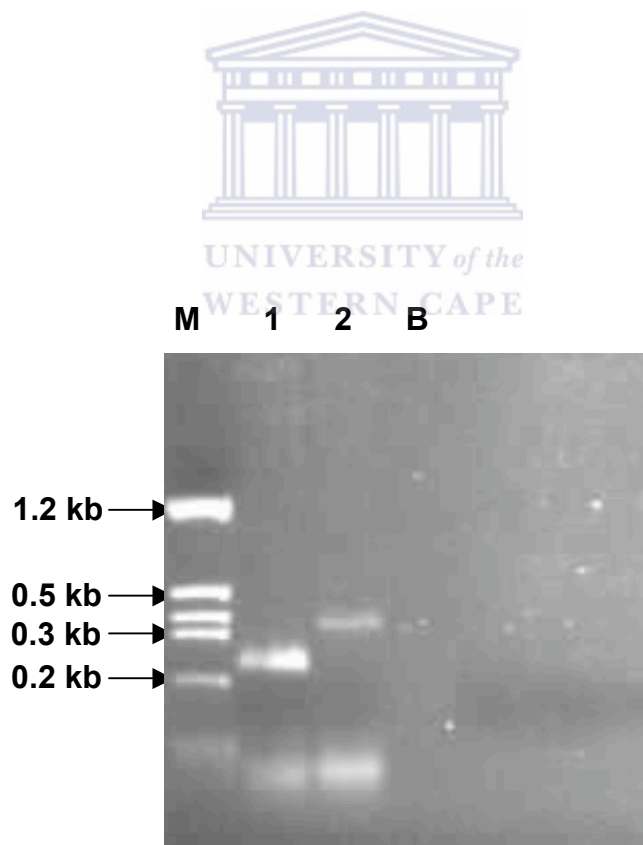


H1 (human) and U6 (mouse) RNA Pol III promoters were PCR amplified using gene specific oligonucleotides (see table 4.1 for sequences) as described in section 2.10.1. Gene specific oligonucleotides were designed to include an Ase I site at the 5' end and Hind III, Bgl II and Ase I sites at the 3' end. An additional six bases was placed between the Hind III and the Bgl II recognition sequences (see figure 4.1). The incorporation of Hind III and Bgl II was performed to facilitate the cloning of the siRNA oligonucleotides into the 3' ends of the respective promoters.

Figure 4.1a diagrammatically represents the PCR strategy used to amplify the U6 and H1 promoters and figure 4.1b the results. From figure 4.1b the expected size fragment of 268



(a)



(b)

Figure 4.1 PCR amplification of the RNA Pol III U6 and H1 promoters.

- (a) A diagrammatical representation of the PCR strategy used to amplify the human H1 and mouse U6 RNA Pol III promoters with the engineered restriction sites indicated.
- (b) Represents the PCR amplification of the human H1 and mouse U6 promoters. PCR products were resolved on a 1.5 % agarose gel. **Lane M.** represents the size marker pTZ,, **lane 1.** the PCR fragment representing the amplified H1 promoter, **lane 2.** The U6 promoter and **lane B.** the water blank

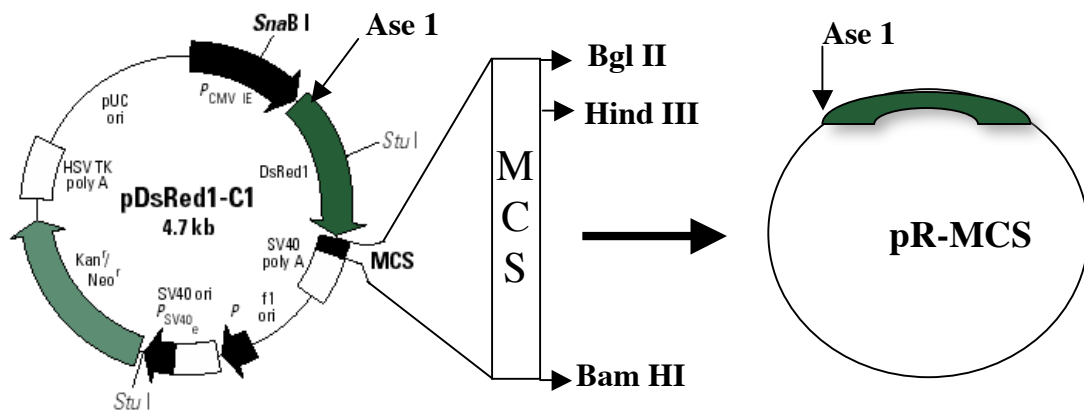
bp representing the human H1 promoter and the expected size fragment of 380 bp representing the mouse U6 promoter was observed. PCR fragments corresponding to both promoters were cloned into the pGEM[®]-T Easy cloning vector as per the manufacturers instructions. Recombinant clones corresponding to both promoters were sequenced using the Big Dye v.3.0 cycle sequencing protocol as described in section 2.11 with the M13 forward and reverse oligonucleotides. The obtained sequencing data were compared to the non-redundant database using BLASTn (Altschul *et al.*, 1990). The results showed complete matches to the database for both promoters (results not shown).

4.3 Cloning of H1 and U6 promoters

4.3.1 Deletion of the MCS from pEGFP-C1 and pDsRed-C1 vectors

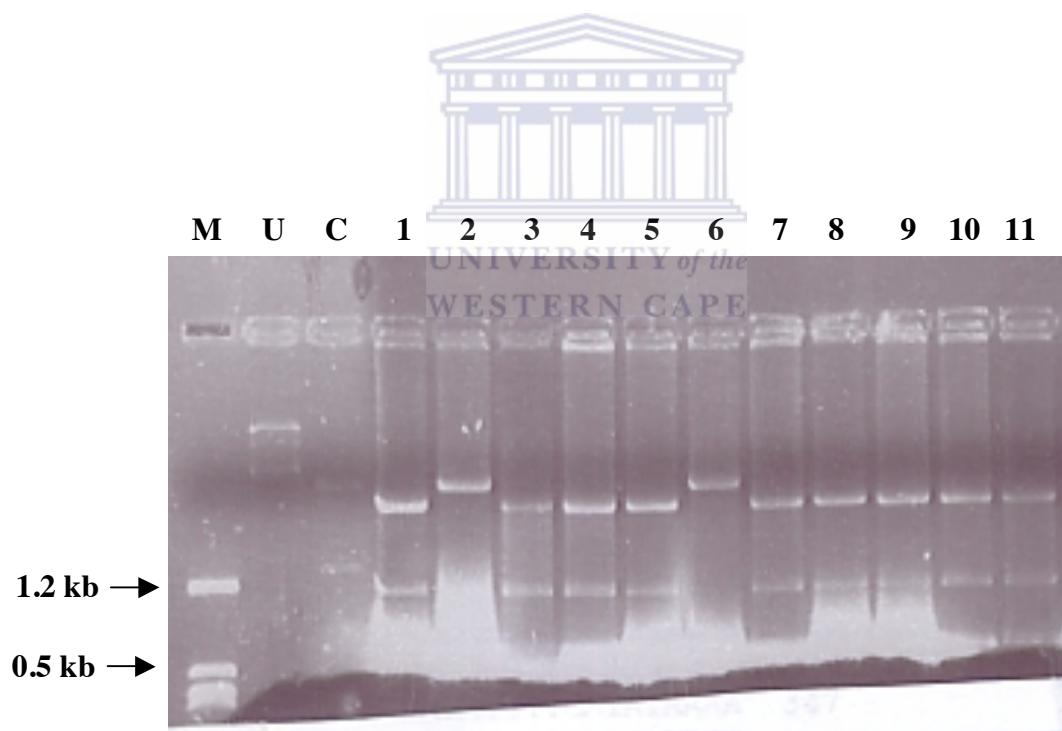
In addition to the pGEM[®]-T Easy vector, both pEGFP-C1 and pDsRed-C1 were used to clone promoter U6 and H1. This would allow for localization of the constructs in cells using fluorescence microscopy.

Firstly the multiple cloning sites (MCS) of pEGFP-C1 and pDsRed-C1 had to be deleted. PCR amplification of U6 and H1 resulted in the addition of a Hind III and Bgl II recognition sequence at the 3' end of both promoters allowing for the subsequent cloning of the siRNA oligonucleotides. Thus with the cloning of U6 and H1 into pEGFP-C1 and pDsRed-C1, an additional recognition site will be created for both restriction endonucleases, with one site already existing in the MCS of both vectors.



(a)

(b)



(c)

Figure 4.2 A diagrammatical representation of the deletion of the MCS (Multiple Cloning Site) from pDsRed-C1 cloning vector.

(a) Represent the graphical map of pDsRed1 and the recognition sites of the endonucleases flanking the MCS.

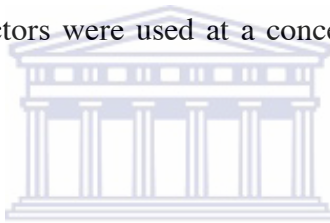
(b) the religated pDsRed1 cloning vector with the MCS deleted.

(c) Screening for MCS deleted pDsRed-C1 vectors using restriction analysis. **M.** represents the size marker pTZ, **U.** uncut pDsRed-C1 plasmid DNA, **C.** control pDsRed-C1 DNA digested with Ase I and Bgl II and **lanes 2 and 6** vectors where the MCS have been deleted. Restriction products were resolved on a 0.8 % agarose gel.

used to construct restriction maps for both vectors. The maps showed the absence of all restriction recognition sequences found within the MCS (data not shown).

4.3.2 Preparing pG-MCS and pR-MCS as cloning vectors

pG-MCS and pR-MCS were cultured overnight and plasmid DNA isolated using the Caesium Chloride/Ethidium bromide fractionation protocol as described in section 2.7.3. Plasmid DNA representing both vectors was digested with Ase I as described in section 2.8.3. Completely digested vectors were diluted to 100 ng and the phosphates removed as described in section 2.8.4. Vectors were used at a concentration of 10 ng/ μ l in ligation reactions.



4.3.3 Cloning of the U6 and H1 promoters

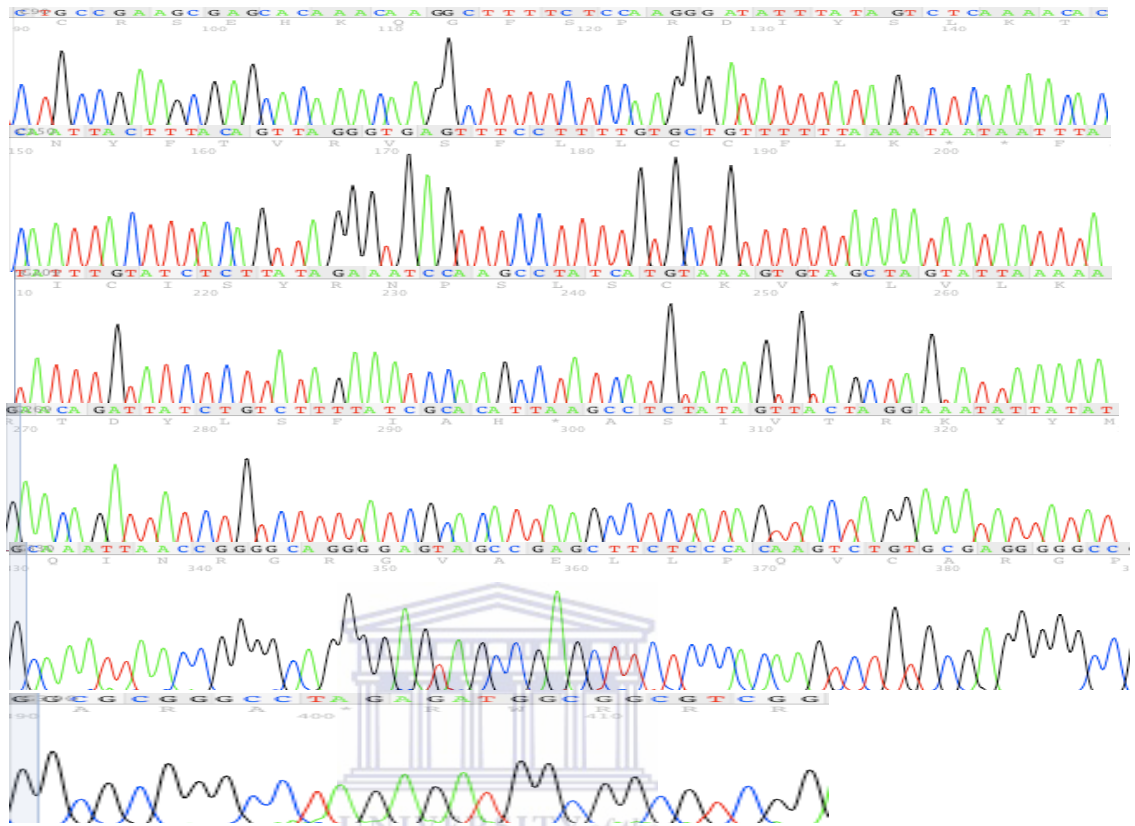
The pGEM[®]-T Easy U6 and H1 recombinant clones were digested with Ase I as described in section 2.8.3 to release the promoters. However, digestion with Ase I produced more than the two expected fragments thus indicating another recognition site for Ase I on the pGEM[®]-T Easy vector. Analysis of the pGEM[®]-T Easy vector nucleotide sequence showed an isoschizomer for Ase I, namely Vsp I. To overcome this the pGEM[®]-T Easy recombinant clones were used as template in a PCR using the M13 universal oligonucleotides as described in section 2.10.2. The resulting U6 and H1 PCR products were digested with Ase I as described in section 2.8.3 and the digested fragments purified using the GFX purification protocol as described in section 2.9.2. The

purified U6 and H1 fragments were serially diluted and used in a ligation reaction with the Ase I digested pG-MCS and pR-MCS vectors respectively as described in section 2.8.4 at a vector to insert ratio of 1:5. Reactions were transformed as described in section 2.6.

4.3.4 Screening for recombinant clones

To identify pG-MCS U6/H1 and pR-MCS U6/H1 recombinant clones several colonies were picked from plates representing the different cloning reactions and used as template in colony PCR analysis as described in section 2.10.3. A common forward primer (Fc) was designed 100 bp upstream of the Ase I recognition site within the pUC region and a common reverse primer (Rc) was designed 100 bp downstream of the Ase I restriction site within the CMV region for both pEGFP-C1 and pDsRed-C1 (see table 4.1). Colonies that were positive for PCR were cultured and subjected to large-scale plasmid isolation using the alkaline lysis procedure as described in section 2.7.2. Plasmid DNA was digested with Ase I to confirm the presence of the insert as described in section 2.8.4.

U6 and H1 cloned into pGEM[®]-T Easy, pG-MCS and pR-MCS were sequenced using the Big Dye v.3.0 cycle sequencing kit as described in section 2.11. Sequence data obtained was compared to the non-redundant database using BLASTn (Altschul *et al.*, 1990). No mismatches were observed for U6 (see figure 4.3) and H1 (H1 data not shown). Vectors were subsequently called GU6 and GH1 (pG-MCS), RU6 and RH1 (pR-MCS) and pU6 and pH1 (pGEM[®]-T Easy) and shall be referred to as such in the subsequent text.



(a)

```

>emb|X06980.1|MMU6SNR Mouse U6 RNA gene
Length=707

Score = 603 bits (326), Expect = 4e-169
Identities = 328/329 (99%), Gaps = 0/329 (0%)
Strand=Plus/Minus

Query  90   CTGCCGAAGCGAGCACAACAAGGCTTTTCTCCAAGGGATATTTATAGTCTCAAAACACA 149
      |||
Sbjct  331   CTGCCGAAGCGAGCACAACAAGGCTTTTCTCCAAGGGATATTTATAGTCTCAAAACACA 272

Query  150   CAATTACTTTACAGTTAGGGTGAGTTTCCTTTTGTGCTGTTTTTTAAAATAATAATTTAG 209
      |||
Sbjct  271   CAATTACTTTACAGTTAGGGTGAGTTTCCTTTTGTGCTGTTTTTTAAAATAATAATTTAG 212

Query  210   TATTTGTATCTCTTATAGAAATCCAAGCCTATCATGTAAAGTGTAGCTAGTATTTAAAAG 269
      |||
Sbjct  211   TATTTGTATCTCTTATAGAAATCCAAGCCTATCATGTAAAGTGTAGCTAGTATTTAAAAG 152

Query  270   AACAGATTATCTGTCTTTTATCGCACATTAAGCCTCTATAGTTACTAGGAAATATTATAT 329
      |||
Sbjct  151   AACAGATTATCTGTCTTTTATCGCACATTAAGCCTCTATAGTTACTAGGAAATATTATAT  92

Query  330   GCAAATTAACCGGGGCAGGGGAGTAGCCGAGCTTCTCCACAAGTCTGTGCGAGGGGGCC 389
      |||
Sbjct  91    GCAAATTAACCGGGGCAGGGGAGTAGCCGAGCTTCTCCACAAGTCTGTGCGAGGGGGCC  32

Query  390   GGCGCGGGCCTAGAGATGGCGGCGTCGGA 418
      |||
Sbjct  31    GGCGCGGGCCTAGAGATGGCGGCGTCGGA  3
  
```

(b)

Figure 4.3 **Sequence data and BLAST results for the RNA Pol III mouse U6 promoter.**

- (a) Shows the sequence traces for the mouse U6 promoter.

- (b) the sequence alignment of the U6 promoter against the non-redundant database using BLASTn.



4.4 Cloning of siRNA oligonucleotides

4.4.1 Identifying siRNA oligonucleotides

siRNA oligonucleotides were identified using the iRNAi version 1.0 oligonucleotide prediction software (<http://mekentosj.com/irnai/>). The full-length annotated mouse RBBP6 nucleotide sequence was used as input data. The sequence included the 5' to 3' untranslated region (UTRs) and the different splice variants. Oligonucleotides were designed using set criteria (see table 4.2). The set criteria will select for oligonucleotides with a Hind III site at the 5' end and a Bgl II site at the 3' end as determined by the iRNAi software. The oligonucleotides were chemically synthesized at Inqaba Biotech at a final concentration of 100 µM. Two sets of oligonucleotides were designed which were designated DWNN-A and B respectively (see table 4.1 for sequences).

Search Sequence for:

Begin: AA	End: TT	n: 19
Search pattern: AA-[N]19-TT		GC content 50%
Forward Primer		Reverse Primer
5' Prefix: GATCCC	5' Prefix: AGCTTTTCCAAAAA	
Loop: TTCAAGAGA	Loop: TCTCTTGAA	
3' Suffix: TTTTGGAAA	3' Suffix: GGG	

Table 4.2 Settings used for the design of siRNA oligonucleotides using the iRNAi v1.0 software.

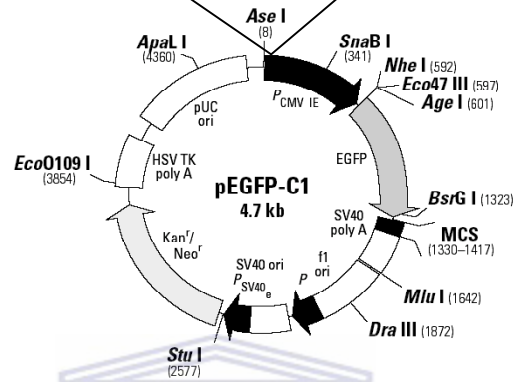
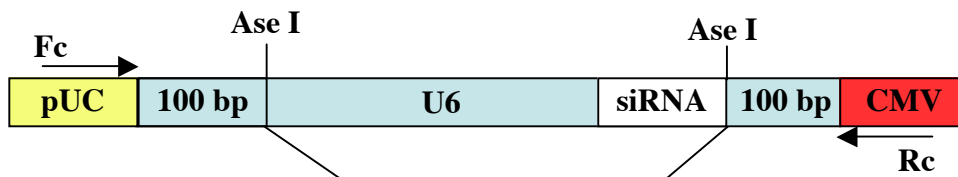
4.4.2 Annealing of siRNA oligonucleotides

Sense and antisense siRNA oligonucleotides were annealed as described in section 2.22. The formation of DNA duplexes was confirmed by electrophoresis on a 12 % polyacrylamide gel (data not shown). For each dsDNA, the mobility on the gel was shifted compared to the ssDNA. Annealing of the forward and the reverse oligonucleotide resulted in the formation of the 5' Hind III and 3' Bgl II restriction sites.

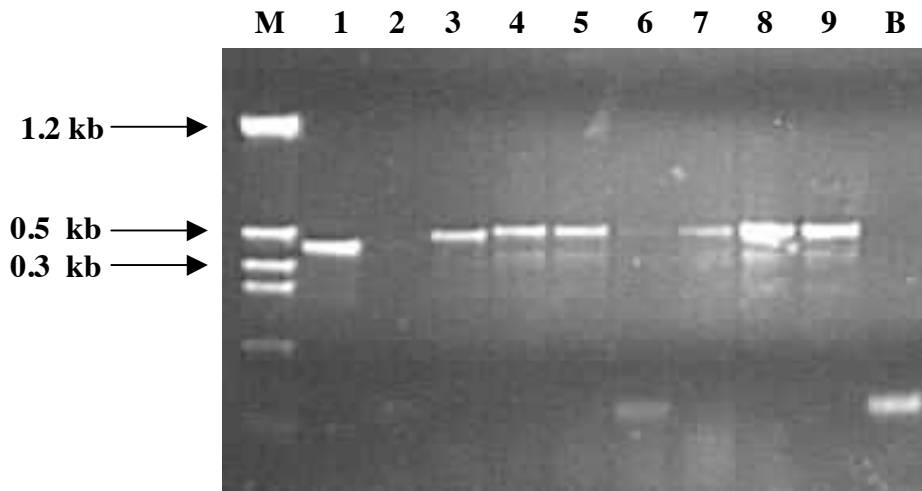
4.4.3 Cloning of siRNA oligonucleotides

All the vectors containing U6 and H1 described in section 4.3.4 were digested with Hind III and Bgl II as described in section 2.8.3. Annealed siRNA oligonucleotides from section 4.4.2 were ligated into the digested vectors as described in section 2.8.4. Colony PCR was used to identify recombinant clones as described in section 2.10.3. The common forward (Fc) and the common reverse (Rc) oligonucleotides were used to identify GU6/H1 and RU6/H1 recombinant clones, whilst pU6/H1 recombinant clones were identified using the M13 universal oligonucleotides.

Figure 4.4 shows the identification of GU6 DWNN-A recombinant clone (GU6A for short). Lane 1 shows the amplification of the U6 promoter using U6 F and U6 R resulting in the expected fragment size of 380 bp. Lane 3 shows the amplification of the U6 promoter using Fc and Rc, thus resulting in a fragment with an additional 200 bp. This increase in product size can be contributed to the position of the oligonucleotides in



(a)



(b)

Figure 4.4 The PCR strategy used to identify GU6A recombinant clones.

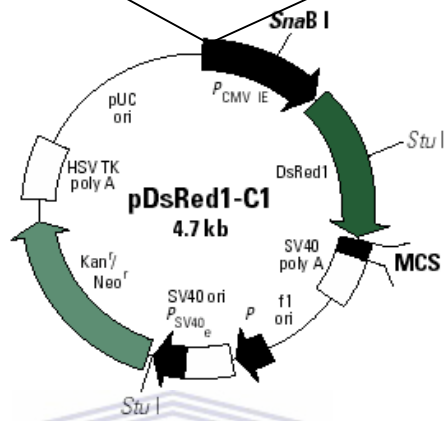
- (a) Schematic representation of the PCR strategy used to identify GU6 siRNA recombinant clones.
- (b) PCR of GU6 siRNA recombinants. clones. Recombinant siRNA clones were identified using colony PCR **M.** represents the size marker pTZ, **lane 2.** represents the PCR amplification of the U6 promoter using the U6 GSPs, **lane B.** represents the water blank and **lane 4.** the PCR amplification of the U6 promoter using Fc and Rc **lanes 5 to 9.** represents the recombinant clones. PCR products were resolved on a 2 % agarose gel.

respect to the Ase I recognition sequence (see figure 4.4a). Lane 4 to 9 represents the recombinant clones. The shift in size of the recombinant clones is marginal which can be contributed to the relatively small size of the siRNA oligonucleotide (64 bp). A higher percentage agarose gel and an extended electrophoresis period should increase the resolution of the PCR fragments.

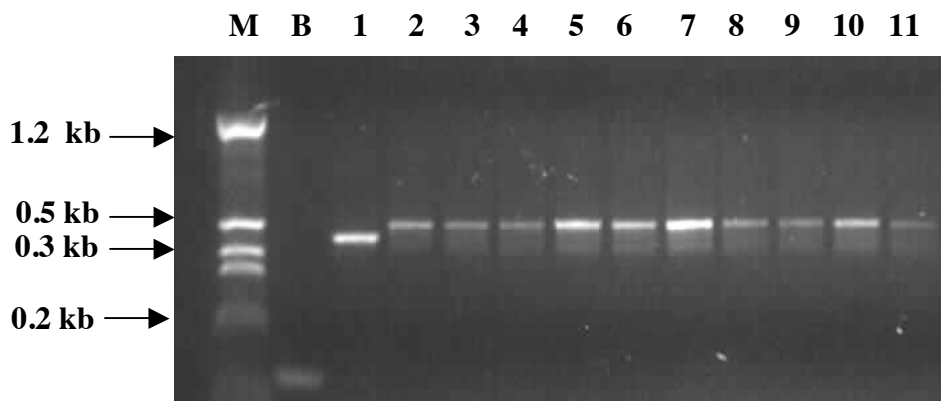
Figure 4.5 shows the identification of RH1B recombinant clones. Lane 1 shows the amplification product of H1 using Fc and Rc, whilst lanes 2 to 11 represents the recombinant clones. Figure 4.5 shows the identification of pU6 recombinant clones with 4.6a showing the pU6A recombinant clones and 4.6b the pU6B recombinant clones.

4.4.4 Sequencing of recombinant siRNA clones

All clones representing the different siRNA constructs were sequencing at the Inqaba Biotech core sequencing facility. GU6/H1 and RU6/H1 siRNA recombinant constructs were sequenced using Fc and Rc oligonucleotides. The pU6/H1 siRNA constructs were sequenced using the M13 universal forward and reverse oligonucleotides. BLASTn (Altschul *et al.*, 1990) were used to compare the sequencing results against the non-redundant database. From the results (see figure 4.7) a complete match was found for DWNN-A against the database (DWNN-B data not shown). Sequencing data also showed the presence of the 5' prefix, loop and 3' suffix sequences. Table 4.3 shows the complete list of sequenced siRNA constructs. Figure 4.8 shows a graphical map of the GU6B vector.



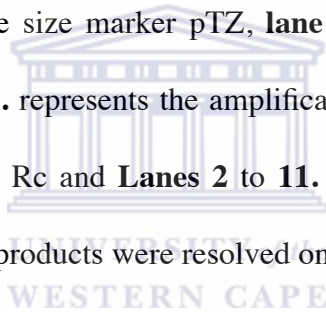
(a)



(b)

Figure 4.5 The PCR strategy used to identify RH1B recombinant clones.

- (a) Schematic representation of the PCR method used to identify RH1 siRNA recombinants.
- (b) The PCR results for the RH1 siRNA recombinants. Lane **M.** represents the size marker pTZ, **lane B.** represents the water blank, **lane 1.** represents the amplification of the H1 promoter using Fc and Rc and **Lanes 2 to 11.** the siRNA recombinant clones. PCR products were resolved on a 2 % agarose gel.



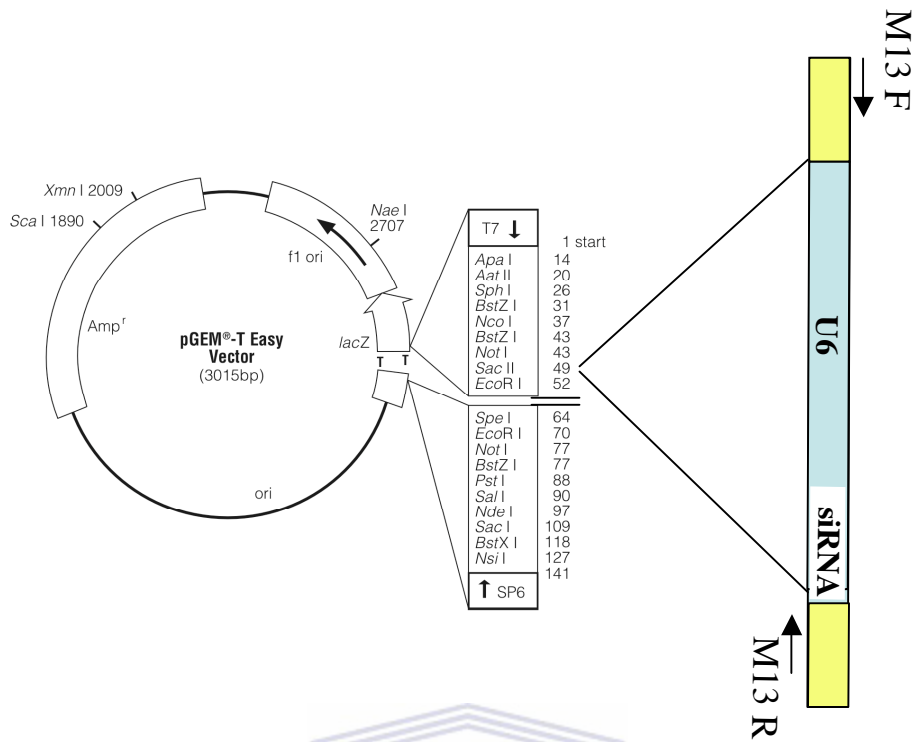
Construct	Cloning vectors			RNA pol III promoters		siRNA oligonucleotides	
	pEGFP-C1	DsRed-C1	pGEM [®] -T-Easy	H1 promoter	U6 promoter	DWNN A	DWNN B
pU6A			✓		✓	✓	
pU6B			✓		✓		✓
pH1A			✓	✓		✓	
pH1B			✓	✓			✓
RU6A		✓			✓	✓	
RU6B		✓			✓		✓
RH1A		✓		✓		✓	
RH1B		✓		✓			✓
GU6A	✓				✓	✓	
GU6B	✓				✓		✓
GH1A	✓			✓		✓	
GH1B	✓			✓			✓

Table 4.3. List of siRNA constructs generated and the nomenclature used in the subsequent chapters.



4.5 Summary

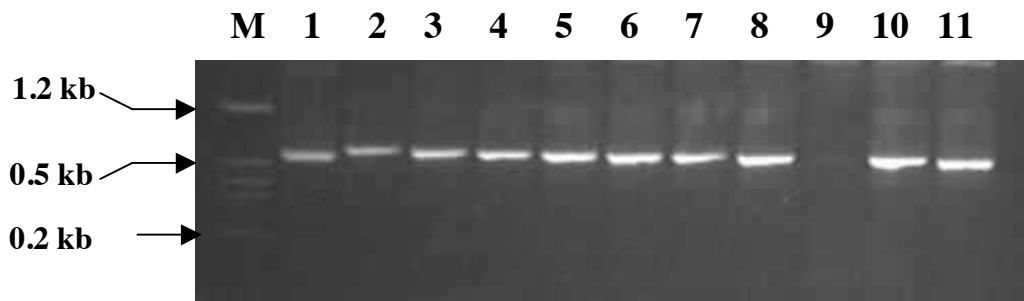
The aim of this chapter was to design several plasmid-based siRNA vectors that would target and ablate the expression of the mouse RBBP6 gene. Plasmid-based RNAi vectors predominantly make use of the RNA pol III type promoters U6 and H1 (Kawasaki and Taira, 2003, Miyagishi and Taira, 2002). The U6 and the H1 promoters were amplified using PCR and cloned into the pGEM[®]-T Easy, pEGFP-C1 and pDsRed-C1 vectors respectively. Oligonucleotides used in the amplification of the promoters were engineered to include an Ase I recognition sequence at both ends allowing for the cloning of the promoters into the Ase I recognition sequence of pEGFP-C1 and pDsRed-C1. Cloning into the pEGFP-C1 and pDsRed-C1 vectors would allow for localization of the target oligonucleotides in cells using fluorescence microscopy. Furthermore, a Hind III



(a)



(b)



(c)

Figure 4.6 The PCR strategy used to identify pU6 siRNA recombinant clones.

(a) Schematic representation of the PCR strategy used to identify pGEM-T Easy siRNA recombinants.

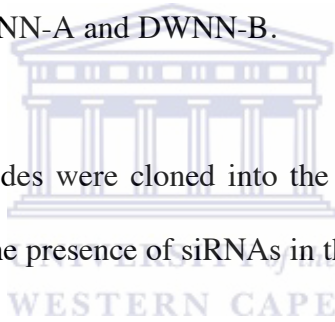
(b) Shows the PCR results of the pU6A recombinant clones
Lane M. represents the size marker pTZ, **lane 1.** represents the positive U6 control and **lanes 2 to 10.** represents the siRNA recombinant clones.

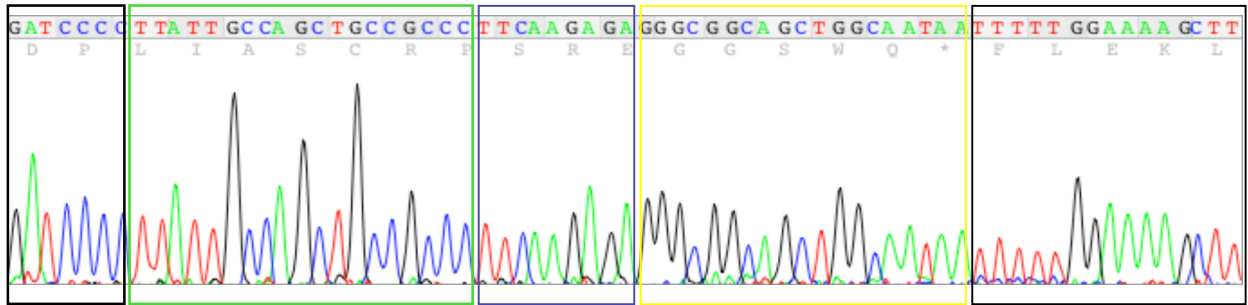
(c) Shows the PCR results of the pU6B recombinant clones
Lane M. represents the size marker pTZ, **lane 1.** represents the positive U6 control and **lanes 2 to 11.** represents the siRNA recombinant clones. PCR products were resolved on a 2 % agarose gel.

and Bgl II recognition sequence were placed at the 3' end of the reverse oligonucleotides for both U6 and H1 preceding Ase I, allowing for the ligation of the siRNA oligonucleotides at the 3' end of the U6 and H1 promoters.

The full-length annotated mouse RBBP6 DNA sequence served as input data and siRNA target sequences were identified using the iRNAi version 1.0 oligonucleotide prediction software. Oligonucleotides were designed based on the criteria listed in table 4.1. The criteria allowed for the incorporation of a Hind III recognition sequence at the 5' end of the siRNA oligonucleotide and a Bgl II at the 3' end. Two targeting oligonucleotides were identified designated DWNN-A and DWNN-B.

Annealed siRNA oligonucleotides were cloned into the U6 and H1 containing vectors. Sequence analysis confirmed the presence of siRNAs in the respective cloning vectors.





GATCCCCTTATTGCCAGCTGCCGCCCTTCAAGAGAGGGCGGCAGCTGGCAATAATTTTTGGAAAAGCTT

5' PREFIX TARGET (SENSE) LOOP TARGET (ANTI-SENSE) 3 SUFFIX

(a)

>[gi|3858884|qb|U83913.1|MMU83913](#) **UEG** Mus musculus proliferation potential-related protein (P2P-R) mRNA, complete cds
Length=5131

Sort alignments for this subject sequence by:
[E value](#) [Score](#) [Percent identity](#)
[Query start position](#) [Subject start position](#)

Score = 38.2 bits (19), Expect = 1.2
Identities = 19/19 (100%), Gaps = 0/19 (0%)
Strand=Plus/Plus

Query 1 TTATTGCCAGCTGCCGCC 19
Sbjct 850 TTATTGCCAGCTGCCGCC 868

Score = 38.2 bits (19), Expect = 1.2
Identities = 19/19 (100%), Gaps = 0/19 (0%)
Strand=Plus/Minus

Query 20 GGGCGGCAGCTGGCAATA 38
Sbjct 868 GGGCGGCAGCTGGCAATA 850

>[gi|1546778|qb|U28789.1|MMU28789](#) **UEG** Mus musculus p53-associated cellular protein PACT mRNA, partial cds
Length=5191

Sort alignments for this subject sequence by:
[E value](#) [Score](#) [Percent identity](#)
[Query start position](#) [Subject start position](#)

Score = 38.2 bits (19), Expect = 1.2
Identities = 19/19 (100%), Gaps = 0/19 (0%)
Strand=Plus/Plus

Query 1 TTATTGCCAGCTGCCGCC 19
Sbjct 701 TTATTGCCAGCTGCCGCC 719

Score = 38.2 bits (19), Expect = 1.2
Identities = 19/19 (100%), Gaps = 0/19 (0%)
Strand=Plus/Minus

Query 20 GGGCGGCAGCTGGCAATA 38
Sbjct 719 GGGCGGCAGCTGGCAATA 701

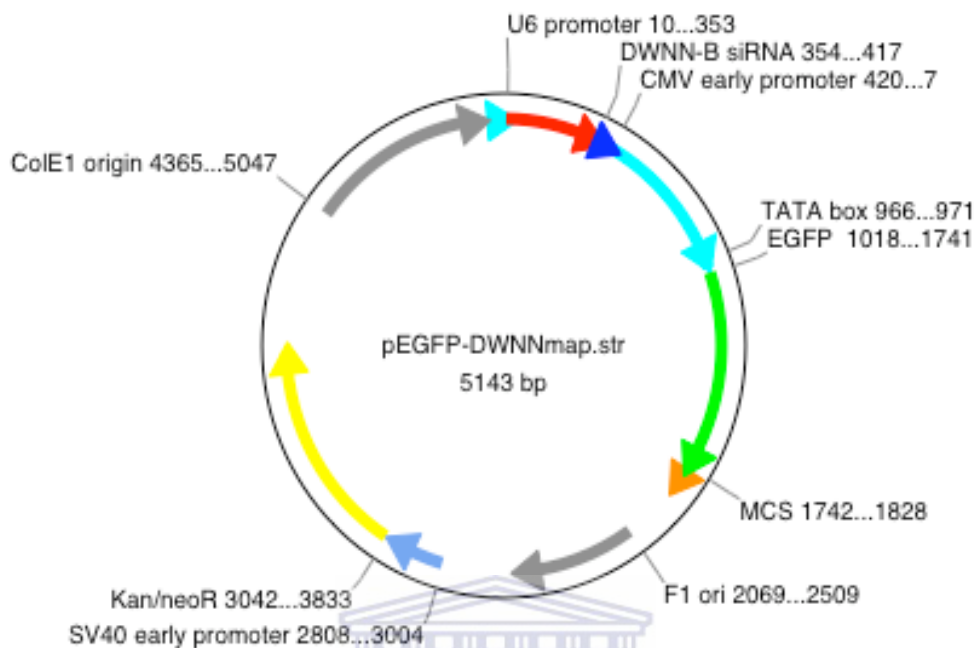
(b)

Figure 4.7 **Sequence and BLAST results of the DWNN-A siRNA oligonucleotide.**

- (a) Shows the sequence traces for the DWNN-A siRNA oligonucleotide.

- (b) The sequence alignment of the DWNN-A siRNA oligonucleotide against the non-redundant database using BLASTn.





(a)

U6 promoter

TATACTAGTTACATCCCTCCGTACGCCGCCATCTCTAGGCCCGCGCCGGCCCCCTCGCAGACT
 TGTGGGAGAAGCTCGGCTACTCCCCTGCCCCGGTTAATTGTCATATAATATTTCTAGTAACT
 ATAGAGGCTTAATGTGCGATAAAAGACAGATAATCTGTTCTTTTTAATACTAGCTACACTTTC
 CATGATAGGCTTGGATTTCTATAAGAGATACAAATACTAAATTATTATTTTAAAAAACAGCAC
 AAAAGGAAACTCACCTAACTGTAAAGTAATTGTGTGTTTTGAGACTATAAATATCCCTTGA
 GAAAAGCCTTGTGTGCTCGCTTCGGCAGA

DWNN-B siRNA

GATCCC TGCAGGGGATCGTCAGGGATTTC AAGAGA AATCCCTGACGATCCCCTGCA
 TTTTGGAAA GCTT

CMV early promoter

GCGATTAATAACTAATGCATGGCGGTAATACGGTTATCCACAGAATCAGGGGATAACGC
 AGGAAAGAACATGTGAGCAAAAAGGCCAGCAAAAAGGCCAGGAACCGTAAAAAGGCCGCG
 TTGCTGGCGTTTTTCCATAGGCTCCGCCCCCTGACGAGCATCACAAAAATCGACGCTC
 AAGTCAGAGGTGGCGAAACCCGACAGGACTATAAAGATACCAGGCGTTTTCCCCCTGGA
 AGCTCCCTCGTGGCGCTCTCTGTTCCGACCCTGCCGTTACCGGATACCTGTCCGCCTT
 TCTCCCTTCGGGAAGCGTGGCGCTTTCTCATAGCTCACGCTGTAGGTATCTCAGTTCCG
 GGAAGGCCGT

(b)

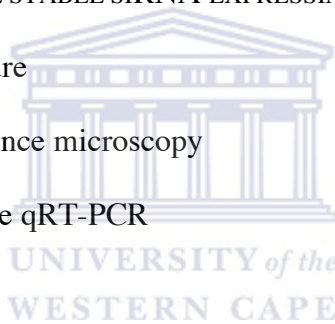
Figure 4.8 Represents the map for the siRNA construct GU6B.

- (a) A graphic representation of the map of GU6B
- (b) The nucleotide of the DWNN-B siRNA, U6 promoter and the CMV early promoter cloned into pEGFP-C1



**CHAPTER 5: INTERFERENCE RNA – EVALUATING THE EFFECT OF
THE siRNA CONSTRUCTS ON THE EXPRESSION OF RBBP6.**

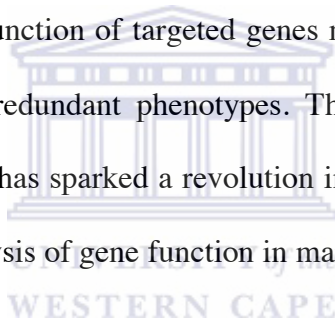
- 5.1 Introduction
- 5.2 TRANSIENT TRANSFECTIONS OF CELLS
 - 5.2.1 Transfection of mouse NIH 3T3 cells with siRNA constructs
 - 5.2.2 Fluorescence microscopy
 - 5.2.3 Real-Time qRT-PCR
- 5.3 GENERATING THE STABLE siRNA EXPRESSING CELL LINE RU6A AND GU6B
 - 5.3.1 Cell culture
 - 5.3.2 Fluorescence microscopy
 - 5.3.3 Real-Time qRT-PCR
- 5.4 SUMMARY



CHAPTER 5: INTERFERENCE RNA – EVALUATING THE EFFECT OF THE siRNA CONSTRUCTS ON THE EXPRESSION OF RBBP6

5.1 Introduction

Reverse genetics, in which a gene is disrupted so that the effect of its loss on an organism can be observed, is a simple way to investigate gene function. Gene targeting by homologous recombination is commonly used to determine gene function in mammals, but it is both costly and time consuming, whilst many organisms are not amenable to such gene targeting methods. The function of targeted genes might not be determined by this approach owing to lethal or redundant phenotypes. The advent of interference RNA (RNAi) directed ‘knockdown’ has sparked a revolution in somatic cell genetics allowing the inexpensive and rapid analysis of gene function in mammals.



Biologists are exploiting RNAi as an experimental tool to find out what genes do. When a gene is activated, its sequence is read to produce messenger RNA (mRNA), which contains the information necessary to manufacture a particular protein. So by using siRNA or double-stranded RNAs that correspond to a specific mRNA sequence, researchers can trick a cell into destroying this mRNA and silencing the gene in question.

In theory, RNAi could be used to treat any disease – forms of cancer, for instance, that are linked to an overactive gene or genes. At present, most of the clinical interest lies in applying RNAi in its natural role as a means of combating pathogenic viruses by

disabling their RNA. Naturally HIV would be an obvious candidate since to date there is no cure or vaccine against the virus.

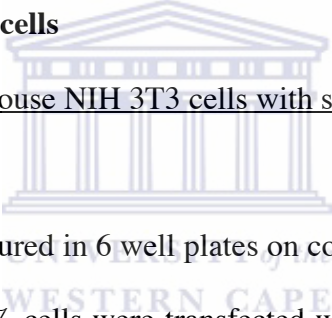
Aims of this chapter:

-Transiently transfect the different siRNA constructs into NIH 3T3 cells and determine the effect on the expression of the RBBP6 gene.

-To generate stable cell lines expressing the DWNN-A and DWNN-B siRNA oligonucleotides.

5.2 Transient transfections of cells

5.2.1. Transfection of mouse NIH 3T3 cells with siRNA constructs



Mouse NIH 3T3 cells were cultured in 6 well plates on cover slips as described in section 2.13.3. At a confluency of 70 % cells were transfected with the different RBPP6 siRNA constructs using the Metafectene™ transfection reagent as described in section 2.14.1. A concentration of 100 ng of DNA per well was used of the respective constructs. Cells were incubated an additional 48 hours post-transfection. The following control experiments were also set up: cells only and cells transfected with pDsRed-C1 and RU6 (vector not containing the siRNA oligonucleotide).

5.2.2 Fluorescence microscopy

Cover slips were removed 48 hours post-transfection and placed into new 6 well plates. Cells were fixed as described in section 2.15.1 and stained with the anti-DWNN domain specific primary antibody and the Alexa Fluor 488 (Green) or 594 (Red) goat anti-rabbit IgG secondary antibodies as described in chapter 2.14.2. The Alexa Fluor 488 secondary antibody was used for cells transfected with pDsRed-C1 siRNA constructs and the Alexa Fluor 594 used where cells were transfected with the pEGFP-C1 siRNA constructs and either of the secondary antibodies if cells were transfected with the pGEM[®]-T Easy siRNA constructs.

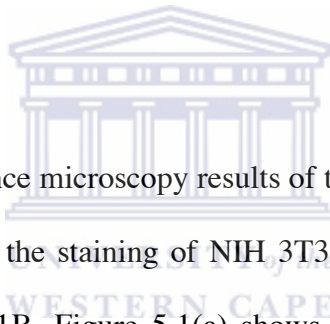
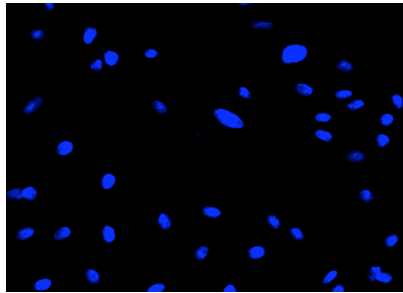
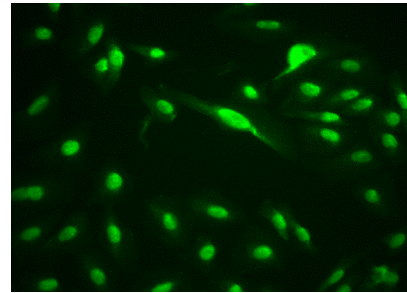


Figure 5.1 shows the fluorescence microscopy results of the analysis of localization of the RBBP6 protein resulting from the staining of NIH 3T3 cell line transiently transfected with the siRNA construct RH1B. Figure 5.1(a) shows the parental cell line NIH 3T3 counterstained with DAPI whilst 5.1(b) shows the cell line stained with the anti-DWNN polyclonal antibody and the Alexa Fluor 488 secondary antibody. Figure 5.1(c) shows the NIH 3T3 cell line transiently transfected with the siRNA construct RH1B and 5.1(d) shows the NIH 3T3 cell line transiently transfected with the siRNA construct RH1B stained with the anti-DWNN antibody and the Alexa Fluor 488 secondary antibody. From these results the nucleus appears to be predominantly stained compared to the surrounding cytoplasm. The fluorescent intensity resulting from the staining of the NIH 3T3 cells, transiently transfected with RH1B appears to be less than that of the NIH 3T3 un-transfected cell line.

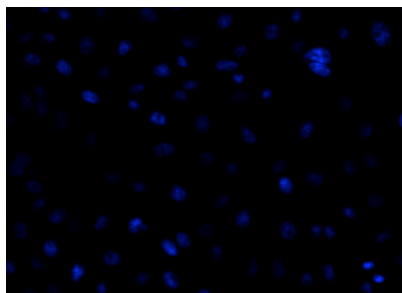


(a)

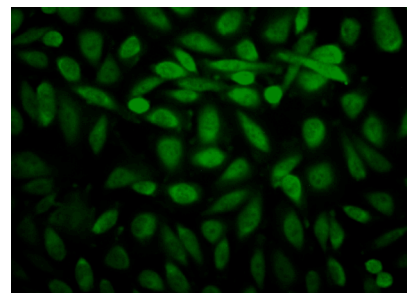


(b)

20X magnification



(c)



(d)

20X magnification

Figure 5.1 Fluorescence microscopy analysis of the localization of the RBBP6 protein in the NIH 3T3 cells transiently transfected with the siRNA construct RH1B.

- (a) NIH 3T3 cells counterstained with DAPI.
- (b) NIH 3T3 cells stained with polyclonal anti-DWNN primary antibody and the goat anti-rabbit Alexa Fluor 488 secondary antibody.
- (c) NIH 3T3 cells transiently transfected with RH1B and counterstained with DAPI.
- (d) NIH 3T3 cells transiently transfected with RH1B stained with the polyclonal anti-DWNN primary antibody and goat anti-rabbit Alexa Fluor 488 secondary antibody.

Figure 5.2 shows the localization of the RBBP6 protein in the NIH 3T3 cells transiently transfected with the siRNA construct RU6A. Figure 5.2(a) shows the parental cell line counterstained with DAPI and (b) shows the parental cell line stained with the anti-DWNN antibody and the Alexa Fluor 488 secondary antibody. Figure 5.2 (c) shows the parental cell line transiently transfected with the siRNA construct RU6A counterstained with DAPI and figure 5.2 (d) shows the NIH 3T3 cell line transiently transfected with the siRNA construct RU6A stained with the anti-DWNN antibody and the Alexa Fluor 488 secondary antibody. The difference in fluorescence intensities can be clearly observed. A marked decrease in fluorescence intensity is observed in the cells transfected with the siRNA construct as seen in figure 5.2(d).

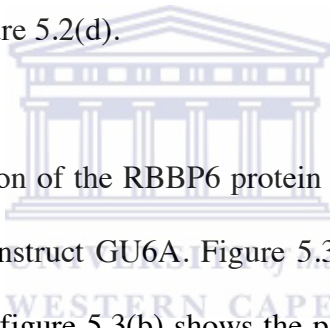
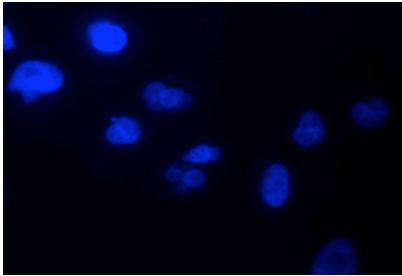
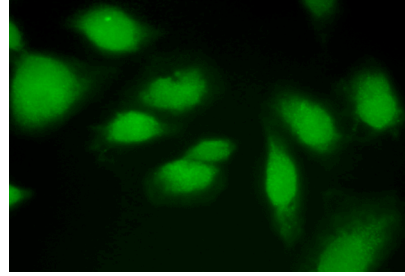


Figure 5.3 shows the localization of the RBBP6 protein in the NIH 3T3 cells transiently transfected with the siRNA construct GU6A. Figure 5.3(a) shows the parental cell line counterstained with DAPI and figure 5.3(b) shows the parental cell line stained with the anti-DWNN antibody and the Alexa Fluor 594 secondary antibody. Figure 5.3(c) shows the parental cell line transiently transfected with the siRNA construct GU6A counterstained with DAPI and figure 5.3(d) shows the NIH 3T3 cell line transiently transfected with the siRNA construct GU6A stained with the anti-DWNN antibody and the Alexa Fluor 594 secondary antibody. The fluorescence is clearly more intense emanating from the parental cell line compared to that in the siRNA expressing cell lines. No observable differences were seen between the parental cell line and those transfected with the control constructs, pDsRed-C1 (cloning vector) and RU6 (U6 promoter cloned into vector only) (data not shown). It can thus be concluded that the effect on RBBP6

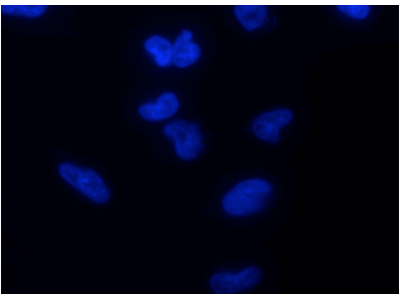


(a)

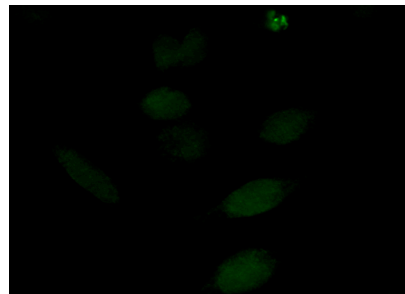


(b)

40X magnification



(c)

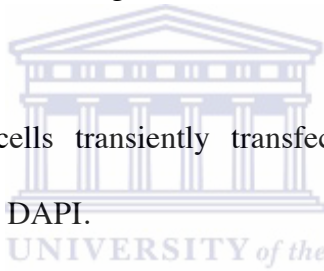


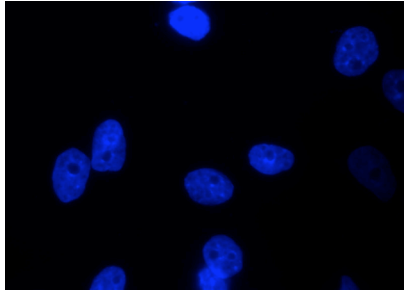
(d)

40X magnification

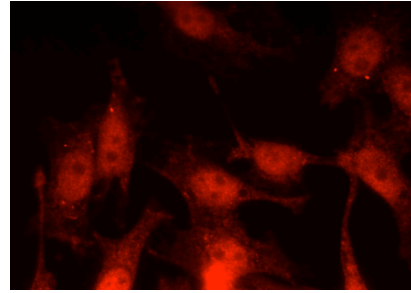
Figure 5.2 Fluorescence microscopy analysis of the localization of the RBBP6 protein in the NIH 3T3 cells transiently transfected with the siRNA construct RU6A.

- (a) NIH 3T3 cells counterstained with DAPI.
- (b) NIH 3T3 cells stained with polyclonal anti-DWNN primary antibody and the goat anti-rabbit Alexa Fluor 488 secondary antibody.
- (c) NIH 3T3 cells transiently transfected with RU6A and counterstained with DAPI.
- (d) NIH 3T3 cells transiently transfected with RU6A stained with the polyclonal anti-DWNN primary antibody and goat anti-rabbit Alexa Fluor 488 secondary antibody.



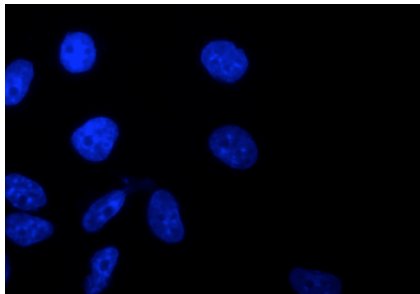


(a)

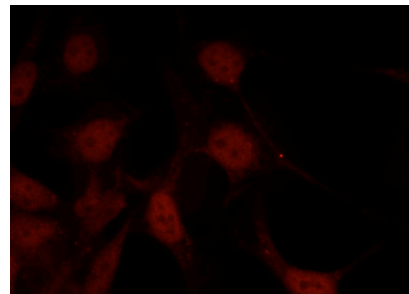


(b)

20X magnification



(c)



(d)

20X magnification

Figure 5.3 Fluorescence microscopy analysis of the localization of the RBBP6 protein in the NIH 3T3 cells transiently transfected with the siRNA construct GU6A.

- (a) NIH 3T3 cells counterstained with DAPI.
- (b) NIH 3T3 cells stained with polyclonal anti-DWNN primary antibody and the goat anti-rabbit Alexa Fluor 594 secondary antibody.
- (c) NIH 3T3 cells transiently transfected with GU6A and counterstained with DAPI.
- (d) NIH 3T3 cells transiently transfected with GU6A stained with the polyclonal anti-DWNN primary antibody and goat anti-rabbit Alexa Fluor 594 secondary antibody.

expression as observed using fluorescence microscopy is a consequence of the cloned siRNA oligonucleotides.

5.2.3 Real-Time qRT-PCR

Total RNA was isolated from NIH 3T3 cells transfected with the different siRNA constructs as well as the parental cell line as described in chapter 2.18 and the RNA resolved on an agarose gel as described in section 2.19 (see figure 5.4). Figure 5.4 shows RNA of high quality with no visible degradation and the 23S and 18S subunits clearly distinguishable. The isolated RNA was used in a cDNA synthesis reaction as described in section 2.20. All cDNA samples were standardized to a concentration of 50 ng and used directly in a Real-Time qRT-PCR as described in section 2.21 using gene specific oligonucleotides against the RBBP gene (see table 4.1).

Figure 5.5 shows the Real-Time qRT-PCR data obtained for the expression of RBBP6 in the NIH 3T3 cell line transiently transfected with the different siRNA vectors with the CP values given for each reaction. From figure 5.5 the expression level of RBBP6 in the NIH 3T3 un-transfected cells were similar to the expression of RBBP6 in the NIH 3T3 cells transfected with the control constructs RU6 and pDsRed-C1. The results shows that the effect on the expression of RBBP6 was unaffected by the cloning vector or the RNA Pol III promoter U6. The siRNA transfected NIH 3T3 cells showed lower CP values compared to the un-transfected NIH 3T3 cell line as well as the NIH 3T3 cell line

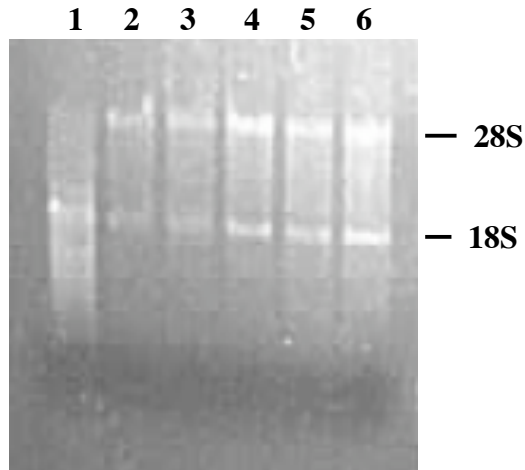


Figure 5.4 Isolation of total RNA from cultured NIH 3T3 cells.

Total RNA was isolated using the TRIzol protocol, resuspended in DEPC treated water and resolved on a 1.2 % agarose gel containing formamide.

Lane 1. Represents RNA isolated from the parental cell line NIH 3T3, **lane 2.** RNA isolated from the NIH 3T3 cell line transfected with pDsRed1, **lane 3** GU6 and **lanes 4, 5 and 6** represents RNA isolated from the NIH 3T3 cells transfected with siRNA constructs GU6B, RH1A and RU6A respectively.

transfected with the control constructs. The siRNA transfected cell lines thus have a lower mRNA copy number of the RBBP6 gene as indicated by the higher CP values.

The Real-Time PCR efficiencies (E) were calculated from the resulting slopes provided by the Real-Time Quantitative PCR software and was calculated according to the equation formulated by Pfaffl (2001) as described in section 2.22. The *gapdh* standard curve was used to calculate the expression level of RBBP6. The expression of RBBP6 was calculated as 100 % in the un-transfected NIH 3T3 cell line and the expression of the gene in the siRNA cell lines calculated relative to it and represented as the mean \pm SD.

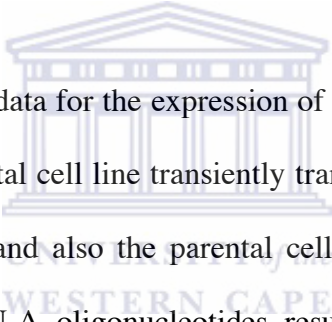
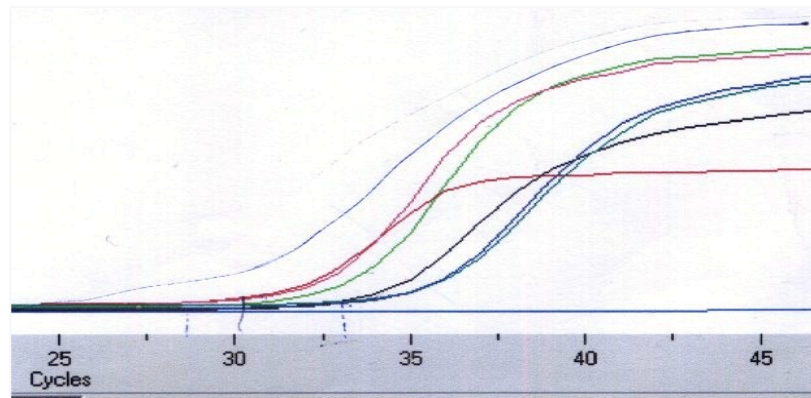


Figure 5.6 shows the analyzed data for the expression of the RBBP6 gene in the parental cell line compared to the parental cell line transiently transfected with the RU6A, RH1A and GU6B siRNA constructs and also the parental cell line transfected with the GU6 control construct. The DWNN-A oligonucleotides resulted in an approximate 65 % decrease compared to 62 % resulting from the DWNN-B oligonucleotide.

5.3 Generating the stable siRNA expressing cell lines RU6A and GU6 B

5.3.1 Cell culture

The parental cell line NIH 3T3 was cultured in a 25 cm³ flask until 80 % confluent as described in section 2.13.3. The cell were transfected with 100 ng of the RNAi constructs RU6A and GU6B using Metafectene™ as described in section 2.14.1. Stable cell lines



	Threshold(CP) value
—◆— GAPDH housekeeping gene	25.86
—◆— Cells only control	30.90
—◆— RU6 only control	31.04
—◆— pDsRed1 only control	32.84
—◆— GU6B	32.08
—◆— GH1A	35.48
—◆— RU6A	35.20
—◆— Blank	

Figure 5.5 Expression analysis of the RBBP6 gene using Real-Time qRT-PCR.

NIH 3T3 cells were transiently transfected with different siRNA constructs. Total RNA was isolated from the cells and cDNA synthesized. The level of expression of the RBBP6 gene was determined in the different cells using Real-Time qRT-PCR analysis.

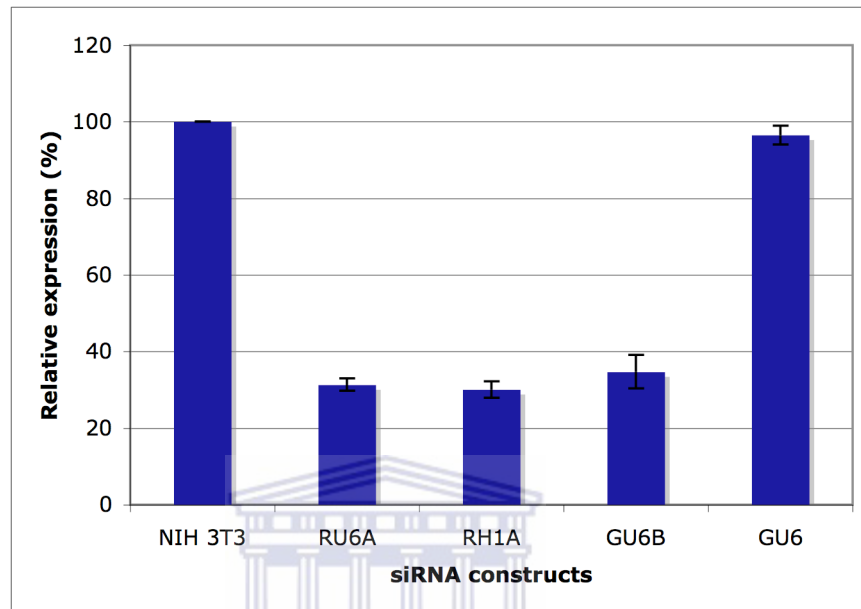


Figure 5.6 The expression level of the RBBP6 gene in cells transiently transfected with different siRNA constructs.

The Real-Time qRT-PCR data (see figure 5.5) was analyzed and presented as a bar graph showing the relative expression level of the RBBP6 gene following the transient transfection of the different siRNA constructs into the NIH 3T3 cell line as the mean \pm SD as independent repeats of the experiment. The GU6 vector were used as a control.

were generated as described in section 2.14.2 using G418. Cells were frozen down and stored at -150°C .

5.3.2 Fluorescence microscopy

Fluorescent microscopy was used to evaluate the expression of the RBBP6 gene in the stable siRNA cell lines RU6A and GU6B. The parental cell line, as well as the stable lines were cultured in 6 well plates in DMEM on cover slips as described in section 2.13.3. Cover slips were removed and the cells fixed as described in section 2.15.1 and stained with the anti-DWNN antibody as described in section 2.15.2. Fluorescence was evaluated using a Zeiss fluorescence microscope and the cells photographed.

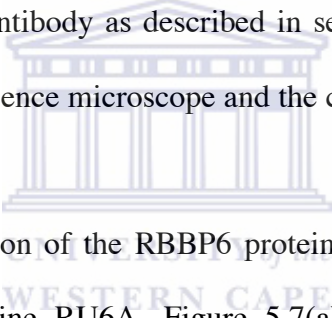
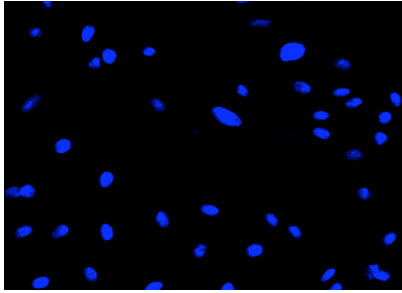
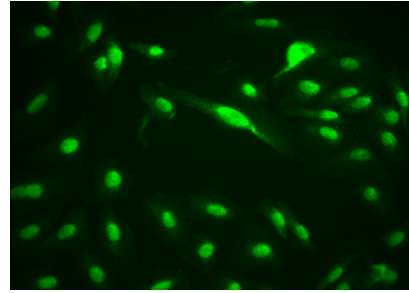


Figure 5.7 shows the localization of the RBBP6 protein in the NIH 3T3 parental cells compared to the stable cell line RU6A. Figure 5.7(a) shows the parental cell line counterstained with DAPI and figure 5.7(b) shows the parental cell line stained with the anti-DWNN antibody and the Alexa Fluor 488 secondary antibody. Figure 5.7(c) shows the stable cell line RU6A counterstained with DAPI and figure 5.7(d) shows the stable cell line RU6A stained with the anti-DWNN antibody and the Alexa Fluor 488 secondary antibody. The fluorescence intensity emanating from the parental cell line was significantly higher than that emanating from the stable cell line. The same was observed for the GU6B cell line (data not shown). However there is clear nuclear staining in the parental cell line compared to the stable cell line RU6A. The fluorescence observed in the stable cell line can be considered cytoplasmic background. This background might be a

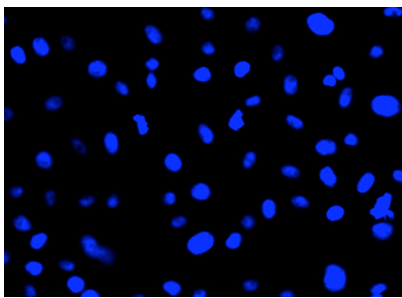


(a)

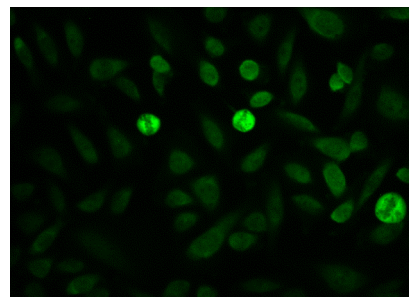


(b)

20X magnification



(c)

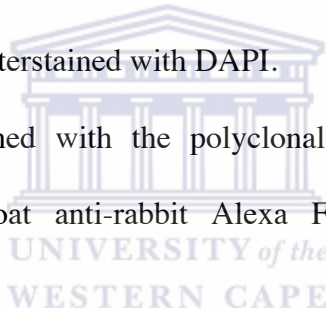


(d)

20X magnification

Figure 5.7 Fluorescence microscopy analysis of the localization of the RBBP6 protein in the stable siRNA expressing RU6A cell line.

- (a) NIH 3T3 cells counterstained with DAPI.
- (b) NIH 3T3 cells stained with polyclonal anti-DWNN primary antibody and the goat anti-rabbit Alexa Fluor 488 secondary antibody.
- (c) RU6A counterstained with DAPI.
- (d) RU6A stained with the polyclonal anti-DWNN primary antibody and the goat anti-rabbit Alexa Fluor 488 secondary antibody.



consequence of the non-specificity of the anti-DWNN antibody since this antibody is polyclonal thus showing cross-reactivity to other proteins in the cell.

5.3.3 Real-Time qRT-PCR

Quantitative RT-PCR was used to determine the level of expression of the RBBP6 gene in the stable cell lines RU6A and GU6B. Stable cell lines and the parental cell line were cultured in DMEM as described in section 2.13.3. Total RNA was extracted using the TRIzol protocol as described in section 2.19 (figure 5.8) and cDNA synthesized as described in section 2.20. The concentrations of the different cDNA synthesized were standardized and 50 ng representing the different samples were used in a Real-Time qRT-PCR using a LightCycler instrument as described in section 2.21 using the RBBP6 forward and reverse oligonucleotides (see table 4.1).

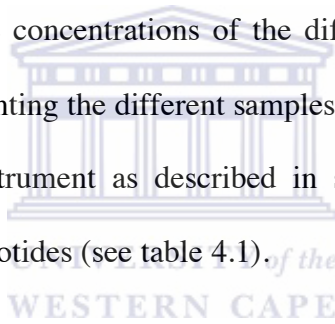


Figure 5.9 shows the Real-Time qRT-PCR data obtained for the expression of RBBP6 in the stable siRNA expressing cell lines RU6A and GU6B with the CP values given for each reaction. The threshold values are significantly lower for the parental cell line and the *gapdh* housekeeping gene compared to the values for GU6B and RU6A. The expression level of the RBBP6 gene is thus significantly lower in the stable cell line compared to the parental cell line NIH 3T3.

The Real-Time PCR efficiencies (E) were calculated from the resulting slopes provided by the Real-Time Quantitative PCR software and was calculated according to the

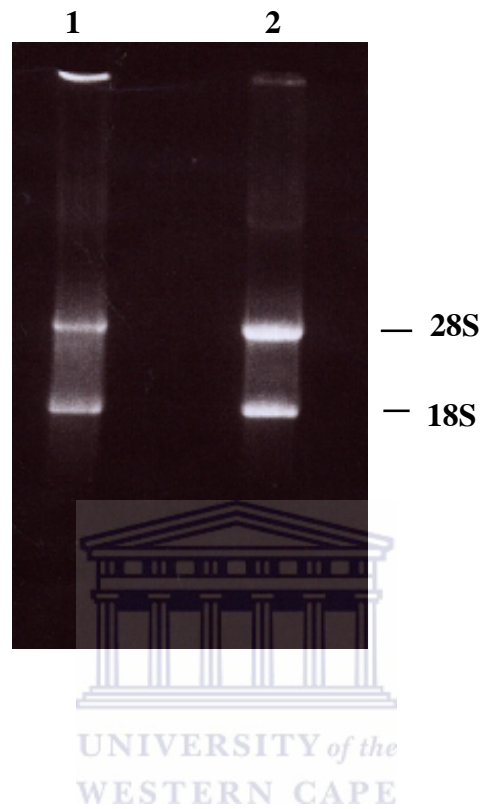


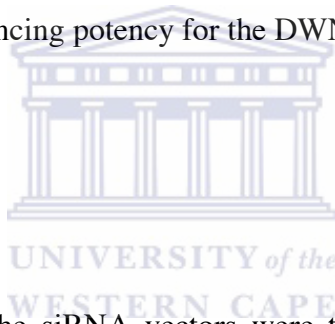
Figure 5.8 Isolation of total RNA from cultured NIH 3T3 cells.

Total RNA was isolated from the RU6A and GU6B stable siRNA expressing cell lines using the TRIZol protocol. RNA was resuspended in DEPC treated water and resolved on a 1.2 % agarose gel containing formamide. **Lane 1.** represents RNA isolated from RU6A and **lane 2.** RNA isolated from GU6B.

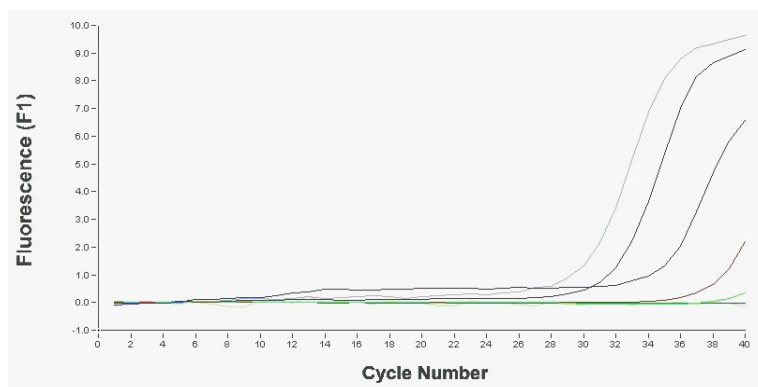
equation formulated by Pfaffl (2001) as described in section 2.22. The *gapdh* standard curve was used to calculate the expression level of RBBP6. The expression of RBBP6 was calculated as 100 % in the un-transfected NIH 3T3 cell line and the expression of the gene in the siRNA stable cell lines calculated relative to it and represented as the mean \pm SD as independent repeats of the experiment.

The expression of RBBP6 was calculated to be 95 % lower in the RU6A stable cell line and 85 % lower in GU6B compared to the expression of RBBP6 in the parental cell line NIH 3T3. These results compare well with those observed for transient transfections indicating a slightly higher silencing potency for the DWNN-A oligonucleotide.

5.4 Summary



In this chapter the effect of the siRNA vectors were tested on the expression of the DWNN protein. Several constructs were designed as described in chapter 4. NIH 3T3 cells were transiently transfected with the different siRNA constructs and stained with the anti-DWNN domain antibody. The results showed a decrease in expression of RBBP6 as observed by fluorescent microscopy. For transiently transfected cells a decrease in fluorescence was observed when compared to the parental cell line. As discussed earlier the anti-DWNN antibody was of a polyclonal nature, which could explain the cytoplasmic background observed.



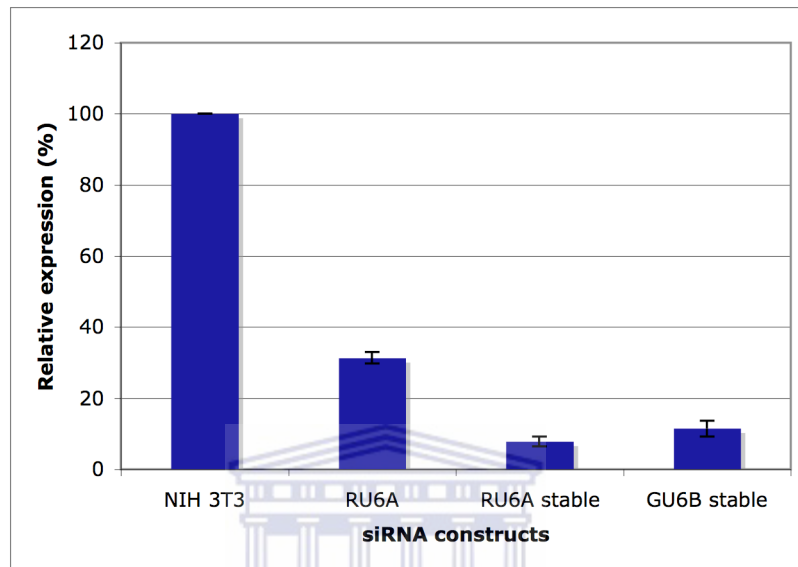
	Threshold (CP) value
NIH 3T3 GADH	29.56
NIH 3T3 RBBP6	31.02
RU6A	34.82
GU6B stable cell line	37.89
RU6A stable cell line	39.80
Blank	

Figure 5.9 Expression level of the RBBP6 gene as determined using Real-Time qRT-PCR analysis.

The stable siRNA expressing cell lines RU6A and GU6B and the NIH 3T3 cell line transiently transfected with RU6A were cultured and total RNA isolated. cDNA was synthesized and analyzed for the expression level of the RBBP6 gene using Real-Time qRT-PCR. The expression level of RBBP6 in the parental cell line NIH 3T3 and the housekeeping gene *gapdh* were used as controls.

Furthermore Real-Time qRT-PCR was used to determine RBBP6 expression following transient transfection of the parental NIH 3T3 cell line with the siRNA constructs. The results showed an average reduction in RBBP6 expression of 63.5 %. Also a slightly higher reduction in RBBP6 expression was observed resulting from the DWNN-A oligonucleotide.

The RU6A and GU6B siRNA constructs were also used to establish stable cell lines. The intensity in fluorescence in the stable cell lines were significantly reduced compared to the parental cell line following immune fluorescence staining for the DWNN domain. This observation was confirmed with Real-Time qRT-PCR data with the reduction of RBBP6 expression calculated at an average of 90 % in the stable siRNA expressing cell lines. The DWNN-A oligonucleotide also resulted in a higher silencing potency as earlier observed in the transient transfection experiments. From these results it can thus be concluded that the expression of the targeted gene RBBP6 was successfully reduced using the RNAi technology.



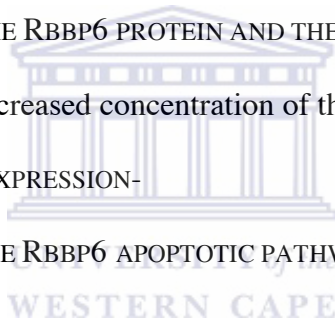
UNIVERSITY of the
WESTERN CAPE

Figure 5.10 The level of expression of the RBBP6 gene.

The Real-Time qRT-PCR data (see figure 5.9) was analyzed and presented as a bar graph showing the relative expression level of the RBBP6 gene in the different cell lines. The graph compares the expression level of the RBBP6 gene in the parental NIH 3T3 cell line to that of the parental cell line transiently transfected with RU6A to the expression of RBBP6 in the stable cell lines RU6A and GU6B. Data are presented as the mean \pm SD as independent repeats of the experiment.

CHAPTER 6: THE EFFECT OF RBBP6 SILENCING ON APOPTOSIS

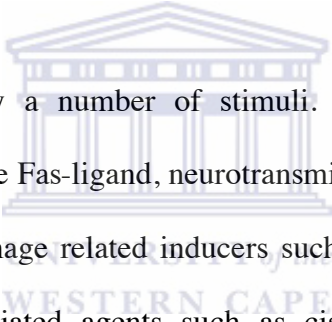
- 6.1 INTRODUCTION
- 6.2 DETERMINING THE OPTIMUM CONCENTRATION OF CAMPTOTHECIN
 - 7.2.1 The Annexin V-PE assay
- 6.3 THE EFFECT OF DWNN SILENCING ON APOPTOSIS
 - 6.3.1 The Annexin V-PE assay
 - 6.3.2 The APOPercentage™ assay
 - 6.3.3 Complementing stable cell lines with a full-length Rbbp6 cDNA
- 6.4 OVER-EXPRESSING THE RBBP6 PROTEIN AND THE EFFECT ON APOPTOSIS
 - 6.4.1 The effect of increased concentration of the RBBP6 on apoptosis
- 6.5 THE EFFECT ON P53 EXPRESSION-
- 6.6 INVESTIGATION OF THE RBBP6 APOPTOTIC PATHWAY
- 6.7 SUMMARY



CHAPTER 6: THE EFFECT OF RBBP6 SILENCING ON APOPTOSIS

6.1 Introduction

Apoptosis is a normal physiological process, which occurs during embryonic development as well as in maintenance of tissue homeostasis. Certain morphological features characterize the apoptosis program. This includes loss of plasma membrane asymmetry and attachment, condensation of the cytoplasm and nucleus and internucleosomal cleavage of DNA (Casciola-Rosen *et al.*, 1996).



Apoptosis can be induced by a number of stimuli. Inducers of apoptosis include physiological factors such as the Fas-ligand, neurotransmitters, growth factor withdrawal, loss of matrix attachment, damage related inducers such as heat shock, viral infection, bacterial toxins, therapy-associated agents such as cisplatin, vincristine, bleomycin, doxorubicin, staurosporine and toxins such as ethanol (Thompson, 1995).

Camptothecin is described in the literature as a chemical compound that will induce apoptosis in cultured cells. Camptothecin, a compound isolated from the plant *Camptotheca acuminata*, has shown significant activity against a broad range of tumours (Liu *et al.*, 2000). The anti-tumour activity of camptothecin can be attributed to its ability to bind the enzyme DNA topoisomerase I. DNA topoisomerase I catalyses the relaxation of super coiled DNA through the cleavage of double stranded DNA and the formation of a phosphotyrosyl bond between the cleaved DNA and the active site tyrosine of the

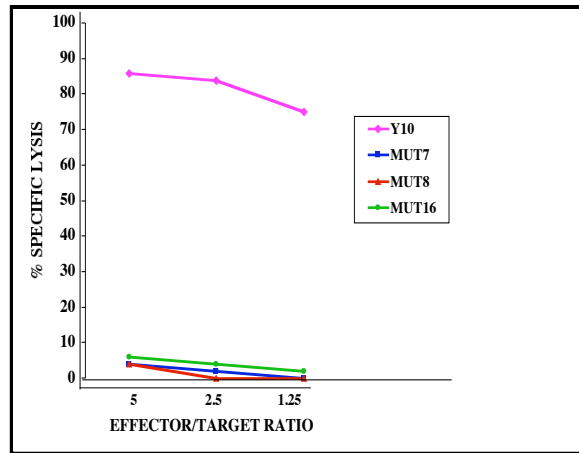


Figure 6.1a LDH release assay of the three hygromycin B/CTL resistant clones 16(3 xHA8)3.5hr, 8(3 x HA8)3.5hr and 7(3 x HA8)3.5hr compared to the Y10 parental cell line, on exposure to the HA-specific K^k restricted CTL clones HA8 and HA11 (George, 1995).

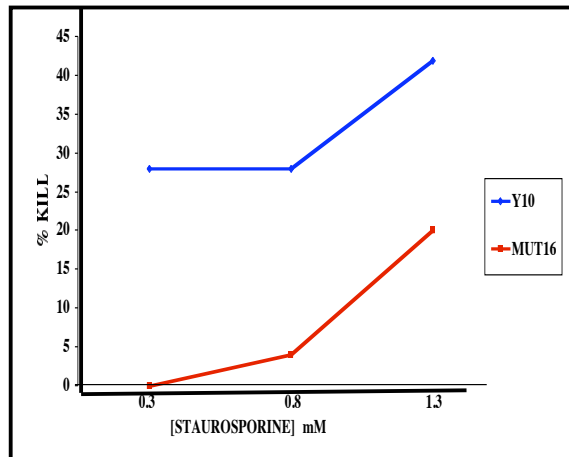


Figure 6.1b LDH release assay of the hygromycin B/CTL resistant clones Mut16(3 xHA8)3.5hr compared to the Y10 parental cell line Y10 on exposure to different concentrations of staurosporine.(Pretorius, 2000).

enzyme (Fiorani and Bjornsti, 2000). The activity of topoisomerase I is inhibited by camptothecin by blocking the re-ligation of the DNA strands after cleavage. Camptothecin reversibly stabilizes the covalent topoisomerase I/DNA complexes and advancing replication forks during the S-phase of the cell cycle contributing to the toxicity of camptothecin by increasing DNA damage, which activates stress-associated signaling pathways that may ultimately induce apoptosis.

DWNN/RBBP6/P2P-R gene was isolated in a genetic screen aimed at identifying novel components of the MHC class I antigen processing and presentation pathways (George, 1995). Several mutant cell lines were generated using a promoter trap mutagenesis strategy in the genetic screen. The mutant cell lines were analyzed for sensitivity to the CTL specific clones HA8 and HA11 using the lactate dehydrogenase (LDH) release assay (George, 1995). Of these cell lines analyzed three showed 100 % resistance to killing by the CTL specific clones, HA8 and HA11 (see figure 6.1a). Further analysis showed that the Mut 16(3xHA8) 3.5hrs cell line, from which the gene was identified, to be resistant to staurosporine-induced apoptosis (Pretorius, 2000) (see figure 6.1b).

P2P-R deficiency, by antisense treatment, restricts cell cycle progression from G1 through S to mitosis in a microtubule-dependent manner and P2P-R deficiency represses UV irradiation-induced apoptosis (Scott and Gao, 2002). Furthermore, Gao and Scott, (2002) showed that P2P-R protein over-expression restricts mitotic progression at prometaphase and promotes mitotic apoptosis. Over-expression of this potential pro-apoptotic region in MCF-7 cells promoted camptothecin-induced apoptosis. The potential

pro-apoptotic region overlaps with the region of P2P-R that is responsible for p53 and single stranded DNA binding (amino acids 1204-1314). (Gao and Scott, 2003).

Recently Li *et al.*, 2007, showed by knocking out the p53-binding domain of the RBBP6 gene using homologous recombination, that the PACT-p53 interaction plays a critical role in embryonic development and tumorigenesis and identify PACT as a member of negative regulators of p53.

A range of biochemical assays were used to detect and quantify the induction of apoptosis in RU6A and GU6B compared to the normal NIH 3T3 cell line. The activation of a particular pathway is dependant on the reagent used to activate apoptosis, its concentration and to some extent the cell type. Due to these considerations different assays that detect different biochemical changes in cells during apoptosis were used to examine the effect of RBBP6 silencing, using RNAi, on apoptosis.

Aims of this chapter:

- Investigate the role of RBBP6 in camptothecin –induced apoptosis, using the stable siRNA expressing cell lines RU6A and GU6B.
- Investigate the effect on p53 expression following the induction of apoptosis.
- Investigate the possible route of apoptosis as mediated by the RBBP6 gene.

6.2 Determining the optimum concentration of camptothecin

6.2.1 The Annexin V-PE assay

This section will deal with determining the optimum concentration of camptothecin needed to cause maximum cell death in the parental NIH 3T3 cell line using the Annexin V-PE assay.

Loss of plasma membrane asymmetry is one of the earliest features characterizing apoptosis. In the apoptotic cells, the membrane phospholipid phosphatidylserine (PS) is translocated from the inner to the outer leaflet of the plasma membrane, thereby exposing PS to the external cellular environment. Annexin V is a 35-36 kDa Ca^{2+} dependant phospholipid-binding protein that has a high affinity for PS and binds to the cells with exposed PS. Since externalization of PS occurs in the earlier stages of apoptosis, Annexin V can identify apoptosis at an earlier stage than assays based on nuclear changes such as DNA fragmentation. Annexin V-PE staining precedes the loss of membrane integrity, which accompanies the latter stages of cell death resulting from either apoptotic or necrotic processes. Therefore staining with Annexin V-PE is typically used in conjunction with a vital dye such as 7-Amino-actinomycin (7-AAD) to allow the identification of early apoptotic cells.

The parental cell line NIH 3T3 was cultured in 6 well plates at a density of 2.4×10^4 cells per well. After culturing the cells for 24 hrs in DMEM as described in section 2.13.3, the cells were treated with different concentrations of camptothecin ranging from 0 to 25

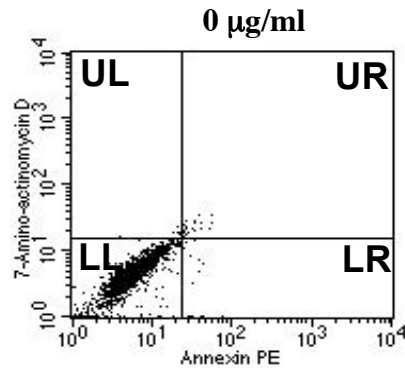
$\mu\text{g/ml}$ for an additional 24 hrs. Following this induction period cells were harvested and assayed using the Annexin V-PE protocol as described in section 2.16.3.

Figure 6.2(i) shows the Annexin V-PE results obtained following the induction of apoptosis in the NIH 3T3 cell line with different concentrations of camptothecin after a 24 hr period. The different quadrants are as follows; UL - necrotic cell population, LL - normal cell population, LR - early apoptotic population and UR - late apoptotic population. From the results a linear increase in the amount of apoptotic cells in parallel with an increase in camptothecin concentration is observed. The combination of the UR and LR quadrants showed 73 % of the parental NIH 3T3 cells to be apoptotic at a concentration of 25 $\mu\text{g/ml}$ camptothecin after 24 hrs. The results were analyzed and presented as a bar graph plotting the mean \pm SD (see figure 6.2(ii)). The data were analyzed for independent repeats of the experiment. A concentration of 25 $\mu\text{g/ml}$ camptothecin induced for 24 hrs was used for all subsequent experiments unless otherwise stated.

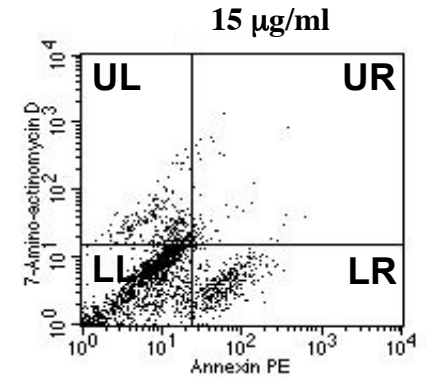
6.3 The effect of RBBP6 silencing on apoptosis

6.3.1 Annexin V-PE assay

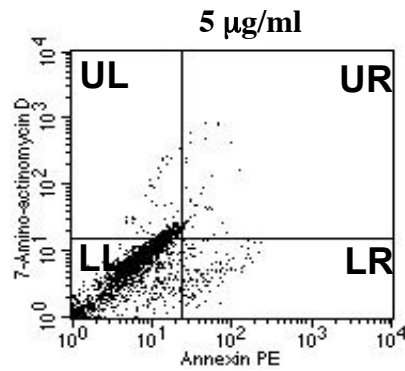
The stable siRNA expressing cell lines, RU6A and GU6B, were cultured in 6 well plates as described in section 2.13.3 alongside the parental cell line NIH 3T3. Following incubation the cells were treated with 15, 20 and 25 $\mu\text{g/ml}$ camptothecin respectively for 24 hrs. Apoptosis was measured using the Annexin V-PE assay as described in section



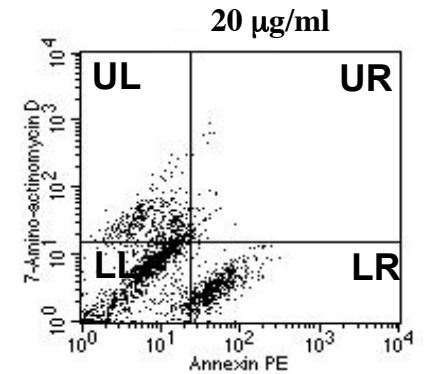
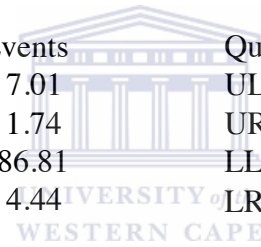
Quad	% Events
UL	0.75
UR	0.26
LL	94.57
LR	4.42



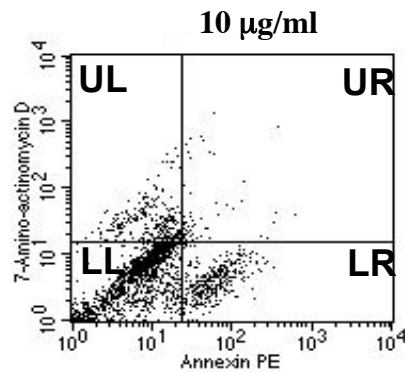
Quad	% Events
UL	12.23
UR	2.99
LL	71.26
LR	13.52



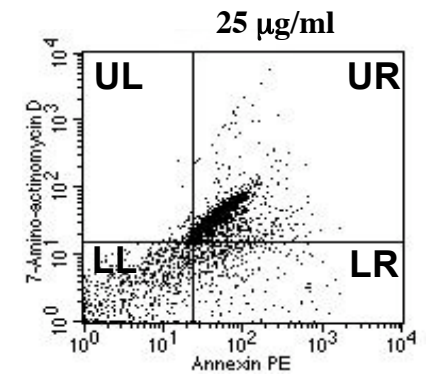
Quad	% Events
UL	7.01
UR	1.74
LL	86.81
LR	4.44



Quad	% Events
UL	17.79
UR	2.35
LL	58.77
LR	21.09



Quad	% Events
UL	10.23
UR	4.63
LL	78.02
LR	7.12



Quad	% Events
UL	2.84
UR	60.44
LL	24.22
LR	12.50

**Figure 6.2(i) Apoptosis analysis of the parental NIH 3T3 cell line
using the Annexin V-PE assay following treatment with
camptothecin.**

The NIH 3T3 cell line was treated with increasing concentrations of camptothecin ranging from 0 to 25 $\mu\text{g/ml}$ for 24 hours and the percentage apoptosis determined using the Annexin V-PE assay on a FACS instrument.

UL - Necrotic cell population

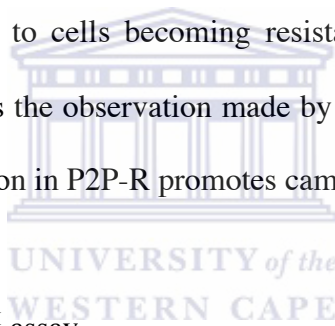
LL - Normal cell population

LR - Early apoptotic population

UR - Late apoptotic population

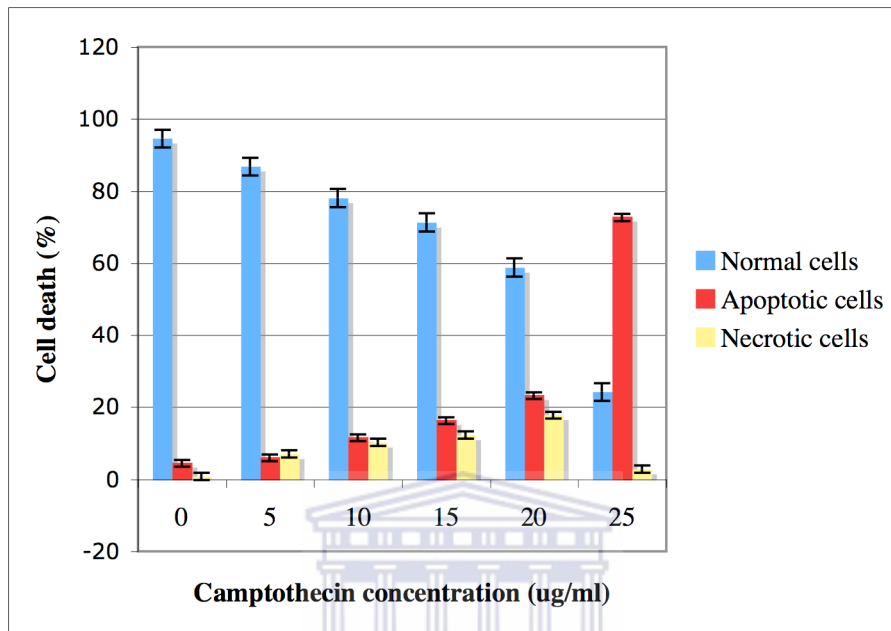


2.16.3 Quadrant statistics were performed on the results and presented as a bar graph (see figure 6.2(iii)). Figure 6.2(iii-a) compares the results obtained for the parental cell line to that for RU6A. From the results less than 5 % of the RU6A cell population were apoptotic compared to 73 % of the parental cell line at any given concentration of camptothecin. Figure 6.2(iii-b) compares the results obtained for the parental cell line to that for GU6B. The results indicates an apoptotic population of less than 10 % for the GU6B cell line compared to the 73 % of the parental cell line at any given concentration of camptothecin. Both RU6A and GU6B showed a significantly lower percentage of apoptotic cells when compared to the parental cell line. These results clearly indicate that the silencing of RBBP6 leads to cells becoming resistant to apoptosis as induced by camptothecin and complements the observation made by Gao and Scott, 2003, that over-expressing a pro-apoptotic region in P2P-R promotes camptothecin-induced apoptosis.



6.3.2 APOPercentage™ assay

This assay works by the accumulation of the APOPercentage™ dye within all cells that are at the mid-phase stage of apoptosis. This stage corresponds with the translocation of phosphatidylserine to the outer surface of the cell membrane (Fadok *et al.*, 1992). In other words, all cells undergoing ‘mid-phase apoptosis’ will be stained fluorescent pink with the APOPercentage™ dye and the percentage of apoptotic cells measured by FACS analysis.



UNIVERSITY of the
WESTERN CAPE

Figure 6.2(ii) Flow cytometric data for the NIH 3T3 cell line following the induction of apoptosis.

The FACS data (see figure 6.2(i)) was analyzed and plotted as the mean \pm SD presenting the percentage cell death versus the camptothecin concentration for the different stages of apoptosis as measured by the Annexin V-PE assay.

The data were analyzed for independent repeats of the experiment.

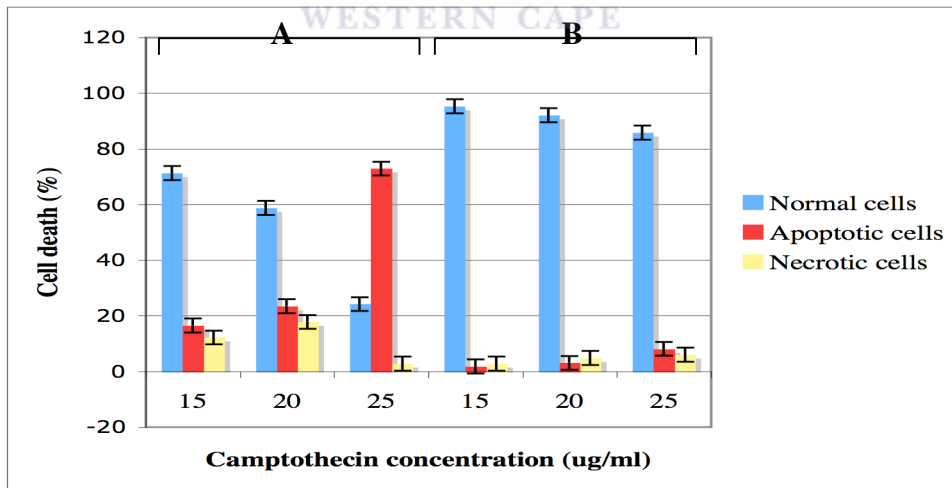
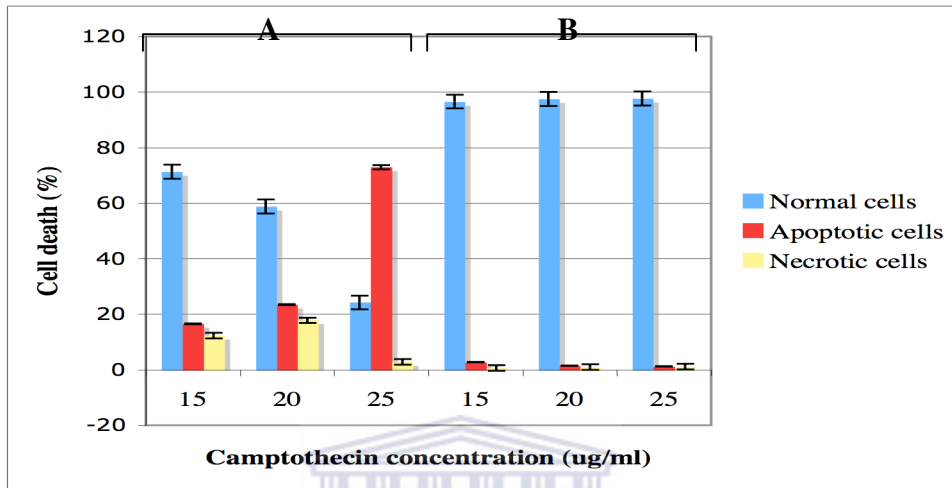
NIH 3T3 and the siRNA expressing stable cell lines were propagated in six well plates as described in section 2.13.3 and treated with 25 µg/ml camptothecin for 24 hours. In order to measure the occurrence of apoptosis the *APOPercentage*TM assay was used as described in section 2.16.2.

Figure 6.3(A) compares the results obtained for the NIH 3T3 cell line with that obtained for RU6A and GU6B using the *APOPercentage*TM assay and 6.3(B) the results analyzed and presented as a bar graph. From figure 6.3(A-ii) 37 % of the parental cell line are undergoing apoptosis compared to 5 % RU6A (figure 6.3A-iii) and 8 % in GU6A (figure 6.3A-v) respectively. Although the stable siRNA expressing cell lines appear to be more resistant, there is however a small difference noted in the results obtained using the Annexin V-PE assay with those obtained using the *APOPercentage*TM assay. Both assays measure apoptosis but at a different stage of the process and this can be considered a contributing factor to the difference noted in the results. Notwithstanding this difference, the results showed a 5-7 fold decrease in sensitivity to apoptosis in GU6B and RU6A respectively.

6.3.3 Complementing stable cell lines with a full-length RBBP6 cDNA

To investigate the role of RBBP6 in apoptosis further, a full-length cDNA (DWNN-200, supplied by Dr A Skepu) was transfected back into stable cell lines. The equivalent of 1 µg representing the cDNA construct was transfected back into RU6A and GU6B using MetafecteneTM as described in section 2.14.1. The expression level of the RBBP6 protein

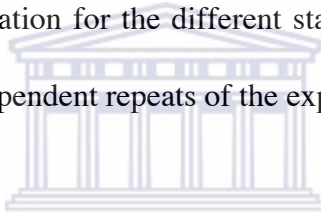
(a)



(b)

Figure 6.2(iii) Flow cytometric data for the NIH 3T3, RU6A and GU6B cell lines following the induction of apoptosis.

The NIH 3T3, RU6A and GU6B cell lines were treated with camptothecin ranging from 15 to 25 $\mu\text{g/ml}$. Apoptosis was measured using the Annexin V-PE assay on a FACS instrument. The FACS data was analyzed and plotted as the mean \pm SD presenting the percentage cell death versus the camptothecin concentration for the different stages of apoptosis. The data were analyzed for independent repeats of the experiment.



- (a) Compares the results obtained for the NIH 3T3 cell line (**Panel A**) to the results obtained for RU6A (**Panel B**).
- (b) Compares the results obtained for the NIH 3T3 cell line (**Panel A**) to that obtained for GU6B (**Panel B**).

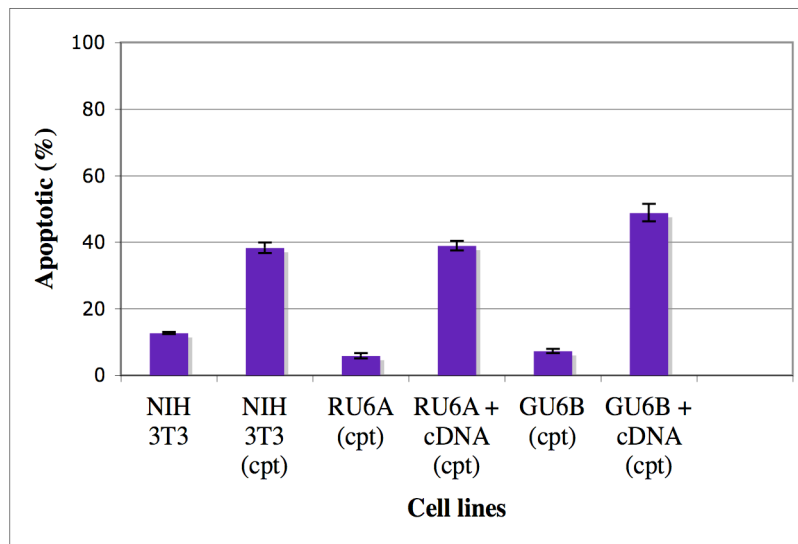
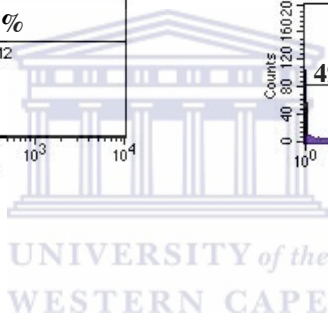
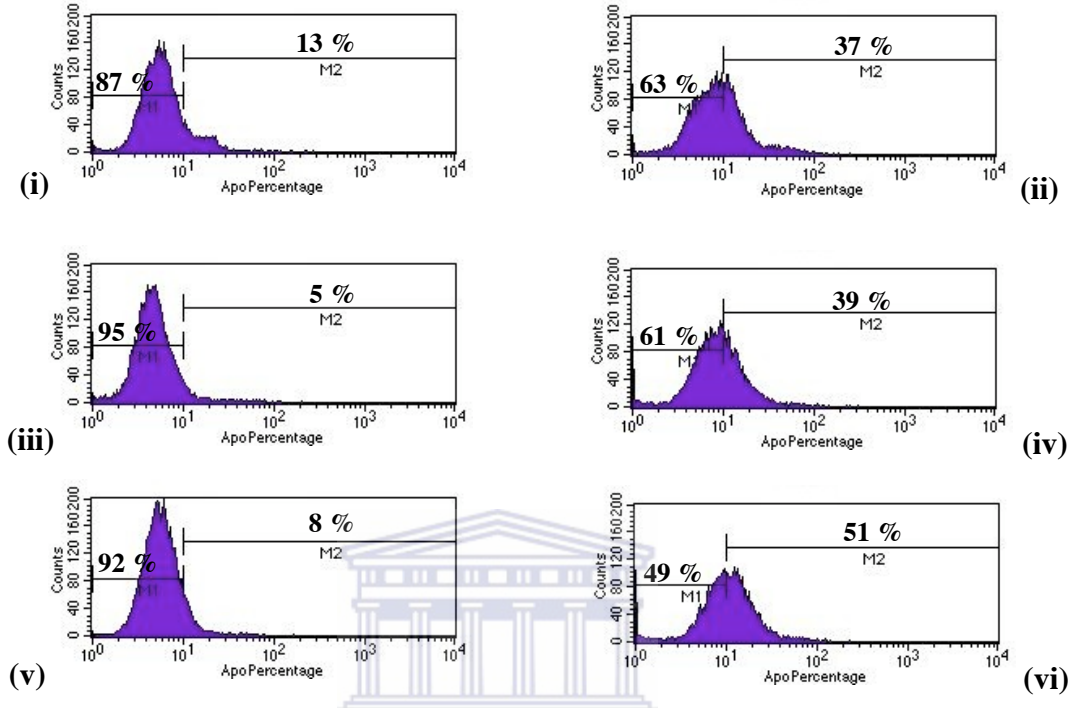
in RU6A and GU6B, following transfection, was measured using Real-Time qRT-PCR and compared to the expression level of the protein in the “knock down” cell lines as well as in the parental cell line (data not shown). The cDNA complemented cell lines were treated with 25 µg/ml camptothecin for 24 hrs and apoptosis measured using the *APOPercentage*TM assay as described in section 2.16.2.

Figure 6.3(A) shows the *APOPercentage*TM assay results obtained for RU6A and GU6B complemented with the full-length RBBP6 cDNA following camptothecin-induced apoptosis and 6.3(B) the data presented as a bar graph plotting the mean ± SD. The data were analyzed for independent repeats of the experiment. From figure 6.3A-iv RU6A sensitivity to apoptosis was restored to the same level as that measured in the parental cell line following transfection of the full-length cDNA. However, the GU6B (see figure 6.3A-vi) cell line showed an apoptotic population of 51% a 1.4 fold increase compared to the parental cell line. From the results it appears that following transfection of the full-length RBBP6 cDNA construct, the parental NIH 3T3 phenotype (sensitivity to camptothecin) is rescued in the RBBP6 negative cell lines, RU6A and GU6B.

6.4 Over-expressing the RBBP6 protein and the effect on Apoptosis

Gao and Scott (2003) showed that in over-expressing a putative pro-apoptotic region of P2P-R in human MCF-7 cells, camptothecin-induced apoptosis were promoted.

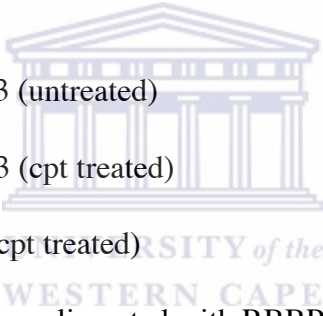
(A)



(B)

Figure 6.3 *APOPercentage*TM assay demonstrating the percentage cell death in different cell lines following camptothecin-induced apoptosis.

The cell lines were treated with 25 µg/ml camptothecin (cpt) for 24 hours and the percentage apoptosis measured using the *APOPercentage*TM assay on a FACS instrument.

- 
- Panel A(i)** NIH 3T3 (untreated)
- (ii)** NIH 3T3 (cpt treated)
- (iii)** RU6A (cpt treated)
- (iv)** RU6A complimented with RBBP6 cDNA (cpt treated)
- (v)** GU6B (cpt treated)
- (vi)** GU6B complimented with RBBP6 cDNA (cpt treated)

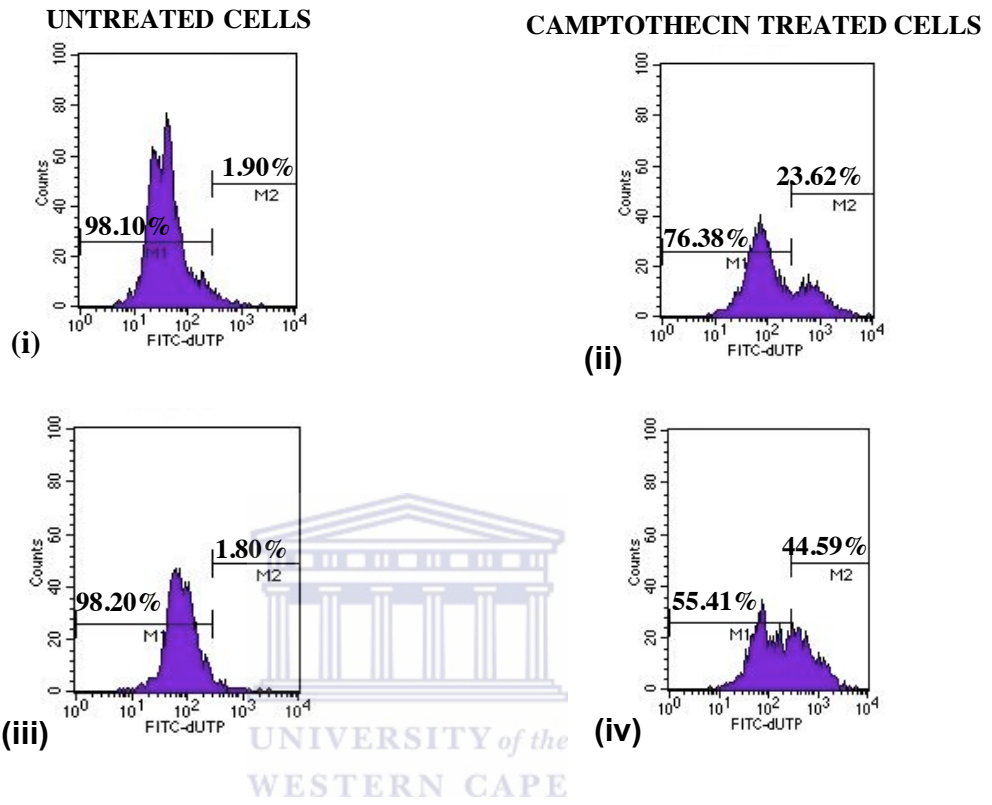
Panel B The analyzed FACS data presented as a bar graph as the mean \pm SD. The data were analyzed for independent repeats of the experiment.

This section will look at the over-expression of the full-length DWNN-200 protein in NIH 3T3 cells and the effect it has on apoptosis induced by camptothecin. NIH 3T3 cells were cultured in 6 well plates as described in section 2.13.3. Cells were transfected with 1 μ g of the DWNN-200 cDNA construct using the Metafectene™ reagent as described in section 2.14.1. The expression level of RBBP6 was calculated at 50 % more in the RBBP6 cDNA transfected NIH 3T3 cell line compared to the un-transfected one as measured using Real-Time qRT-PCR (data not shown).

Apoptosis was induced 48 hrs post-transfection with 25 μ g/ml of camptothecin. Cells were harvested after 48 hrs to ensure that cells undergoing apoptosis were in the late stage and evaluated for apoptosis using the APO-Direct/TUNEL assay as described in section 2.16.4. Extensive DNA degradation is a characteristic event, which occurs in the late stages of apoptosis. Cleavage of the DNA may yield double-stranded, low molecular weight DNA fragments (mono- and oligonucleosomes) as well as single strand breaks (“nicks”) in high molecular weight DNA. These DNA strand breaks can be detected by enzymatic labeling of the free 3'-OH termini with modified nucleotides (X-dUTP, X = biotin, DIG or fluorescein). Suitable labeling enzymes include DNA polymerase (nick translation) and terminal deoxynucleotidyl transferase (end labeling) which are utilized by the TUNEL assay or alternatively known as TdT-mediated X-dUTP nick end labeling (Heatwole, 1999).

Figure 6.4(A) shows the TUNEL results obtained for the NIH 3T3 cell line following the induction of apoptosis using camptothecin and 6.4(B) the results analyzed and presented

(A)



(B)

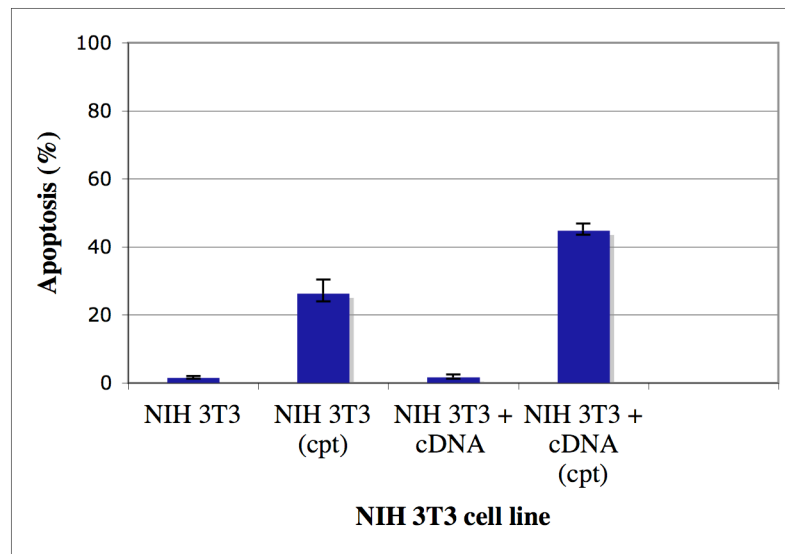


Figure 6.4 TUNEL assay measuring apoptosis in the NIH 3T3 cell line

NIH 3T3 cells were complimented with the full-length RBBP6 cDNA construct followed by treatment with 25 $\mu\text{g/ml}$ camptothecin for 48 hrs. Apoptosis were measured before and after the transfection of the RBBP6 cDNA using the TUNEL assay on a FACS instrument.

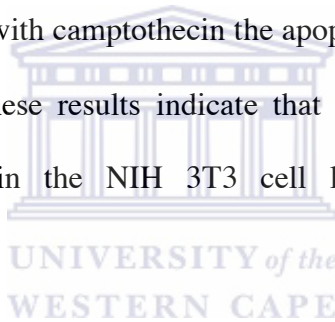
- Panel A(i)** NIH 3T3 cells (untreated)
- (ii)** NIH 3T3 cells (treated)
- (iii)** NIH 3T3 complimented with cDNA (untreated)
- (iv)** NIH 3T3 complimented with cDNA (treated)

WESTERN CAPE

Panel B The analyzed FACS data presented as a bar graph as the mean \pm SD. The data were analyzed for independent repeats of the experiment.

as a bar graph. From figure 6.4(Ai-ii) the NIH 3T3 cell line show an apoptotic population of 24 % following induction of apoptosis compared to 2 % in the un-induced cell population.

Figure 6.4 (Aiii-iv) compares the NIH 3T3 cell transfected with the full-length cDNA (un-induced) to that transfected with the full-length cDNA followed by treatment with camptothecin. Experiment 6.4(Ai) served as control to compensate for the effect over-expression alone might have on the NIH 3T3 cells. From the data it is clear that the effect of over-expression was negligible. In the NIH 3T3 cells over-expressing the RBBP6 protein followed by treatment with camptothecin the apoptotic population doubled (44.56 % compared to 23.62 %). These results indicate that over-expression of the RBBP6 protein promotes apoptosis in the NIH 3T3 cell line following treatment with camptothecin.

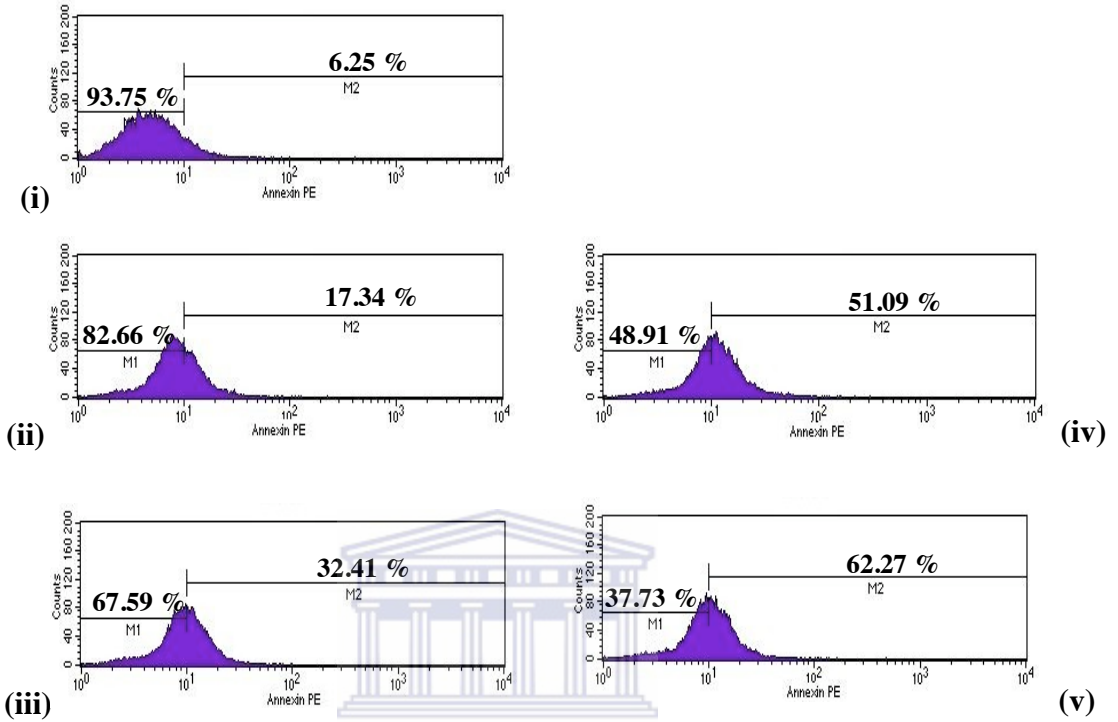


6.4.1 The effect of increased concentration of RBBP6 on Apoptosis

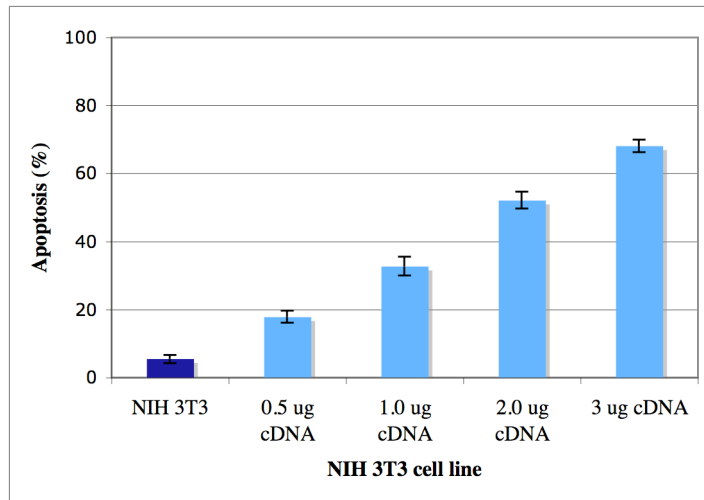
Previously 1 μg of the full-length RBBP6 cDNA was transfected into NIH 3T3 cells and the cells treated with camptothecin. Using the TUNEL assay the amount of apoptosis was measured. This section will examine the effect on apoptosis as the concentration of the full-length RBBP6 cDNA is increased in NIH 3T3 cells.

NIH 3T3 cells were cultured in 6 well plates till 70 % confluent as described in section 2.13.3. Different concentrations of the cDNA was transfected using Metafectene™ as

(A)



UNIVERSITY of the
WESTERN CAPE



(B)

- NIH 3T3 (untreated)
- NIH 3T3 + RBBP6 cDNA(treated)

Figure 6.5 *APOPercentage*TM assay demonstrating the percentage cell death in the NIH 3T3 cell line.

The NIH cell line were transfected with the RBBP6 cDNA with concentrations ranging from 0.5 to 3.0 $\mu\text{g/ml}$. The transfected cells were treated with 25 $\mu\text{g/ml}$ camptothecin for 24 hours and the percentage apoptosis measured using the *APOPercentage*TM assay on a FACS instrument.

Panel A(i) NIH 3T3 un-transfected

(ii) NIH 3T3 - 0.5 $\mu\text{g/ml}$

(iii) NIH 3T3 - 1.0 $\mu\text{g/ml}$

(iv) NIH 3T3 - 2.0 $\mu\text{g/ml}$

(v) NIH 3T3 - 3.0 $\mu\text{g/ml}$

Panel B The analyzed FACS data presented as a bar graph as the mean \pm SD. The data were analyzed for independent repeats of the experiment.

described in section 2.14.1. Following transfection of the cDNA construct, cells were treated with camptothecin for 24 hrs. The apoptotic population was measured using the Annexin V-PE assay as described in section 2.16.3. This assay was used to clearly distinguish between an apoptotic and a necrotic population.

Figure 6.5(A) shows the Annexin V-PE (necrotic population excluded so that only true apoptotic cells are measured) results for the NIH 3T3 cell line transfected with increased concentrations of the full-length RBBP6 cDNA and treated with camptothecin and 6.5(B) the results analyzed and presented as a bar graph plotting the mean \pm SD. The data were analyzed for independent repeats of the experiment. From the results there is a linear increase in the apoptotic population in parallel with an increase in the RBBP6 protein expression. The necrotic cell population remained the same (data not shown). Thus there seems to be no toxic effect on the NIH 3T3 cells resulting from the over-expression of the RBBP6 protein.

6.5 The effect on p53 expression

Many forms of apoptosis are mediated by p53 dependant mechanisms (Haupt *et al.*, 1997, Moll and Zaika, 2001). Mechanisms that can also be directly influenced by the action of Rb1 (Bates and Vousden, 1999). Gao and Scott (2002) showed that apoptosis mediated through P2P-R was independent of both p53 and Rb as Soas2 cells lack p53 and functional Rb1. However Li *et al.* (2007) showed that knockdown of endogenous PACT

using homologous recombination resulted in p53 accumulation *in vivo* and induced apoptosis and cell cycle growth retardation in a p53 dependant manner.

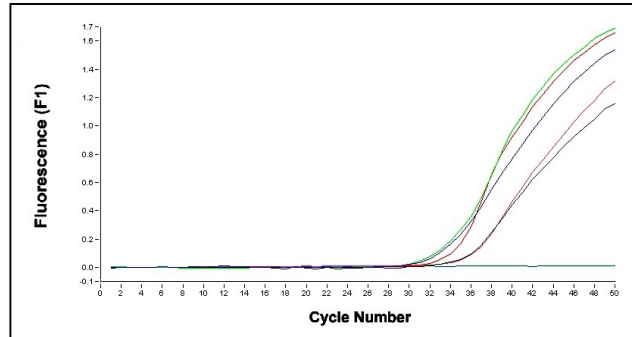
This section will aim to evaluate the effect on p53 expression in the RBBP6 negative cell line, RU6A and the parental cell line, NIH 3T3 on various levels. Firstly, p53 expression in the un-induced wild type NIH 3T3 cells will be compared to the same line following induction of apoptosis via camptothecin. These experiments in turn will be compared to p53 expression in the NIH 3T3 cell line over-expressing the RBBP6 protein. Secondly, p53 expression will be evaluated in the RU6A cell line before and after camptothecin-induced apoptosis.



All cell lines in this section were cultured in DMEM as described in section 2.13.3. Cells were plated in duplicate in 6 well plates, one set of cells were left untreated and served as control whilst the second set of cells, were treated with 25 µg/ml camptothecin for 24 hrs. Total RNA was isolated from all the cells using the TRIzol method as described in section 2.19 and cDNA synthesized as described in section 2.20. The synthesized cDNAs were standardized and subjected to Real-Time qRT-PCR analysis as described in section 2.21. Mouse p53 specific oligonucleotides were used (see table 6.1 for sequences) and the *gapdh* housekeeping gene used as reference gene to quantify the relative p53 expression.

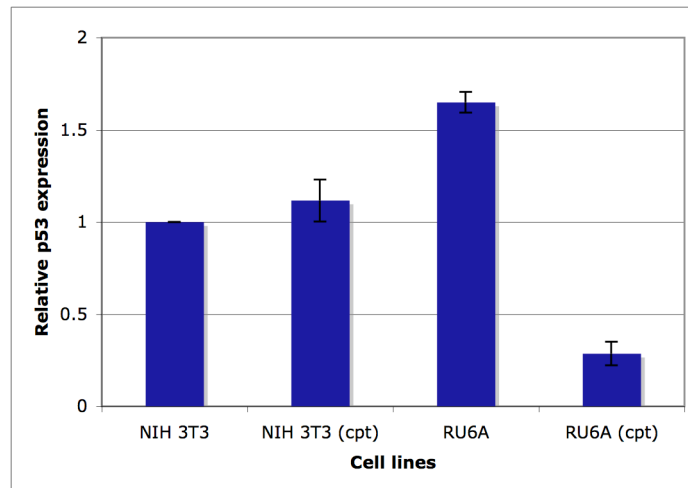
Figure 6.6(A) shows the Real-Time qRT-PCR data obtained for the expression of p53 with the CP values given for each reaction. The Real-Time PCR efficiencies (E) were calculated from the resulting slopes provided by the Real-Time Quantitative PCR

(a)



Threshold (CP) value

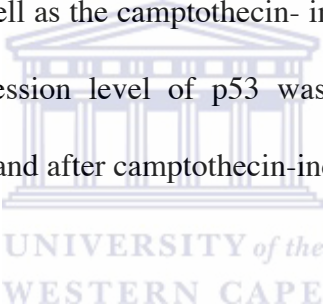
3T3 p53	33.62
3T3+RBBP6 cDNA (cpt) p53	34.52
3T3 (cpt) p53	34.21
3T3	35.90
RU6A (cpt) p53	36.09
Blank GAPDH	



(b)

Figure 6.6 Expression analysis of the p53 gene using Real-Time qRT-PCR.

The NIH 3T3 cell line was transfected with the full-length RBBP6 cDNA. Following transfection the cell line were treated with 25 $\mu\text{g/ml}$ camptothecin for 24 hrs. The expression level of p53 was determined in the cDNA complimented cell line and compared to the expression of p53 in the un-induced as well as the camptothecin- induced NIH 3T3 cell line. Furthermore the expression level of p53 was also determined in the RU6A cell line before and after camptothecin-induced apoptosis.

- 
- (a) Represents the Real-Time qRT-PCR data using a LightCycler instrument.
- (b) The analyzed FACS data presented as a bar graph as the mean \pm SD. The data were analyzed for independent repeats of the experiment.

software and was calculated according to the equation formulated by Pfaffl (2001) as described in section 2.22. The *gapdh* standard curve was used to calculate the relative expression level of p53 and the data represented as the mean \pm SD in figure 6.6(B).

From figure 6.6(B) no differences were observed in the expression of p53 in the NIH 3T3 cell line before and after camptothecin-induced apoptosis. Similarly no difference was observed in p53 expression in the NIH 3T3 cell line following transfection of the full-length RBBP6 cDNA and subsequent induction of apoptosis. The results suggest that camptothecin-induced apoptosis in the NIH 3T3 cell line are independent of observable changes in p53 expression.



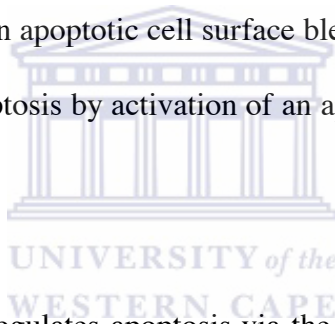
However, the results for RU6A are different compared to those observed for the parental NIH 3T3 cells. In the RU6A cell line (data not shown in figure 6.6(A) the expression of p53 is higher than that observed for the parental NIH 3T3 cell line. There is an approximate 2-fold higher p53 expression in the RU6A cell line compared to the NIH 3T3 cell line. Following the induction of apoptosis however, there is a decrease in the expression of p53 in the RU6A cell line of approximately 4-fold.

From the results the following observations can be made. Firstly, there are no change in the expression of p53 in the NIH 3T3 cell line expressing endogenous RBBP6 before and after the induction of apoptosis as well as in the NIH 3T3 cell line over-expressing the RBBP6 protein treated with camptothecin. Secondly, p53 expression appears to increase

in the RBBP6 negative cell line, RU6A and subsequently decreases after treatment with camptothecin.

6.6 Investigation of the RBBP6 apoptotic pathway

Apoptosis is signalled via three major biochemical routes in mammalian cells. In the study by Gao and Scott, 2002, they showed P2P-R localization to the mitochondria indicating a possible intrinsic mechanism. The intrinsic route responds to most pro-apoptotic signals, which emanates largely from the mitochondrion. However, they also showed localization of P2P-R in apoptotic cell surface blebs, suggesting that P2P-R over-expression might promote apoptosis by activation of an apoptotic pathway that originates from the cell surface.



The Bcl-2 family of proteins regulates apoptosis via the intrinsic pathway. Bcl-2 family members are key regulators of apoptosis and are over expressed in many malignancies even without the presence of the tumour (Reed, 1997). The Bcl-2 family includes pro-apoptotic members such as Bax, and anti-apoptotic members such Bcl-2.

Anti-apoptotic Bcl-2 members act as repressors of apoptosis by blocking the release of cytochrome-c, whereas pro-apoptotic members act as promoters. These effects are more dependent on the balance between Bcl-2 and Bax than on Bcl-2 quantity alone (Reed, 1997). This section will investigate a possible intrinsic route of apoptosis mediated by RBBP6 by looking at the expression of Bcl-2 and Bax in the NIH 3T3 cell line and

compare it to expression of Bcl-2 and Bax in the RU6A cell line.

The NIH 3T3 and RU6A cell lines were cultured in DMEM as described in section 2.13.3. Cells were plated in duplicate with one set of the cells treated with camptothecin and the other set left untreated. Total RNA was isolated from all the cells using the TRIzol method as described in section 2.19. and cDNA synthesized as described in section 2.20. The synthesized cDNA was standardized and analyzed in a qRT-PCR as described in section 2.21 using gene specific oligonucleotides against Bax and Bcl-2. The Real-Time PCR efficiencies (E) were calculated from the resulting slopes provided by the Real-Time Quantitative PCR software and was calculated according to the equation formulated by Pfaffl (2001) as described in section 2.22. The *gapdh* standard curve was used to calculate the relative expression level of Bax and Bcl-2 and the data represented as the mean \pm SD in figure 6.7.

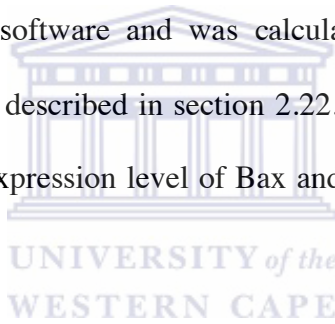
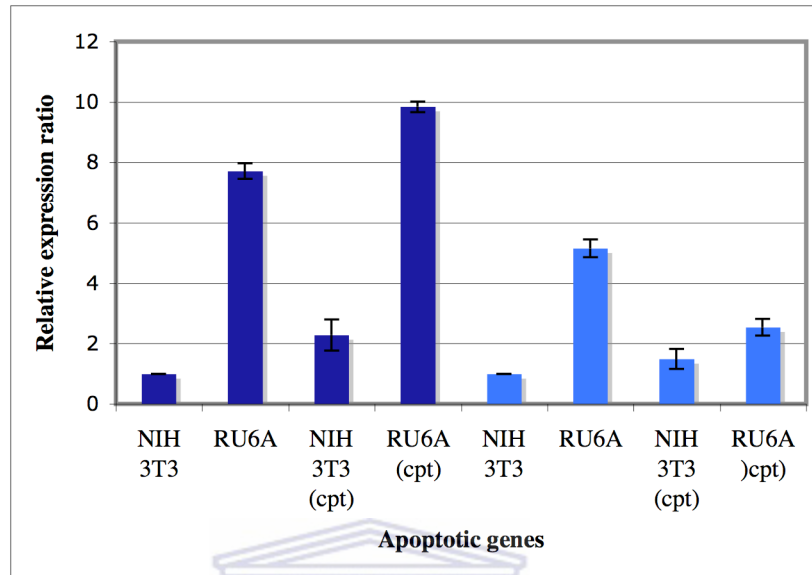


Figure 6.7 compares the relative expression ratio of Bcl-2 in the NIH 3T3 cell line compared to the RU6A cell line before and after the induction of apoptosis using camptothecin. The expression ratio of Bcl-2 was calculated as 1.0 in the un-treated NIH 3T3 cell line whilst Bcl-2 expression in the RU6A cell line was 8-fold higher than its expression in the parental cell line.

Following camptothecin-induced apoptosis in the NIH 3T3 cell line the relative expression of Bcl-2 increased 2-fold compared to its expression in the un-induced NIH 3T3 control cell line. The expression of Bcl-2 in the RU6A cell line following the



■ Bcl-2 anti-apoptotic

■ Bax pro-apoptotic

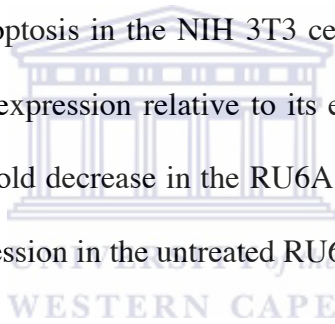
Figure 6.7 Shows the relative expression ratios of the pro-apoptotic Bax versus the anti-apoptotic Bcl-2 gene.

The relative expression ratios of Bcl-2 and Bax were determined in the NIH 3T3 and RU6A cell lines before and after treatment with camptothecin (cpt). The expression of the pro-apoptotic gene Bax and the anti-apoptotic gene Bcl-2 was determined using Real-Time qRT-PCR. The data was analyzed and presented as the mean \pm SD. The data were analyzed for independent repeats of the experiment.

induction of apoptosis showed an approximate 1.3-fold increase compared to its expression in the untreated RU6A cell line and a 10-fold increase compared to its expression in the parental NIH 3T3 cell line.

Figure 6.7 compares the relative expression ratio of Bax in the NIH 3T3 and RU6A cell lines before and after the induction of apoptosis. From the results the expression of Bax are given as 1.0 in the NIH 3T3 cell line. The expression of Bax in the RU6A cell line was calculated at 5-fold higher compared to its expression in the NIH 3T3 cell line.

Following the induction of apoptosis in the NIH 3T3 cell line using camptothecin, Bax showed a 1.5-fold increase in expression relative to its expression in the untreated NIH 3T3 cell line and showed a 2-fold decrease in the RU6A cell line following induction of apoptosis compared to its expression in the untreated RU6A cell line.



6.8 Summary

Several lines of evidence implicated RBBP6 in the process of apoptosis. Gao and Scott, 2003, showed that over-expressing the P2P-R protein promotes apoptosis induced by camptothecin whilst Li *et al.*, 2007, showed targeting the PACT protein using homologous recombination also promotes apoptosis. This chapter focused on the role of the RBBP6 in apoptosis using the RNA interference (RNAi) technique of gene targeting. Two cell lines, RU6A and GU6B, were established which stably express siRNA oligonucleotides targeting different regions of the RBBP6 gene.

Primer	Sequence	Position
m-p53F	5' TGA AAC GCC GAC CTA TCC TTA 3'	829-849
m-p53R	5' GGC ACA AAC ACG AAC CTC AA 3'	901-920
mGAPDH F	5' GGT GGC AGA GGC CTT TG 3'	798-814
mGAPDH R	5'TGC CGA TTT AGC ATC TCC TT 3'	847-866
Bax F	5'GCC CTT TTG CTT CAG GGT TT 3'	139-158
Bax R	5' TCC AAT GTC CAG CCC ATG AT 3'	220-240
Bcl-2 F	5' GACAGAAGATCATGCCGTCC 3'	871-890
Bcl-2 R	5' GGTACCAATGGCACTTCAAG 3'	1156-1175

Table 6.1 List of oligonucleotides used in this chapter.

After determining the optimum concentration of camptothecin needed to induce 100 % killing in the parental NIH 3T3 cell line, the stable cell lines RU6A and GU6B were treated with the same concentration of camptothecin and different apoptosis assays used to determine the extent of induction of cell death. The use of different assay systems would allow for the evaluation of apoptosis at different stages of the process.

The Annexin V-PE assay system allow for the evaluation of cells in early apoptosis as well as to discriminate between cells undergoing necrosis from those undergoing apoptosis. From the results obtained both stable cell lines were significantly more resistant to apoptosis induced by camptothecin, with the RU6A cell line being more resistant than the GU6B cell line. At a concentration of 25 µg/ml camptothecin over a 24

hr period of induction, 73 % of the parental cells were in the early stage of apoptosis compared to 1 % of the RU6A cell population and 5 % of the GU6 cell population.

The *APOPercentage*TM assay was used to assay apoptosis at the mid-phase stage of apoptosis. The results obtained using this assay confirm those observed with the Annexin V-PE assay. The stable cell lines were resistant to camptothecin-induced apoptosis compared to the NIH 3T3 cell line. The *APOPercentage*TM assay showed 5 % of the RU6A and 8 % of the GU6B cell populations to be apoptotic. However, the percentage apoptosis measured in the un-induced NIH 3T3 cell population using the Annexin V-PE assay was higher than the percentage apoptosis measured in the same cell line using the *APOPercentage*TM assay. This difference can possibly be explained by the fact that both assays look at different stages of the apoptosis process. Notwithstanding this difference, the stable siRNA expressing cell lines showed significant resistance to apoptosis induced by camptothecin and it can thus be concluded that targeting the expression of RBBP6 *in vivo*, causes cells to become resistant to apoptosis placing the RBBP6 gene in the category of pro-apoptotic genes.

To further examine the role of RBBP6 in apoptosis, the stable cell lines were complemented with a full-length cDNA corresponding to the complete protein, DWNN-200, followed by treatment with camptothecin. Following transfection of the full-length cDNA DWNN-200 into the RU6A cell line, sensitivity to camptothecin was restored to the same level as that observed in the parental cell line NIH 3T3. However, the GU6B cell line showed an apoptotic population higher than the NIH 3T3 cell line following the

transfection of DWNN-200. From the qRT-PCR data, silencing of the RBBP6 gene, using the DWNN-A siRNA oligonucleotide compared to the DWNN-B siRNA oligonucleotide, was more effective and showed that this difference lends support to the observations made by Holen *et al.*, 2002, who showed that targeting different regions of a given mRNA gave different results. They carried out limited tiling of different siRNA across a region of the human coagulation trigger factor gene (TF) shifting the siRNA target site by only three nucleotides at a time resulted in different degrees of silencing.

Next the effect of over-expressing DWNN-200 on apoptosis was evaluated. The DWNN-200 cDNA was transfected into the NIH 3T3 cell line and subsequently treated with camptothecin. Utilizing the TUNEL apoptosis assay, the results showed a two-fold increase in the NIH 3T3 cell population (45 %) following transfection of DWNN-200 compared to the NIH 3T3 cells (23,62 %) expressing endogenous RBBP6. The NIH 3T3 cell line transfected with DWNN-200 without camptothecin treatment showed an apoptotic population of only 2 %, suggesting that the RBBP6 protein alone does not have any apoptotic effect on the NIH 3T3 cells. The results clearly implicate and strengthen RBBP6 involvement in camptothecin-induced apoptosis. Furthermore the NIH 3T3 cell line were transfected with increasing concentrations of the DWNN-200 cDNA construct. The cells showed a linear increase in the apoptotic population with an increase in the cDNA concentration. It was concluded from this study that over-expression of the RBBP6 protein had no toxic effect on the cell.

The study by Gao and Scott, 2002 that showed P2P-R protein over-expression restricts mitotic progression at prometaphase and promotes mitotic apoptosis, was done using Saos2 cells lacking p53 and a functional Rb1. They concluded that apoptosis induced by camptothecin was independent of p53. Li *et al.*, 2007, however, shown that the targeting of PACT leads to increased apoptosis in a p53 dependant manner. In this chapter the expression of p53 was measured in the parental cell line NIH 3T3 and compared to the expression of p53 following camptothecin-induced apoptosis in the same cell line. Since the RU6A cell lines showed a higher resistance to apoptosis, both the p53 and Bax/Bcl-2 experiments were only carried out using this cell line. The results showed no change in expression of p53 using Real-Time qRT-PCR analysis. In addition the NIH 3T3 cell line were transfected with the DWNN-200 cDNA constructs and apoptosis was induced. The results were similar than observed before, no measurable differences were observed in the expression of p53. However, in the RU6A cell line, the expression of p53 was slightly higher than its expression in the NIH 3T3 cell line treated with camptothecin, whilst the expression of p53 decreased in the RU6A cell line following camptothecin-induced apoptosis.

This chapter also dealt with the possible route of apoptosis that RBBP6 might be involved in by looking at the expression of Bcl-2 and Bax. The anti-apoptotic gene Bcl-2 and the pro-apoptotic gene Bax had been implicated in the intrinsic route of apoptosis. In this study the expression of both genes were studied before and after the induction of apoptosis in the NIH 3T3 cell line and compared to the their expression in the RU6A cell line.

In the NIH 3T3 cell line before induction of apoptosis the expression of both genes were at what can be considered basal level. As proposed by the “rheostat” model, (Kroemer, 1997) the relative ratio of expression between Bax and Bcl-2 regulates apoptosis. From the results the ratio of Bcl-2/bax in the NIH 3T3 cell following induction of apoptosis showed a slightly higher expression of Bcl-2 than Bax. The RU6A cell line showed an approximate 5 fold higher expression level of Bcl-2 compared to Bax following camptothecin-induced apoptosis keeping in mind that the RU6A cell were almost completely resistant to apoptosis. The ratio of Bcl-2/bax in the untreated NIH 3T3 cell line were also similar (1:1) whilst in the untreated RU6A cell line the expression of Bcl-2 was higher than Bax yet not at the same level as observed in the cell line following induction of apoptosis. Although the results do not clearly implicate RBBP6 in the intrinsic route of apoptosis it strongly suggests a role for Bcl-2 and Bax in apoptosis in conjunction with RBBP6. Li *et al.*, 2007, showed the transcription levels of p21 and Bax increased in the PACT *-/-* embryos and concluded that PACT can inhibit the expression of p53 and thus the expression of p53 target genes.

**CHAPTER 7: THE EFFECT OF SILENCING OF THE RBBP6 GENE ON
THE CELL CYCLE.**

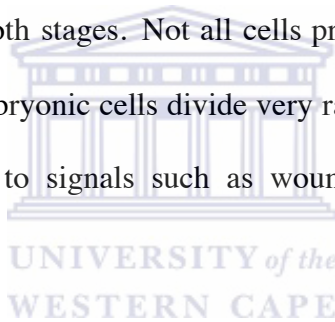
- 7.1 INTRODUCTION
- 7.2 CELL CYCLE ANALYSIS OF RU6A AND GU6B
- 7.3 THE EFFECT OF APOPTOSIS ON THE CELL CYCLE
- 7.4 SUMMARY



CHAPTER 7: THE EFFECT OF SILENCING OF THE RBBP6 GENE ON THE CELL CYCLE

7.1 Introduction

The objective of the cell cycle in most cases is to produce two daughter cells that are accurate copies of the parent. The cell cycle integrates a continuous growth cycle, an increase in cell mass, with a discontinuous division or chromosome cycle, the replication and partitioning of the genome into two daughter cells. Successful cellular replication requires the cell to integrate both stages. Not all cells proceed through the stages of the cell cycle at the same rate. Embryonic cells divide very rapidly, while mature cells might divide rarely, or in response to signals such as wounding, or not at all (Evan and Vousden, 2001).



There are four cell cycle phases with the cell starting out at the completion of mitosis (M phase) whilst the chromosomal DNA is replicated during the S phase (synthetic phase). The remaining phases are gaps between mitosis and the S phase. G1 (first gap phase) is the interval between mitosis and DNA replication. The G2 phase (second gap phase) is the interval between the completion of DNA replication and mitosis. Transitions out of gap phases (G1, G2) are regulated by cyclins and cyclin dependent kinases (CDKs). Cyclins are only present at certain times during the cell cycle. MPF (Maturation Promoting Factor) includes the CDK and cyclins that triggers progression through the cell cycle (see fig. 7.1).

Both p53 and pRb, known regulators of the cell cycle, are regulated by CDKs. pRb is subjected to regulation by many factors, including E2F and cyclin D1. The hypo-phosphorylated pRb, complexes with E2F, which serves as a transcriptional activator of cyclin D1 by binding to its promoter. Inactivation of pRb phosphorylation via the cyclin D/CDK complex in late G1 would not only release E2F transcription factors, but would also decrease cyclin D1 expression (Ekholm and Reed, 2000). Interestingly, E2F release from pRb is associated with cell proliferation; however, above a certain threshold E2F has the potential to trigger apoptosis (Seville *et al.*, 2005).

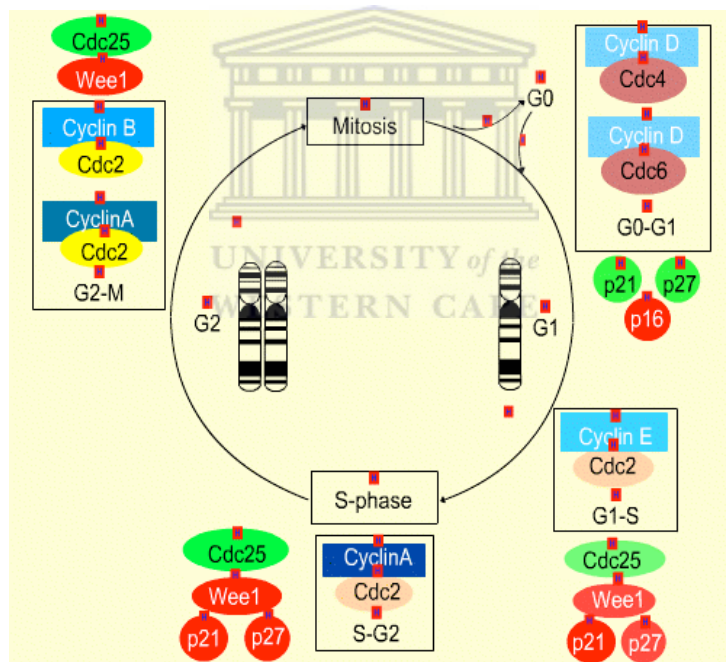


Figure 7.1 Represents a schematic representation of the cell cycle and proteins that regulate the different checkpoints. (www.reactome.org/figures/CellCycle)

The p21^{WAF/CIP1} protein is a cyclin dependant kinase inhibitor that associates with a class of CDKs and inhibits their kinase activities leading to cell cycle arrest and the

dephosphorylation of pRb. Furthermore the p21^{WAF/CIP1} protein is a p53 inducible protein that inactivates the cyclin CDK complexes, blocking the cell cycle progression in the G1-S transition and is also highly expressed in cells undergoing either G1 arrest or apoptosis by either p53-dependent or p53-independent mechanisms (el-Deiry *et al.*, 1994, Michieli *et al.*, 1994).

p53 acts as a tumour suppressor gene and control entry into the S phase of the cell cycle and plays many important roles in cell proliferation. Mutations of the p53 gene inactivate its suppressor activity and its role in tumour progression (Oka *et al.*, 2000). The p53 tumour suppressor gene encodes a transcriptional factor central in the regulation of cell growth, DNA repair and apoptosis induction. Its activity requires the induction of several target genes, including MDM2 and p21^{WAF1} (Trocone *et al.*, 1998).

p53 (Simons *et al.*, 1995) and Rb (Sakai *et al.*, 1995) have both been shown to bind to mammalian RBBP6, suggesting a possible role for RBBP6 in the regulation of these two proteins similar to that played by MDM2 (Hsieh *et al.*, 1999), and thus it is possible to propose a model for the integration of the regulation of transcription, cell cycle control and apoptosis. Given the fact that the DWNN domain can be independently expressed in vertebrates, an interesting possibility is that the function of RBBP6 is to DWNNylate other proteins like p53 and Rb in a fashion similar to ubiquitin and ubiquitin-like proteins.

Several studies have implicated RBBP6 involvement in the cell cycle. Gao and Scott, 2002, showed that P2P-R over-expression promotes both prometaphase arrest in mitosis and mitotic apoptosis. In their study mitotic cells showed a tenfold increase in immunoreactive P2P-R protein. During mitosis, the distribution of P2P-R protein also changed from a primary nucleolar localization in interphase cells to the periphery of chromosomes in mitotic cells (Gao *et al.*, 2002). These findings suggest that P2P-R might serve a functional role in mitosis.

Furthermore, P2P-R deficiency, using anti-sense technology, restricts cell cycle progression from G1 through S to mitosis in a microtubule-dependent manner and represses UV irradiation-induced apoptosis (Scott and Gao, 2002). Recently Li *et al.*, 2007, showed that the growth of the cell line U20S were significantly retarded compared H1299, a p53 null cell line, following silencing of PACT using shRNA, suggesting that PACT is essential for cell growth in a p53 dependant manner.

Aim of this chapter;

- To study the effect on the cell cycle following the silencing of the RBBP6 gene in NIH 3T3 cells.

7.2 Cell cycle analysis of RU6A and GU6B

Both stable siRNA expressing cell lines, RU6A and GU6B, as well as the parental cell line NIH 3T3 were cultured in 6 well plates for 12, 18, 24 and 48 hrs as described in

section 2.13.3. At the indicated time points, cells were removed from the wells and prepared for cell cycle analysis as described in section 2.17. The cells were analyzed using a FACS instrument as described in section 2.15. The data was analyzed with the FlowJo v8.5.3 software using the Dean/Jett/Fox statistical program (Tree Star Inc.) and represented as the percentage of cells within each phase.

Figure 7.2 shows the FACS results of the cell cycle analysis of the NIH 3T3, RU6A and GU6B cell lines at the 12-hour time point. Figure 7.2(a) shows the FACS data and 7.2(b) the data analyzed and represented as a bar graph plotting the mean \pm SD. From the results there are a higher proportion of cells in the G1 phase in the RU6A (81 %) and GU6B (78 %) cell lines compared to the same phase in the NIH 3T3 (60 %) cell line. There are approximately 20 % more cells in the G1 phase for RU6A and GU6B compared to the NIH 3T3 cell line.

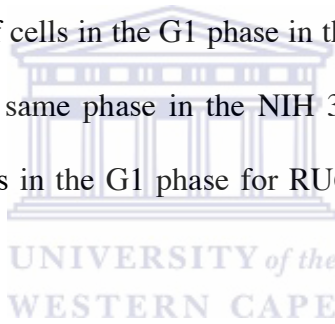
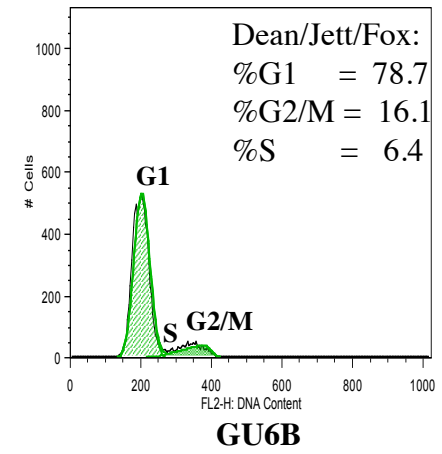
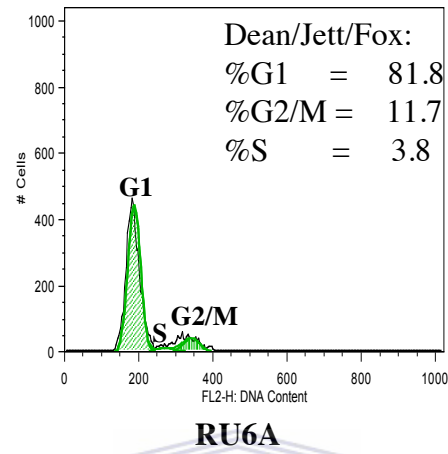
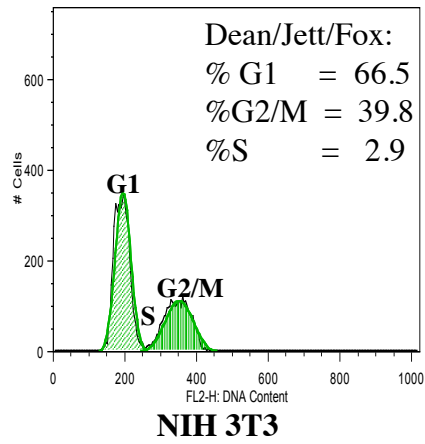
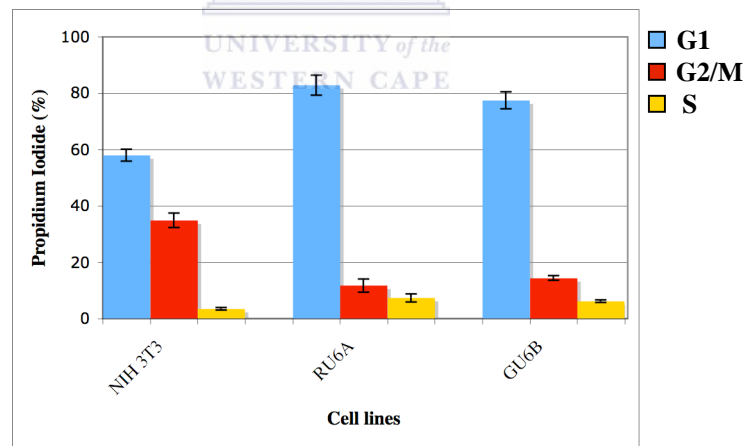


Figure 7.3 shows the FACS results of the cell cycle analysis of the NIH 3T3, RU6A and GU6B cell lines at the 18-hour time point. Figure 7.3(a) shows the FACS data and 7.3(b) the data analyzed and represented as a bar graph plotting the mean \pm SD. At the 18 hour time point the distribution of the NIH 3T3 cells are more or less equal in the G1 and G2/M phase with a slightly higher proportion of cells in the G2/M phase and a clearly defined S phase. Both RU6A (65 %) and GU6B (49 %) showed a higher proportion of the cell population in G1 compared to the NIH 3T3 cells (38 %). However, the proportion of cells in the G1 phase, are 16 % lower in the GU6B population compared to RU6A.



(a)

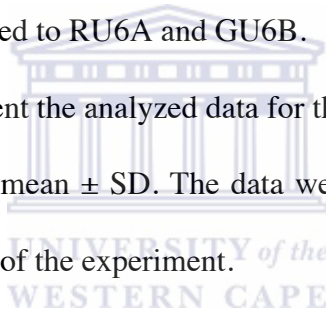


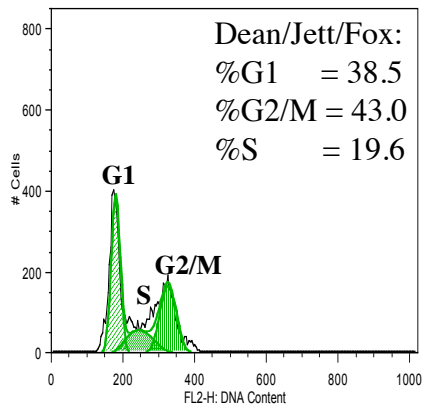
(b)

Figure 7.2 FACS results of the cell cycle analysis of the NIH 3T3, RU6A and GU6B cell lines at the 12 hour time-point.

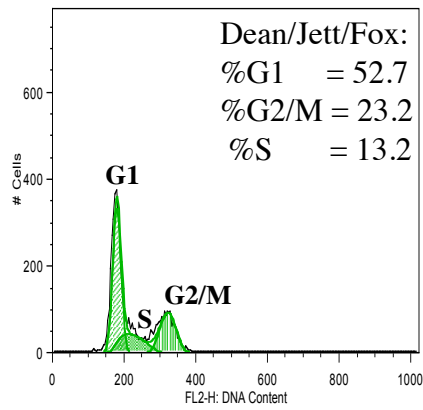
The NIH 3T3, RU6A and GU6B cell lines were cultured and at the 12 hour time-point the cells were analyzed for the different stages of the cell cycle using Propidium iodide staining on a FACS instrument.

- (a) Shows the cell cycle results of the NIH 3T3 cell line compared to RU6A and GU6B.
- (b) Represent the analyzed data for the cell cycle results as the mean \pm SD. The data were analyzed for independent repeats of the experiment.

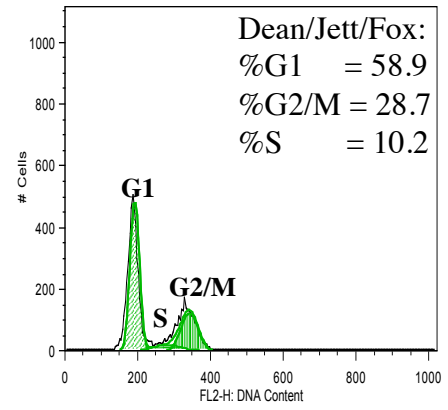




NIH 3T3

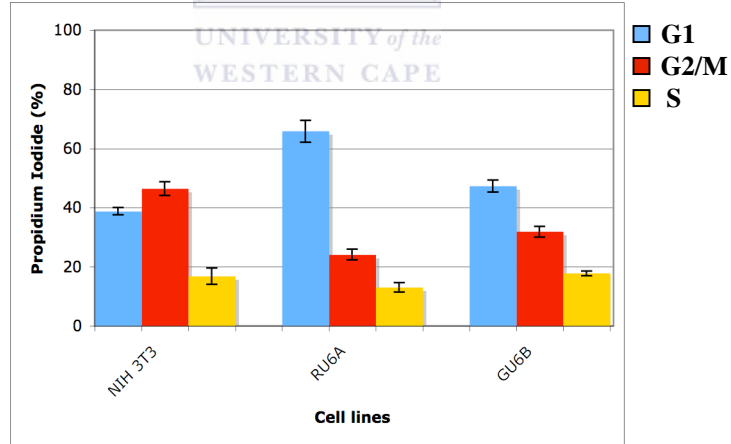


RU6A



GU6B

(a)



(b)

Figure 7.3 FACS results of the cell cycle analysis of the NIH 3T3, RU6A and GU6B cell lines at the 18 hour time-point.

The NIH 3T3, RU6A and GU6B cell lines were cultured and at the 18 hour time-point the cells were analyzed for the different stages of the cell cycle using Propidium iodide staining on a FACS instrument.

- (a) Shows the cell cycle results of the NIH 3T3 cell line compared to RU6A and GU6B
- (b) Represent the analyzed data for the cell cycle results as the mean \pm SD. The data were analyzed for independent repeats of the experiment.

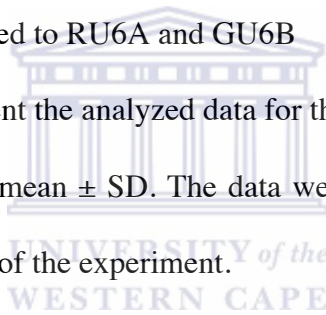
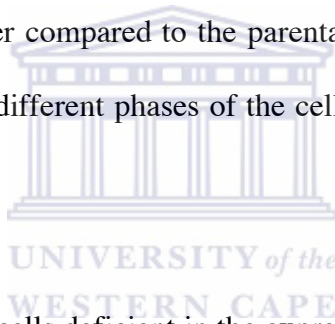
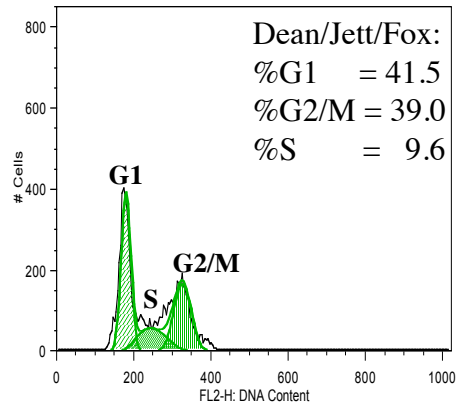


Figure 7.4(a) shows the FACS results of the cell cycle analysis of the NIH 3T3, RU6A and GU6B cell lines at the 24 hour point and figure 7.4(b) the analyzed data at the 24 hour time point presented as bar graph plotting the mean \pm SD. The results show that the population of cells in G1 are still higher in RU6A (68 %) and GU6B (65 %) compared to the NIH 3T3 (45 %) cell population. Significantly at this time point though, is that G1 for both RU6A and GU6B are showing an almost equal proportion of cells compared to the 16 % difference observed at the 24-hour time point.

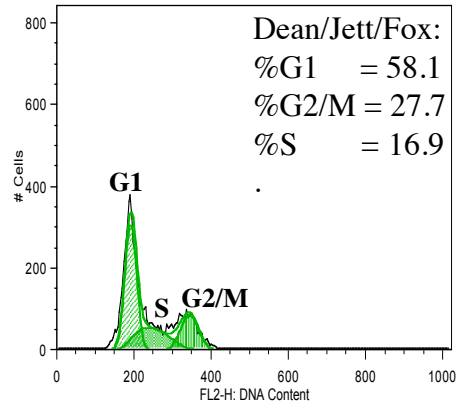
At the 48 hr analysis time point (see figure 7.5) the percentage of cells found in G1 for RU6A and GU6B is still higher compared to the parental cell line. NIH 3T3. However, the distribution of cells in the different phases of the cell cycle appears to be similar for RU6A and GU6B.



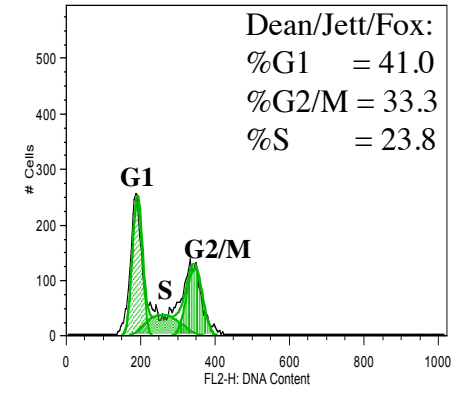
From the results it is clear that cells deficient in the expression of RBBP6 are restricted at the G1 phase of the cell cycle. There also seems to be distinct differences in the distribution of the RU6A cell population compared to the GU6B population between G1 and G2/M at the 18 and 24-hour time points. Generally, more cells seemed to be restricted in the G1 phase of the cell cycle for the RU6A cell population. This result is consistent with those observed for apoptosis analysis and qRT-PCR, that the silencing effect exerted by DWNN-A compared to that exerted by DWNN-B is more potent.



NIH 3T3

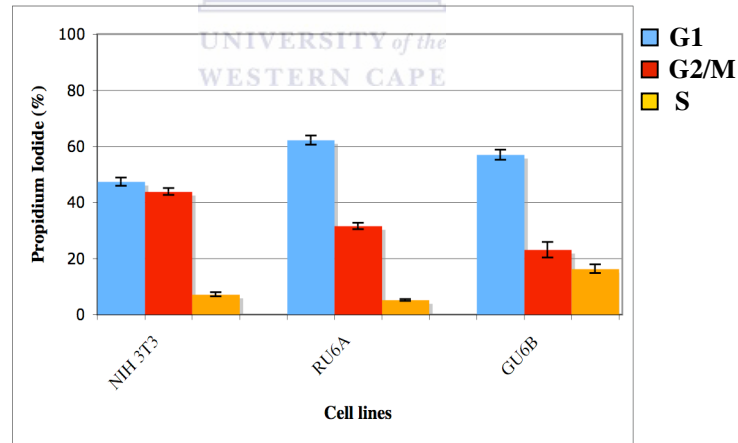


RU6A



GU6B

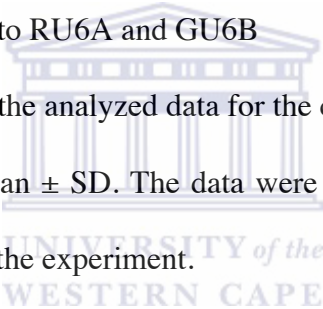
(a)

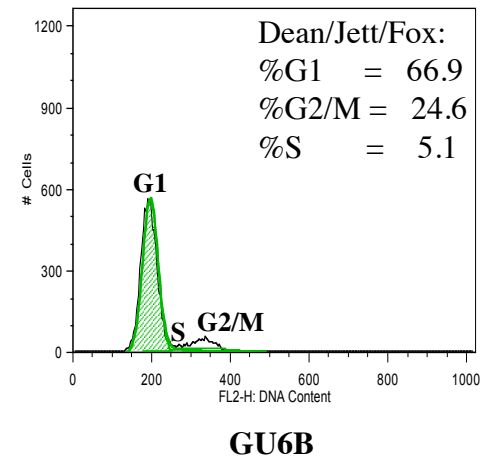
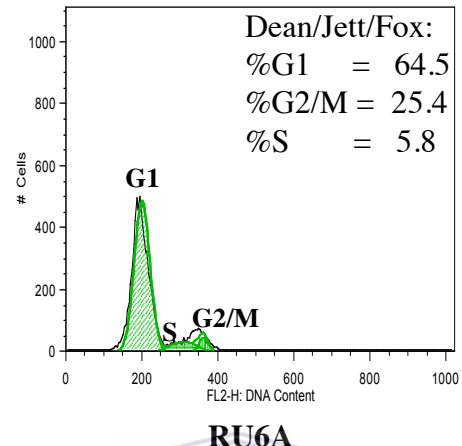
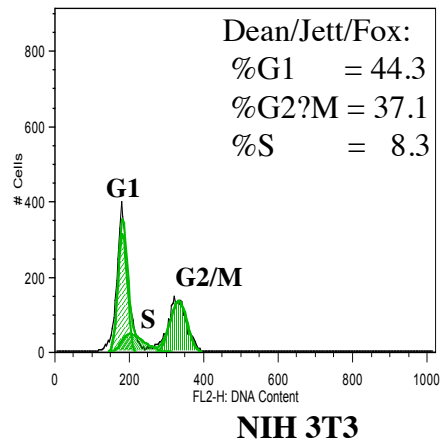


(b)

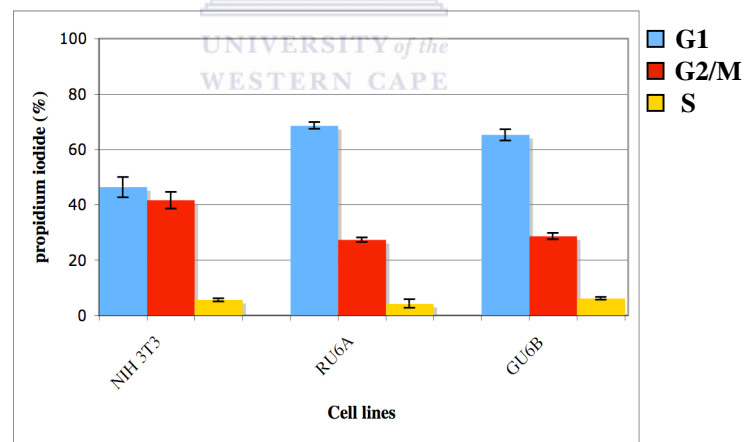
Figure 7.4 FACS results of the cell cycle analysis of the NIH 3T3, RU6A and GU6B cell lines at the 24 hour time-point.

The NIH 3T3, RU6A and GU6B cell lines were cultured and at the 24 hour time-point the cells were analyzed for the different stages of the cell cycle using Propidium iodide staining on a FACS instrument.

- (a) Shows the cell cycle results of the NIH 3T3 cell line compared to RU6A and GU6B
- (b) Represent the analyzed data for the cell cycle results as the mean \pm SD. The data were analyzed for independent repeats of the experiment.
- 



(a)

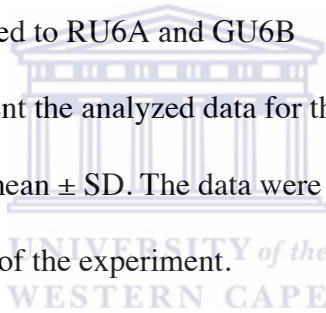


(b)

Figure 7.5 FACS results of the cell cycle analysis of the NIH 3T3, RU6A and GU6B cell lines at the 48 hour time-point.

The NIH 3T3, RU6A and GU6B cell lines were cultured and at the 48 hour time-point the cells were analyzed for the different stages of the cell cycle using Propidium iodide staining on a FACS instrument.

- (a) Shows the cell cycle results of the NIH 3T3 cell line compared to RU6A and GU6B
- (b) Represent the analyzed data for the cell cycle results as the mean \pm SD. The data were analyzed for independent repeats of the experiment.



7.2 The effect of apoptosis on the cell cycle

This section will investigate the effect of camptothecin-induced apoptosis on the cell cycle. The 24 hour time point will be used, as this period was shown to be optimal for maximum apoptosis to occur in the parental cell line as described in section 6.2.

Both the stable siRNA expressing cell lines, RU6A and GU6B, as well as the parental cell line NIH 3T3 were cultured in 6 well plates as described in section 2.13.3. The cells were treated with 25 $\mu\text{g/ml}$ camptothecin for 24 hours. At the indicated time point, cells were removed from the wells and prepared for cell cycle analysis as described in section 2.17 using the PI solution. The cells were analyzed using FACS analysis as described in section 2.15. The collected data was analyzed using the FlowJo v8.5.3 software (Tree Star Inc.).

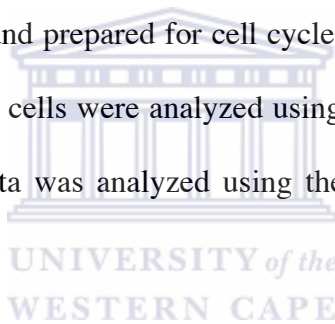


Figure 7.6 shows the FACS result for the NIH 3T3 cell line compared to that for RU6A and GU6B before and after the induction of apoptosis. The FACS data was analyzed and presented as a bar graph plotting the mean \pm SD. From figure 7.6 the parental NIH 3T3 cell line shows a pronounced sub G1 apoptotic population of approximately 60 %. The existence of a clearly defined G1 and G2/M phases are absent with less than 50 % of the cells distributed between the phases. Cells exiting the S phase appear to undergo apoptosis since there is almost a complete lack of the G2/M phase.

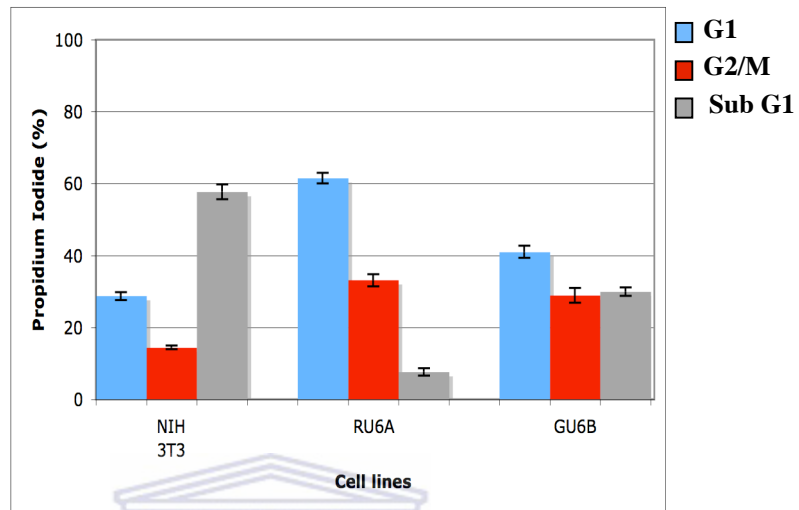
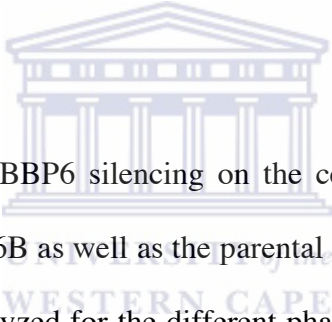


Figure. 7.6 Represent the cell cycle results measured on a FACS instrument following camptothecin-induced apoptosis.

The NIH 3T3, RU6A and GU6B cell lines were cultured and apoptosis induced with 25 µg/ml camptothecin and at the 24 hour time point, the cells were analyzed for the different stages of the cell cycle using the Propidium iodide solution on a FACS instrument. The data was analyzed and represented as the mean ± SD. The data were analyzed for independent repeats of the experiment.

The GU6B cell line shows an apoptotic population similar to that of the parental cell, yet there is a distinguishable G1 and G2/M phase with a higher proportion of cells in the G1 phase. The RU6A cells, shows a significantly lower apoptotic population with the G1 phase still showing a higher concentration of cells. A higher proportion of the RU6A cell population remains restricted in the G1 phase with fewer cells undergoing apoptosis compared to the parental cell line as well as RU6B. These observations are consistent with those made in the previous chapter, that RU6A cells are more resistant to apoptosis induced by camptothecin than GU6B.

7.3 Summary



In this chapter the effect of RBBP6 silencing on the cell cycle was investigated. The stable cell lines RU6A and GU6B as well as the parental cell line NIH 3T3 were cultured and at selected time points analyzed for the different phases of the cell cycle. Cells were analyzed following Propidium iodide staining on a FACS instrument.

At the 12-hour time point the G1 population in RU6A and GU6B were significantly higher than the same population in the NIH 3T3 cells. An approximate difference of 20 % was calculated between the RBBP6 negative cell lines and the NIH 3T3 cell line. At the 18-hour time point, RU6A and GU6B still had higher proportion of cells in the G1 phase compared to the NIH 3T3 cell line, however the G1 phase of RU6A had a 16 % higher proportion of cells compared to the same phase in GU6B. However at the 24 and 48-hour time points the difference was absent. The G1 population for RU6A and GU6B showed

an equal proportion of cells, which is still higher than that for the NIH 3T3 cells. The difference between RU6A and GU6B might be contributed to the efficacy of the different siRNA oligonucleotides. From chapter 5.3.3 the expression of RBBP6 in the RU6A cell line was shown to be lower than its expression in GU6B using qRT-PCR.

The different cell lines were also treated with camptothecin for 24 hours, after which they were analyzed for the different phases of the cell cycle. The highest population of apoptotic cells was observed in the NIH 3T3 cells. The GU6B cell line showed an apoptotic population similar to that of the parental cell line. However, the GU6B cell line showed distinct distribution of cells throughout the different phases of the cell cycle with a high proportion of cells in G1. The NIH 3T3 cells showed no discernable phases with most of the cells in the sub G1 (apoptotic) population. RU6A showed a relatively small apoptotic population compared to both NIH 3T3 and GU6B. The G1 phase is still very pronounced in this cell line. The results from this chapter shows deficiency in RBBP6 results in cells being restricted in the G1 phase of the cell cycle and are consistent with observations by Gao and Scott, 2002, Li *et al.*, 2007.

CHAPTER 8: GENERAL DISCUSSION

- 8.1 INTRODUCTION
- 8.2 EXPRESSION ANALYSIS OF THE RBBP6 PROMOTERS IN CELL CULTURE (CHAPTER THREE)
- 8.3 INTERFERENCE RNA- CONSTRUCTION OF MOUSE RBBP6 siRNA VECTORS (CHAPTER FOUR)
- 8.4 INTERFERENCE RNA- TESTING THE EFFECT OF siRNA CONSTRUCTS ON THE EXPRESSION OF RBBP6 (CHAPTER FIVE)
- 8.5 THE EFFECT OF RBBP6 SILENCING ON APOPTOSIS (CHAPTER SIX)
- 8.6 THE EFFECT OF RBBP6 SILENCING ON THE CELL CYCLE (CHAPTER SEVEN)
- 8.7 CONCLUSION
- 8.8 FUTURE WORK



CHAPTER 8: GENERAL DISCUSSION

8.1 Introduction

An investigation using promoter-trapping technology led to the identification of a novel hamster gene homologous to the human cDNA 21c4 (Genbank:T25012) (Frigerio *et al.*, 1995). This cDNA was completely sequenced and shown to be a 0.9 kb cDNA clone encoding a 118 amino acid protein (Rees *et al.*, unpublished). The corresponding gene was found to be located on human chromosome 16p12.2, upstream of the previously identified RBBP6/PACT/P2P-R gene. Analysis of cDNA sequences showed that the sequence coded for the previously unidentified N-terminus of the RBBP6 protein (Dlamini *et al.*, in prep), which were named the DWNN domain.

RBBP6 has been shown to suppress the binding of p53 to DNA, (Sakai *et al.*, 1995) and to block the binding of the adenovirus E1A protein to Rb (Witte and Scott, 1997, Simons *et al.*, 1997) suggesting that the interactions with both tumour suppressor proteins are biologically relevant. RBBP6 strongly localizes to chromosomes during mitosis and to nuclear speckles, which are believed to be the main sites of activity for pre-mRNA splicing and processing, during interphase (Gao *et al.*, 2002, Yoshitake *et al.*, 2004). Over-expression of P2P-R has been shown to lead to cell cycle arrest and apoptosis (Gao and Scott, 2002, Gao and Scott, 2003). The yeast homologue, Mpe1p, forms part of the Yeast Cleavage and Polyadenylation Factor and is essential for the specific cleavage and polyadenylation of pre-mRNA (Vo *et al.*, 2001).

Yoshitake *et al.* (2004) reported that RBBP6 is strongly up regulated in oesophageal cancer cells, and high levels of expression correlate with higher rates of proliferation in cultured oesophageal cancer cell and low survival rates in cancer patients. Cytotoxic T cells specific for RBBP6-derived peptides were able to lyse oesophageal cancer cells in culture, and to produce regression of oesophageal tumours in mice xenograft models.

Furthermore, since p53 and Rb have both been shown to bind to mammalian RBBP6, it is possible that RBBP6 plays a role in the regulation of these two proteins similar to that played by MDM2 (Hsieh *et al.*, 1999) suggesting a possible model for the integration of the regulation of transcription, cell cycle control and apoptosis. Given the fact that the DWNN domain can be independently expressed in vertebrates, an interesting possibility is that the function of RBBP6 is to DWNNylate other proteins.

Pugh *et al.* (2006), using NMR structural analysis showed that DWNN is a novel ubiquitin-like domain found only at the N-terminus of the RBBP6 family of splicing-associated proteins. They proposed that the ubiquitin-like structure of the domain greatly increases the likelihood that RBBP6 functions through some form of ubiquitin-like modification. Furthermore, the fact that the DWNN domain is independently expressed in higher vertebrates implies that the domain may itself function as a novel ubiquitin-like modifier of other proteins.

Li *et al.* (2007), demonstrated that the disruption of PACT in mice leads to early embryonic lethality before embryonic day 7.5 (E7.5), accompanied by an accumulation

of p53 and widespread apoptosis. This lethality can be partially rescued by p53-null and thus prolonged survival to E11.5. They also showed that endogenous PACT could interact with Hdm2 and enhance Hdm2-mediated ubiquitination and degradation of p53 as a result of the increase of the p53-Hdm2 affinity. Consequently, PACT represses p53-dependent gene transcription. Knockdown of PACT significantly attenuates the p53-Hdm2 interaction, reduces p53 poly-ubiquitination, and enhances p53 accumulation, leading to both apoptosis and cell growth retardation. Taken together, their data demonstrate that the PACT-p53 interaction plays a critical role in embryonic development and tumorigenesis and identifies PACT as a member of negative regulators of p53.



The aim of this thesis was investigate the effect of RBBP6 silencing on apoptosis and the cell cycle using RNAi technology and to better understand the existence of two promoters for the RBBP6 gene.

8.2 Expression analysis of the RBBP6 promoters in cell culture (Chapter three)

Genetic analysis of the RBBP6 gene showed the presence of two promoters responsible for the expression of the different transcripts of the gene. The promoters were designated Promoter 0 (P0) and Promoter P1 (P1). To better understand the existence of two promoters for the RBBP6 gene the Enhanced Green Fluorescent Protein (EGFP) and the Red Fluorescent Protein (DsRed1) were placed under the transcriptional control of P0 and P1 respectively. Using a combination of fluorescence microscopy, FACS analysis and Real-Time qRT-PCR, the activity of P0 appeared to be higher than that of P1 in the

Hek 293T cell line. However, following the induction of apoptosis using camptothecin, the transcriptional activity of both promoters increased. The increase in P1 activity was marginal compared to the increase in P0 activity. From the results it can thus be suggested that the activity of the two promoters can be increased under certain cellular conditions.

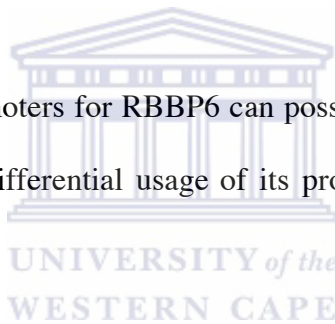
The presence of two promoters for one gene is not unique. The differential usage of dual promoters has been described for several of the *Ly-49* genes (Saleh *et al.*, 2002). The Ly49A NK cell receptor interacts with MHC class I molecules on target cells and negatively regulates NK cell-mediated target cell lysis. The distal promoter of some Ly-49 genes was shown to have promoter activity in fetal cells and in bone marrow cells, possibly linking its usage to the initiation of *Ly-49* expression in NK cells (Saleh *et al.*, 2002). In addition, the mouse *NKR-P1C* gene has also recently been shown to have a novel upstream non-coding exon that is differentially used during NK cell development, as well as a DNase I HSS (hypersensitive site) upstream of the gene (Ljusic *et al.*, 2003).

Studies have also indicated that in dual promoter systems the activity of the one promoter can control the activity of the other one during preferential promoter usage (Wilhelm *et al.*, 2003, Dobbelstein *et al.*, 2005). The p73 protein is one of two homologues of the tumour suppressor p53, it is expressed in different isoforms as a result of differential promoter usage and alternative splicing (Yang and McKeon, 2000). Like p53, p73 has been implicated in apoptosis (Jost *et al.*, 1997). In contrast with p53 however, the p73 gene has two distinct promoters coding for two protein isoforms with opposite effects.

These isoforms contain a transactivation domain at their amino terminal ends and they are collectively termed TAp73, while the transactivation proficient TAp73 shows pro-apoptotic effects, the amino-terminal-deleted DeltaNp73 has an anti-apoptotic function. Indeed, the relative expression of these two proteins is related to the prognosis of several cancers (Dobbelstein *et al.*, 2005).

TAp73 is able to transactivate its own second promoter, thus inducing the expression of the anti-apoptotic DeltaNp73 isoform. Therefore, the balance between TAp73 and DeltaNp73 finely regulates cellular sensitivity to death (Dobbelstein *et al.*, 2005).

Thus the presence of two promoters for RBBP6 can possibly be an indication of various functions for the gene, with differential usage of its promoters under different cellular conditions.

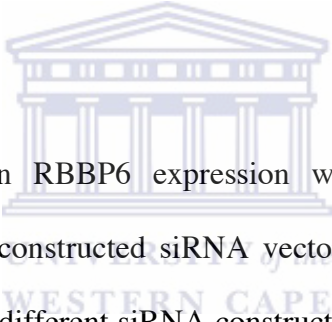


8.3 Interference RNA – Construction of mouse RBBP6 siRNA vectors. (Chapter four)

The aim of this chapter was to construct several siRNA vectors to target the DWNN gene. The U6 and H1 promoters were used to drive the expression of the silencing siRNAs. Both RNA Polymerase III promoters U6 and H1 were PCR amplified and cloned into pGEM[®]-T Easy as well as into pEGFP-C1 and pDsRed-C1. However, the multiple cloning site region of pEGFP-C1 and pDsred-C1 was deleted, as its presence will interfere with the cloning of the siRNA oligonucleotides downstream of U6 and H1.

Two siRNA oligonucleotides were identified with the iRNAi version 1.0 oligonucleotide prediction software (<http://mekentosj.com/irnai>) using the full-length annotated mouse RBBP6 nucleotide sequence as input data. Two distinct siRNA oligonucleotides were identified targeting different regions of the mouse RBBP6 gene, which were designated DWNN-A and DWNN-B respectively. The identified siRNA oligonucleotides were subsequently cloned in the different U6 and H1 vectors with sequence analysis revealing the correct nucleotide sequences for all the siRNA vectors constructed.

8.4 Interference RNA – Testing the effect of the siRNA constructs on the expression of RBBP6 (Chapter five)



In this chapter the effect on RBBP6 expression was investigated following the transfection of the previously constructed siRNA vectors. Firstly NIH 3T3 cells were transiently transfected with the different siRNA constructs. Fluorescence microscopy and Real-Time qRT-PCR were used to evaluate the effect on RBBP6 expression.

From the fluorescence microscopy data differences were observed resulting from the effect of the different siRNA constructs. The DWNN-A siRNA appeared to be slightly more effective than the DWNN-B siRNA. This observation was consistent with the data obtained for Real-Time qRT-PCR. The difference was slight, approximately 3 %, and can possibly not be considered significant.

It is important to consider that transfection rates in culture vary considerably and can be quite low, particularly with primary cells. For example, if the transfection efficiency is only 50 %, then the maximum effect one could detect with a highly efficient siRNA could be $\leq 2x$. Therefore knowledge about the transformation efficiency of a particular cell type is paramount if the data is to be interpretable. For this reason different transfection reagents were tested to achieve the highest efficiency in the NIH 3T3 cell line. The Metafectene™ transfection reagent showed the highest efficiency in the NIH 3T3 cell line using the pEGFP-C1 vector as control.

Another approach to validating the effectiveness of a siRNAs is to quantify the level of the target protein. For this reason Real-Time qRT-PCR was used, to determine the level of RBBP6 expression. Because siRNAs target mRNAs, and not proteins, the maximal effect on the level of protein expression will occur after the preexisting pool of protein has undergone its normal decay. Transfection of dividing cells with siRNAs exerts only a transient effect, with maximal mRNA knockdown occurring somewhere between days 1-4 after transfection, depending on the cell type, and then gradually attenuating (Cullen, 2006). Therefore, long-lived proteins may show only a modest knockdown using methods like Western blots even if the RNAi effect at the mRNA level is readily detectable. Since the protein turnover of RBBP6 at this point is not known, Real-Time qRT-PCR was seen as the most effective method in quantifying the level of knockdown.

Two stable cell lines, 3T3 GU6B and RU6A were also established. Both cell lines showed significant decreases in expression of RBBP6 as measured by fluorescence

microscopy and Real-Time qRT-PCR. However, a greater decrease was observed in the RU6A cell line suggested a more potent silencing effect exerted by the DWNN-A siRNA.

8.5 The effect of RBBP6 silencing on Apoptosis. (Chapter six)

In this chapter the effect of RBBP6 silencing was investigated using the stable cell lines RU6A and GU6B. Camptothecin was used to induce apoptosis over a 24-hour period and the percentage cell death measured using different assays that evaluate the process at its various stages.

Both the Annexin V-PE and APOPercentage™ assays showed that the stable cell lines were significantly resistant to apoptosis compared to the parental NIH 3T3 cell line. The RU6A cell line showed a slightly higher resistance to apoptosis compared to GU6B and this can possibly relate to the difference observed in the silencing potency mediated by the different siRNA oligonucleotides. Furthermore, the RBBP6 cDNA construct, DWNN-200, was transfected back into the stable cell lines, restoring their sensitivity to camptothecin-induced apoptosis.

The DWNN-200 construct was also over-expressed in the NIH 3T3 cell line and this caused an increase in apoptosis as assayed with the TUNEL assay. A linear increase in the cDNA construct concentration transfected showed an increase in apoptosis in the NIH 3T3 cell line.

Next, the effect on p53 expression was investigated. In the parental NIH 3T3 cell line, no effect was observed on p53 expression before and after camptothecin-induced apoptosis. This results was also observed following RBBP6 over-expression and induction of apoptosis mediated by camptothecin. However, in the RU6A cell line, an increase was observed in p53 expression before the induction of apoptosis whilst the expression decreased following induction of apoptosis.

Finally, a possible intrinsic route of apoptosis was investigated involving RBBP6 by evaluating the expression of Bax (pro-apoptotic)/Bcl-2 (anti-apoptotic). The expression ratio of both genes had been implicated in the intrinsic route of apoptosis (Reed, 1997). In the resting (un-induced) NIH 3T3 cell line the expression ratio of Bax/Bcl-2 was equal. This observation was consistent with the “rheostat” model, that the relative ratio of expression between Bcl-2/Bax is responsible for regulation of apoptosis (Kroemer, 1997). This ratio however changes following camptothecin-induced apoptosis. In the NIH 3T3 cell line, following apoptosis, the expression level of Bax is slightly lower than that of Bcl-2. In the RU6A cell line the expression of Bcl-2 is much higher than Bax, whereas both genes shows an increased expression in the RBBP6 negative line, RU6A, compared to the NIH 3T3 cell line. This difference increases further following induction of apoptosis. These observations are consistent with the apoptosis resistant phenotype of the RU6A cell line. Also the study by Li *et al.* (2007) showed an increase in Bax expression in PACT^{-/-} embryos.

How does the current study compare to results observed by other groups? RBBP6 is clearly implicated in apoptosis. Gao and Scott, 2003, showed that over-expression of the p53-binding domain, promotes camptothecin-induced apoptosis, whilst Li *et al.*, 2007, showed by targeting the same domain using homologous recombination that apoptosis is promoted. The current study showed targeting RBBP6 using RNAi technology results in cells, which show increased resistance to apoptosis induced by camptothecin.

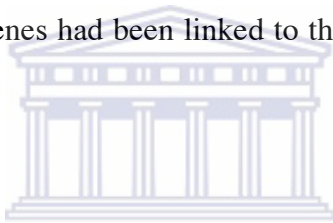
The inconsistencies between the different studies can be a consequence of the different methods used to study RBBP6 function. In the Gao and Scott (2003) study the expressed protein lacked residues 1 to 199, which includes the DWNN domain (residues 1-118) (see figure 1.11). The results observed might be a consequence of the absence of these residues, since protein function are dependent on its proper folding of all participating domains. The absence of these amino acids could result in improper folding and a truncated protein.

Li *et al.* (2007) targeted exons 12 and 13 of the PACT gene, replacing it with a neomycin resistance cassette. Although not indicated by their study, other domains might have retained their functionality since null alleles are more likely to be generated by deleting or recombining a selection cassette into more 5' exons rather than exons that encode the C-terminus of the protein, since under these circumstances minimal portions of the wild-type polypeptide would be made.

In the current study RNAi was used to target the expression of RBBP6. This method is not without its drawbacks. Protein expression is not completely suppressed that it can be considered a null mutation. Since the results showed an average “knock-down” of 95 % in the stable cell lines, there is still residual protein present in the cell. Thus the results from each study should be interpreted on the merits of the different techniques used. Notwithstanding these discrepancies the involvement of RBBP6 in apoptosis cannot be denied.

What is the possible mechanism of RBBP6 involvement in apoptosis? Many forms of apoptosis are mediated by transcription-dependant mechanisms (Haupt *et al.*, 1997, Ding *et al.*, 2000). Over-expression of P2P-R promoted mitotic apoptosis (Gao and Scott, 2002), which had to be independent of transcription because essentially all transcriptional activity is suppressed in mitotic cells (Salem *et al.*, 1998). However, p53 and other factors might influence mitotic apoptosis by other mechanisms. From the study of Li *et al.*, PACT inhibits the transcriptional activity of p53. Knockdown of PACT in U206 cells increased p53 transcriptional activity, indicating that endogenous PACT negatively regulates p53. Furthermore, a slight increase in p53 expression was observed in PACT^{-/-} embryos using RT-PCR, which is consistent with the observation that PACT affects the rate and/or stabilizes the p53 protein. A similar increase in p53 expression was observed in the current study in the RU6A (RBBP6 negative) cell line. Also an increase in p21 and Bax was observed in PACT^{-/-} embryos (Li *et al.*, 2007), demonstrating that PACT can inhibit the transcriptional activity of p53 and p53 targeted genes. A similar increase in Bax expression was seen in the current study.

Which route of apoptosis is possible affected by the activity of RBBP6? Since cellular apoptosis seems to ultimately target the mitochondria (Finkel, 2001) the possibility exists that the RBBP6 protein might localize in the mitochondria to facilitate apoptosis with the association of p53, since p53 can also show mitochondrial localization (Marchenko *et al.*, 2000). In this regard, small P2P-R spots were observed in the cytoplasm in mitotic cells that could represent mitochondria (Gao and Scott, 2002). In the current study further evidence was provided for a possible intrinsic route of apoptosis. The expression ratio of bcl-2 and bax showed an increase in the RU6A (RBBP6 negative cell line), which showed an additional increase following the induction of apoptosis. The activation and increased expression of both genes had been linked to the intrinsic pathway of apoptosis (Reed, 1994).



Gao and Scott, 2002, also showed the localization of P2P-R in apoptotic cell surface blebs, suggesting that RBBP6 promotes apoptosis by the activation of the apoptotic pathway that originates from the cell surface (extrinsic pathway) and might influence the sub-plasmalemmal aggregation of the Fas death receptors that leads to the activation of the associated caspases (Strasser *et al.*, 2000).

8.6 The effect of RBBP6 silencing on the cell cycle. (Chapter seven)

In this chapter it was observed that RBBP6 deficient cells are restricted in the G1 phase with a higher proportion of the RU6A cells in G1 compared to GU6B. In this study the full-length mouse RBBP6 gene was targeted using the RNAi gene targeting technology.

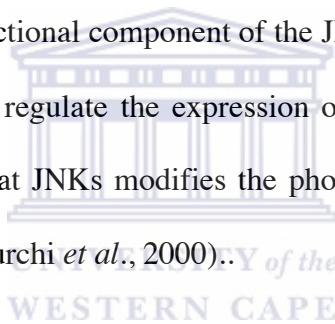
RBBP6 binds to both the p53 and Rb tumour suppressors (Witte and Scott, 2002, Simons *et al.*, 1997). Since both p53 and Rb are key regulators of the cell cycle, the possibility exist that in a RBBP6 negative cell regulatory control of the cell cycle will be absent causing the cell to be restricted in the cell cycle. The observation that p53 activity is controlled by RBBP6 (Li *et al.*, 2007), raises the possibility that this regulatory control also extents to Rb. From this study it was similarly shown that the targeting of RBBP6 in the U203 cell line, resulting in cell growth suppression in a p53 dependant manner. In the H1266 (p53 negative cell line) RBBP6 deficiency showed no suppression of cell growth.

What possible mechanisms might influence cell cycle control mediated by RBBP6? Gao and Scott (2002) suggested that adequate levels of the RBBP6 protein must be present in cells to progress from G1 through S to mitosis efficiently via the induction of AP1-and JNK-dependant pathways. RBBP6 could have one or more roles in the AP1 and JNK-dependant signaling pathways. The protein could be required to facilitate the expression of AP1 factors and/or JNKs via effects on RNA metabolism. This mechanism could possibly be based on evidence that the RBBP6 protein is an RNA binding protein (Witte and Scott, 1997) furthermore it localizes to the nucleolus in interphase mammalian cells (Gao *et al.*, 2002).

RBBP6 might also influence the stability and localization of AP1 factors. This is plausible since the protein shares characteristics with type A hnRNP proteins ((Mino *et al.*, 1989) which are known to function as chaperones and nuclear transport proteins (Shahied *et al.*, 2001). The protein might similarly be involved in AP1 signaling via

effects on the serum response factor and its interactions with the serum response element. This possibility is implicated by the fact that terminally differentiated and senescent cells that are deficient in RBBP6 show repression in the inducible expression of some AP1 factors because of the nuclear exclusion of the serum response factors that prevents its binding to and activation of the serum response element (Ding *et al.*, 2001). Terminally differentiated and senescent cells, that has loss the ability to induce AP1 factors and that shows a deficiency in expression of P2P-R, lacks the ability to progress through the cell cycle (Witte and Scott, 1997, Scott and Witte, 1992).

Finally, RBBP6 could be a functional component of the JNK activation system. Chen and Tan, 2000, showed that JNKs regulate the expression of multiple transcription factors, whilst other studies showed that JNKs modifies the phosphorylation of c-Jun and other proteins (Catani *et al.*, 2001, Turchi *et al.*, 2000).



8.7 Conclusion

In this study the RNAi gene targeting strategy was used to explore the physiological function of the DWNN protein. Furthermore the existence of two promoters for the gene was also investigated.

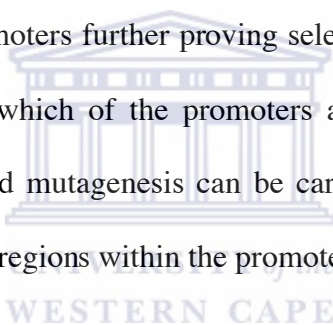
In an attempt to investigate the role played by the RBBP6 gene, several experiments have been undertaken and the following conclusions were drawn:

- (a) The activity of P0 appears to be stronger than that of P1, also the activity of P0 is increased following the induction of apoptosis as induced by camptothecin.
- (b) Gene targeting by interference RNA (RNAi) proved to be fast and efficient method in producing RBBP6 'knock out' cell lines.
- (c) Using different siRNA oligonucleotides to target the same gene can have different silencing effects on a gene. As was shown in this study the DWNN A-siRNA had a more potent silencing effect compared to the DWNN B-siRNA.
- (d) Silencing the RBBP6 using RNAi renders cells resistant to apoptosis induced by camptothecin. Also over-expression of RBBP6 promotes camptothecin-induced apoptosis.
- (e) The induction of apoptosis as mediated by RBBP6 is dependent of p53.
- (f) Apoptosis mediated by RBBP6 follows a possible intrinsic route suggested by the change in expression of Bcl-2 and Bax in the RU6A cell line.
- (g) Finally, silencing of the RBBP6 gene causes G1 arrest suggesting a possible

role in the cell cycle.

8.8 Future work

The presence of two promoters for one gene is not uncommon in any genome yet it is not the norm. To investigate this phenomenon further, the existing constructs can be used to study the effect of other physiological stresses like DNA damage induced by UV light. This would shed more light on the selective promoter activity under different cellular conditions. Since this thesis showed the efficiency of RNAi, siRNA oligonucleotides can be designed to target both promoters further proving selective activity of each promoter. Once it has been established which of the promoters are more active under different cellular conditions, site-directed mutagenesis can be carried out on specific residues to establish the crucial regulatory regions within the promoters responsible for its activity.



In terms of RBBP6 involvement in apoptosis new biological systems need to be developed wherein cells can be induced to over-express full-length RBBP6 under the control of a promoter that can be regulated or induced. This would make it possible to better define the kinetics and mechanisms by which native RBBP6 influences apoptosis and mitosis. The possibility that RBBP6 interacts with other mitotic regulatory factors needs to be evaluated by immunoprecipitation and confocal co-localization studies.

Also the role of RBBP6 in the cell cycle needs to be fully established. Interaction between the protein and regulators of the cell cycle should be established and the role of

RBBP6 in the AP1 and JNK pathways proven. Finally, correlations need to be established between human carcinogenesis and the molecular characteristics of RBBP6.



REFERENCES

Abbas, AK, Lichtman, AH and Pober, JS. (1997) Cellular and Molecular Immunology. third edition. WB Saunders Company.

Adams JM and Cory S. (1998) The Bcl-2 protein family: arbiters of cell survival. *Science*. **281**: 1322-1326.

Agrawal N, Dasaradhi PV, Mohammed A, Malhotra P, Bhatnagar RK, Mukherjee SK. (2003) RNA interference: biology, mechanism, and applications. *Microbiol Mol Biol Rev*. **67**: 657-85.

Albert TK, Lemaire M, van Berkum NL, Gentz R, Collart MA, Timmers HT. (2000) Isolation and characterization of human orthologs of yeast CCR4-NOT complex subunits. *Nucleic Acids Res*. **28**: 809-817.

Albert TK, Hanzawa H, Legtenberg YI, de Ruwe MJ, van den Heuvel FA, Collart MA, Boelens R, Timmers HT. (2002) Identification of a ubiquitin-protein ligase subunit within the CCR4-NOT transcription repressor complex. *Embo J*. **21**: 355-364.

Alnemri ES, Livingston DJ, Nicholson DW, Salvesen G, Thornberry NA, Wong WW, Yuan J. (1996) Human ICE/CED-3 protease nomenclature. *Cell*. **87**: 171-175.

Altschul SF, Gish W, Miller W, Myers EW, Lipman DJ. (1990) Basic local alignment search tool. *J Mol Biol.* **215**: 403-410.

Amano K, Furuno T, Nakanishi M. (2006) Conditioned medium from feeder STO cells increases the attachment of mouse embryonic stem cells. *Biol Pharm Bull.* **29**: 1747-50.

Amarzguioui M, Rossi JJ, Kim D. (2005) Approaches for chemically synthesized siRNA and vector-mediated RNAi. *FEBS Lett.* **579**: 5974-81.

Anantharaman V, Koonin EV, Aravind L. (2002) Comparative genomics and evolution of proteins involved in RNA metabolism. *Nucleic Acids Res.* **30**: 1427–1464.

Applebaum J, Shimon H, Sela BA, Belmaker RH, Levine J. (2004) Homocysteine levels in newly admitted schizophrenic patients. *J Psychiatr Res.* **38**: 413-416.

Aravind L and Koonin EV. (2000) The U box is a modified RING finger - a common domain in ubiquitination. *Curr Biol.* **10**: R132-134.

Ashkenazi A and Dixit VM. (1998) Death receptors: signaling and modulation. *Science.* **281**: 1305-1308.

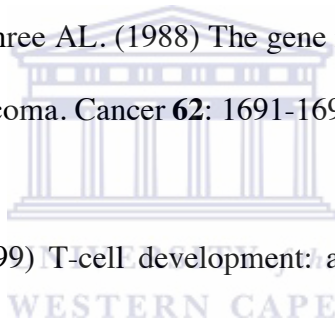
Baldin V, Lukas J, Marcote MJ, Pagano M, Draetta G. (1993) Cyclin D1 is a nuclear protein required for cell cycle progression in G1. *Genes Dev* **7**: 812-821.

Bass BL. (2000) Double-stranded RNA as a template for gene silencing. *Cell* **101**: 235-238.

Bates S and Vousden KH. (1999) Mechanisms of p53-mediated apoptosis. *Cell Mol Life Sci.* **55**: 28-37.

Baulcombe D. (1999) Viruses and gene silencing in plants. *Arch Virol Suppl.* **15**: 189-201.

Benedict WF, Fung YK, Murphree AL. (1988) The gene responsible for the development of retinoblastoma and osteosarcoma. *Cancer* **62**: 1691-1694.



Benoist C and Mathis D. (1999) T-cell development: a new marker of differentiation state. *Curr Biol.* **9**: 59-61.

Bernstein E, Caudy AA, Hammond SM, Hannon GJ. (2001) Role for a bidentate ribonuclease in the initiation step of RNA interference. *Nature.* **409**: 363-366.

Bertrand JR, Pottier M, Vekris A, Opolon P, Maksimenko A, Malvy C. (2002) Comparison of antisense oligonucleotides and siRNAs in cell culture and *in vivo*. *Biochem Biophys Res Commun.* **296**: 1000-1004.

Birnboim HC and Doly J. (1979) A rapid alkaline extraction procedure for screening recombinant plasmid DNA. *Nucleic Acids Res.* **7**: 1513-1523.

Bitko V and Barik S. (2001) Phenotypic silencing of cytoplasmic genes using sequence-specific double-stranded short interfering RNA and its application in the reverse genetics of wild type negative-strand RNA viruses. *BMC Microbiol.* **1**: 34-41.

Blaszczyk J, Tropea JE, Bubunenko M, Routzahn KM, Waugh DS, Court DL, Ji X. (2001) Crystallographic and modeling studies of RNase III suggest a mechanism for double-stranded RNA cleavage. *Structure.* **9**: 1225-1236.

Bosher JM, Dufourcq P, Sookhareea S, Labouesse M. (1999) RNA interference can target pre-mRNA: consequences for gene expression in a *Caenorhabditis elegans* operon. *Genetics.* **153**: 1245-1256.

Braciale TJ, Morrison LA, Sweetser MT, Sambrook J, Gething MJ, Braciale VL. (1987) Antigen presentation pathways to class I and class II MHC-restricted T lymphocytes. *Immunol Rev.* **98**: 95-114.

Bradley A and Robertson E. (1986) Embryo-derived stem cells: a tool for elucidating the developmental genetics of the mouse. *Curr Top Dev Biol.* **20**: 357-371.

Breitschopf K, Bengal E, Ziv T, Admon A, Ciechanover A. (1998) A novel site for ubiquitination: the N-terminal residue, and not internal lysines of MyoD, is essential for conjugation and degradation of the protein. *EMBO J.* **17**: 5964-5973.

Caplen NJ, Zheng Z, Falgout B, Morgan RA. (2002) Inhibition of viral gene expression and replication in mosquito cells by dsRNA-triggered RNA interference. *Mol Ther.* **6**: 243-251.

Carmell MA and Hannon GJ. RNase III enzymes and the initiation of gene silencing. *Nat Struct Mol Biol.* **11**: 214-8.

Carr AM. (2000) Cell cycle. Piecing together the p53 puzzle. *Science.* **287**: 1765-1766.

Casadaban MJ and Cohen SN. (1980) Analysis of gene control signals by DNA fusion and cloning in *Escherichia coli*. *J Mol Biol.* **138**: 179-207.

Casciola-Rosen L, Nicholson DW, Chong T, Rowan KR, Thornberry NA, Miller DK, Rosen A. (1996) Apopain/CPP32 cleaves proteins that are essential for cellular repair: a fundamental principle of apoptotic death. *J Exp Med.* **183**: 1957-64.

Catani MV, Rossi A, Costanzo A, Sabatini S, Levrero M, Melino G, Avigliano L. (2001) Induction of gene expression via activator protein-1 in the ascorbate protection against UV-induced damage. *Biochem J.* **356**: 77-85.

Chang C, Simmons DT, Martin MA, Mora PT. (1979) Identification and partial characterization of new antigens from simian virus 40-transformed mouse cells. *J Virol.* **31**: 463-471.

Chavez-Reyes A, Parant JM, Amelse LL, de Oca Luna RM, Korsmeyer SJ, Lozano G. (2003) Switching mechanisms of cell death in mdm2- and mdm4-null mice by deletion of p53 downstream targets. *Cancer Res.* **63**: 8664-8669.

Chen SM, Takiff HE, Barber AM, Dubois GC, Bardwell JC, Court DL. (1990) Expression and characterization of RNase III and Era proteins: Products of the rnc operon of *Escherichia coli*. *J Biol Chem.* **265**: 2888-2895.

Chen YR and Tan TH. (2000) The c-Jun N-terminal kinase pathway and apoptotic signaling (review). *Int J Oncol.* **16**: 651-62.

Chinnaiyan AM, O'Rourke K, Tewari M, Dixit VM. (1995) FADD, a novel death domain-containing protein, interacts with the death domain of Fas and initiates apoptosis. *Cell.* **81**: 505-512.

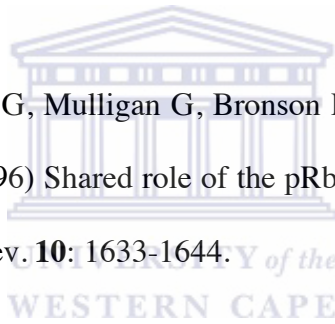
Choo Y and Klug A. (1997) Physical basis of a protein-DNA recognition code. *Curr Opin Struct Biol.* **7**: 117-125.

Chung S, Andersson T, Sonntag KC, Björklund L, Isacson O, Kim KS. (2002) Analysis of different promoter systems for efficient transgene expression in mouse embryonic stem cell lines. *Stem Cells*. **20**: 139-45.

Clancy, J. (1998) *Basic concepts in Immunology*. McGraw-Hill Companies. pp 1-11.

Clarke R, Smith AD, Jobst KA, Refsum H, Sutton L, Ueland PM. (1998) Folate, vitamin B12, and serum total homocysteine levels in confirmed Alzheimer disease. *Arch Neurol* **55**: 1449-1455.

Cobrinik D, Lee MH, Hannon G, Mulligan G, Bronson RT, Dyson N, Harlow E, Beach D, Weinberg RA, Jacks T. (1996) Shared role of the pRb-related p130 and p107 proteins in limb development. *Genes Dev*. **10**: 1633-1644.



Coburn GA and Cullen BR. (2002) Potent and specific inhibition of human immunodeficiency virus type 1 replication by RNA interference. *J Virol*. **76**: 9225-9231.

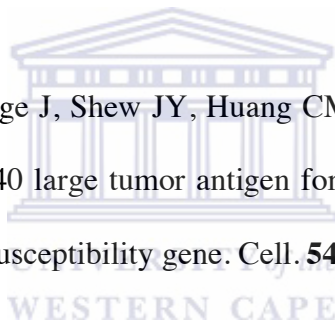
Cohen SN, Chang AC, Hsu L. (1972) Non-chromosomal antibiotic resistance in bacteria: genetic transformation of *Escherichia coli* by R-factor DNA. *Proc Natl Acad Sci U S A*. **69**: 2110-4.

Crowe PD, Van Arsdale TL, Walter BN, Ware CF, Hession C, Ehrenfels B, Browning JL, Din WS, Goodwin RG, Smith CA. (1994) A lymphotoxin-beta-specific receptor. *Science*. **264**: 707-710.

Cullen BR. (2006) Enhancing and confirming the specificity of RNAi experiments. *Nat Methods*. **3**: 677-81.

Darmon AJ, Nicholson DW, Bleackley RC. (1995) Activation of the apoptotic protease CPP32 by cytotoxic T-cell-derived granzyme B. *Nature*. **377**: 446-448.

DeCaprio JA, Ludlow JW, Figge J, Shew JY, Huang CM, Lee WH, Marsilio E, Paucha E, Livingston DM. (1988) SV40 large tumor antigen forms a specific complex with the product of the retinoblastoma susceptibility gene. *Cell*. **54**: 275-283.



del Peso L, Gonzalez VM, Nunez G. (1998) *Caenorhabditis elegans* EGL-1 disrupts the interaction of CED-9 with CED-4 and promotes CED-3 activation. *J Biol Chem*. **273**: 33495-33500.

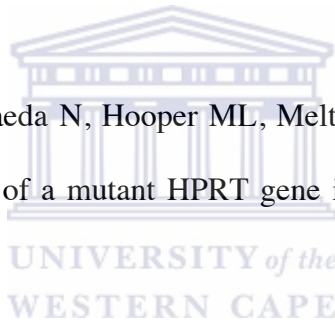
DeLeo AB, Jay G, Appella E, Dubois GC, Law LW, Old LJ. (1979) Detection of a transformation-related antigen in chemically induced sarcomas and other transformed cells of the mouse. *Proc Natl Acad Sci U S A*. **76**: 2420-2424.

Ding HF, Lin YL, McGill G, Juo P, Zhu H, Blenis J, Yuan J, Fisher DE. (2000) Essential role for caspase-8 in transcription-independent apoptosis triggered by p53. *J Biol Chem.* **275**: 38905-11.

Ding W, Gao S, Scott RE. (2001) Senescence represses the nuclear localization of the serum response factor and differentiation regulates its nuclear localization with lineage specificity. *J Cell Sci.* **114**: 1011-8.

Dobbelstein M, Strano S, Roth J, Blandino G. (2005) p73-induced apoptosis: a question of compartments and cooperation. *Biochem Biophys Res Commun.* **331**: 688-693.

Doetschman T, Gregg RG, Maeda N, Hooper ML, Melton DW, Thompson S, Smithies O. (1987) Targeted correction of a mutant HPRT gene in mouse embryonic stem cells. *Nature.* **330**: 576-578.



Dudley NR and Goldstein B. (2003) RNA interference: silencing in the cytoplasm and nucleus. *Curr Opin Mol Ther.* **5**: 113-7.

Dupuis M, Schaerer E, Krause KH, Tschopp J. (1993) The calcium-binding protein calreticulin is a major constituent of lytic granules in cytolytic T lymphocytes. *J Exp Med.* **177**: 1-7.

Durfee T, Mancini MA, Jones D, Elledge SJ, Lee WH. (1994) The amino-terminal region of the retinoblastoma gene product binds a novel nuclear matrix protein that co-localizes to centers for RNA processing. *J Cell Biol.* **127**: 609-622.

Dykxhoorn DM, Novina CD, Sharp PA. (2003) Killing the messenger: short RNAs that silence gene expression. *Nat Rev Mol Cell Biol.* **4**: 457-467.

Dyson N. (1994) pRb, p107 and the regulation of the E2F transcription factor. *J Cell Sci Suppl.* **18**: 81-87.

Dyson N, Howley PM, Munger K, Harlow E. (1989) The human papilloma virus-16 E7 oncoprotein is able to bind to the retinoblastoma gene product. *Science.* **243**: 934-937.

Eikelboom JW, Lonn E, Genest J, Jr., Hankey G, Yusuf S. (1999) Homocyst(e)ine and cardiovascular disease: a critical review of the epidemiologic evidence. *Ann Intern Med.* **131**: 363-375.

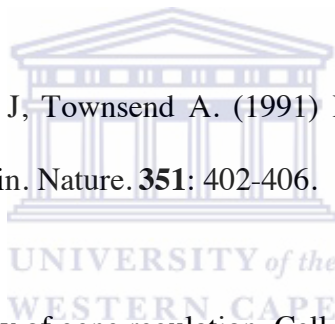
el-Deiry WS, Harper JW, O'Connor PM, Velculescu VE, Canman CE, Jackman J, Pietenpol JA, Burrell M, Hill DE, Wang Y, *et al.* (1994) WAF1/CIP1 is induced in p53-mediated G1 arrest and apoptosis. *Cancer Res.* **54**: 1169-1174.

el-Deiry WS, Tokino T, Velculescu VE, Levy DB, Parsons R, Trent JM, Lin D, Mercer WE, Kinzler KW, Vogelstein B. (1993) WAF1, a potential mediator of p53 tumor suppression. *Cell*. **75**: 817-825.

Ekholm SV and Reed SI (2000) Regulation of G(1) cyclin-dependent kinases in the mammalian cell cycle. *Curr Opin Cell Biol*. **12**: 676-84.

Elbashir SM, Lendeckel W, Tuschl T. (2001) RNA interference is mediated by 21- and 22-nucleotide RNAs. *Genes Dev*. **15**: 188-200.

Elliott T, Cerundolo V, Elvin J, Townsend A. (1991) Peptide-induced conformational change of the class I heavy chain. *Nature*. **351**: 402-406.



Emerson BM. (2002) Specificity of gene regulation. *Cell*. **109**: 267-70.

Evan GI and Vousden KH. (2001) Proliferation, cell cycle and apoptosis in cancer. *Nature*. **411**: 342-8.

Fadok VA, Voelker DR, Campbell PA, Cohen JJ, Bratton DL, Henson PM. (1992) Exposure of phosphatidylserine on the surface of apoptotic lymphocytes triggers specific recognition and removal by macrophages. *J Immunol*. **148**: 2207-2216.

Fairall L, Schwabe JW, Chapman L, Finch JT, Rhodes D. (1993) The crystal structure of a two zinc-finger peptide reveals an extension to the rules for zinc-finger/DNA recognition. *Nature*. **366**: 483-487.

Feil R. (2007) Conditional somatic mutagenesis in the mouse using site-specific recombinases. *Handb Exp Pharmacol*. **178**: 3-28.

Fernandes-Alnemri T, Armstrong RC, Krebs J, Srinivasula SM, Wang L, Bullrich F, Fritz LC, Trapani JA, Tomaselli KJ, Litwack G, Alnemri ES. (1996) In vitro activation of CPP32 and Mch3 by Mch4, a novel human apoptotic cysteine protease containing two FADD-like domains. *Proc Natl Acad Sci U S A*. **93**: 7464-7469.

Finkel E. (2001) The mitochondrion: is it central to apoptosis? *Science*. **292**: 624-6.

Fiorani P and Bjornsti MA. (2000) Mechanisms of DNA topoisomerase I-induced cell killing in the yeast *Saccharomyces cerevisiae*. *Ann N Y Acad Sci*. **922**: 65-75.

Fire A, Xu S, Montgomery MK, Kostas SA, Driver SE, Mello CC. (1998) Potent and specific genetic interference by double-stranded RNA in *Caenorhabditis elegans*. *Nature*. **391**: 806-811.

Franch T, Petersen M, Wagner EG, Jacobsen JP, Gerdes K. (1999) Antisense RNA regulation in prokaryotes: rapid RNA/RNA interaction facilitated by a general U-turn loop structure. *J Mol Biol*. **294**: 1115-25.

Fraser AG, Kamath RS, Zipperlen P, Martinez-Campos M, Sohrmann M, Ahringer J. (2000) Functional genomic analysis of *C. elegans* chromosome I by systematic RNA interference. *Nature*. **408**: 325-330.

Fribourg S, Kellenberger E, Rogniaux H, Poterszman A, Van Dorsselaer A, Thierry JC, Egly JM, Moras D, Kieffer B. (2000) Structural characterization of the cysteine-rich domain of TFIIF p44 subunit. *J Biol Chem*. **275**: 31963-31971.

Frigerio JM, Berthézène P, Garrido P, Ortiz E, Barthelémy S, Vasseur S, Sastre B, Seleznieff I, Dagorn JC, Iovanna JL. (1995) Analysis of 2166 clones from a human colorectal cancer cDNA library by partial sequencing. *Hum Mol Genet*. **4**: 37-43.

Fung-Leung WP and Mak TW. (1992) Embryonic stem cells and homologous recombination. *Curr Opin Immunol*. **4**: 189-194.

Gao S and Scott RE. (2002) P2P-R protein over-expression restricts mitotic progression at prometaphase and promotes mitotic apoptosis. *J Cell Physiol*. **193**: 199-207.

Gao S and Scott RE. (2003) Stable over-expression of specific segments of the P2P-R protein in human MCF-7 cells promotes camptothecin-induced apoptosis. *J Cell Physiol*. **197**: 445-452.

Gao S, Witte MM, Scott RE. (2002) P2P-R protein localizes to the nucleolus of interphase cells and the periphery of chromosomes in mitotic cells, which show maximum P2P-R immunoreactivity. *J Cell Physiol.* **191**: 145-154.

Ge Q, McManus MT, Nguyen T, Shen CH, Sharp PA, Eisen HN, Chen J. (2003) RNA interference of influenza virus production by directly targeting mRNA for degradation and indirectly inhibiting all viral RNA transcription. *Proc Natl Acad Sci U S A.* **100**: 2718-2723.

George AE. (1995) A new method for isolating genes involved in the processing and presentation of antigens to cytotoxic T cells. (D.Phil. Thesis). University of Oxford.

Gessner JE, Grussenmeyer T, Dumbosky M, Schmidt RE. (1996) Separate promoters from proximal and medial control regions contribute to the natural killer cell-specific transcription of the human FcγRIII-A (CD16-A) receptor gene. *J Biol Chem.* **271**: 30755-64.

Gitlin L, Karelsky S, Andino R. (2002) Short interfering RNA confers intracellular antiviral immunity in human cells. *Nature.* **418**: 430-434.

Glazko GV, Koonin EV, Rogozin IB, Shabalina SA. (2003) A significant fraction of conserved noncoding DNA in human and mouse consists of predicted matrix attachment regions. *Trends Genet.* **19**: 119-124.

Gonczy P, Echeverri C, Oegema K, Coulson A, Jones SJ, Copley RR, Duperon J, Oegema J, Brehm M, Cassin E, Hannak E, Kirkham M, Pichler S, Flohrs K, Goessen A, Leidel S, Alleaume AM, Martin C, Ozlu N, Bork P, Hyman AA. (2000) Functional genomic analysis of cell division in *C. elegans* using RNAi of genes on chromosome III. *Nature*. **408**: 331-336.

Gordon JW. (1994) Transgenic mouse models of hepatocellular carcinoma. *Hepatology*. **19**: 538-539.

Grana X, Garriga J, Mayol X. (1998) Role of the retinoblastoma protein family, pRb, p107 and p130 in the negative control of cell growth. *Oncogene*. **17**: 3365-3383.

Green D and Kroemer G. (1998) The central executioners of apoptosis: caspases or mitochondria? *Trends Cell Biol.* **8**: 267-271.

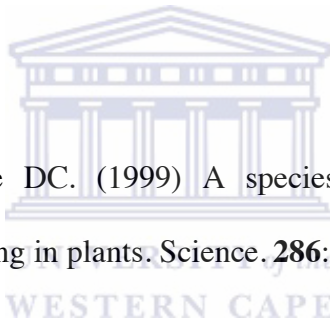
Green DR and Reed JC. (1998) Mitochondria and apoptosis. *Science*. **281**: 1309-1312.

Grishok A, Pasquinelli AE, Conte D, Li N, Parrish S, Ha I, Baillie DL, Fire A, Ruvkun G, Mello CC. (2001) Genes and mechanisms related to RNA interference regulate expression of the small temporal RNAs that control *C. elegans* developmental timing. *Cell*. **106**: 23-34.

Gross A, Yin XM, Wang K, Wei MC, Jockel J, Milliman C, Erdjument-Bromage H, Tempst P, Korsmeyer SJ. (1999) Caspase cleaved BID targets mitochondria and is required for cytochrome c release, while BCL-XL prevents this release but not tumor necrosis factor-R1/Fas death. *J Biol Chem.* **274**: 1156-1163.

Gui JF, Lane WS, Fu XD. (1994) A serine kinase regulates intracellular localization of splicing factors in the cell cycle. *Nature.* **369**: 678-682.

Haas AL and Siepmann TJ. (1997) Pathways of ubiquitin conjugation. *FASEB J.* **11**: 1257-1268.



Hamilton AJ and Baulcombe DC. (1999) A species of small antisense RNA in posttranscriptional gene silencing in plants. *Science.* **286**: 950-2

Hammond SM, Bernstein E, Beach D, Hannon GJ. (2000) An RNA-directed nuclease mediates post-transcriptional gene silencing in *Drosophila* cells. *Nature.* **404**: 293-296.

Hanks M, Wurst W, Anson-Cartwright L, Auerbach AB, Joyner AL. (1995) Rescue of the En-1 mutant phenotype by replacement of En-1 with En-2. *Science.* **269**: 679-682.

Harbour JW and Dean DC. (2000) The Rb/E2F pathway: expanding roles and emerging paradigms. *Genes Dev.* **14**: 2393-2409.

Harbour JW, Luo RX, Dei Santi A, Postigo AA, Dean DC. (1999) Cdk phosphorylation triggers sequential intramolecular interactions that progressively block Rb functions as cells move through G1. *Cell*. **98**: 859-869.

Haupt S, Berger M, Goldberg Z, Haupt Y. (2003) Apoptosis - the p53 network. *J Cell Sci*. **116**: 4077-4085.

Haupt Y, Maya R, Kazanietz A, Oren M. (1997) Mdm2 promotes the rapid degradation of p53. *Nature*. **387**: 296-299.

Hayes MP, Berrebi GA, Henkart PA. (1989) Induction of target cell DNA release by the cytotoxic T lymphocyte granule protease granzyme A. *J Exp Med*. **170**: 933-946.

Heatwole VM. (1999) TUNEL assay for apoptotic cells. *Methods Mol Biol*. **115**: 141-8.

Hengartner MO and Horvitz HR. (1994) Programmed cell death in *Caenorhabditis elegans*. *Curr Opin Genet Dev*. **4**: 581-586.

Hermeking H, Lengauer C, Polyak K, He TC, Zhang L, Thiagalingam S, Kinzler KW, Vogelstein B. (1997) 14-3-3 sigma is a p53-regulated inhibitor of G2/M progression. *Mol Cell*. **1**: 3-11.

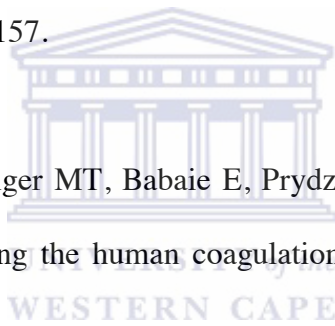
Hirose Y and Manley JL. (2000) RNA polymerase II and the integration of nuclear events. *Genes Dev.* **14**: 1415-1429.

Hjalt T and Wagner EG. (1992) The effect of loop size in antisense and target RNAs on the efficiency of antisense RNA control. *Nucleic Acids Res.* **20**: 6723-6732.

Hochstrasser M. (2000) Biochemistry. All in the ubiquitin family. *Science.* **289**: 563-564.

Hochstrasser M. (2000) Evolution and function of ubiquitin-like protein-conjugation systems. *Nat Cell Biol.* **2**: 153-157.

Holen T, Amarzguioui M, Wiiger MT, Babaie E, Prydz H. (2002) Positional effects of short interfering RNAs targeting the human coagulation trigger Tissue Factor. *Nucleic Acids Res.* **30**: 1757-1766.



Holm L and Sander C, (1993) Protein structure comparison by alignment of distance matrices. *J Mol Biol.* **233**: 123-138.

Hsieh JK, Chan FS, O'Connor DJ, Mittnacht S, Zhong S, Lu X. (1999) RB regulates the stability and the apoptotic function of p53 via MDM2. *Mol Cell.* **3**: 181-193.

Huang Y and Carmichael GG. (1996) A suboptimal 5' splice site is a cis-acting determinant of nuclear export of polyomavirus late mRNAs. *Mol Cell Biol.* **16**: 6046-6054.

Huibregtse JM, Scheffner M, Beaudenon S, Howley PM. (1995) A family of proteins structurally and functionally related to the E6-AP ubiquitin-protein ligase. *Proc Natl Acad Sci U S A.* **92**: 5249-56.

Irwin M, Marin MC, Phillips AC, Seelan RS, Smith DI, Liu W, Flores ER, Tsai KY, Jacks T, Vousden KH, Kaelin WG, Jr. (2000) Role for the p53 homologue p73 in E2F-1-induced apoptosis. *Nature.* **407**: 645-648.

Ishiura S, Matsuda K, Koizumi H, Tsukahara T, Arahata K, Sugita H. (1990) Calcium is essential for both the membrane binding and lytic activity of pore-forming protein (perforin) from cytotoxic T-lymphocyte. *Mol Immunol.* **27**: 803-807.

Ishizuka A, Saito K, Siomi MC, Siomi H. (2006) In vitro precursor microRNA processing assays using *Drosophila* Schneider-2 cell lysates. *Methods Mol Biol.* **342**: 277-86.

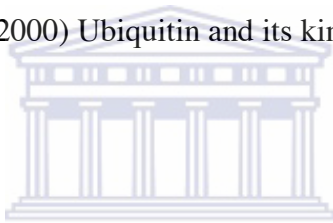
Itoh N, Yonehara S, Ishii A, Yonehara M, Mizushima S, Sameshima M, Hase A, Seto Y, Nagata S. (1991) The polypeptide encoded by the cDNA for human cell surface antigen Fas can mediate apoptosis. *Cell.* **66**: 233-243.

Jacobsen SE, Running MP, Meyerowitz EM. (1999) Disruption of an RNA helicase/RNase III gene in Arabidopsis causes unregulated cell division in floral meristems. *Development*. **126**: 5231-5243.

Jaenisch R. (1988) Transgenic animals. *Science*. **240**: 1468-1474.

Jeanmougin F, Thompson JD, Gouy M, Higgins DG, Gibson TJ. (1998) Multiple sequence alignment with Clustal X. *Trends Biochem Sci*. **23**: 403–405.

Jentsch S and Pyrowolakis G. (2000) Ubiquitin and its kin: how close are the family ties? *Trends Cell Biol*. **10**: 335-42.



Joazeiro CA and Weissman AM. (2000) RING finger proteins: mediators of ubiquitin ligase activity. *Cell*. **102**: 549-552.

Jost CA, Marin MC, Kaelin WG, Jr. (1997) p73 is a simian [correction of human] p53-related protein that can induce apoptosis. *Nature*. **389**: 191-194.

Joyner AL, Skarnes WC, Rossant J. (1989) Production of a mutation in mouse En-2 gene by homologous recombination in embryonic stem cells. *Nature*. **338**: 153-156.

Joyner AL, Zervas. (2006) Genetic inducible fate mapping in mouse: establishing genetic lineages and defining genetic neuroanatomy in the nervous system. *Dev Dyn*. **235**: 2376-85.

Kamihira M, Ono K, Esaka K, Nishijima K, Kigaku R, Komatsu H, Yamashita T, Kyogoku K, Iijima S. (2005) High-level expression of single-chain Fv-Fc fusion protein in serum and egg white of genetically manipulated chickens by using a retroviral vector. *J Virol.* **79**: 10864-74.

Kamijo T, Zindy F, Roussel MF, Quelle DE, Downing JR, Ashmun RA, Grosveld G, Sherr CJ. (1997) Tumor suppression at the mouse INK4a locus mediated by the alternative reading frame product p19ARF. *Cell.* **91**: 649-659.

Kanduc D, Mittelman A, Serpico R, Sinigaglia E, Sinha AA, Natale C, Santacrose R, Di Corcia MG, Lucchese A, Dini L, Pani P, Santacrose S, Simone S, Bucci R, Farber E. (2002) Cell death: apoptosis versus necrosis (review). *Int J Oncol.* **21**: 165-170.

Kapadia SB, Brideau-Andersen A, Chisari FV. (2003) Interference of hepatitis C virus RNA replication by short interfering RNAs. *Proc Natl Acad Sci U S A.* **100**: 2014-2018.

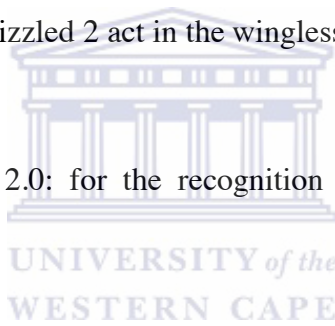
Kataoka T, Schroter M, Hahne M, Schneider P, Irmeler M, Thome M, Froelich CJ, Tschopp J. (1998) FLIP prevents apoptosis induced by death receptors but not by perforin/granzyme B, chemotherapeutic drugs, and gamma irradiation. *J Immunol.* **161**: 3936-3942.

Kato J, Matsushime H, Hiebert SW, Ewen ME, Sherr CJ. (1993) Direct binding of cyclin D to the retinoblastoma gene product (pRb) and pRb phosphorylation by the cyclin D-dependent kinase CDK4. *Genes Dev.* **7**: 331-342.

Kawasaki H and Taira K. (2003) Short hairpin type of dsRNAs that are controlled by tRNA (Val) promoter significantly induce RNAi-mediated gene silencing in the cytoplasm of human cells. *Nucleic Acids Res.* **31**: 700-707.

Kennerdell JR and Carthew RW. (1998) Use of dsRNA-mediated genetic interference to demonstrate that frizzled and frizzled 2 act in the wingless pathway. *Cell.* **95**: 1017-1026.

Knudsen S. (1999) Promoter 2.0: for the recognition of Pol II promoter sequences. *Bioinformatics* **15**: 356-361.



Knudson AG, Jr. (1971) Mutation and cancer: statistical study of retinoblastoma. *Proc Natl Acad Sci U S A.* **68**: 820-823.

Korsmeyer SJ. (1995) Regulators of cell death. *Trends Genet.* **11**: 101-105.

Krammer PH. (2000) CD95's deadly mission in the immune system. *Nature.* **407**: 789-795.

Krippner A, Matsuno-Yagi A, Gottlieb RA, Babior BM. (1996) Loss of function of cytochrome c in Jurkat cells undergoing fas-mediated apoptosis. *J Biol Chem.* **271**: 21629-21636.

Kroemer G. (1997) The proto-oncogene Bcl-2 and its role in regulating apoptosis. *Nat Med.* **3**: 614-20.

Kroemer G, Petit P, Zamzami N, Vayssiere JL, Mignotte B. (1995) The biochemistry of programmed cell death. *FASEB J.* **9**: 1277-1287.

Krueger A, Baumann S, Krammer PH, Kirchhoff S. (2001) FLICE-inhibitory proteins: regulators of death receptor-mediated apoptosis. *Mol Cell Biol.* **21**: 8247-8254.

Kubbutat MH, Jones SN, Vousden KH. (1997) Regulation of p53 stability by Mdm2. *Nature.* **387**: 299-303.

Kupfer A, Singer SJ, Dennert G. (1986) On the mechanism of unidirectional killing in mixtures of two cytotoxic T lymphocytes. Unidirectional polarization of cytoplasmic organelles and the membrane-associated cytoskeleton in the effector cell. *J Exp Med.* **163**: 489-498.

Lakin ND and Jackson SP. (1999) Regulation of p53 in response to DNA damage. *Oncogene.* **18**: 7644-7655.

Lane DP and Crawford LV. (1979) T antigen is bound to a host protein in SV40-transformed cells. *Nature*. **278**: 261-263.

Larionov A, Krause A, Miller W. (2005) A standard curve based method for relative real time PCR data processing. *BMC Bioinformatics*. **6**: 62-78.

Lee CW and La Thangue NB. (1999) Promoter specificity and stability control of the p53-related protein p73. *Oncogene*. **18**: 4171-81.

Lee EY, To H, Shew JY, Bookstein R, Scully P, Lee WH. (1988) Inactivation of the retinoblastoma susceptibility gene in human breast cancers. *Science*. **241**: 218-221.

Lee MH, Williams BO, Mulligan G, Mukai S, Bronson RT, Dyson N, Harlow E, Jacks T. (1996) Targeted disruption of p107: functional overlap between p107 and Rb. *Genes Dev*. **10**: 1621-1632.

Lee WH, Bookstein R, Lee EY. (1988) Studies on the human retinoblastoma susceptibility gene. *J Cell Biochem*. **38**: 213-227.

Lehner PJ, Hewitt EW, Romisch K. (2000) Antigen presentation: peptides and proteins scramble for the exit. *Curr Biol*. **10**: 839-842.

Levine AJ. (1997) p53, the cellular gatekeeper for growth and division. *Cell*. **88**: 323-331.

Li H, Zhu H, Xu CJ, Yuan J. (1998) Cleavage of BID by caspase 8 mediates the mitochondrial damage in the Fas pathway of apoptosis. *Cell*. **94**: 491-501.

Li L, Deng B, Xing G, Teng Y, Tian C, Cheng X, Yin X, Yang J, Gao X, Zhu Y, Sun Q, Zhang L, Yang X, He F. (2007) PACT is a negative regulator of p53 and essential for cell growth and embryonic development. *Proc Natl Acad Sci U S A*. **104**: 7951-6.

Li T, Evdokimov E, Shen RF, Chao CC, Tekle E, Wang T, Stadtman ER, Yang DC, Chock PB. (2004) Sumoylation of heterogeneous nuclear ribonucleoproteins, zinc finger proteins, and nuclear pore complex proteins: a proteomic analysis. *Proc Natl Acad Sci U S A*. **101**: 8551-8556.

Liakopoulos D, Doenges G, Matuschewski K, Jentsch S. (1998) A novel protein modification pathway related to the ubiquitin system. *EMBO J*. **17**: 2208-14.

Lin FL, Sperle K, Sternberg N. (1985) Recombination in mouse L cells between DNA introduced into cells and homologous chromosomal sequences. *Proc Natl Acad Sci U S A*. **82**: 1391-1395.

Lissy NA, Davis PK, Irwin M, Kaelin WG, Dowdy SF. (2000) A common E2F-1 and p73 pathway mediates cell death induced by TCR activation. *Nature*. **407**: 642-645.

Liu LF, Desai SD, Li TK, Mao Y, Sun M, Sim SP. (2000) Mechanism of action of camptothecin. *Ann N Y Acad Sci*. **922**: 1-10.

Livingston DM and Shivdasani R. (2001) Toward mechanism-based cancer care. *JAMA*. **285**: 588-593.

Ljutic B, Carlyle JR, Zúñiga-Pflücker JC. (2003) Identification of upstream cis-acting regulatory elements controlling lineage-specific expression of the mouse NK cell activation receptor, NKR-P1C. *J Biol Chem*. **278**: 31909-17.

Lowe SW and Lin AW. (2000) Apoptosis in cancer. *Carcinogenesis*. **21**: 485-495.

Lowin B, Hahne M, Mattmann C, Tschopp J. (1994) Cytolytic T-cell cytotoxicity is mediated through perforin and Fas lytic pathways. *Nature*. **370**: 650-652.

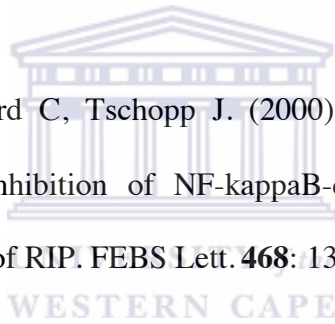
Lundberg AS and Weinberg RA. (1998) Functional inactivation of the retinoblastoma protein requires sequential modification by at least two distinct cyclin-cdk complexes. *Mol Cell Biol*. **18**: 753-761.

Marchenko ND, Zaika A, Moll UM. (2000) Death signal-induced localization of p53 protein to mitochondria. A potential role in apoptotic signaling. *J Biol Chem.* **275**: 16202-12.

Marchetto MC, Correa RG, Menck CF, Muotri AR. (2006) Functional lentiviral vectors for xeroderma pigmentosum gene therapy. *J Biotechnol.* **126**: 424-30.

Martienssen RA. (1998) Functional genomics: probing plant gene function and expression with transposons. *Proc Natl Acad Sci U S A.* **95**: 2021-2026.

Martinon F, Holler N, Richard C, Tschopp J. (2000) Activation of a pro-apoptotic amplification loop through inhibition of NF-kappaB-dependent survival signals by caspase-mediated inactivation of RIP. *FEBS Lett.* **468**: 134-136.



Masuda H, Miller C, Koeffler HP, Battifora H, Cline MJ. (1987) Rearrangement of the p53 gene in human osteogenic sarcomas. *Proc Natl Acad Sci U S A.* **84**: 7716-7719.

Matthews JM and Sunde M. (2002) Zinc fingers--folds for many occasions. *IUBMB Life.* **54**: 351-355.

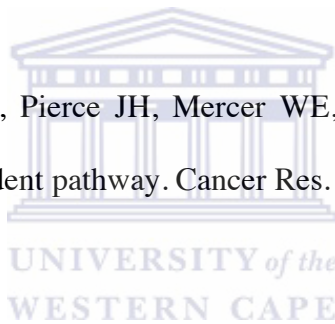
Maubach G, Lim MC, Zhang CY, Zhuo L. (2006) GFAP promoter directs lacZ expression specifically in a rat hepatic stellate cell line. *World J Gastroenterol.* **12**: 723-30.

McManus MT and Sharp PA. (2002) Gene silencing in mammals by small interfering RNAs. *Nat Rev Genet.* **3**: 737-747.

Meek DW. (1999) Mechanisms of switching on p53: a role for covalent modification? *Oncogene.* **18**: 7666-7675.

Mercie P, Garnier O, Lascoste L, Renard M, Closse C, Durrieu F, Marit G, Boisseau RM, Belloc F. (2000) Homocysteine-thiolactone induces caspase-independent vascular endothelial cell death with apoptotic features. *Apoptosis.* **5**: 403-411.

Michieli P, Chedid M, Lin D, Pierce JH, Mercer WE, Givol D. (1994) Induction of WAF1/CIP1 by a p53-independent pathway. *Cancer Res.* **54**: 3391-5.



Minoo P, Sullivan W, Solomon LR, Martin TE, Toft DO, Scott RE. (1989) Loss of proliferative potential during terminal differentiation coincides with the decreased abundance of a subset of heterogeneous ribonuclear proteins. *J Cell Biol.* **109**: 1937-46.

Miura M, Zhu H, Rotello R, Hartweg EA, Yuan J. (1993) Induction of apoptosis in fibroblasts by IL-1 beta-converting enzyme, a mammalian homolog of the *C. elegans* cell death gene *ced-3*. *Cell.* **75**: 653-660.

Miyagishi M and Taira K. (2002) Development and application of siRNA expression vector. *Nucleic Acids Res Suppl.* **2**:113-114.

Miyagishi M and Taira K. (2002) U6 promoter-driven siRNAs with four uridine 3' overhangs efficiently suppress targeted gene expression in mammalian cells. *Nat Biotechnol.* **20**: 497-500.

Moens CB, Auerbach AB, Conlon RA, Joyner AL, Rossant J. (1992) A targeted mutation reveals a role for N-myc in branching morphogenesis in the embryonic mouse lung. *Genes Dev.* **6**: 691-704.

Moll UM and Zaika A. (2001) Nuclear and mitochondrial apoptotic pathways of p53. *FEBS Lett.* **493**: 65-9.

Monaco JJ. (1992) A molecular model of MHC class-I-restricted antigen processing. *Immunol Today.* **13**: 173-179.



Morgenbesser SD, Williams BO, Jacks T, DePinho RA. (1994) p53-dependent apoptosis produced by Rb-deficiency in the developing mouse lens. *Nature.* **371**: 72-74.

Morrison LA, Braciale VL, Braciale TJ. (1986) Distinguishable pathways of viral antigen presentation to T lymphocytes. *Immunol Res.* **5**: 294-304.

Muller H, Lukas J, Schneider A, Warthoe P, Bartek J, Eilers M, Strauss M. (1994) Cyclin D1 expression is regulated by the retinoblastoma protein. *Proc Natl Acad Sci U S A.* **91**: 2945-2949.

Muller SR, Sullivan PD, Clegg DO, Feinstein SC. (1990) Efficient transfection and expression of heterologous genes in PC12 cells. *DNA Cell Biol.* **9**: 221-9.

Nagata S. (1997) Apoptosis by death factor. *Cell.* **88**: 355-365.

Nayler O, Stratling W, Bourquin JP, Stagljar I, Lindemann L, Jasper H, Hartmann AM, Fackelmayer FO, Ullrich A, Stamm S. (1998) SAF-B protein couples transcription and pre-mRNA splicing to SAR/MAR elements. *Nucleic Acids Res.* **26**: 3542-3549.

Ngo H, Tschudi C, Gull K, Ullu E. (1998) Double-stranded RNA induces mRNA degradation in *Trypanosoma brucei*. *Proc Natl Acad Sci U S A.* **95**: 14687-14692.

Nicholson DW. (1999) Caspase structure, proteolytic substrates, and function during apoptotic cell death. *Cell Death Differ.* **6**: 1028-1042.

Novotny J, Diegel S, Schirmacher H, Mohrle A, Hildebrandt M, Oberstrass J, Nellen W. (2001) Dictyostelium double-stranded ribonuclease. *Methods Enzymol.* **342**: 193-212.

Nykanen A, Haley B, Zamore PD. (2001) ATP requirements and small interfering RNA structure in the RNA interference pathway. *Cell.* **107**: 309-321.

Oka A, Harima Y, Harima K, Ostapenko VV, Tanaka Y, Ohnishi T, Sawada S. (2000) Determination of p53-mediated transactivational ability in radiation-treated cervical cancer. *Cancer Detect Prev.* **24**: 275-82.

Onodera M. (2004) Delivery of genes to hematopoietic stem cells. *Methods Mol Biol.* **246**: 527-39.

Oren M. (1999) Regulation of the p53 tumor suppressor protein. *J Biol Chem.* **274**: 36031-36034.

Ormerod MG, Orr RM, Peacock JH. (1994) The role of apoptosis in cell killing by cisplatin: a flow cytometric study. *Br J Cancer.* **69**: 93-100.

Outinen PA, Sood SK, Liaw PC, Sarge KD, Maeda N, Hirsh J, Ribau J, Podor TJ, Weitz JI, Austin RC. (1998) Characterization of the stress-inducing effects of homocysteine. *Biochem J.* **332** : 213-221.

Pan G, Ni J, Wei YF, Yu G, Gentz R, Dixit VM. (1997) An antagonist decoy receptor and a death domain-containing receptor for TRAIL. *Science.* **277**: 815-818.

Pasquinelli AE. (2002) MicroRNAs: deviants no longer. *Trends Genet.* **18**: 171-173.

Paule MR and White RJ. (2000) Survey and summary: transcription by RNA polymerases I and III. *Nucleic Acids Res.* **28**: 1283-1298.

Peter ME, Medema JP, Krammer PH. (1997) Does the *Caenorhabditis elegans* protein CED-4 contain a region of homology to the mammalian death effector domain? *Cell. Death Differ.* **4**: 523-525.

Pfaffl MW. (2001) A new mathematical model for relative quantification in real-time RT-PCR. *Nucleic Acid Research.* **29**: 1-16.

Pieters J. (1997) MHC class II restricted antigen presentation. *Curr Opin Immunol.* **9**: 89-96.



Pomerantz J, Schreiber-Agus N, Liegeois NJ, Silverman A, Alland L, Chin L, Potes J, Chen K, Orlov I, Lee HW, Cordon-Cardo C, DePinho RA. (1998) The Ink4a tumor suppressor gene product, p19Arf, interacts with MDM2 and neutralizes MDM2's inhibition of p53. *Cell.* **92**: 713-723.

Pretorius A. (2000) Identification and isolation of novel components of the antigen presentation and processing pathway via the MHC class I molecule. (MSc thesis). University of the Western Cape.

Provost P, Dishart D, Doucet J, Friendewey D, Samuelsson B, Radmark O. (2002) Ribonuclease activity and RNA binding of recombinant human Dicer. *EMBO J.* **21**: 5864-5874.

Pugh DJ, Eiso AB, Faro A, Lulya PT, Hoffmann E, Rees DJ. (2006) DWNN, a novel ubiquitin-like domain, implicates RBBP6 in mRNA processing and ubiquitin-like pathways. *BMC Struct Biol.* **6**: 1-11.

Qiu S, Adema CM, Lane T. (2005) A computational study of off-target effects of RNA interference. *Nucleic Acids Res.* **33**: 1834-47.

Quelle DE, Cheng M, Ashmun RA, Sherr CJ. (1997) Cancer-associated mutations at the INK4a locus cancel cell cycle arrest by p16INK4a but not by the alternative reading frame protein p19ARF. *Proc Natl Acad Sci U S A.* **94**: 669-673.

Ramelot TA, Cort JR, Yee AA, Semesi A, Edwards AM, Arrowsmith CH, Kennedy MA. (2003) Solution structure of the yeast ubiquitin-like modifier protein Hub1. *J Struct Funct Genomics.* **4**: 25–30.

Ramsdell F, Seaman MS, Miller RE, Tough TW, Alderson MR, Lynch DH. (1994) *gld/gld* mice are unable to express a functional ligand for Fas. *Eur J Immunol.* **24**: 928-933.

Reed JC. (1997) Bcl-2 family proteins: strategies for overcoming chemoresistance in cancer. *Adv Pharmacol.* **41**: 501-532.

Reed R and Magni K. (2001) A new view of mRNA export: separating the wheat from the chaff. *Nat Cell Biol.* **3**: 201-4.

Regner M and Mullbacher A. (2004) Granzymes in cytolytic lymphocytes--to kill a killer? *Immunol Cell Biol.* **82**: 161-169.

Renz A and Fackelmayer FO. (1996) Purification and molecular cloning of the scaffold attachment factor B (SAF-B), a novel human nuclear protein that specifically binds to S/MAR-DNA. *Nucleic Acids Res.* **24**: 843-849.

Robberson BL, Cote GJ, Berget SM. (1990) Exon definition may facilitate splice site selection in RNAs with multiple exons. *Mol Cell Biol.* **10**: 84-94.

Rotzschke O and Falk K. (1991) Naturally-occurring peptide antigens derived from the MHC class-I-restricted processing pathway. *Immunol Today.* **12**: 447-455.

Rouvier E, Luciani MF, Golstein P. (1993) Fas involvement in Ca(2+)-independent T cell-mediated cytotoxicity. *J Exp Med.* **177**: 195-200.

Rudy A, Kowalska I, Straczkowski M, Kinalska I. (2005) Homocysteine concentrations and vascular complications in patients with type 2 diabetes. *Diabetes Metab.* **31**: 112-117.

Saijo M, Sakai Y, Kishino T, Niikawa N, Matsuura Y, Morino K, Tamai K, Taya Y. (1995) Molecular cloning of a human protein that binds to the retinoblastoma protein and chromosomal mapping. *Genomics.* **27**: 511-519.

Sakai Y, Saijo M, Coelho K, Kishino T, Niikawa N, Taya Y. (1995) cDNA sequence and chromosomal localization of a novel human protein, RBQ-1 (RBBP6), that binds to the retinoblastoma gene product. *Genomics.* **30**: 98-101.

Salcedo M, Taja L, Utrera D, Chavez P, Hidalgo A, Perez C, Benitez L, Castaneda C, Delgado R, Gariglio P. (2002) Changes in retinoblastoma gene expression during cervical cancer progression. *Int J Exp Pathol.* **83**: 275-286.

Saleh A, Makrigiannis AP, Hodge DL, Anderson SK. (2002) Identification of a novel Ly49 promoter that is active in bone marrow and fetal thymus. *J Immunol.* **168**: 5163-9.

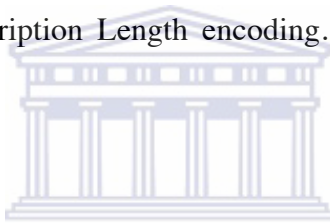
Salem C, El-Alfy M, Leblond CP. (1998) Changes in the rate of RNA synthesis during the cell cycle. *Anat Rec.* **250**: 6-12.

Sarin A, Haddad EK, Henkart PA. (1998) Caspase dependence of target cell damage induced by cytotoxic lymphocytes. *J Immunol.* **161**: 2810-2816.

Sarin A, Williams MS, Alexander-Miller MA, Berzofsky JA, Zacharchuk CM, Henkart PA. (1997) Target cell lysis by CTL granule exocytosis is independent of ICE/Ced-3 family proteases. *Immunity*. **6**: 209-215.

Schlegel J, Peters I, Orrenius S, Miller DK, Thornberry NA, Yamin TT, Nicholson DW. (1996) CPP32/apopain is a key interleukin 1 beta converting enzyme-like protease involved in Fas-mediated apoptosis. *J Biol Chem*. **271**: 1841-1844.

Schug J and Overton GC. (1997) Modeling transcription factor binding sites with Gibbs Sampling and Minimum Description Length encoding. *Proc Int Conf Intell Syst Mol Biol*. **5**: 268-71.



Scorrano L and Korsmeyer SJ. (2003) Mechanisms of cytochrome c release by proapoptotic BCL-2 family members. *Biochem Biophys Res Commun*. **304**: 437-444.

Scott RE, Giannakouros T, Gao S, Peidis P. (2003) Functional potential of P2P-R: a role in the cell cycle and cell differentiation related to its interactions with proteins that bind to matrix associated regions of DNA? *J Cell Biochem*. **90**: 6-12.

Seville LL, Shah N, Westwell AD, Chan WC. (2005) Modulation of pRB/E2F functions in the regulation of cell cycle and in cancer. *Curr Cancer Drug Targets*. **5**: 159-70.

Shahied L, Braswell EH, LeStourgeon WM, Krezel AM. (2001) An anti-parallel four-helix bundle orients the high-affinity RNA binding sites in hnRNP C: a mechanism for RNA chaperonin activity. *J Mol Biol.* 2001 **305**: 817-28.

Sharma P, Senthilkumar RD, Brahmachari V, Sundaramoorthy E, Mahajan A, Sharma A, Sengupta S. (2006) Mining literature for a comprehensive pathway analysis: a case study for retrieval of homocysteine related genes for genetic and epigenetic studies. *Lipids Health Dis.* **5**: 1-12.

Shew JY, Ling N, Yang XM, Fodstad O, Lee WH. (1989) Antibodies detecting abnormalities of the retinoblastoma susceptibility gene product (p110RB) in osteosarcomas and synovial sarcomas. *Oncogene Res.* **4**: 205-214.

Shi L, Kraut RP, Aebersold R, Greenberg AH. (1992) A natural killer cell granule protein that induces DNA fragmentation and apoptosis. *J Exp Med.* **175**: 553-566.

Shi Y and Berg JM. (1996) DNA unwinding induced by zinc finger protein binding. *Biochemistry.* **35**: 3845-3848.

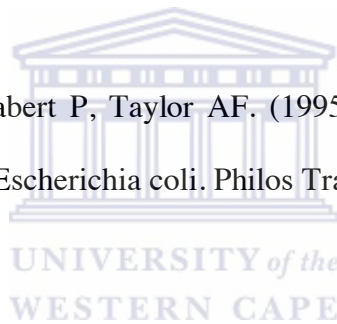
Shresta S, Heusel JW, Macivor DM, Wesselschmidt RL, Russell JH, Ley TJ. (1995) Granzyme B plays a critical role in cytotoxic lymphocyte-induced apoptosis. *Immunol Rev.* **146**: 211-221.

Siegel RM. (2006) Caspases at the crossroads of immune-cell life and death. *Nat Rev Immunol.* **6**: 308-317.

Silva JM, Hammond SM, Hannon GJ. (2002) RNA interference: a promising approach to antiviral therapy? *Trends Mol Med.* **8**: 505-508.

Simons A, Melamed-Bessudo C, Wolkowicz R, Sperling J, Sperling R, Eisenbach L, Rotter V. (1997) PACT: cloning and characterization of a cellular p53 binding protein that interacts with Rb. *Oncogene.* **14**: 145-155.

Smith GR, Amundsen SK, Dabert P, Taylor AF. (1995) The initiation and control of homologous recombination in *Escherichia coli*. *Philos Trans R Soc Lond B Biol Sci.* **347**: 13-20.



Smith J and Rothstein R. (1995) A mutation in the gene encoding the *Saccharomyces cerevisiae* single-stranded DNA-binding protein Rfa1 stimulates a RAD52-independent pathway for direct-repeat recombination. *Mol Cell Biol.* **15**: 1632-1641.

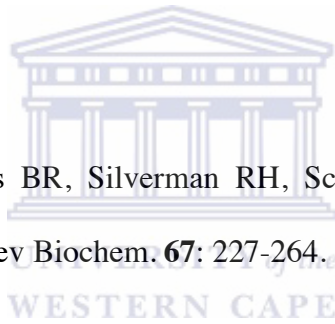
Smithies O, Gregg RG, Boggs SS, Koralewski MA, Kucherlapati RS. (1985) Insertion of DNA sequences into the human chromosomal beta-globin locus by homologous recombination. *Nature.* **317**: 230-234.

Stacey A, Schnieke A, McWhir J, Cooper J, Colman A, Melton DW. (1994) Use of double-replacement gene targeting to replace the murine alpha-lactalbumin gene with its human counterpart in embryonic stem cells and mice. *Mol Cell Biol.* **14**: 1009-1016.

Stachelek JL and Liskay RM. (1988) Accuracy of intrachromosomal gene conversion in mouse cells. *Nucleic Acids Res.* **16**: 4069-4076.

Stanger BZ, Leder P, Lee TH, Kim E, Seed B. (1995) RIP: a novel protein containing a death domain that interacts with Fas/APO-1 (CD95) in yeast and causes cell death. *Cell.* **81**: 513-523.

Stark GR, Kerr IM, Williams BR, Silverman RH, Schreiber RD. (1998) How cells respond to interferons. *Annu Rev Biochem.* **67**: 227-264.



Stougaard P, Molin S, Nordstrom K. (1981) RNAs involved in copy-number control and incompatibility of plasmid R1. *Proc Natl Acad Sci U S A.* **78**: 6008-6012.

Strasser A, O'Connor L, Dixit VM. (2000) Apoptosis signaling. *Annu Rev Biochem.* **69**: 217-45.

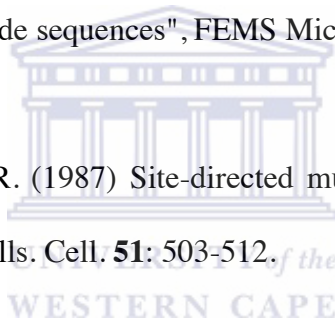
Svoboda P. (2007) Off-targeting and other non-specific effects of RNAi experiments in mammalian cells. *Curr Opin Mol Ther.* **9**: 248-57.

Takahashi T, Tanaka M, Brannan CI, Jenkins NA, Copeland NG, Suda T, Nagata S. (1994) Generalized lymphoproliferative disease in mice, caused by a point mutation in the Fas ligand. *Cell*. **76**: 969-976.

Talanian RV, Yang X, Turbov J, Seth P, Ghayur T, Casiano CA, Orth K, Froelich CJ. (1997) Granule-mediated killing: pathways for granzyme B-initiated apoptosis. *J Exp Med*. **186**: 1323-1331.

Tatiana A. Tatusova, Thomas L. Madden, (1999) "Blast 2 sequences - a new tool for comparing protein and nucleotide sequences", *FEMS Microbiol Lett*. **174**: 247-250.

Thomas KR and Capecchi MR. (1987) Site-directed mutagenesis by gene targeting in mouse embryo-derived stem cells. *Cell*. **51**: 503-512.



Thompson CB. (1995) Apoptosis in the pathogenesis and treatment of disease. *Science*. **267**: 1456-1462.

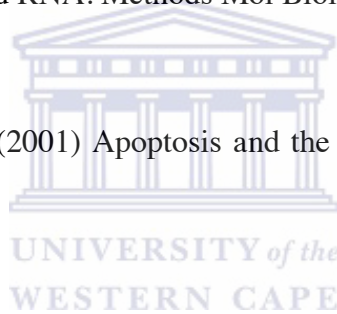
Thornberry NA. (1997) The caspase family of cysteine proteases. *Br Med Bull*. **53**: 478-490.

Thornberry NA, Bull HG, Calaycay JR, Chapman KT, Howard AD, Kostura MJ, Miller DK, Molineaux SM, Weidner JR, Aunins J, *et al.* (1992) A novel heterodimeric cysteine protease is required for interleukin-1 beta processing in monocytes. *Nature*. **356**: 768-774.

Thornberry NA and Lazebnik Y. (1998) Caspases: enemies within. *Science*. **281**: 1312-1316.

Timmons L. (2006) Construction of plasmids for RNA interference and in vitro transcription of double-stranded RNA. *Methods Mol Biol*. **351**: 109-17.

Tomei LD and Umansky SR. (2001) Apoptosis and the heart: a brief review. *Ann N Y Acad Sci*. **946**: 160-168.



Tomizawa J, Itoh T, Selzer G, Som T. (1981) Inhibition of ColE1 RNA primer formation by a plasmid-specified small RNA. *Proc Natl Acad Sci U S A*. **78**: 1421-1425.

Townsend AR, Gotch FM, Davey J. (1985) Cytotoxic T cells recognize fragments of the influenza nucleoprotein. *Cell*. **42**: 457-467.

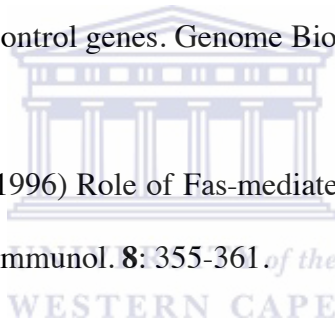
Troncone G, Martinez JC, Palombini L, De Rosa G, Mugica C, Rodriguez JA, Zeppa P, Di Vizio D, Lucariello A, Piris MA (1998) Immunohistochemical expression of mdm2 and p21WAF1 in invasive cervical cancer: correlation with p53 protein and high risk HPV infection. *J Clin Pathol*. **51**: 754-60.

Turchi L, Loubat A, Rochet N, Rossi B, Ponzio G. (2000) Evidence for a direct correlation between c-Jun NH2 terminal kinase 1 activation, cyclin D2 expression, and G(1)/S phase transition in the murine hybridoma 7TD1 cells. *Exp Cell Res.* **261**: 220-8.

Tuschl T, Zamore PD, Lehmann R, Bartel DP, Sharp PA. (1999) Targeted mRNA degradation by double-stranded RNA in vitro. *Genes Dev.* **13**: 3191-3197.

Vandesompele J, De Preter K, Pattyn F, Poppe B, Van Roy N, De Paepe A, Speleman F. (2002) Accurate normalization of real-time quantitative RT-PCR data by geometric averaging of multiple internal control genes. *Genome Biol.* **3**: 1-11.

Van Parijs L and Abbas AK. (1996) Role of Fas-mediated cell death in the regulation of immune responses. *Curr Opin Immunol.* **8**: 355-361.



Vo LT, Minet M, Schmitter JM, Lacroute F, Wyers F. (2001) Mpe1, a zinc knuckle protein, is an essential component of yeast cleavage and polyadenylation factor required for the cleavage and polyadenylation of mRNA. *Mol Cell Biol.* **21**: 8346-8356.

Volarevic S, Pende M, Pullen N. (1999) Manipulating mammalian genome by gene targeting. *Croat Med J.* **40**: 368-374.

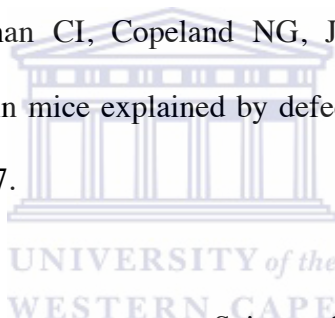
von Melchner H and Ruley HE. (1989) Identification of cellular promoters by using a retrovirus promoter trap. *J Virol.* **63**: 3227-33.

Wadhwa R, Kaul SC, Miyagishi M, Taira K. (2004) Vectors for RNA interference. *Curr Opin Mol Ther.* **6**: 367-72.

Wajant H. (2002) The Fas signaling pathway: more than a paradigm. *Science.* **296**: 1635-1636.

Walsh CM, Glass AA, Chiu V, Clark WR. (1994) The role of the Fas lytic pathway in a perforin-less CTL hybridoma. *J Immunol.* **153**: 2506-2514.

Watanabe-Fukunaga R, Brannan CI, Copeland NG, Jenkins NA, Nagata S. (1992) Lymphoproliferation disorder in mice explained by defects in Fas antigen that mediates apoptosis. *Nature.* **356**: 314-317.



Weinberg RA. (1991) Tumor suppressor genes. *Science.* **254**: 1138-1146.

Weinberg RA. (1995) The retinoblastoma protein and cell cycle control. *Cell.* **81**: 323-330.

Werner A. (2005) Natural antisense transcripts. *RNA Biol.* **2**: 53-62.

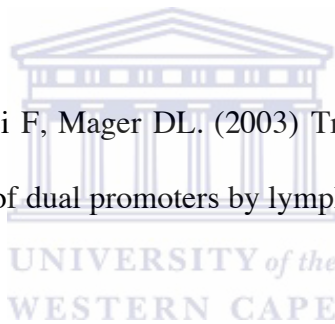
Whitton JL and Oldstone MB. (1989) Class I MHC can present an endogenous peptide to cytotoxic T lymphocytes. *J Exp Med.* **170**: 1033-1038.

Whyte P, Buchkovich KJ, Horowitz JM, Friend SH, Raybuck M, Weinberg RA, Harlow E. (1988) Association between an oncogene and an anti-oncogene: the adenovirus E1A proteins bind to the retinoblastoma gene product. *Nature*. **334**: 124-129.

Wianny F and Zernicka-Goetz M. (2000) Specific interference with gene function by double-stranded RNA in early mouse development. *Nat Cell Biol*. **2**: 70-75.

Wildin RS, Wang HU, Forbush KA, Perlmutter RM. (1995) Functional dissection of the murine Ick distal promoter. *J Immunol*. **155**: 1286-95.

Wilhelm BT, Landry JR, Takei F, Mager DL. (2003) Transcriptional control of murine CD94 gene: differential usage of dual promoters by lymphoid cell types. *J Immunol*. **171**: 4219-26.



Wilkinson CR, Dittmar GA, Ohi MD, Uetz P, Jones N, Finley D. (2004) Ubiquitin-like protein Hub1 is required for pre-mRNA splicing and localization of an essential splicing factor in fission yeast. *Curr Biol*. **14**: 2283–2288.

Williamson P, Schlegel RA. (2002) Transbilayer phospholipid movement and the clearance of apoptotic cells. *Biochim Biophys Acta*. **1585**: 53-63.

Witte MM and Scott RE. (1997) The proliferation potential protein-related (P2P-R) gene with domains encoding heterogeneous nuclear ribonucleoprotein association and Rb1 binding shows repressed expression during terminal differentiation. *Proc Natl Acad Sci U S A.* **94**: 1212-1217.

Wolf BB, and Green DR. (1999) Suicidal tendencies: apoptotic cell death by caspase family proteinases. *J Biol Chem.* **274**: 20049-20052.

Wu X, Bayle JH, Olson D, Levine AJ. (1993) The p53-mdm-2 autoregulatory feedback loop. *Genes Dev.* **7**: 1126-1132.

Wyllie AH. (1997) Apoptosis: an overview. *Br Med Bull.* **53**: 451-465.



Xue D and Horvitz HR. (1997) *Caenorhabditis elegans* CED-9 protein is a bi-functional cell-death inhibitor. *Nature.* **390**: 305-308.

Yang A and McKeon F. (2000) P69 and P73: P53 mimics, menaces and more. *Nat Rev Mol Cell Biol.* **1**: 199-207.

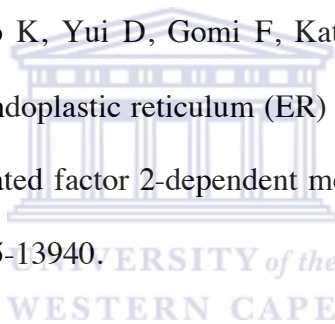
Yang X, Khosravi-Far R, Chang HY, Baltimore D. (1997) Daxx, a novel Fas-binding protein that activates JNK and apoptosis. *Cell.* **89**: 1067-1076.

Yap DB, Hsieh JK, Chan FS, Lu X. (1999) mdm2: a bridge over the two tumour suppressors, p53 and Rb. *Oncogene*. **18**: 7681-7689.

Yewdell JW and Bennink JR. (1989) Brefeldin A specifically inhibits presentation of protein antigens to cytotoxic T lymphocytes. *Science*. **244**: 1072-1075.

Yewdell JW, Bennink JR, Hosaka Y. (1988) Cells process exogenous proteins for recognition by cytotoxic T lymphocytes. *Science*. **239**: 637-640.

Yoneda T, Imaizumi K, Oono K, Yui D, Gomi F, Katayama T, Tohyama M. (2001) Activation of caspase-12, an endoplasmic reticulum (ER) resident caspase, through tumor necrosis factor receptor-associated factor 2-dependent mechanism in response to the ER stress. *J Biol Chem*. **276**: 13935-13940.



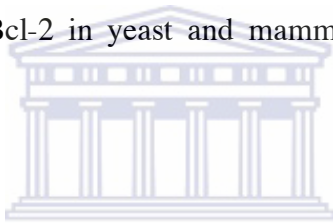
Yoshitake Y, Nakatsura T, Monji M, Senju S, Matsuyoshi H, Tsukamoto H, Hosaka S, Komori H, Fukuma D, Ikuta Y, Katagiri T, Furukawa Y, Ito H, Shinohara M, Nakamura Y, Nishimura Y. (2004) Proliferation potential-related protein, an ideal esophageal cancer antigen for immunotherapy, identified using complementary DNA microarray analysis. *Clin Cancer Res*. **10**: 6437-6448.

Yu JY, DeRuiter SL, Turner DL. (2002) RNA interference by expression of short-interfering RNAs and hairpin RNAs in mammalian cells. *Proc Natl Acad Sci U S A*. **99**: 6047-6052.

Zang WQ, Veldhoen N, Romaniuk PJ. (1995) Effects of zinc finger mutations on the nucleic acid binding activities of Xenopus transcription factor IIIA. *Biochemistry*. **34**: 15545-52.

Zauberman A, Flusberg D, Haupt Y, Barak Y, Oren M. (1995) A functional p53-responsive intronic promoter is contained within the human mdm2 gene. *Nucleic Acids Res*. **23**: 2584-2592.

Zha H and Reed JC. (1997) Heterodimerization-independent functions of cell death regulatory proteins Bax and Bcl-2 in yeast and mammalian cells. *J Biol Chem*. **272**: 31482-31488.



Zhang C, Kawauchi J, Adachi MT, Hashimoto Y, Oshiro S, Aso T, Kitajima S. (2001) Activation of JNK and transcriptional repressor ATF3/LRF1 through the IRE1/TRAF2 pathway is implicated in human vascular endothelial cell death by homocysteine. *Biochem Biophys Res Commun*. **289**: 718-724.

Zhang H, Kolb FA, Brondani V, Billy E, Filipowicz W. (2002) Human Dicer preferentially cleaves dsRNAs at their termini without a requirement for ATP. *EMBO J*. **21**: 5875-5885.

Zheng H, Hasty P, Brenneman MA, Grompe M, Gibbs RA, Wilson JH, Bradley A. (1991) Fidelity of targeted recombination in human fibroblasts and murine embryonic stem cells. *Proc Natl Acad Sci U S A.* **88**: 8067-8071.

Zou H, Henzel WJ, Liu X, Lutschg A, Wang X. (1997) Apaf-1, a human protein homologous to *C. elegans* CED-4, participates in cytochrome c-dependent activation of caspase-3. *Cell.* **90**: 405-413.

